Role of the adaptor protein (AP) complexes AP-1, AP-3, and AP-4 in protein sorting and vesicular trafficking in the human malaria parasite *Plasmodium falciparum*

-Dissertation-

With the aim of achieving a doctoral degree at the Faculty of

Mathematics, Informatics and Natural Sciences

Department of Biology

University of Hamburg

submitted by

José Jesús Cubillán Marín

Hamburg, 2025

Ich versichere, dass dieses gebundene Exemplar der Dissertation und das in elektronischer Form eingereichte Dissertationsexemplar (über den Docata-Upload) und das bei der Fakultät (zuständiges Studienbüro bzw. Promotionsbüro Physik) zur Archivierung eingereichte gedruckte gebundene Exemplar der Dissertationsschrift identisch sind.

I, the undersigned, declare that this bound copy of the dissertation and the dissertation submitted in electronic form (via the Docata upload) and the printed bound copy of the dissertation submitted to the faculty (responsible Academic Office or the Doctoral Office Physics) for archiving are identical.

Hamburg, den 11.07.2025	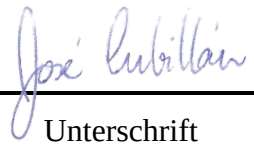
Ort, Datum	Unterschrift

Day of oral defence: 04.07.2025

1. Dissertation reviewer: Dr. Tobias Spielmann

2. Dissertation reviewer: Prof. Dr. Tim Gilberger

Member of the examination committee: Dr. Hannah Michaela Behrens

Chair of the examination committee: Prof. Dr. Tobias Lenz

Eidesstattliche Versicherung

Hiermit versichere ich an Eides statt, die vorliegende Dissertationsschrift selbst verfasst und keine anderen als die angegebenen Hilfsmittel und Quellen benutzt zu haben.

Sofern im Zuge der Erstellung der vorliegenden Dissertationsschrift generative Künstliche Intelligenz (gKI) basierte elektronische Hilfsmittel verwendet wurden, versichere ich, dass meine eigene Leistung im Vordergrund stand und dass eine vollständige Dokumentation aller verwendeten Hilfsmittel gemäß der Guten wissenschaftlichen Praxis vorliegt. Ich trage die Verantwortung für eventuell durch die gKI generierte fehlerhafte oder verzerrte Inhalte, fehlerhafte Referenzen, Verstöße gegen das Datenschutz- und Urheberrecht oder Plagiate.

Affidavit

I hereby declare and affirm that this doctoral dissertation is my own work and that I have not used any aids and sources other than those indicated.

If electronic resources based on generative artificial intelligence (gAI) were used in the course of writing this dissertation, I confirm that my own work was the main and value-adding contribution and that complete documentation of all resources used is available in accordance with good scientific practice. I am responsible for any erroneous or distorted content, incorrect references, violations of data protection and copyright law or plagiarism that may have been generated by the gAI.

Hamburg, den 11.07.2025

Ort, Datum

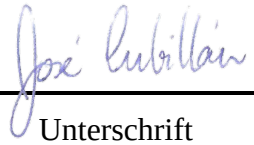

Unterschrift

Language certificate

I am a native speaker, have read the present PhD thesis and hereby confirm that it complies with the rules of the English language.

Mittelbiberach, 22.05.2025

City, Date

Sheila Mainye

Summary

Malaria is a parasitic disease caused by apicomplexan parasites of the genus *Plasmodium*. Of the five species of parasites that infects humans, *Plasmodium falciparum* is the deadliest species, and is responsible for almost all malaria deaths worldwide. Despite the highly complex life cycle of the parasite, with different stages developing in the mosquito vector and the human host, the pathogenesis of malaria is restricted to the erythrocytic schizogony. This phase of the life cycle, also termed erythrocytic cycle, is established upon the entry of the parasites into the human bloodstream, where they invade red blood cells (RBCs) and undergo asexual multiplication within a parasitophorous vacuole (PV). The parasites multiply until the conclusion of the schizogony, at which point the newly formed parasites egress under rupture of the host cell and subsequently invade new RBCs. A distinctive feature of the *Plasmodium* parasites is the formation of highly specialised, unique invasion-related organelles – the apical secretory organelles: micronemes, rhoptries and dense granules; and the inner membrane complex (IMC) – at the end of the schizogony. These organelles, which are exclusively present in the merozoites, are critical for the process of invasion into RBCs.

As eukaryotic model organisms, the endomembrane system of malaria parasites consists of a set of classical organelles – the nucleus, endoplasmic reticulum (ER), Golgi apparatus, endosome and mitochondrion – as well as the apicoplast, food vacuole (FV) and the invasion organelles. With the exception of micronemes, rhoptries, dense granules and the IMC, which are formed during schizogony, almost all the membrane organelles are present during the entire blood stage development of the parasite. An intriguing aspect of the secretory pathway is the supposed rudimentary nature of the Golgi apparatus, which lacks the characteristic stacked cisternae observed in many model organisms. The Golgi apparatus has a spatially separated cis-Golgi and trans-Golgi compartment, and it is believed that the exit face of the Golgi retains the capacity to mediate the delivery of cargoes to their correct cellular destination. However, it remains unclear which cytosolic components are involved in the post-Golgi trafficking and in the biogenesis of invasion organelles.

In eukaryotic models, the heterotetrameric adaptor protein (AP) complexes are among of the most significant components responsible for the post-Golgi trafficking and endocytosis. With the exception of AP-2, which is involved in endocytosis, the post-Golgi adaptors AP-1, AP-3, AP-4 and AP-5 orchestrate the trafficking between the trans-Golgi, early/late endosomes, lysosomes and plasma membrane. In the context of malaria parasites, both general and specialised organelles depend on faithful protein transport to mediate host cell invasion and for intracellular survival. However, the role of adaptors in the parasite and the comparability of the sorting machinery with model organisms is unclear.

The present thesis investigated the function of the post-Golgi adaptors AP-1, AP-3 and AP-4 (with AP-5 not being a subject of study due to its status as a pseudogene) on the protein sorting and vesicular trafficking in the human malaria parasite *P. falciparum*. The selection-linked integration (SLI) approach was employed to generate transgenic parasites that endogenously expressed C-terminally 2xFKBP-GFP-2xFKBP-tagged versions of the μ-subunits of the AP-1, AP-3 and AP-4 complexes. These parasite lines were utilised to study their function (by knock sideways), colocalization with markers to determine their cellular location and proxiome (by DiQ-BioID) to identify their interactors.

The results of live-cell fluorescence microscopy images demonstrated that all three adaptors were localised in clathrin-positive areas at the trans-Golgi. Of note, AP-1 appeared to occupy more of the clathrin-positive areas in comparison to AP-3 and AP-4, which seemingly resided in distinct regions within the trans-Golgi.

Growth curve analyses demonstrated that conditional inactivation of AP-1 resulted in phenotypes of growth arrest in trophozoites (when the adaptor was inactivated in ring stages) or arrested in schizonts (when the adaptor was inactivated before cytokinesis). Instead, the inactivation of AP-3 and AP-4 led to a defective invasion. Hence, all three adaptors were found to be important for the survival of the parasites.

As AP-1 exhibited the most pronounced effect, a range of different organellar markers were used to investigate its impact on trophozoite- and schizont-stage parasites. In the arrested trophozoites the ER and cis-Golgi remained intact, whereas the trans-Golgi was partially disrupted as suggested by a partial dispersal of the trans-Golgi markers Rab6 and AP-3μ, as well as clathrin (scaffolding protein of AP-1 vesicles). In contrast, sortilin (a canonical cargo receptor of AP-1) was observed to be missorted to the parasite plasma membrane (PPM) and subsequently internalised via endocytosis to the FV. Some sortilin also remained in a trans-

Golgi-like localisation. It is noteworthy that the default pathway of secretory proteins and protein export remained unaffected, suggesting that the AP-1 machinery plays a role in the events of sortilin and clathrin-dependent vesicular trafficking. A detailed analysis of the arrested schizonts revealed that the biogenesis of apical secretory and the IMC, as well as the cytokinesis process, were found to be compromised. This provides an explanation for the inability of the AP-1 knock sideways parasites to egress and invade new RBCs.

Despite the defective invasion phenotype exhibited by AP-3 and AP-4 knock sideways, no evidence of a defect in the integrity of apical organelles or the IMC was observed, with the exception of the microneme marker AMA1, which exhibited a small amount of AMA1 showing a diffuse pattern in the cytoplasm beside its physiological localisation. This finding indicates that both AP-3 and AP-4 adaptors sort specific cargoes to the specialised invasion organelles rather than impacting the integrity of these organelles.

Proxiomes from live cells then revealed a remarkable similarity in the configuration of the adaptor sorting machinery between the parasite and evolutionarily distant model organisms, but also unconventional features in relation to the composition of AP vesicle machinery, transmembrane cargoes and potential destination compartments. In some cases, contrasting with those observed in model organisms. The proxiomes of AP-1 and AP-4 identified the scaffolding protein clathrin and the accessory protein tepsin as common interacting partners for both adaptors, suggesting that the AP-1 and AP-4 machineries incorporate clathrin and tepsin in the vesicles. In addition, AP-1 recognised the multiligand receptor sortilin, while AP-4 sorted multi-transmembrane proteins. AP-1 appeared to facilitate the sorting of cargoes to VPS9-positive compartments, whereas AP-4 defines a potential trafficking pathway to acidocalcisomes. Finally, the proxiome of AP-3 did not identify coat or accessory proteins, and no cargoes were detected. However, the identification of components of the Mon1/Ccz1 and HOPS/CORVET complexes suggests that AP-3 sorts cargo vesicles to endosomal compartments resembling to those described for AP-3 in model organisms. Overall, this thesis revealed unexpected exchangeability of key elements in otherwise surprisingly conserved adaptor sorting pathways in malaria parasites.

Zusammenfassung

Malaria ist eine parasitäre Krankheit, die durch Apikomplexa-Parasiten der Gattung *Plasmodium* verursacht wird. Von den fünf Parasitenarten, die den Menschen infizieren, ist *Plasmodium falciparum* die tödlichste Art und für fast alle Malaria-Todesfälle weltweit verantwortlich. Trotz des hochkomplexen Lebenszyklus des Parasiten mit verschiedenen Stadien, die sich im Mückenvektor und im menschlichen Wirt entwickeln, ist die Pathogenese der Malaria auf die erythrozytäre Schizogonie beschränkt. Diese Phase des Lebenszyklus, die auch als erythrozytärer Zyklus bezeichnet wird, beginnt mit dem Eintritt der Parasiten in den menschlichen Blutkreislauf, wo sie in die roten Blutkörperchen eindringen und sich in einer parasitophoren Vakuole (PV) ungeschlechtlich vermehren. Die Parasiten vermehren sich bis zum Abschluss der Schizogonie, bei der die neu gebildeten Parasiten durch Platzen der Wirtszelle entweichen und anschließend neue Erythrozyten befallen. Eine Besonderheit der *Plasmodium*-Parasiten ist die Bildung hochspezialisierter, einzigartiger, mit der Invasion verbundener Organellen - die apikalen sekretorischen Organellen: Mikroneme, Rhoptrien und dichte Granula sowie der innere Membrankomplex (IMC) - am Ende der Schizogonie. Diese Organellen, die ausschließlich in den Merozoiten vorhanden sind, sind für den Prozess der Invasion in die Erythrozyten entscheidend.

Als eukaryotische Modellorganismen besteht das Endomembransystem von Malariaparasiten aus einer Reihe klassischer Organellen - dem Kern, dem endoplasmatischen Retikulum (ER), dem Golgi-Apparat, dem Endosom und dem Mitochondrium - sowie dem Apikoplast, der Nahrungsvakuole (FV) und den Invasionsorganellen. Mit Ausnahme von Mikronemen, Rhoptrien, dichten Granula und der IMC, die während der Schizogonie gebildet werden, sind fast alle Membranorganellen während der gesamten Entwicklung des Parasiten im Blutstadium vorhanden. Ein faszinierender Aspekt des sekretorischen Weges ist die vermutlich rudimentäre Natur des Golgi-Apparates, dem die charakteristischen gestapelten Zisternen fehlen, die in vielen Modellorganismen beobachtet werden. Der Golgi-Apparat verfügt über ein räumlich getrenntes cis-Golgi- und trans-Golgi-Kompartiment, und man geht davon aus, dass die Ausgangsfläche des Golgi die Fähigkeit behält, die Ladungen an ihren richtigen zellulären

Bestimmungsort zu befördern. Es bleibt jedoch unklar, welche zytosolischen Komponenten am Post-Golgi-Trafficking und an der Biogenese von Invasionsorganellen beteiligt sind.

In eukaryontischen Modellen gehören die heterotetrameren Adaptorprotein (AP)-Komplexe zu den wichtigsten Komponenten, die für den Post-Golgi-Traffic und die Endozytose verantwortlich sind. Mit Ausnahme von AP-2, das an der Endozytose beteiligt ist, steuern die Post-Golgi-Adaptoren AP-1, AP-3, AP-4 und AP-5 den Transport zwischen trans-Golgi, frühen/späten Endosomen, Lysosomen und Plasmamembran. Im Zusammenhang mit Malariaparasiten sind sowohl allgemeine als auch spezialisierte Organellen auf einen zuverlässigen Proteintransport angewiesen, um das Eindringen in die Wirtszelle und das intrazelluläre Überleben zu ermöglichen. Die Rolle der Adaptoren im Parasiten und die Vergleichbarkeit der Sortiermaschinerie mit Modellorganismen ist jedoch unklar.

In der vorliegenden Arbeit wurde die Funktion der Post-Golgi-Adaptoren AP-1, AP-3 und AP-4 (wobei AP-5 aufgrund seines Status als Pseudogen nicht untersucht wurde) für die Proteinsortierung und den vesikulären Transport im menschlichen Malariaparasiten *P. falciparum* untersucht. Mit Hilfe des SLI-Ansatzes (Selection-Linked Integration) wurden transgene Parasiten erzeugt, die endogen C-terminal 2xFKBP-GFP-2xFKBP-markierte Versionen der μ-Untereinheiten der AP-1-, AP-3- und AP-4-Komplexe exprimierten. Diese Parasitenlinien wurden zur Untersuchung ihrer Funktion (durch Knock-Sideways), der Kolokalisierung mit Markern zur Bestimmung ihres zellulären Standorts und des Proxioms (durch DiQ-BioID) zur Identifizierung ihrer Interaktoren verwendet.

Die Ergebnisse der Fluoreszenzmikroskopie in lebenden Zellen zeigten, dass alle drei Adaptoren in Clathrin-positiven Bereichen im trans-Golgi lokalisiert waren. Bemerkenswert ist, dass AP-1 mehr der Clathrin-positiven Bereiche zu besetzen schien als AP-3 und AP-4, die anscheinend in verschiedenen Regionen innerhalb des trans-Golgi zu finden waren.

Wachstumskurvenanalysen zeigten, dass die bedingte Inaktivierung von AP-1 zu einem Wachstumsstillstand bei Trophozoiten (wenn der Adaptor im Ringstadium inaktiviert wurde) oder zu einem Stillstand bei Schizonten (wenn der Adaptor vor der Zytokinese inaktiviert wurde) führte. Stattdessen führte die Inaktivierung von AP-3 und AP-4 zu einer mangelhaften Invasion. Somit erwiesen sich alle drei Adaptoren als wichtig für das Überleben der Parasiten.

Da AP-1 die stärkste Wirkung zeigte, wurde eine Reihe verschiedener organellarer Marker verwendet, um seine Auswirkungen auf Parasiten im Trophozoiten- und Schizontenstadium zu untersuchen. In den angehaltenen Trophozoiten blieben das ER und das cis-Golgi intakt,

während das trans-Golgi teilweise gestört war, wie eine teilweise Dispersion der trans-Golgi-Marker Rab6 und AP-3µ sowie Clathrin (Gerüstprotein der AP-1-Vesikel) nahelegt. Im Gegensatz dazu wurde beobachtet, dass Sortilin (ein kanonischer Ladungsrezeptor von AP-1) zur Plasmamembran (PPM) des Parasiten fehlverteilt und anschließend durch Endozytose in FV internalisiert wurde. Ein Teil von Sortilin verblieb auch in einer trans-Golgi ähnlichen Lokalisation. Bemerkenswert ist, dass der Standardweg der sekretorischen Proteine und des Proteinexports nicht beeinträchtigt wurde, was darauf hindeutet, dass die AP-1-Maschinerie eine Rolle im Sortilin- und Clathrin-abhängigen vesikulären Transport spielt. Eine detaillierte Analyse der angehaltenen Schizonten ergab, dass die Biogenese der apikalen sekretorischen Organellen und der IMC sowie der Zytokineseprozess beeinträchtigt waren. Dies ist eine Erklärung für die Unfähigkeit der AP-1-Knock-Sideways-Parasiten, aus den Erythrozyten auszutreten und in neue Erythrozyten einzudringen.

Trotz des defekten Invasionsphänotyps von AP-3 und AP-4 knock sideways Parasiten wurden keine Anzeichen für eine Beeinträchtigung der Integrität der apikalen Organellen oder des IMC beobachtet, mit Ausnahme des Mikronemenmarkers AMA1, der neben seiner physiologischen Lokalisierung eine geringe Menge von AMA1 mit einem diffusen Muster im Zytoplasma aufwies. Dieser Befund deutet darauf hin, dass sowohl AP-3- als auch AP-4-Adaptoren spezifische Ladungen zu den spezialisierten Invasionsorganellen sortieren und nicht die Integrität dieser Organellen beeinträchtigen.

Proxiome aus lebenden Zellen zeigten dann eine bemerkenswerte Ähnlichkeit in der Konfiguration der Adaptor-Sortiermaschinerie zwischen dem Parasiten und evolutionär entfernten Modellorganismen, aber auch unkonventionelle Merkmale in Bezug auf die Zusammensetzung der AP-Vesikelmaschinerie, der Transmembranfrachten und der potenziellen Zielkompartimente. In einigen Fällen stehen sie im Gegensatz zu denen, die in Modellorganismen beobachtet werden. In den Proxiomen von AP-1 und AP-4 wurden das Gerüstprotein Clathrin und das akzessorische Protein Tepsin als gemeinsame Interaktionspartner für beide Adaptoren identifiziert, was darauf hindeutet, dass die AP-1- und AP-4-Maschinerien Clathrin und Tepsin in die Vesikel einbauen. Darüber hinaus erkannte AP-1 den Multiligandenrezeptor Sortilin, während AP-4 Multitransmembranproteine sortierte. AP-1 scheint die Sortierung von Ladungen zu VPS9-positiven Kompartimenten zu erleichtern, während AP-4 einen potenziellen Trafficking-Weg zu Acidocalcisomen definiert. Schließlich wurden im Proxiom von AP-3 keine Hüll- oder Zubehörproteine identifiziert, und es wurden keine Ladungen nachgewiesen. Die Identifizierung von Komponenten der Mon1/Ccz1- und

HOPS/CORVET-Komplexe deutet jedoch darauf hin, dass AP-3 Frachtvesikel in endosomale Kompartimente sortiert, die denen ähneln, die für AP-3 in Modellorganismen beschrieben wurden. Insgesamt ergab diese Arbeit eine unerwartete Austauschbarkeit von Schlüsselelementen in ansonsten überraschend konservierten Adaptor-Sortierwegen in Malariaparasiten.

Table of contents

List of figures

List of tables

Abbreviations

aa *amino acids*
AMA1 *apical membrane antigen 1*
ANTH *AP180 N-terminal homology*
AP *adaptor protein*
ARS *Ring-stage Survival Assay*
BC *Before Christ*
BS(D) *Blasticidin S (deaminase)*
Ca *calcium*
CALM *clathrin assembly lymphoid myeloid leukaemia*
CHC *clathrin heavy chain*
CLAG3.1, 3.2 *cytoadherence-linked asexual gene 3.1, 3.2*
CLAPs *clathrin associated sorting proteins*
CLC *clathrin light chain*
CME *clathrin-mediated endocytosis*
COPI *coatomer complex I*
CORVET C *core endosomal vacuole tethering*
CRT *chloroquine resistance transporter*
DAPI *4',6-diamidino-2-phenylindole*
DARC *Duffy antigen receptor for chemokines*
DIC *differential interference contrast*
DHE *dihydroethidium*
DMSO *dimethyl sulfoxide*
dNTPs *desoxynucelotide phosphates*
DPAP1 *dipeptidyl aminopeptidase 1*
DTT *1,4-dithiothreitol*
LDL *low-density lipoprotein*
MFS *malaria freezing solution*
mSca *mScarlet*
MSRP6 *MSP7-related protein 6*
MSP1 *merozoite surface protein 1*
MTS *malaria thawing solution*
MTV1 *modified transport to the vacuole 1*
Neo *neomycin phosphotransferase II*
NLS *nuclear localisation signal*
NPPs *new permeation pathways*
NTD *N-terminal domain*
p *pellet*
PBS *phosphate buffered saline*
PCR *polymerase chain reaction*
PEXEL *Plasmodium export element*
P. falciparum Plasmodium falciparum
*Pf*EMP1 *Plasmodium falciparum erythrocyte membrane protein 1*
PI(3)P *phosphatidylinositol-3-phosphate*
PIESP2 *Plasmodium-infected erythrocyte surface protein 2*
PIPES *piperazine-N,N'-bis(2-ethanesulphonic acid)*
PNEP *PEXEL-negative exported protein*
PPIX *protoporphyrin IX*
PPM *parasite plasma membrane*
PTEX *protein translocon of exported proteins*
PV *parasitophorous vacuole*

EBA-181/175/-140 *erythrocyte-binding antigen 181/175/140*
EBL *erythrocyte-binding like*
E. coli Escherichia coli
EEF *exoerythrocytic forms*
EGF *epidermal growth factor*
EPS15 *EGFR Protein tyrosine kinase Substrate #15*
EM *electron microscopy*
endo *endogenous*
ENTH *epsin N-terminal homology*
ER *endoplasmic reticulum*
ERGIC *ER-Golgi intermediate compartment*
EtBr *ethidium bromide*
EXP1, 2 *exported protein 1, 2*
FHF *fused toes homolog-Hook-FHIP*
FKBP *FK506 binding protein*
FRB FKBP *rapamycin binding domain*
FV *food vacuole*
fw *forward*
G6PD *glucose-6-phosphate dehydrogenase*
GA-TGN *Golgi-associated TGN*
GalNAc *N-Acetylgalactosamine*
GFP *green fluorescent protein*
GGA: *Golgi-localised, γ-ear-containing*
GI-TGN *Golgi-independent TGN*
GPA/C *glycophorin A/C*
HbS *sickle haemoglobin*
hDHFR *human dihydrofolate reductase*
HEPES *4-(2-Hydoxyethyl)-1-piperazineethanesulfonicacid*
HOPS *homotypic fusion and vacuole protein sorting*
P. vivax Plasmodium vivax
PVM *parasitophorous vacuole membrane*
RBC *red blood cell*
RESA *ring-infected erythrocyte surface antigen*
RhopH 2, 3 *high-molecular-weight rhoptry protein 2, 3*
RON2, 4, 5, 8 *rhoptry neck protein 2, 4, 5 ,8*
ROP *rhoptry bulb protein*
RPMI *Roswell Park Memorial Institute (medium)*
RSA *rhoptry secretory apparatus*
RUSC1, 2 *run and SH3-domain containing proteins 1, 2*
rv *reverse*
SBP1 *skeleton-binding protein 1*
SCA *sickle-cell anaemia*
SERA5 *serine-rich antigen 5*
SLI *selection-linked integration*
SLiMs *short linear motifs*
SORTLR *sortilin-like receptor*
SP *signal peptide*
SPG11 *spastic paraplegia 11*
SPG15 *spastic paraplegia 15*
SNARE *soluble N-ethylmaleimide-sensitive-factor attachment protein receptor*
SUB1 *subtilisin-like protease 1*
TE *Tris-EDTA*
TEMED *N, N, N, N-Tetramethylethylenediamin*
TGN
T. gondii Toxoplasma gondii
TM(D) *transmembrane (domain)*

hpi *hours post invasion*

HSP101 *heat shock protein 101*

IFA *immunofluorescence assay*

IMC *inner membrane complex*

iRBC *infected red blood cell*

(k)bp (kilo) *base pairs*

K13 *Kelch13*

MC(s) *Maurer's clefts*

TVN *tubovesicular network*

V-ATPases *vacuolar-type H^+-ATPases*

VHS *Vps-27, Hrs and STAM*

VPS41 *Vacuolar protein sorting-associated protein 41 homolog*

WHO *World Health Organisation*

WR *WR99210*

yDHODH *yeast dihydroorotate dehydrogenase*

2A T2A *skip peptide*

7xGGGGS *7x glycine-serine-linker*

1. Introduction

1.1 Malaria

1.1.1 Historical Overview

Malaria is an ancient disease that has profoundly shaped the history of human beings. The earliest records of malaria-like illnesses were described in Chinese medical texts from 2700 BC, Mesopotamian clay tablets from 2000 BC, Egyptian papyri from 1570 BC, writings from the Vedic period in India dated to 1500-800 BC, and Greek texts from 850 BC (Institute of Medicine (US) Committee on the Economics of Antimalarial Drugs, 2004; Cox, 2010). In these historical documents, a distinct feature to describe this disease was the presence of periodic fever in people living in marshy places (Cox, 2010; Nosten et al., 2022). Molecular genetic studies have revealed that the most famous pharaoh, King Tutankhamun, and several members of his family, experienced repeated episodes of *Plasmodium falciparum* infections, and this disease was identified as the most probable cause of death (Hawass et al., 2010), although this cause of death is controversial (Timmann & Meyer, 2010).

The term ‘malaria’ is derived from the Italian words *mal* and *aria* which mean ‘bad air’ which likely arose from an association of marshy regions with the disease. The first documented observation of malaria parasites under the microscope was conducted by Charles Louis Alphonse Laveran in 1880, who identified the organism in the blood of patients infected with malaria (Cox, 2010).

1.1.2 Evolution and host adaptations

Phylogenetic studies have indicated that malaria parasites have co-evolved with non-human primates in Africa. It is suggested that the emergence of *P. falciparum* occurred from gorillas in Sub-Saharan Africa within the past 10,000 years, whereas *Plasmodium vivax* is believed to have emerged from *P. vivax*-like parasites that infected chimpanzees and gorillas in Central

Africa (see Figure 1) (Joy et al., 2003; Liu et al., 2010, 2014; Loy et al., 2017; Sharp et al., 2024).

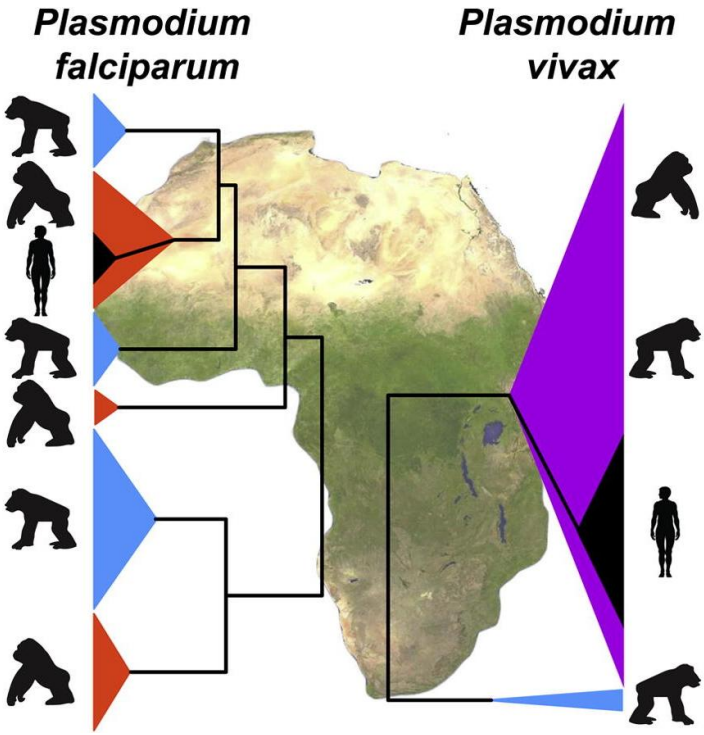

Figure 1 Origin of the human malaria parasites *P. falciparum* and *P. vivax* in Africa.
Phylogenetic analysis shows the origin of *P. falciparum* from gorillas, and *P. vivax* from chimpanzees and gorillas. Mitochondrial and nuclear DNA fragments of *Plasmodium* primate, *Laverania* primate, rodent, bird and reptile parasites were used for the molecular analysis (from (Loy et al., 2017)).

During the course of human history, the *Plasmodium* parasites have exerted a considerable degree of selective pressure on the genome of human populations in geographical regions where malaria is endemic (Kwiatkowski, 2005; Weatherall, 2008; Kariuki & Williams, 2020). This has been supported by the establishment of the FY*O allele of the human Duffy antigen receptor for chemokines (DARC) in African population, where this mutation has been linked to resistance to *P. vivax* infections (McManus et al., 2017). Furthermore, the genetic mutation of the β globin gene that produces sickle haemoglobin (HbS), responsible for sickle-cell anaemia (SCA) (Piel et al., 2010), has been shown to promote protection against malaria, although its effectiveness varies depending on the parasite genotype (Band et al., 2022). Moreover, it has been demonstrated that high frequency of α^{+}-thalassaemia protects against severe malaria caused by *P. falciparum* (Flint et al., 1986; Allen et al., 1997); whereas the deficiency of glucose-6-phosphate dehydrogenase (G6PD) provides partial protection against

malaria (Ruwende & Hill, 1998), although it can hinder the efficacy of anti-malarial treatments against *P. vivax*, such as primaquine, which cause haemolytic anaemia in patients with G6PD (A-) deficiency (Fanello et al., 2008; Chu et al., 2017).

1.1.3 *Plasmodium* species infecting humans

Malaria is an endemic vector-borne disease caused by protozoan parasites belonging to the genus *Plasmodium*, which are transmitted by female *Anopheles* mosquito vectors. The genus *Plasmodium* belongs to the order Haemosporida (Phylum Apicomplexa), whose species have been described as having a polyphyletic origin (Figure 2) (Outlaw & Ricklefs, 2011; Galen et al., 2018). At present, more than 200 species of *Plasmodium* are known to infect a variety of organisms, including reptiles, birds and mammals. Of these, five *Plasmodium* species have been described as infecting humans – *P. falciparum*, *P. vivax*, *P. malariae*, *P. ovale* and *P. knowlesi* (White, 2008).

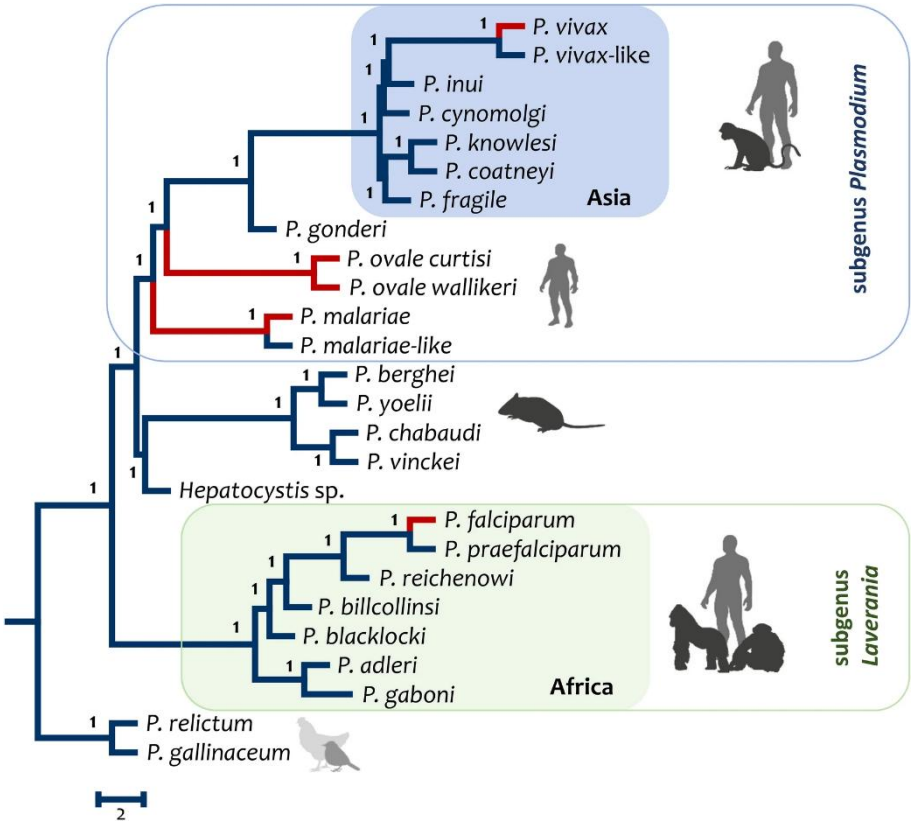

Figure 2. Phylogenetic analyses of *Plasmodium* spp. based on 1028 single copy orthologous genes. *Plasmodium* species were clustered in the subgenera *Plasmodium*, *Vinckeia* and *Laverania*. Human infecting *Plasmodium* species are represented by red branches. *Plasmodium ovale* is divided into two

subspecies: *P. ovale curtisi* and *P. ovale wallikeri*. *Plasmodium gallinaceum* and *Plasmodium relictum* were used to estimate the root of the primate-rodent malaria tree (from (Escalante et al., 2022)).

Some studies have suggested that human malaria is caused by six species instead of five, on the basis of the presence of two genetically distinct but morphologically indistinguishable species of *P. ovale*, named *P. ovale curtisi* and *P. ovale wallikeri* (Sutherland et al., 2010; Ansari et al., 2016; Snounou et al., 2024).

In recent years, the occurrence of zoonotic infections caused by non-human primate malaria parasites has been a subject of increasing attention. The most notable example is zoonotic malaria caused by *P. knowlesi*, the fifth human-infecting malaria parasite (Singh et al., 2004; White, 2008), which is naturally maintained in long-tailed and pig-tailed macaques, and banded leaf monkeys in South East Asia (Jeyaprakasam et al., 2020). Furthermore, a number of additional reports of emergent zoonotic transmissions have been documented for the non-human primate malaria parasites *P. cynomolgi* (Ta et al., 2014), geographically limited in Southeast Asia, and *P. simium* (Brasil et al., 2017), restricted to the Atlantic Forest of south and south-eastern Brazil. A recent study (Yap et al., 2021) reported that the detection of several non-primate malaria species – including *P. inui*, *P. coatneyi*, *P. inui-like* and *P. simiovale* – in addition to *P. knowlesi* and *P. cynomolgi*, in indigenous Malaysian communities has underscored the significance of zoonotic malaria transmission as a potential threat to human health (Faust & Dobson, 2015; Voinson et al., 2022).

1.1.4 Distribution and epidemiology of malaria

Human malaria is widely distributed in tropical and subtropical regions, where parasites coexist geographically with their respective female *Anopheles* mosquito vectors (Sinka et al., 2012). These geographic regions are characterised by the combination of environmental factors – such as temperature, rainfall, humidity, wind and daylight duration – that support parasite and vector survival (Kelly-Hope et al., 2009; Rossati et al., 2016). In conjunction with the capacity of vectors to transmit parasites, the impact of climate change, and the emergence and spread of anti-malarial drug resistance, these factors render this parasitic disease difficult to eradicate in the endemic regions (White, 2004; Caminade et al., 2014).

In 2023, the World Health Organization (WHO) estimated a total of 263 million cases of malaria and 597,000 deaths from malaria globally, with predominant cases and deaths reported

in children under five years of age (WHO, 2024). The vast majority of malaria cases (94 %) and deaths (95 %) was observed in the WHO African Region, followed by the WHO Eastern Mediterranean Region (4 % of cases and 3 % of deaths). The remaining WHO regions (South-East Asia, Western Pacific and Americas) accounted for approximately 2% of cases and 2 % of deaths (WHO, 2024; Daily & Parikh, 2025).

Among human malaria species, *P. falciparum* was responsible for approximately 97% of malaria cases worldwide in 2023. This parasite is highly endemic in sub-Saharan Africa (Figure 3A), while *P. vivax*, responsible for about 3.5% of malaria cases worldwide, is endemic in South America, South and Southeast Asia, the Western Pacific and Oceania (Figure 3B) (WHO, 2024; Daily & Parikh, 2025).

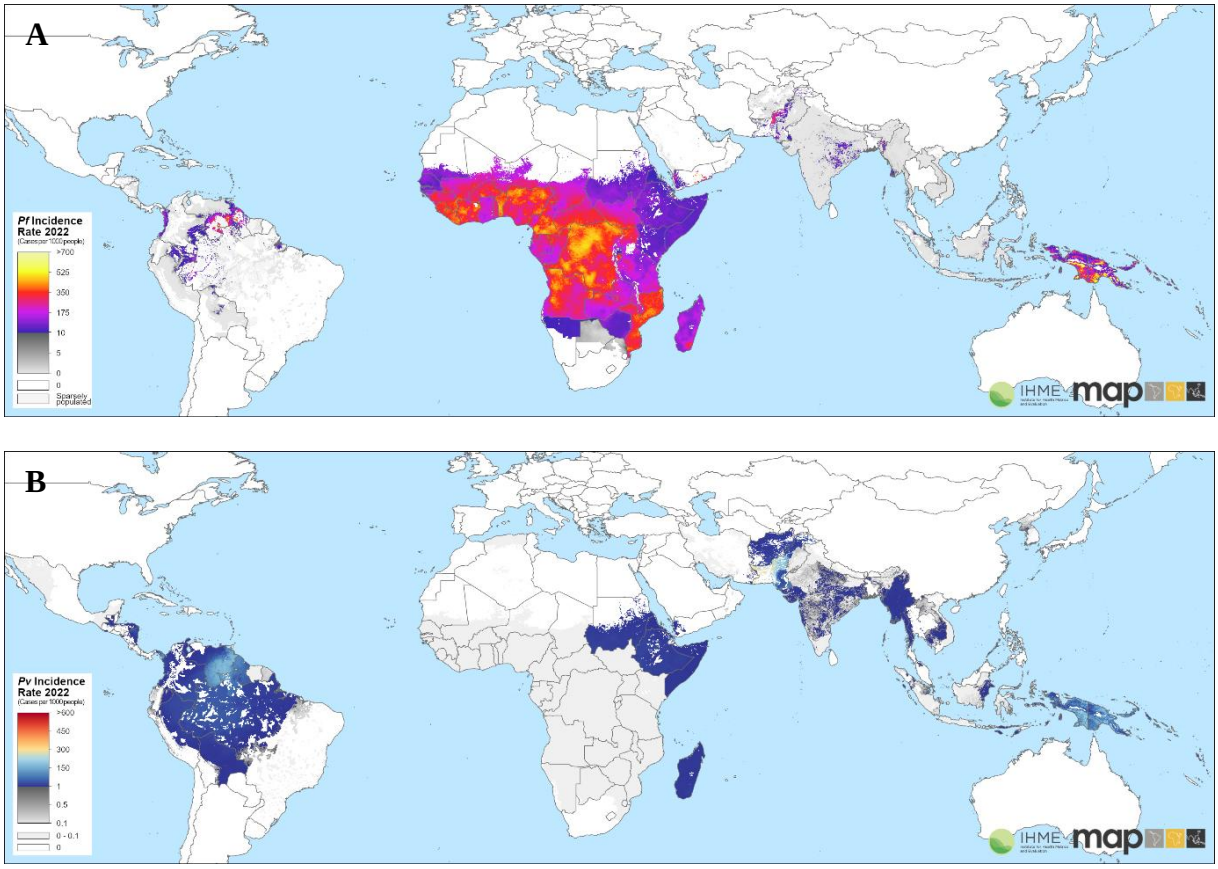

Figure 3. The incidence rate of *P. falciparum* and *P. vivax* malaria in 2022.
Clinical cases per 1,000 population per annum of *P. falciparum* **(A)** and *P. vivax* **(B)**. Colours show incidence rate from high (yellow for *P. falciparum*, red for *P. vivax*) to low (white). Grey colour in *P. falciparum* (sparsely populated) and *P. vivax* (very low) (from www.malariaatlas.org).

1.2 *Plasmodium* biology

1.2.1 Life cycle of *Plasmodium falciparum*

The life cycle of *P. falciparum* parasite alternates between two distinct organisms: the human and the female *Anopheles* mosquito. The parasite undergoes asexual replication (schizogony) in humans and sexual reproduction (sporogony) in the mosquito (Figure 4).

1.2.1.1 Schizogony in the liver and in erythrocytes

The schizogonic cycle begins with the inoculation of sporozoites (the infective stage of the parasite for humans) into the skin of a human host by an infected female *Anopheles* mosquito (Figure 4). Subsequent to this, sporozoites actively migrate through the dermis and enter the blood circulation. Upon reaching at the liver, sporozoites traverse host cells and invade hepatocytes, where they reside within a parasitophorous vacuole (PV) and initiate asexual development into clinically-silent liver stages or exoerythrocytic forms (EEF) (Amino et al., 2006; Prudêncio et al., 2006; De Niz et al., 2017). The hepatic development of this parasite stage leads to multiple rounds of DNA replication and nuclear division, followed by cytokinesis to generate thousands of exoerythrocytic merozoites in the hepatocyte, in a developmental process known as exoerythrocytic schizogony (Scheiner et al., 2024). After 2 to 16 days (depending on the species of malaria parasite) of liver-stage development, exoerythrocytic merozoites are packaged as merozoite-filled vesicles, known as merosomes, which bud from the infected hepatocyte into the liver sinusoids (Sturm et al., 2006; Baer et al., 2007; Scheiner et al., 2024). Merosomes remain intact in the bloodstream until they reach the lung, where they rupture, releasing the merozoites into the circulation (Baer et al., 2007). The exoerythrocytic merozoites then invade red blood cells (RBCs), thus initiating the erythrocytic cycle (also called erythrocytic schizogony). Once within the RBC, the parasite establishes develops in a PV and sequentially progresses through the asexual stages termed ring, trophozoite, and schizont. During late schizogony, parasites undergo asynchronous nuclear division and cytokinesis to generate 16-32 merozoites. Upon egress, these merozoites invade new RBCs (Cowman et al., 2012; Voß et al., 2023). Each erythrocytic cycle of *P. falciparum* takes around 48 hours (Bozdech et al., 2003) (the stages of this cycle are described in detail in section 1.2.2). During the erythrocytic schizogony, a small proportion of parasites commit to sexual development in

order to form the male and female gametocytes (the infective stages of the parasite for mosquito vectors) (Josling & Llinás, 2015).

1.2.1.2 Sporogony

The sporogonic cycle commences during a new feeding event, when a female *Anopheles* mosquito takes up mature gametocyte-containing blood from an infected human host (Figure 4). Once in the mosquito midgut lumen, the activation of gametocytes to gametes is triggered by a combination of microenvironmental factors, including a decrease in temperature (16-24°C), a shift in extracellular pH (~7.2 to 8), elevated cytosolic Ca^{2+} levels, and exposure to the mosquito-derived tryptophan metabolite xanthurenic acid (Billker et al., 1998, 2004; Bennink et al., 2016; Dash et al., 2022). During this process, male gametocytes undergo multiple rounds of DNA replication and nuclear division to form eight highly motile, flagellated microgametes in a process called exflagellation, while female gametocytes transform into a single macrogamete (Dash et al., 2022). Subsequently, male gametes fuse with female gametes to form a zygote, which undergoes a transformation into a mobile and invasive ookinete. Then ookinetes rapidly traverse the midgut epithelium and develop into sessile oocysts beneath the basal lamina. Within the oocyst, sporogony occurs, producing thousands of sporozoites. Following rupture of the oocyst, the sporozoites are released into the haemocoel and enter the salivary glands, where they await to be transmitted to a new human host (Josling & Llinás, 2015; Dash et al., 2022).

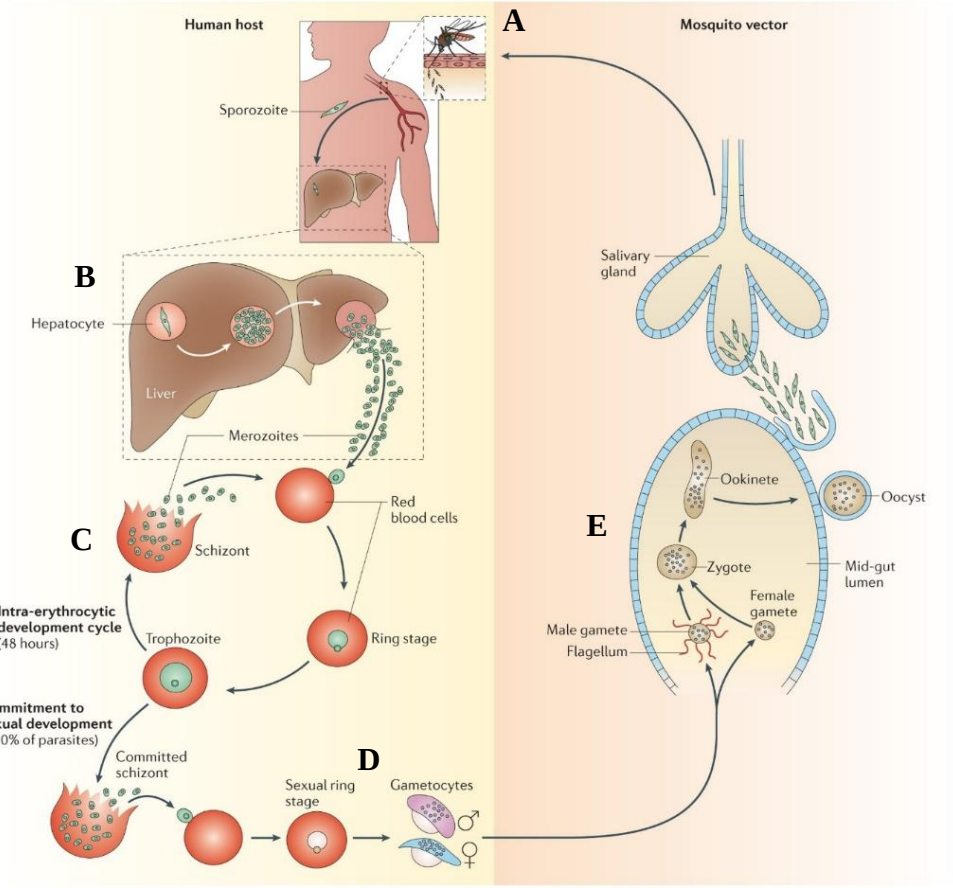

Figure 4. Life cycle of *Plasmodium falciparum* parasites.
(A) During a blood meal by an infected female *Anopheles* mosquito, sporozoites are inoculated into the skin of the human host and subsequently travel into the liver (Prudêncio et al., 2006). **(B)** Parasites invade hepatocytes and form thousands of exoerythrocytic merozoites that are released into the bloodstream (Scheiner et al., 2024). **(C)** Merozoites invades RBCs and develop into ring, trophozoite and schizont stage during growth in the host cell. The released merozoites re-invade RBCs, leading to continuous multiplication in the blood. **(D)** Some intracellular parasites commit to form gametocytes (Josling & Llinás, 2015). **(E)** Mature gametocytes are taken up during a new blood meal of an *Anopheles* mosquito. Within the midgut lumen, parasites undergo fertilisation and maturation, followed by traversing the midgut epithelial cell wall and development to oocysts, which form sporozoites (Dash et al., 2022). These parasites migrate to the salivary glands, where they await another blood meal (modified from (Josling & Llinás, 2015)).

1.2.2 Asexual blood stages of *Plasmodium falciparum*

During the asexual erythrocytic cycle, the parasite undergoes a series of distinct developmental stages with different purposes. These are described in detail in the next sections.

1.2.2.1 Ring stage

Upon invasion of RBCs, the parasites are referred to as the ring stage, due to their ring-like appearance in Giemsa smears. This phase of the development in RBCs takes approximately 18 hours to complete (Figure 5). The parasites establish themselves within the PV that is generated during invasion and separates the parasite from the host cell. Immediately after invasion it starts to dismantle the invasion-related membrane compartments (e.g., rhoptries and the inner membrane complex (IMC)) (Torii et al., 1989; Bannister et al., 2003; Hanssen et al., 2013; Riglar et al., 2013). Ring stage has been described to be highly dynamic and mobile in shape, undergoing repeated transitions from an ameboid form to a disc-shaped form (Grüring et al., 2011; Fréville et al., 2025) that in in electron microscopy studies was shown to result from a cup shape of the parasite (Bannister et al., 2004). While the ring stage is considered to be metabolically less active than other stages and originally was considered to not endocytose host cell cytosol (Abu Bakar et al., 2010), food vacuole like structures have been detected (Bannister et al., 2004) and uptake of host cell cytosol shortly after invasion was recently demonstrated (Birnbaum et al., 2020). In parallel, the export machinery is established by trafficking specific parasite proteins into the host cell, thereby inducing the formation of Maurer's clefts and remodelling the architecture of the host cell (Bannister et al., 2004; Marti et al., 2004; Grüring et al., 2011; McMillan et al., 2013). Maurer's clefts function as a sorting platform for the trafficking of exported proteins to the RBC membrane (Mundwiler-Pachlatko & Beck, 2013).

The ring stage is also relevant in artemisinin resistance, as it is the stage that survives high drug concentrations in resistant parasites and where this can be measured in the laboratory using the Ring-stage Survival Assay (ARS) (Witkowski et al., 2013). It is noteworthy that rings are the sole intracellular stage found in the blood circulation of patients naturally infected with *P. falciparum*, as after completion of host cell modifications the parasites cytoadhere in the vasculature of major organs to evade splenic passage that eliminates later stages (Rowe et al., 1997; Smith et al., 2000; Salanti et al., 2003).

1.2.2.2 Trophozoite stage

The ring stage progresses into the trophozoite stage in a short transition phase of about 4 hours where the morphology of the parasite changes from the ring into a filled circle (Grüring et al., 2011). The development of trophozoite-stage parasites ranges from one- to four- nuclei (~18 to 34 hours post-invasion) (Figure 5). This stage is characterised by a significant increase in

parasite size compared to the ring stage, primarily due to the active ingestion and digestion of host cell haemoglobin. Furthermore, a notable morphological feature is the presence of well-defined hemozoin crystals within the FV, a brown pigment that is a produced to prevent the toxic effects of free haem (Jani et al., 2008).

The uptake of host cytosolic material is facilitated by cytostomal invaginations that lead to the transport of host cell cytosol to the FV (Milani et al., 2015). Trophozoites exhibit elevated metabolic activity, as they not only catabolise haemoglobin but also initiate preparations for DNA replication and subsequent schizogony (Ben Mamoun et al., 2001; Bozdech et al., 2003).

In parallel, the parasite, which has already established its protein export machinery, virulence factors and Maurer's clefts in the host cytosol in the ring stage (see section 1.2.2.1) (Marti et al., 2004; Grüring et al., 2011), orchestrates the trafficking of the *P. falciparum* Erythrocyte Membrane Protein 1 (PfEMP1) to the surface of the infected RBC (Douki et al., 2003; McMillan et al., 2013). PfEMP1 is the major cytoadherence factor that mediate for the sequestration of the infected RBC within the microvasculature, particularly in brain vessels (Kyes et al., 2007). As results of this sequestration, trophozoites are typically absent from peripheral blood smears in patients with *P. falciparum* malaria (Silamut et al., 1999).

1.2.2.3 Schizont stage

The transition from the trophozoite to schizont stage occurs when parasite prepares to form its progeny (Figure 5), During this phase, the parasites undergo multiple rounds of DNA replication and asynchronous nuclear division (Klaus et al., 2022). This is accompanied by the elongation and branching of the mitochondrion and apicoplast, in preparation for their segregation into the daughter merozoites (Rudlaff et al., 2020; Liffner et al., 2023; Verhoef et al., 2024). In this phase the biogenesis of highly specialised invasion-related organelles, such as rhoptries, micronemes, dense granules and the IMC, takes place. These organelles are derived from the trans-Golgi compartment (Bannister et al., 2000b, 2003; Yeoman et al., 2011). The centriolar plaque and its associated proteins serve as anchoring platform that tether nucleus in division to the parasite plasma membrane (PPM) during mitosis, as well as to the mitochondrion. Around this anchoring platform, the apical secretory organelles (rhoptries and micronemes) and the IMC are formed (Liffner et al., 2023). Following nuclear division, organelle biogenesis and organellar segregation, the process of cytokinesis takes place, resulting in the formation of daughter merozoites that inherit a specific set of membrane

organelles. The basal complex facilitates the abscission of the daughter merozoites by separating the nascent pellicle (IMC and PPM) from the residual body, which contains parasite-derived waste, including the hemozoin (Rudlaff et al., 2020; Liffner et al., 2023). Toward the end of erythrocytic schizogony, a calcium-dependent signalling cascade triggers the discharge of exosome contents into the PV lumen (Yeoh et al., 2007). Among these, the subtilisin-like protease (SUB1) plays a critical role by activating egress factors, such as the MSP1/6/7 complex and members of serine repeat antigen (SERA) family, which are papain-like cysteine proteases (Yeoh et al., 2007). Upon the coordinated breakdown of both PV membrane (PVM) and RBC membrane, the merozoites are released to the extracellular space, where they invade new RBCs (Wickham et al., 2003).

Like trophozoites, schizonts are also sequestered in the microvasculature, and are therefore not detected in peripheral blood smears of patients with *P. falciparum* malaria (Silamut et al., 1999).

1.2.2.4 Merozoite stage

The egressed merozoite is the invasive form of the parasite for RBCs. Merozoites are among the most diminutive eukaryotic cells, with a diameter of between 1.2 to 1.5 µm (Bannister et al., 2000a). As described in section 1.2.2.3, merozoites are equipped with a set of specialised apical secretory organelles – micronemes, rhoptries and dense granules – as well as the IMC. These organelles are essential for orchestrating the multi-step invasion process, which includes initial attachment, reorientation, tight junction formation, internalisation with the subsequent shedding of the surface coat of merozoites (invasion), and sealing of the PV and RBC membranes (post-invasion) (Cowman et al., 2012).

The survival period of merozoites after egress is remarkably short, with a typical duration of up to 15 minutes as determined under *in vitro* conditions, time after that they lose their viability and invasive capacity (Gilson & Crabb, 2009; Boyle et al., 2010). During this brief time period, merozoites must rapidly invade new RBCs to continue the erythrocytic cycle.

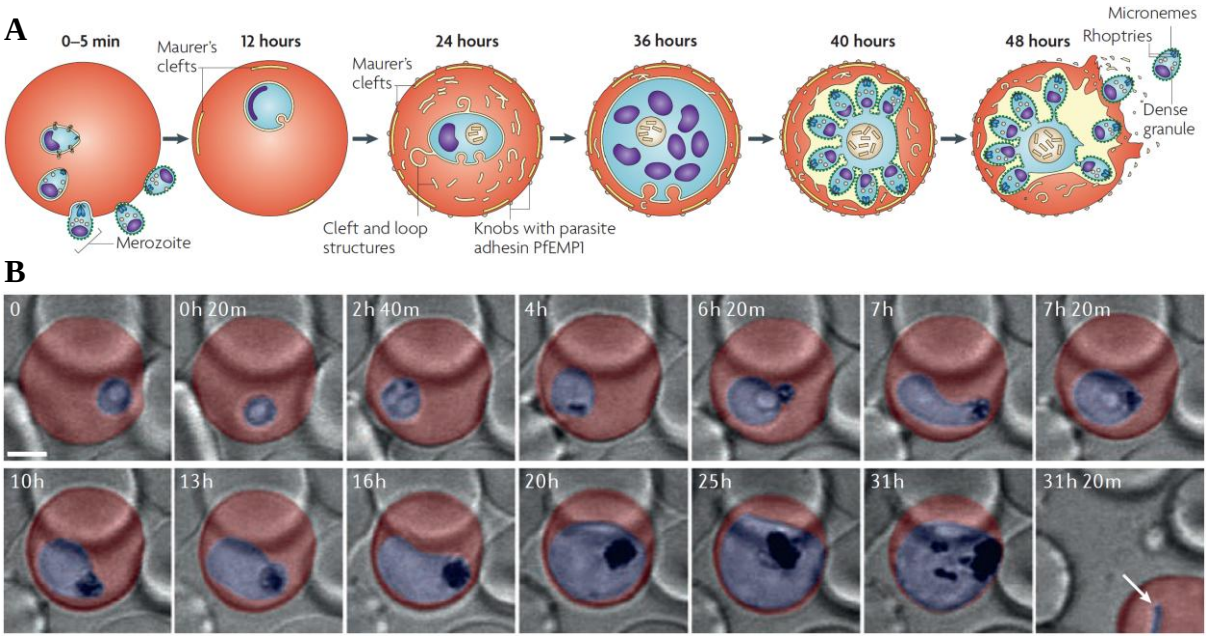

Figure 5. Asexual blood stage development of *P. falciparum*.
(A) Schematic representation of asexual parasite development of *P. falciparum* (modified from Maier et al., 2009). **(B)** 3D microscopy over time (4D imaging) of *P. falciparum* blood stages using confocal microscopy. A series of selective time points in a single differential interference contrast (DIC) z-section of the stacks were acquired at 20-minute intervals, capturing the dynamic of parasite development (from ring stage to schizont stage). Black: hemozoin crystal in the FV of the parasite; artificial colours were assigned as follows: red (RBC) and blue (parasite body); white arrow (at the 31h 20m time point): newly formed ring stage; h: hours post-initiation of time-lapse microscopy imaging: m: minutes post-initiation of time-lapse microscopy imaging. Scale bar: 2 µm (modified from (De Niz et al., 2017).

1.3.3 Endomembrane system in malaria parasites

1.3.3.1 Classical organelles – nucleus, endoplasmic reticulum (ER), Golgi apparatus and mitochondrion

Similar to eukaryotic organism models, malaria parasites possess a classical set of organelles, including the nucleus, the endoplasmic reticulum (ER) and the Golgi apparatus, and the mitochondrion. The ER has been described as surrounding the parasite nuclei with additional "horn-like" projections (Tonkin et al., 2006b). The Golgi apparatus has been described to lack of the classical stacked flat cisternae that are observed in most eukaryotic cells (Van Wye et al., 1996; Bannister et al., 2000a). In contrast, the parasites possess a functional, but potentially rudimentary unstacked Golgi apparatus (Van Wye et al., 1996; Bannister et al., 2000a), similar to that in *Saccharomyces cerevisiae* (Preuss et al., 1992), with the cis-Golgi compartment being

close, but spatially distinguishable from the trans-Golgi compartment (Van Wye et al., 1996; Struck et al., 2005, 2008).

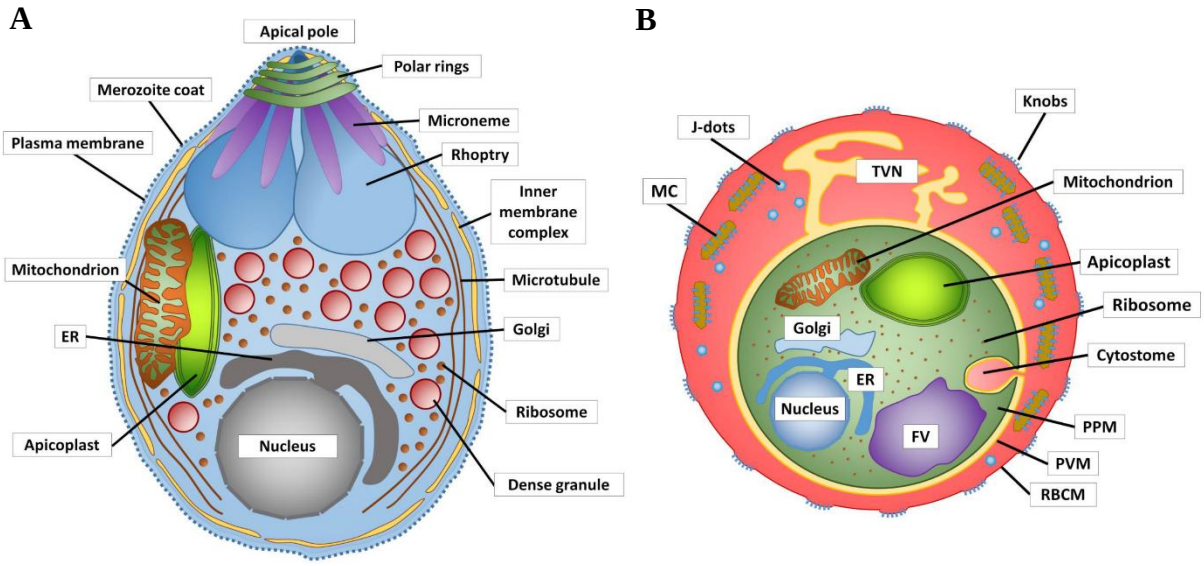

Figure 6. Endomembrane and exomembrane system in *P. falciparum*.
(A and B) Organelles and membrane structures are shown for merozoite (A) and trophozoite stage parasite. ER: endoplasmic reticulum; FV: food vacuole; PPM: parasite plasma membrane; PVM: parasitophorous vacuole membrane; TVN: tubovesicular network; MC: Maurer's cleft; RBCM: RBC membrane (modified from (Flammersfeld et al., 2018).

The parasite also harbours a unique mitochondrion that is important for its development (van Dooren et al., 2006). This double-membrane bound organelle possesses a small genome (about 6 kb), encoding just three proteins (Cox1, Co3 and Cytb) but not tRNAs (Vaidya et al., 1989, 1993; Wilson & Williamson, 1997; Vaidya & Mather, 2009). In contrast to the function of human mitochondria in the respiratory chain for production of energy, the mitochondrial electron transport machinery in malaria blood-stage parasites appears to be essential in the pyrimidine biosynthesis (Painter et al., 2007; Vaidya & Mather, 2009). A recent study (Verhoef et al., 2024) has shown that the mitochondrion is closely associated with the apicoplast during the schizogony.

1.3.3.2 Food vacuole (FV) and endosomal structures

The FV is a highly specialised acidic, lysosome-like organelle that is important for the digestion of haemoglobin (Francis et al., 1997) and the acquisition of nutrients in the parasite (Spielmann et al., 2020). The cytostomal structure serves as the main entrance for host cell cytosolic

components to be directed towards the FV (Spielmann et al., 2020). The metabolism of haemoglobin results in the production of amino acids – a process facilitated by aspartic proteases (plasmepsins), cysteine proteases (falcipains), and metalloproteases (falcilysins) (Francis et al., 1997; Eggleson et al., 1999; Klemba, et al., 2004a; Drew et al., 2008) – and in the release of toxic free haem, which is subsequently detoxified by crystallisation into haemozoin within the FV lumen (Chugh et al., 2013). This process is tightly regulated and forms the foundation for the mechanism of action of several antimalarial drugs, including chloroquine and other aminoquinoline drugs, which interfere with haem detoxification or compromise the integrity of the FV membrane (Egan, 2008; Ismail et al., 2016). The FV has a low pH (pH ~5.2), maintained by vacuolar-type H^+-ATPases (V-ATPases), which is optimal for the enzymatic activity of resident proteases and for haemozoin formation (Saliba et al., 2003).

The parasite also possesses a so far poorly defined endosome that retains certain features found in late endosomes of eukaryotic cells and is positive for the retromer complex and Ras-related protein (Rab7) (Krai et al., 2014). In contrast, the FV and endosomal intermediates are positive for the early endosomal marker PI(3)P (Tawk et al., 2010; Jonscher, 2018). Recently, the cellular localisation of components of the homotypic fusion and vacuole protein sorting (HOPS) and class C core endosomal vacuole tethering (CORVET) complex were described in malaria parasite, supporting the evidence of endosomal structures, which are expected to receive cargo vesicles from the trans-Golgi compartment and sort them to specialised organelles (Mesén-Ramírez et al., 2025).

Although the precise nature of the endosomes is not fully elucidated, primarily due to the complexity and organisation of the parasite, as well as the lack of specific markers to identify them, these organelles might function as intermediate compartments between the trans-Golgi and rhoptries (Krai et al., 2014).

1.3.3.3 Apicoplast

The apicoplast is a non-photosynthetic plastid derived from a secondary endosymbiotic event, which is reflected in its organization within four surrounding membranes (McFadden & Yeh, 2017; Lemgruber et al., 2013). This organelle plays essential roles in different metabolic pathways, including fatty acid and isoprenoid biosynthesis, as well as contributing to haem biosynthesis (Ralph et al., 2004; Lim & McFadden, 2010). Interestingly, in blood stages, the

synthesis of isopentenyl pyrophosphate (IPP), a key intermediate in the isoprenoid pathway, is indispensable for parasite survival (Yeh & DeRisi, 2011). Similar to the mitochondrion, many nuclear-encoded proteins are targeted to this organelle, suggesting that apicoplast genes have been transferred to the nuclear genome (Waller et al., 1998). Its 35-kb circular DNA genome encodes only 30 proteins involved in gene expression, mostly tRNAs and rRNAs, which are necessary for its maintenance and function (Wilson et al., 1996; Gardner et al., 2002; Arisue et al., 2012). The division and segregation of the apicoplast is a tightly regulated process during schizogony, ensuring its coordinated inheritance by daughter merozoites (Verhoef et al., 2024).

1.3.3.4 Invasion-related organelles – micronemes, rhoptries, dense granules and the inner membrane complex (IMC)

During the schizogony the biogenesis of unique invasion-related organelles and the process of cytokinesis to form new daughter merozoites is initiated (Klaus et al., 2022; Voß et al., 2023). Each merozoite is equipped with a set of apical secretory organelles – micronemes, rhoptries and dense granules – as well as the IMC, a double membrane located beneath the PPM (Hanssen et al., 2013). The biogenesis of micronemes, rhoptries, dense granules and the IMC has been suggested to form from the fusion of Golgi-derived vesicles (Bannister et al., 2000b, 2003; Yeoman et al., 2011). The secretory organelles are spatially positioned at the apical pole of the merozoite and the discharge their contents in a rapid and highly coordinated sequence that facilitate the host cell invasion.

1.3.3.4.1 Micronemes

The micronemes are long-necked, bottle-shaped secretory vesicles measuring approximately 160 nm in length and 65 nm in width (Bannister et al., 2003). Each merozoite contains up to 40 micronemes, clustered around the rhoptry necks at the apical pole (Bannister et al., 2000b). Micronemes have been described as heterogeneous in composition, with proteins such as apical membrane antigen 1 (AMA1) and erythrocyte binding antigen 175 (EBA175) residing in distinct subsets of micronemes (Healer et al., 2002; Liffner et al., 2023) while other microneme-like organelles carry egress relevant proteins (Yeoh et al., 2007). Besides EBA175 and AMA1, micronemes contains further proteins involved in the invasion process, including EBA140, EBA181 (Cowman et al., 2012). Once merozoites egress, AMA1 is translocated from the

micronemes to the merozoite surface (Narum & Thomas, 1994; Healer et al., 2002), where it interacts with the rhoptry macromolecular complex rhoptry neck protein (RON2/4/5/8) embedded in the RBC membrane to form the tight junction necessary for invasion (Lamarque et al., 2011). In contrast, EBA175 facilitates the RBC recognition by binding to host receptor Glycophorin A (Sim et al., 1994).

1.3.3.4.2 Rhoptries

The rhoptries are twinned pear-shaped organelles, which are divided into neck and basal bulb regions, with the neck region oriented toward the apical tip of the parasite, whereas the bulb region lies close to the Golgi cisternae (Bannister et al., 2000b; Hanssen et al., 2013). It has been described that rhoptry-resident proteins are trafficked from the trans-Golgi compartment to the nascent rhoptries during schizogony (Bannister et al., 2000b; Liffner et al., 2021). The rhoptry content is abundant with some specific proteins located in the neck while other are exclusively located in the bulb (Counihan et al., 2013; Liffner et al., 2021). Upon reorientation of the merozoite to bring the apical pole to the site of host cell membrane contact, rhoptry content is discharged sequentially, neck first, followed by bulb, during and after the invasion (Cowman et al., 2012; Counihan et al., 2013; Liffner et al., 2021). During these steps, the pair of rhoptries are partially or totally fused, with the tip docking to an apical vesicle, forming the rhoptry secretory apparatus (RSA) (Martinez et al., 2022). Interestingly, rhoptry discharge is a process highly regulated by calcium signals (Singh et al., 2010).

1.3.3.4.3 Dense granules

The dense granules are the final apical organelle to secret their contents during the invasion process (Torii et al., 1989; Riglar et al., 2013). These organelles are very dense, specialised secretory vesicles and in malaria parasites are formed very late during the schizogony (Vallintine & van Ooij, 2023). In contrast to rhoptries, which are positioned at the apical pole of the parasite and gradually secrete their contents through the RSA during the invasion process, dense granules discharge their contents by fusing their membrane with the PPM (Bullen et al., 2012). Dense granules harbour the components of the *Plasmodium* translocon of exported protein (PTEX) complex, EXP2, HSP101 and PTEX150 (Bullen et al., 2012), which is released in the forming PV and is inserted in the PV membrane (De Koning-Ward et al., 2009). It has been described that EXP2 functions both as a nutrient-permeable channel and as a central

component of the PTEX machinery, essential for protein export into the host cell (De Koning-Ward et al., 2009; Garten et al., 2018).

1.3.3.4.4 The inner membrane complex (IMC)

The IMC is a flattened membrane organelle that underlies the PPM and is connected to the Parasite's cytoskeleton (Kono et al., 2012). This organelle is formed de novo during the cytokinesis, originating from the apical end of each developing merozoite, and anchored to the centriolar plaque. The apical ring, Golgi and rhoptries are segregated alongside the centriolar plaque during the merozoite formation (Liffner et al., 2023). The IMC, form a multi-layered membrane structure known as the pellicle (Kono et al., 2016). A dynamic ring structure called the basal complex functions as contractile ring and promotes the separation of daughter cells from the residual body, and define the basal end of each merozoite (Kono et al., 2016; Liffner et al., 2023). The IMC is implicated in critical functions, such as in motility and invasion as well as conferring mechanical stability and shape to the merozoite, and to serve as a scaffold during the formation of daughter merozoites (Kono et al., 2012). After RBC invasion, the IMC is rapidly disassembled within approximately 10 minutes (Riglar et al., 2013).

1.4 Protein sorting and vesicular trafficking machinery in eukaryotic cells

In eukaryotic cells, proteins destined for the secretory pathway are synthesised in the ER, from which they are transported to the ER-Golgi intermediate compartment (ERGIC) and subsequently to the Golgi cisternae (Bonifacino & Glick, 2004; Appenzeller-Herzog & Hauri, 2006). This vesicle-dependent process is mediated by the coat protein complex II (COPII), which is responsible for anterograde transport from the ER to the Golgi (Aridor et al., 1995). The retrieval of proteins is facilitated by coatomer complex I (COPI), which is responsible for the retrograde transport from the Golgi to the ER via coated vesicles (Aridor et al., 1995). During the anterograde trafficking towards and through the cis-Golgi, secretory proteins undergo multiple post-translational modifications (e.g., glycosylation, phosphorylation, lipid modification) that are essential for sorting and proper function at their final destination compartments.

After the cis-Golgi, protein reach the trans-Golgi network which serves as a central hub for protein sorting and trafficking within the cell (Griffiths & Simons, 1986). The trans-Golgi

network is composed of spatially distinct subzones, each responsible for directing cargo proteins to specific destinations, including endosomes, lysosomes, vacuoles, or the plasma membrane. The following sections focus on the vesicle formation and protein sorting events in the context of post-Golgi vesicle trafficking.

1.4.1 Vesicle formation in post-Golgi sorting

Vesicle formation is initiated with the budding of a vesicle from the donor membrane. Cytosolic factors such adaptor protein (AP) complexes – AP-1 to AP-5 (see section 1.4.2) – are recruited onto the donor membrane, by interacting with sorting signals located in the cytosolic tail of transmembrane protein cargoes (Park & Guo, 2014). These transmembrane proteins are either themselves the cargo that is to be transported (e.g., transporters), or are cargo receptors (e.g., sortilin, mannose-6-phosphate receptors) that have the capacity to bind other proteins that are the cargo (Tan & Gleeson, 2019). The adaptors play a role in selecting cargo, initiating the formation of vesicles and targeting these vesicles to their respective destination compartments.

In order to carry out these functions, adaptors attach to the membrane either directly – by inserting amphipathic helices or recognising specific phospholipids – or indirectly, by recruiting accessory factors such as ENTH- and ANTH-domain containing proteins (Heldwein et al., 2004). Adaptors also recruit coat proteins such as clathrin, and, in cooperation with accessory factors, drive the curvature of the donor membrane, leading to vesicle formation and budding (Makowski et al., 2020). Each type of adaptor mediates transport to different destination compartments.

Once the vesicle is budding from the donor membrane, a membrane fission event – mediated by dynamin – occurs, thereby separating the vesicle from the donor membrane (Bonifacino & Glick, 2004). The coated vesicles then undergo an uncoating step, during which all the vesicle-associated cytosolic factors are released, exposing tether proteins that are essential for vesicle tethering on the vesicle surface. These tethering factors facilitate the docking of the vesicle to the target compartment, followed by the fusion of the cargo-carrying vesicles, in a process mediated by SNARE proteins (Bonifacino & Glick, 2004). The released adaptors and other cytosolic factors are recycled for subsequent rounds of vesicle formation.

Clathrin and ENTH/ANTH-domain containing proteins are known to play a pivotal role in the process of membrane curvature induction and vesicle budding (Makowski et al., 2020). For instance, AP-1 and AP-2 interact with clathrin to form clathrin-coated vesicles (Zeno et al.,

2021). However, AP-4 and AP-5 do not interact with clathrin, raising the question of how the curvature for vesicle formation is achieved in the absence of interaction with canonical coat proteins. A recent study (Begley et al., 2024) demonstrated that AP-3 in yeast possesses the intrinsic ability to induce membrane curvature through amphipathic helices present in its subunits. This finding provides a model for how vesicle budding might occur independently of a coat or other accessory proteins.

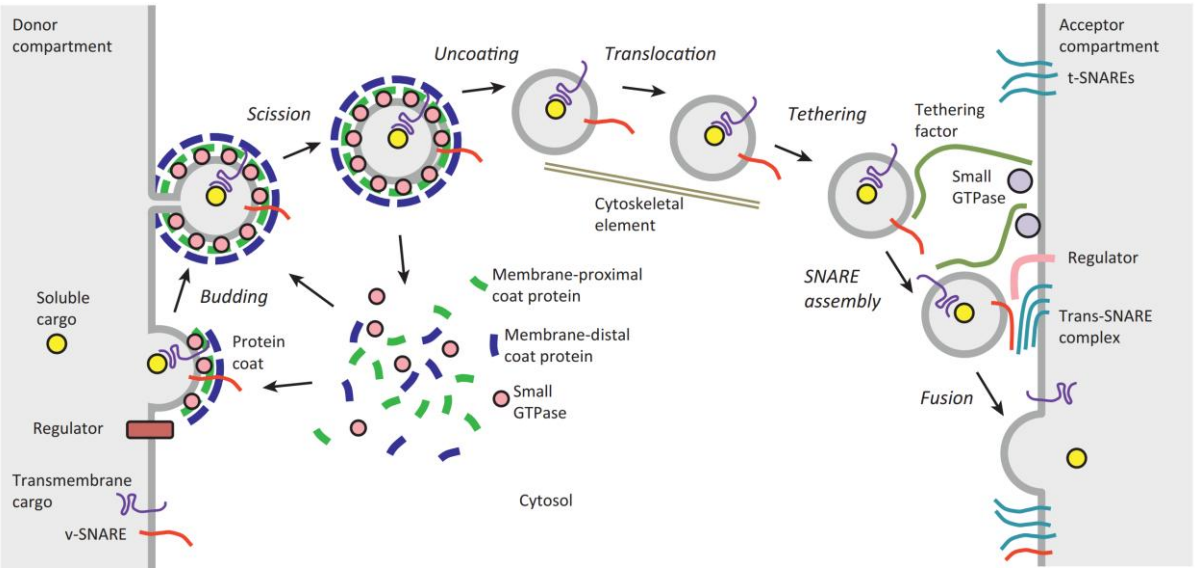

Figure 7. Steps of vesicle formation and fusion.
Cytosolic factors are recruited onto the donor compartment membrane via interaction with transmembrane protein cargoes (purple and red) and lipids, promoting vesicle budding (Bonifacino & Glick, 2004). Transmembrane proteins can also function as carriers for luminal cargoes (yellow), i.e. function as cargo receptors. The scission process involves the separation of the cargo-carrying vesicle from the donor membrane (Parkar et al., 2009). During the trafficking, the vesicle undergoes a uncoating process, whereby the release of the cytosolic factors into the cytosol occurs, and these are recycled for a new event of vesicle formation. Uncoated vesicles expose tethering factors (green) and SNARE proteins (red), which are essential for the proper vesicular tethering and fusion to the acceptor compartment membrane (Bonifacino & Glick, 2004). Transmembrane and soluble cargoes are transferred to the destination compartment (from (Bonifacino, 2014b)).

1.4.2 Adaptor protein (AP) complexes

In eukaryotic model organisms, the AP complexes play key roles in the sorting of cargo proteins into secretory and endocytic trafficking pathways (Dacks & Robinson, 2017). These adaptors select and facilitate the packaging of transmembrane cargo proteins into specific vesicles, thereby directing their transport to the correct cellular destinations (Huang et al., 2019; Shimizu et al., 2021; Wong-Dilworth et al., 2023; Stockhammer et al., 2024a). To date, five

heterotetrameric adaptors (AP-1 to AP-5) have been described, each consisting of two large subunits (one each of γ/α/δ/ε/ζ and β1-5, ~100kDa) complexed with one medium subunit (μ1-5, ~50kDa) and one small subunit (σ1-5, ~20kDa) (Hirst et al., 2011). The adaptors function as an entire heterotetramer complex and are spatially represented in three parts: trunk (core domain), hinge and ears (or appendage domain) (Beacham et al., 2019). Here, the N-terminal domain of the large subunits (one each of γ/α/δ/ε/ζ and β1-5), in conjunction with the medium (μ1-5) and small (σ1-5) subunits organise the trunk, whereas the C-terminal domain of the large subunits (one each of γ/α/δ/ε/ζ and β1-5) form the ears and protrude from the trunk, connected by the hinge. It is important to note that, depending on the adaptor, the ear domain contains specific binding pockets for interacting with accessory factors (e.g., tepsin, epsin, EPS15) while the hinge contains binding sites to bind coat protein (e.g., clathrin).

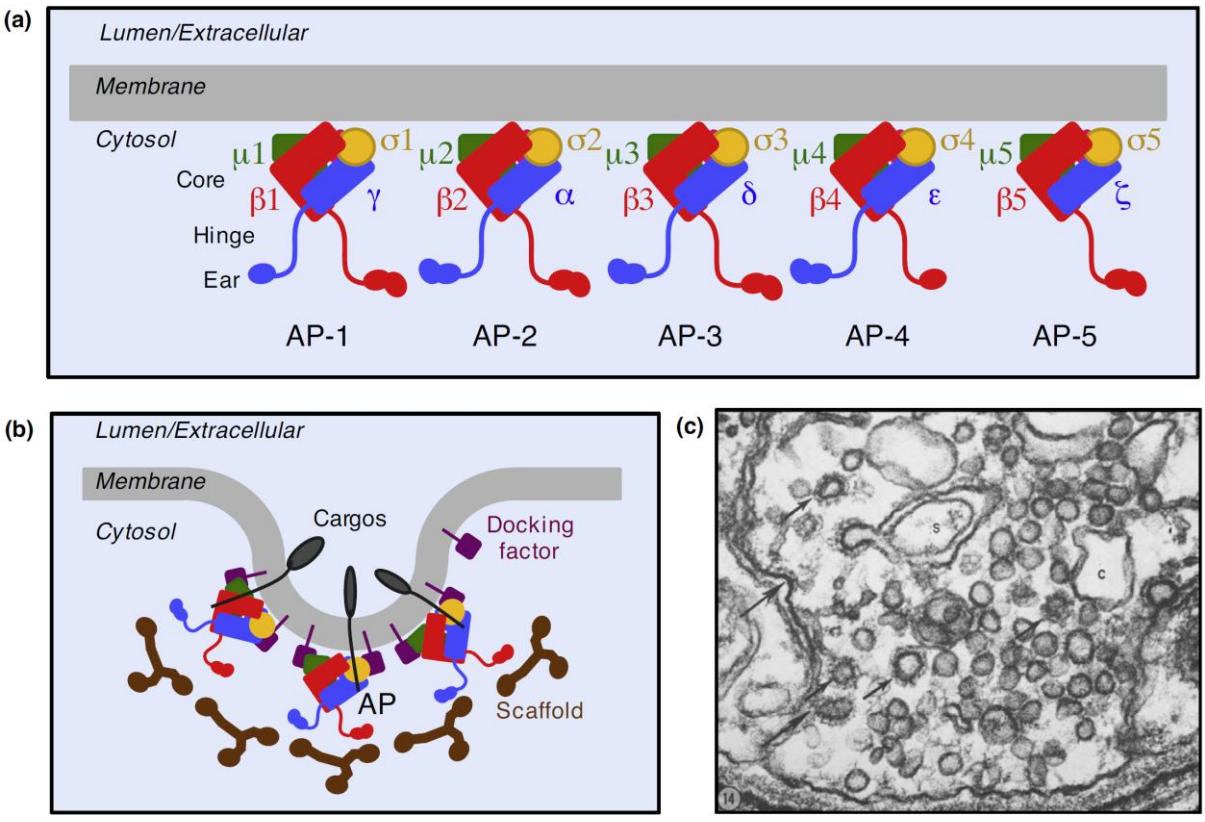

Figure 8. AP complexes.
A) Schematic representation of adaptors (AP-1 to AP-5) showing their subunit composition and organization (core, hinge and ear). **B)** illustration of the architecture of the clathrin/AP-coated vesicle in formation. Adaptors recognise their transmembrane cargo and recruit scaffold proteins. Docking factors are present for vesicle tethering. **C)** clathrin-coated pits and vesicles (arrows) at the presynaptic axon terminal (from (Guardia et al., 2018)).

Adaptors exhibit distinct conformational states based on whether they are inactive or active (Beacham et al., 2019). The cytosolic state or close conformation (inactive) is characterised by the occlusion of the binding sites for tyrosine- and leucine-based sorting motif signals of the cargo proteins, as well as the binding pockets for headgroups of membrane lipids and clathrin-binding boxes, which avoid unspecific interactions with coat and accessory factors, lipids and transmembrane cargoes. In the membrane-bound state, or open conformation (active) when the complex is binding competent, these binding sites are exposed (Ren et al., 2013; Kovtun et al., 2020; Schoppe et al., 2021; Mai et al., 2025).

Multiple subunit isoforms of AP-1, AP-2 and AP-3 complexes have been reported in different organisms (Nakatsu & Ohno, 2003; Mattera et al., 2011; Hirst et al., 2013; Teh et al., 2013; Yamaoka et al., 2013).

AP-1, AP-3, AP-4 and AP-5 have been shown to orchestrate vesicular transport between the trans-Golgi network (TGN) and endosomal and lysosomal compartments, whereas AP-2 is involved in endocytosis (see Figure 8) (Park & Guo, 2014; Paczkowski et al., 2015; Dell'Angelica & Bonifacino, 2019; Sanger et al., 2019).

1.4.2.1 AP-1 complex

AP-1 is located at the TGN or endosomes (Figure 9) and associates with the scaffold protein clathrin to form clathrin-coated vesicles (Robinson, 2004). Specifically, this adaptor interacts with of N-terminal domain (NTD) of the clathrin heavy chain via a consensus clathrin box motif [(L(L,I)(D,E,N)(L,F)(D,E)] located within the hinge region of the γ and β1 subunits (Shih et al., 1995; Doray & Kornfeld, 2001).

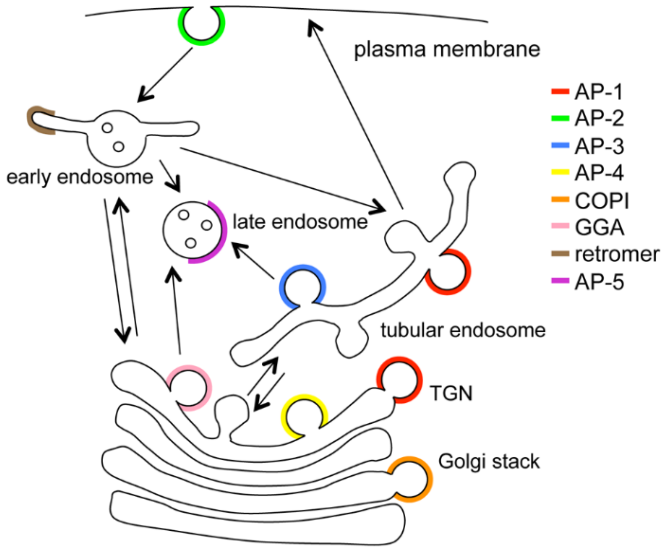

Figure 9. Trafficking pathways mediate by AP complexes.
Each AP complex (AP-1 to AP-5), as well other coat proteins (COP1, GGA and retromer) are represented in different colours and mediates different vesicular trafficking pathways. Black arrows indicate the directionality of the vesicle transport. AP: adaptor protein complex; GGA: Golgi-localised, γ-ear-containing, ADP-ribosylation factor-binding protein; TGN: trans-Golgi network (from (Hirst et al., 2011).

The process of recruitment of AP-1 onto the target membrane is facilitated by the GTPase Arf1 and phosphatidylinositol 4 phosphate (PI(4)P) (Stamnes & Rothman, 1993; Wang et al., 2003). Furthermore, the μ1 and β1 subunits of this complex have been shown to recognise tyrosine- and dileucine-based sorting motifs located in the cytosolic tail of transmembrane protein cargoes (Ohno et al., 1995; Rapoport et al., 1998). Despite the conflicting evidence on the directionality of AP-1-mediated vesicular trafficking (retrieval or anterograde) (Buser et al., 2018, 2022), a recent study (Robinson et al., 2024) demonstrated that AP-1 retrieves cargoes from the post-Golgi compartments (early and recycling endosomes) back to the TGN in mammalian cells. This retrograde transport function of AP-1 has been consistently reported in other mammalian studies (Meyer et al., 2000; Holloway et al., 2013), as well as in yeast (Valdivia et al., 2002; Foote & Nothwehr, 2006). It is noteworthy that this adaptor is also involved in the trafficking of cargo proteins to the basal plasma membrane in polarised cells (Bonifacino, 2014b; Duncan, 2022). In plants, AP-1 has been found at the Golgi-independent TGN (GI-TGN, a transit compartment located between the TGN and plasma membrane involved in the secretory pathway, also known as the free TGN) (Kang et al., 2011; Shimizu et al., 2021). It has been hypothesised that this adaptor may deliver proteins from GI-TGN to the

Golgi-associated TGN (GA-TGN, proximal to the Golgi apparatus and involved in the vacuolar trafficking) (Shimizu et al., 2021; Shimizu & Uemura, 2022).

In alveolates, such as the apicomplexan parasite *Toxoplasma gondii*, AP-1 has been found to colocalise with the trans-Golgi markers SORTLR and GalNAc (Venugopal et al., 2017) at the trans-Golgi compartment, and plays an essential role in the biogenesis of rhoptries and micronemes. Additionally, it has been shown to be involved in cell division (Ngô et al., 2003; Venugopal et al., 2017), exhibiting a phenotype that is similar to that of clathrin when inactivated (Pieperhoff et al., 2013).

1.4.2.2 AP-2 complex

This adaptor interacts with clathrin and coordinates clathrin-mediated endocytosis (CME) from the plasma membrane of eukaryotic cells (Boucrot et al., 2010). The recruitment of this adaptor to the plasma membrane is carried out by binding to phosphatidylinositol 4,5-bisphosphate (PI(4,5)P2), and tyrosine- and dileucine-based sorting motifs present in the cytosolic tail of cargo proteins (Ohno et al., 1995; Gaidarov & Keen, 1999). Interestingly, the CME process is not fully AP-2-dependent, as AP-2-depleted HeLa cells have been observed to internalise cargoes such as epidermal growth factor (EGF) and low-density lipoprotein (LDL) receptors from the plasma membrane in the absence of this adaptor (Motley et al., 2003). This is also supported by studies in yeast (Huang et al., 1999; Yeung et al., 1999) and *Dictyostelium* (Macro et al., 2012).

Conversely, a non-canonical AP-2-dependent endocytosis machinery has been demonstrated to be functional in apicomplexan parasites. AP-2 is associated with the cytostome in *Plasmodium* (Birnbaum et al., 2020; Henrici et al., 2020) and micropore in *Toxoplasma* (Koreny et al., 2023; Wan et al., 2023). However, these highly specialised endocytic mechanisms function in a clathrin-independent manner, suggesting that this scaffold protein is not involved in endocytosis-related roles in these parasites (Birnbaum et al., 2020; Henrici et al., 2020; Koreny et al., 2023; Wan et al., 2023).

1.4.2.3 AP-3 complex

This adaptor is at the trans-Golgi or endosomes and mediated the vesicle transport of transmembrane cargoes to lysosomes and lysosome-related organelles (LRO) in flies and

mammalian cells (Simpson et al., 1996, 1997; Ooi et al., 1997; Peden et al., 2004), and from the TGN to vacuoles in yeast (Cowles et al., 1997; Stepp et al., 1997) and plant (Zwiewka et al., 2011).

The process of AP-3 recruitment onto membrane is also facilitated by the GTPase Arf1 (Ooi et al., 1998). A recent study (Begley et al., 2024) of AP-3 vesicle formation in yeast has described that the δ and μ3 subunits of this adaptor contain two amphipathic helices that are inaccessible when the adaptor is inactive. Upon activation, these amphipathic helices are exposed, thereby suggesting the capability of AP-3 to deform membranes in cooperation with Arf1 (Begley et al., 2024). Despite the absence of C-terminal appendage domains in their δ and β3 subunits, and their inability to interact with coat and accessory proteins, the disordered hinge regions of these large subunits are indispensable for vesicle budding from the TGN and sorting to the lysosome (Leih et al., 2024).

The involvement of clathrin in AP-3-dependent vesicle transport is controversial, with previous studies indicating an interaction with this coat protein (Dell'Angelica et al., 1998; Drake et al., 2000), whereas other studies suggest that no interaction is required in mammalian cells and yeast (Simpson et al., 1996; Zlatic et al., 2013; Schoppe et al., 2020). Furthermore, other AP-3-associated factors are less clearly defined. VPS41 (a homotypic fusion and vacuole protein sorting (HOPS) component) was in earlier work suggested to be a coat of AP-3 vesicles but now is believed to be involved in capturing AP-3 vesicles at the lysosomal destination compartment rather than being a permanent coat component (Rehling et al., 1999; Angers & Merz, 2009; Cabrera et al., 2010; Asensio et al., 2013; Schoppe et al., 2020). Based on these results, AP3 vesicles appear to have distinct requirements for coat or accessory proteins compared to AP-1, AP-2, AP-4 and AP-5.

1.4.2.4 AP-4 complex

This adaptor was the fourth adaptor described as a member of the AP complex family (Dell'Angelica et al., 1999; Hirst et al., 1999). AP-4 is located at the TGN, and it has been suggested to mediate anterograde vesicular transport of transmembrane cargoes (e.g., amyloid precursor protein (APP)) from the TGN to endosomes in HeLa cells (Burgos et al., 2010; Toh et al., 2017), the basolateral sorting in epithelial cells (Simmen et al., 2002) and polarised sorting in neurons (Matsuda et al., 2008). This adaptor also plays a role in the biogenesis of

autophagosomes by trafficking the scramblase autophagy related 9 (ATG9) from the TGN to the endosomes or pre-autophagosomes (Mattera et al., 2017; Davies et al., 2018).

In contrast to AP-1, AP-2 and AP-3 adaptors, AP-4 does not interact with clathrin (Dell'Angelica et al., 1999; Hirst et al., 1999). As described for AP-1 and AP-2, which interact with ENTH-domain containing proteins (see sections 1.4.2.1, 1.4.2.2 and 1.4.3.2), AP-4 is associated with an ENTH and VHS/ENTH-like domain containing protein known as tepsin (Borner et al., 2012), which possesses two phylogenetically conserved motifs in its unstructured C-terminus that bind AP-4 (Mattera et al., 2015). Furthermore, the run and SH3-domain containing proteins 1 (RUSC1) and 2 (RUSC2) (Davies et al., 2018) and the fused toes homolog-Hook-FHIP (FHF) complex (Mattera et al., 2020) have been identified as accessory factors for AP-4.

The μ4 subunit has been shown to preferentially recognise the non-canonical tyrosine-based signal motif (YXXΦE) (Burgos et al., 2010; Ross et al., 2014), as well as non-canonical phenylalanine-based residues (di-aromatic residue (FXF), phenylalanine-based motifs (FGSV) and FR motif (Yap et al., 2003) in cargo proteins.

In plants, AP-4 has been located in specific subdomains of the TGN and is responsible for the vacuolar sorting pathway (Fuji et al., 2016; Müdsam et al., 2018; Shimizu et al., 2021; Yoshinari et al., 2024). In contrast, in model organisms such as yeast, flies and worms, this adaptor has been lost in the course of evolution (Hirst et al., 2013).

1.4.2.5 AP-5 complex

AP-5 is the most recently identified member of the AP complex family (Hirst et al., 2011). This adaptor has been found to be located in late endosomes and lysosomes in HeLa cells (Hirst et al., 2011, 2013) and it is involved in the retrieval of cargoes from late endosomes to the TGN (Hirst et al., 2018). AP-5 does not interact with clathrin or ENTH/ANTH/VHS-like accessory proteins. Instead, AP-5 has been demonstrated to interact with the accessory proteins spatacsin (spastic paraplegia 11, SPG11) and spastizin (spastic paraplegia 15, SPG15), which have been suggested to function as scaffolding proteins (Hirst et al., 2011, 2013). Despite the absence of conserved amino acid residues that recognise tyrosine-based sorting signals in the μ5 subunit in comparison to the μ1-4 subunits, it has been described that the recruitment of the AP-5:SPG11-SPG15 complex to the membrane is dependent on its interaction with PI3P molecules, thereby promoting membrane curvature and autolysosome tubulation (Mai et al., 2025). As

described for AP-4, AP-5 adaptor has been lost in yeast, *Drosophila* and *C. elegans* in the course of evolution (Hirst et al., 2013).

1.4.3 Coat and accessory proteins

During endocytic and secretory trafficking, specific cytosolic factors can be recruited onto donor membranes to shape and drive the formation of cargo-carrying coated vesicles (Bonifacino & Glick, 2004). As mentioned in previous sections, some of these factors include coat proteins and accessory proteins.

Coat proteins are present in many trafficking routes and have been described to facilitate the generation of curvature and budding of vesicles. There are three major classes of vesicle coats: COPII, COPI and clathrin. The first two scaffold proteins, COPII and COPI coat complexes, are involved in the bidirectional trafficking of vesicles between the ER and Golgi cisternae. A third scaffold protein, clathrin, coordinates the post-Golgi trafficking of clathrin-coated vesicles and CME (Robinson, 2015).

1.4.3.1 Clathrin

Clathrin is a scaffold protein that plays a central role in vesicle formation during clathrin-mediated trafficking. Structurally, clathrin is organised as a triskelion composed of three heavy chains (~190 kDa), each associated with a single light chain (~25 kDa), which radiate from a central hub (Kirchhausen & Harrison, 1981; Ungewickell & Branton, 1981). Each heavy chain comprises several distinct regions: an N-terminal β-propeller domain containing seven WD40 repeats, followed by the linker, ankle, distal segment, knee, and proximal segment (Fotin et al., 2004). The light chain binds to the proximal segment of the heavy-chain.

The N-terminal domain (NTD) of the clathrin heavy chain contains four adaptor-binding pockets that are indispensable for the interaction with adaptor proteins such as AP-1, AP-2 and Arrestins (Ter Haar et al., 2000). These binding motif boxes – termed clathrin box, W-box, Arrestin box and Royle box - serve as interaction sites for short linear motifs (SLiMs) located in intrinsically disordered regions of adaptor proteins (Kovtun et al., 2020; Prichard et al., 2021).

During clathrin-mediated vesicular trafficking, clathrin is recruited to donor membranes by interacting with the clathrin box motifs present in the hinge region of the large subunits of AP-

1 and AP-2 complexes. The assembly of clathrin triskelions at the membrane surface leads to the induction of membrane curvature, ultimately leading to the formation of a polyhedral cage-like structure around the budding vesicle (Kirchhausen et al., 2014; Kovtun et al., 2020). In this context, adaptors form the inner layer of the coat vesicles, directly interacting with both membrane, cargo and coat, whereas clathrin forms the outer scaffold.

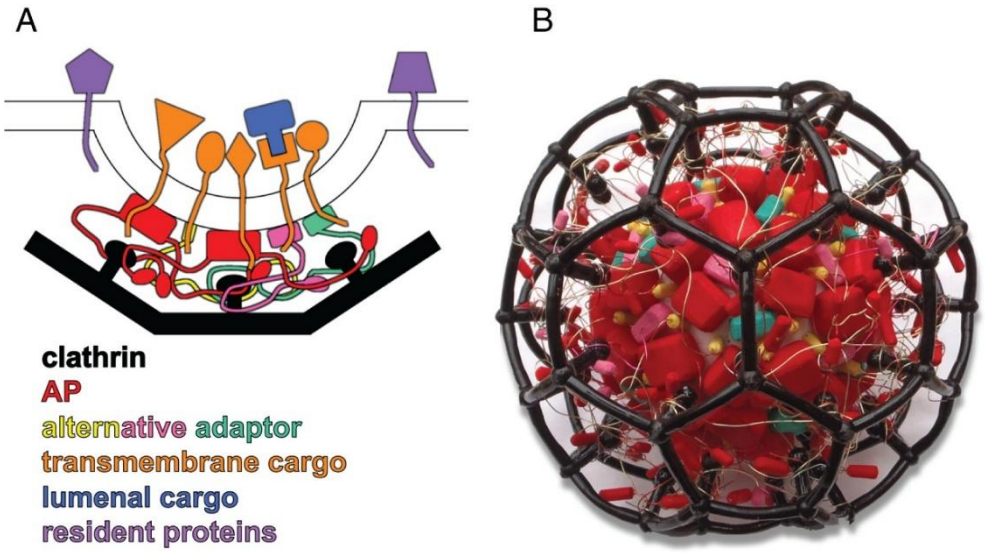

Figure 10. Model of clathrin-coated bud and coated vesicle.
(A) Budding vesicle shows clathrin, adaptors (AP-1 or AP-2), accessory proteins (e.g., ENTH proteins), transmembrane cargoes (e,g., sortilin), lumenal cargoes, and resident transmembrane proteins of the donor membrane. **(B)** A clathrin-coated vesicle. From (Robinson, 2015).

In the presence of sorting signals in the cytosolic tail of transmembrane cargoes, AP-1 is recruited onto the trans-Golgi or endosome membranes, and AP-2 is recruited to the plasma membrane, and AP-1/AP-2-associated clathrin-coated vesicles bud from their respective donor membranes, facilitating protein sorting and trafficking in different trafficking routes within the cell.

1.4.3.2 ENTH/ANTH/VHS-domain containing proteins

In addition to coat proteins, a group of accessory proteins containing Epsin N-terminal homology (ENTH)-, AP180 N-terminal homology (ANTH)- and Vps27, Hrs and STAM (VHS) domains are recruited to both coated and non-coated vesicles (De Craene et al., 2012). These proteins possess the ENTH, ANTH or VHS domain in their N-terminus, which have properties

to bind phospholipids, tubulin and microtubules (ENTH and ANTH), and transmembrane protein cargoes (VHS domain) and are subclassifications of a similar fold (Lohi et al., 2002; Legendre-Guillemin et al., 2004; De Craene et al., 2012; Archuleta et al., 2017). The disordered C-terminus contains binding sites for different components of the vesicular generation machinery, such as clathrin-binding motifs, α-ear binding motifs, γ-ear/GAE-domain binding motifs, NPF motifs and ubiquitin-interacting motifs (Legendre-Guillemin et al., 2004).

In mammalian cells, the ENTH-domain containing protein EpsinR (also known as Clint1 or Enthoprotin) binds to phosphoinositides PI(4)P and PI(5)P and weakly associates with PI(3,4)P2 via the ENTH domain (Hirst et al., 2003; Mills et al., 2003). In contrast, the disordered C-terminus possesses the γ-ear/GAE-domain binding motif, which facilitates the interaction with the γ appendage, as well as the clathrin box (DLF motif), that allows binding to the NTD of clathrin (Kalthoff et al., 2002; Wasiak et al., 2002; Hirst et al., 2003; Mills et al., 2003).

During AP-2-dependent CME, some ENTH and ANTH proteins are required for the coated pit to pinch off to form a coated vesicle. These AP-2-related accessory proteins are known as clathrin associated sorting proteins (CLAPs), and typically possess an N-terminal ENTH or ANTH domain for binding phospholipids, and a C-terminal intrinsically disordered region (IDR), that contains multiple linear binding sites for clathrin (via the clathrin box) and AP-2 (interacting with appendages and hingers of α and β2 subunits). During the initiation of CME, AP-2 interacts with the ANTH protein assembly protein AP180 (in neurons) or its ubiquitous paralog clathrin assembly lymphoid myeloid leukaemia (CALM) (Hao et al., 1999; Naudi-Fabra et al., 2024), as well as the ENTH-domain protein Epsin1 (Hawryluk et al., 2006). As described for AP-2 (see section 1.4.2.2), both AP180/CALM and Epsin1 have been reported to interact with PI(4,5)P2 at the plasma membrane .

Tepsin (tetra-epsin) is an ENTH-domain protein distantly related to other proteins with an N-terminal ENTH-domain (Archuleta et al., 2017). It also contains a VHS/ENTH-like domain downstream of the ENTH domain followed by an unstructured C-terminus (Borner et al., 2012; Archuleta et al., 2017). Tepsin interacts exclusively with the AP-4 complex (Borner et al., 2012). Phylogenetic studies on tepsin have demonstrated that this accessory factor belongs to a monophyletic clade that diverged from epsins early in the evolutionary history of eukaryotes, although its ENTH domain is closely related to that of EpsinR (Hirst et al., 2003; Borner et al., 2012; Archuleta et al., 2017). A structural and functional comparison with other ENTH proteins has shown that tepsin lacks two alpha helices (helix0 and helix8) and a lipid-binding pocket in

its ENTH domain, which is required to bind phospholipids (Archuleta et al., 2017). Similarly, its VHS/ENTH-like domain lacks one alpha helix (helix 8), indicating that this domain does not mediate known VHS functions, such as the recognition of dileucine-based sorting motif in transmembrane cargoes or ubiquitin (Archuleta et al., 2017). Interestingly, both ENTH and VHS/ENTH-like domains are very similar to each other than to most other domains in either family (Archuleta et al., 2017). Furthermore, tepsin has two phylogenetically conserved amino acid motifs described to bind to the appendages of the ε- and β4 subunits of AP-4 in its unstructured C-terminus that both are responsible for the membrane recruitment via the AP-4 complex (Mattera et al., 2015). As reported for the AP-4 complex, tepsin also does not interact with clathrin in agreement with the absence of clathrin box motifs in its sequence (Frazier et al., 2016). In the absence of scaffolding proteins, tepsin was suggested as an accessory or structural component of AP-4 vesicles (Frazier et al., 2016). However, in one instance an interaction between tepsin-like proteins and clathrin has been described: modified transport to the vacuole 1 (MTV1), a distantly related tepsin ortholog in plants, interacts with clathrin through a slightly modified version of the clathrin binding box (LIDTGD) (Sauer et al., 2013).

Recently, tepsin was described to play a functional role in the formation of AP-4 vesicles and the delivery or recycling of ATG9A-positive vesicles (Wallace et al., 2024). It was suggested that AP-4 and tepsin have coevolved in different eukaryotic groups (Borner et al., 2012). However, in other key model systems, such as yeast (*S. cerevisiae*), worms (*C. elegans*) and flies (*D. melanogaster*), both vesicular components were lost (Borner et al., 2012).

1.5 Secretory pathway in malaria parasites

Plasmodium parasites are widely regarded to possess a relatively primitive secretory pathway represented by an unstacked Golgi apparatus (Van Wye et al., 1996; Bannister et al., 2000a). This feature makes it interesting to understand the basis of trafficking. The presence of unique organelles, many of which are specialised for host cell invasion, indicate a need for elaborate sorting capacities.

Plasmodium proteins destined for secretion contain a signal peptide (SP) sequence to enter the ER, where they are trafficked via vesicles to the cis-Golgi (similar to that described in classical models) (Deponte et al., 2012). Upon arrival to the trans-Golgi compartment, some secretory proteins are delivered to invasion-related organelles such as micronemes, rhoptries, dense granules and the IMC (Tonkin et al., 2006a). As these invasion-related organelles and their

precursor compartments are formed mostly from Golgi-derived vesicles, it is expected that vesicular trafficking pathways oriented towards these organelles during schizogony must exist. In addition, specific proteases destined to the FV are transported to the PV lumen or cytostomal structures, where they are subsequently internalised during endocytosis (e.g., dipeptidyl aminopeptidase 1 (DPAP1) and Plasmepsin II) (Klemba, et al., 2004a, b). Proteins destined to the PPM, and possibly also those beyond the confines of the parasite, are likely trafficked via default pathway (Tonkin et al., 2006a). Furthermore, it has been described those proteins destined to the apicoplast can be delivered to this organelle from either the ER or the Golgi (Tonkin et al., 2006b; Heiny et al., 2014).

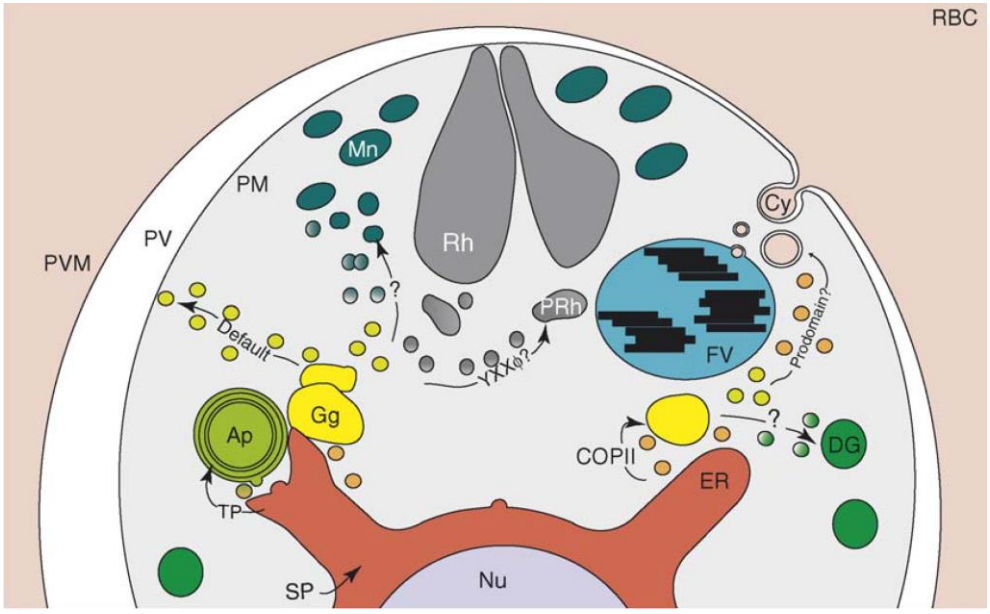

Figure 11. Multiple secretory pathways in *P. falciparum* parasites.
Schematic representation shows multiple routes used for the parasite to sort proteins into vesicles to different destination compartments. Proteins destinated for secretion contain a signal peptide (SP) to enter the secretory pathway. Nu: nucleus; ER: endoplasmic reticulum; TP: transit peptide; Ap: apicoplast; Gg: Golgi compartment; YXXΦ?: tyrosine-based sorting motif; Mn: micronemes; Rh: rhoptries; PRh: Rhoptry precursor; DG; dense granules; FV: food vacuole (containing haemozoin crystals); Cy: cytostome; PM: plasma membrane; PV: parasitophorous vacuole; PVM: PV membrane; RBC: red blood cell (from (Tonkin et al., 2006a)).

1.5.1 Adaptor protein (AP) complexes in malaria parasites

In malaria parasites, the mechanism by which adaptors select, package and sort protein cargoes into vesicles to the specialised and general cellular destinations remains poorly understood, but likely depends on sorting events at the trans-Golgi (Struck et al., 2008; Krai et al., 2014; Hallée

et al., 2018a). Homology searches and phylogenetic analyses were used to identify the AP complexes in *P. falciparum* (Nevin & Dacks, 2009). This study identified the presence of AP-1, AP-2, AP-3 and AP-4 complexes in the genome of the parasite (Nevin & Dacks, 2009), whereas AP-5 was identified as a pseudogene (Hirst et al., 2011). Since then, experimental studies on adaptors have been lacking in this parasite, with the exception of AP-1 and AP-2.

The AP-1 complex was described as exhibiting a perinuclear localisation throughout the erythrocytic cycle of the parasite, and as partially overlapping with the resident rhoptry proteins, RAP1 and Clag3.1, in the schizont stage. However, no functional data on this adaptor was provided (Kaderi Kibria et al., 2015).

In the case of the AP-2 complex, a number of studies have revealed the involvement of this adaptor in Artemisinin resistance (Henriques et al., 2015; Adams et al., 2018; Birnbaum et al., 2020; Henrici et al., 2020). Furthermore, localisation studies showed that AP-2 was confined to a compartment in close proximity to the DV and colocalised with the artemisinin-resistant marker Kelch13 (Birnbaum et al., 2020; Henrici et al., 2020) at the cytostome (Tutor et al., 2023). Fitting with this location, parasites with functionally inactivated AP-2 exhibited a reduction in the haemoglobin uptake into the parasite, indicating an endocytosis defect (Birnbaum et al., 2020). Conditional knock out studies of *ap-2* also detected a defect in organellar integrity during schizont maturation and merozoite biogenesis (Henrici et al., 2020). Surprisingly, colocalisation studies showed that AP-2 did not colocalise with clathrin, indicating that this adaptor is involved in clathrin-independent endocytosis and does not interact with clathrin in *P. falciparum* (Birnbaum et al., 2020; Henrici et al., 2020). These findings were analogous to the observations described for *T. gondii* (Koreny et al., 2023; Wan et al., 2023) and findings suggesting that clathrin is restricted to the trans-Golgi (Pieperhoff et al., 2013). Furthermore, DiQ-BioID of clathrin identified AP-1 and AP-4 subunits as potential interacting partners, but not AP-2 subunits (Birnbaum et al., 2020) (Figure 12), suggesting that clathrin function is restricted to the post-Golgi trafficking and the possibility of an unconventional configuration of vesicle adaptor coats in *P. falciparum* compared to well-studied organisms. In addition, the inactivation of CHC resulted in a merozoite and schizont phenotype that avoided the invasion of new RBCs, but that only partial inactivation of CHC prevented firm conclusions on the phenotype and therefore the role of CHC for the parasite remains unclear (Jonscher, 2018). Of note, this BioID also identified the clathrin light chain (CLC) of the parasite (Birnbaum et al., 2020).

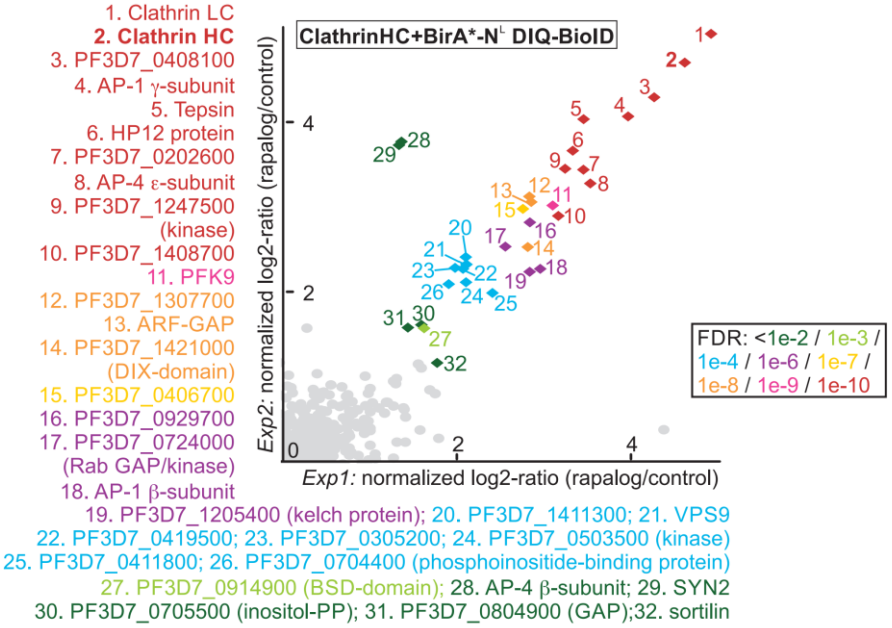

Figure 12. DiQ-BioID of clathrin HC.
DiQ-BioID was performed using parasites with endogenous 2xFKBP-GFP tagged CHC that episomally express the biotinylizer BirA*-FRB-mCherry. DiQ-BioID was induced by addition of rapalog. Biotinylated proteins were listed according to their log2 enrichment, and coloured according to their FDR value. Proxiome of clathrin identified the γ and β1/2 subunits of the AP-1 complex, as well as the ε and β subunits of the AP-4 complex. The AP-4 accessory protein tepsin was also enriched (from (Birnbaum et al., 2020)).

However, both AP-3 and AP-4 have not been studied so far in apicomplexan parasites. In relation to AP-5, database searches indicated that this adaptor was consistently lost for species of the subgenus *Laverania* (e.g., *P. falciparum*, *P. praefalciparum*, *P. reichenowi*, *P. billcollinsi*, *P. blackloki*, *P. adheri* and *P. gaboni*), but not in non-*Laverania* species of the subgenera *Plasmodium* (*P. vivax*, *P. malariae*; *P. ovale* and *P. knowlesi*) and Vinckeia (e.g., *P. berghei*, *P. chabaudi*, *P. vinckei* and *P. yoelii*).

1.5.2 Clathrin and ENTH/VHS-domain proteins in malaria parasites

As in eukaryotic model organisms, the genome of *P. falciparum* parasite contains genes encode clathrin heavy chain (CHC) and clathrin light chain (CLC). Of these, CHC is highly conserved across the eukaryotic kingdom (Jonscher, 2018), whereas CLC showed only a limited sequence similarity to CLC in model organisms (Birnbaum et al., 2020). It has been previously described that CHC is constitutively expressed during the blood stage development of the parasite and

exhibit a perinuclear localisation (Jonscher, 2018). In that dissertation, Jonscher also showed that the conditional inactivation of CHC was critical for parasite development (Jonscher, 2018).

In contrast to model organisms that express a variety of ENTH-domain containing proteins (Legendre-Guillemin et al., 2004; De Craene et al., 2012), malaria parasites possess a sole epsin-like protein known as EpsL (Flemming, 2015; Kibria et al., 2016). This protein was slightly enriched in the Eps15 proxiome and significantly enriched in one out of four replicates in the Kelch13 proxiome (Jonscher, 2018; Birnbaum et al., 2020). Colocalisation studies between EpsL and EPS15 confirmed that EpsL resides or is close to the Kelch13 compartment (Flemming, 2015), where also AP-2 is located (Birnbaum et al., 2020), indicating EpsL may be an endocytosis protein associated with AP-2. In contrast, the epsin ortholog in *T. gondii* has been reported to colocalise and interact with AP-1 at the trans-Golgi (Venugopal et al., 2017).

An ENTH and VHS/ENTH-domain containing protein termed tepsin has been also identified in the parasite (Borner et al., 2012). This protein was highly enriched in the clathrin proxiome and pulldown (Birnbaum et al., 2020; Henrici et al., 2020) (Figure 12). At that time, the enrichment of tepsin in the CHC BioID was considered to be due to the presence of AP-4 in this BioID (Birnbaum et al., 2020). Overall, the configuration of clathrin, the adaptors and the accessory proteins such as ENTH domains in the parasite's vesicular trafficking system remained largely unclear.

1.6 Aims of the thesis

Although the AP complex-mediated post-Golgi vesicular machinery has been described as highly conserved across eukaryotic organisms – facilitating cargo sorting from the TGN to different destination compartments, such as endosomes, lysosomes and the plasma membrane – its configuration has not yet been studied in the human malaria parasite *Plasmodium falciparum*. Notably, the comparably simple secretory pathway combined with the presence of a unique repertoire of specialised organelles, makes malaria parasites a compelling system for investigating vesicle trafficking to the different cellular destinations. The importance of the specialised organelles for the critical process of host cell invasion further raises the interest to understand the vesicular trafficking processes involved in the biogenesis of these organelles and for the faithful sorting of the large number of different kinds of proteins transported to these organelles.

Therefore, the aim of this thesis was to investigate the roles of the post-Golgi adaptors AP-1, AP-3 and AP-4 in vesicle trafficking and protein sorting in malaria blood stage parasites by localising these adaptors in the parasite cell, assessing their function and by identifying the proteins they operate with, to obtain comprehensive overview of the adaptor-mediated vesicle trafficking machinery in these parasites.

2. Materials

2.1 Bacterial and *Plasmodium* strains

Table 1. List of *E. coli* and *P.falciparum* strains

Escherichia coli XL-10 Gold	Tet^r Δ(mcrA)183 Δ(mcrCB-hsdSMR-mrr)173 endA1 supE44 thi-1 recA1 gyrA96 relA1 lac Hte [F' proAB lacIqZΔM15 Tn10 (Tetr) Amy Camr]
Plasmodium falciparum 3D7	Derived from "limiting dilution cloning" of NF54 isolate (MRA-1000) (Walliker et al., 1987)

2.2 Chemicals

Table 2**.** List of chemicals

Name	**Manufacturer**
1,4,-dithiothreitol (DTT)	Biomol, Hamburg
4',6-diamidino-2-phenylindole (DAPI)	Roche, Mannheim
Agar-Aga	BectonDickinson, Heidelberg
Acetic acid	Roth, Karlsruhe
Aceton	Roth, Karlsruhe
Agarose	Invitrogen, Karlsruhe
Albumax II	GIBCO, LIFE TECHNOLOGIES, USA
Ampicillin	Roche, Mannheim

Biotin	Sigma-Aldrich, Steinheim
Blasticidin S (BSD)	LIFE TECHNOLOGIES, USA
Concovalin A (ConA)	Sigma-Aldrich, Steinheim
Desoxynucleotides (dNTPs)	Thermo Scientific, Lithuania
Dihydroethidium (DHE)	Cayman, Ann Arbor, USA
Dulbecco`s Phosphate Buffered Saline (DPBS)	PAN, Biotech, Aidenbach
Dimethyl sulfoxide (DMSO)	SIGMA ALDRICH, USA
DSM1	BEI resources
1,4-dithiothreitol (DTT)	BIOMOL, Hamburg
Ethanol (EtOH)	Roth, Karlsruhe
Ethidium bromide (EtBr)	Sigma-Aldrich, Steinheim
Ethylenediaminetetraacetic acid (EDTA)	BIOMOL, Hamburg
Formaldehyde	Polysciences Warrington/USA
Glutaraldehyde (25%)	Roth, Karlsruhe
Gentamycin	RATIOPHARM, Ulm
G418 disulfate salt	Sigma-Aldrich, Steinheim
Giemsa`s azur, eosin, methylene blue solution	Merck, Darmstadt
Glycerol	Merck, Darmstadt
D-Glucose	MERCK, Darmstadt
Hoechst 33342	Cheomdex, Switzerland
Hydrochloric acid (HCl)	MERCK, Darmstadt

Hypoxanthine	SIGMA ALDRICH, Steinheim
Isopropanol	Roth, Karlsruhe
Magnesium chloride (MgCl2)	Merck, Darmstadt
Methanol	Roth, Karlsruhe
2-[N-(7-nitrobenz-2-oxa-1,3-diazol-4-yl)amino]-2-deoxy-D-glucose (2-NBDG)	INVITROGEN, USA
β-Nicotinamide adenine dinucleotide hydrate (NAD)	SIGMA ALDRICH, Steinheim
Percoll	GE Healthcare, Sweden
Piperazine-N,N'-bis(2-ethanesulphonic acid) (PIPES)	SIGMA ALDRICH, Steinheim
Polyethylene glycol 8000 (PEG-8000)	ROTH, Karlsruhe
Potassium chloride (KCl)	MERCK, Darmstadt
Potassium di-hydrogen phosphate (KH2PO4)	MERCK, Darmstadt
Potassium hydroxide (KOH)	ROTH, Karlsruhe
Protease inhibitor cocktail (“Complete Mini”)	Roche, Mannheim
Rapalog (A/C Heterodimerizer AP21967)	Takara Bio Inc, USA
RPMI (Roswell Park Memorial Institute)-Medium	Applichem, Darmstadt
Saponin	Sigma, Steinheim
Sodium acetate (NaOAc)	Merck, Darmstadt
Sodium hydrogen carbonate ($NaHCO_3$)	Merck, Darmstadt
di-Sodium hydrogen phosphate (Na_2HPO_4)	ROTH, Karlsruhe
Sodium di-hydrogen phosphate (NaH_2PO_4)	ROTH, Karlsruhe

Sodium hydroxide (NaOH)	Merck, Darmstadt
Sodium chloride (NaCl)	GERBU, Gaiberg
Sodium dodecyl sulfate (SDS)	Applichem, Darmstadt
Sorbitol	SIGMA ALDRICH, Steinheim
Triton X-100	Biomol, Hamburg
Tris base	ROTH, Karlsruhe
Tris-EDTA (TE)	INVITROGEN, Karlsruhe
Water for molecular biology (Ampuwa®)	Fresenius Kabi Bad, Homburg
WR99210 (WR)	Jacobus Pharmaceuticals Washington, USA
OsO_4	Electron Microscopy Sciences
Uranyl Acetate	Agar Scientific LTD
Yeast extract	SIGMA ALDRICH, Steinheim
6x DNA-loading dye purple	NEB, Ipswich/USA
10x Fire-polymerase buffer	SOLIS BIODYNE
10x Cutsmart buffer	NEB, Ipswich/USA

2.3 Kits

Table 3. List of kits

Name	**Manufacturer**
Monarch Genomic DNA Purification Kit	NEB, Ipswich, USA

NucleoSpin, Gel and PCR clean-up	Macherey-Nagel, Düren
NucleoSpin, Plasmid	Macherey-Nagel, Düren
PureYield™ Plasmid Midiprep System	Promega, Walldorfm Germany
QIAamp DNA Mini Kit	Qiagen, Hilden
QIAGEN Plasmid Midi Kit	Qiagen, Hilden

2.4 DNA and protein ladders

Table 4. List of DNA and protein ladders

Name	**Manufacturer**
GeneRuler™1000 bp ladder	Thermo Fisher, Waltham MA (USA)

2.5 Solution, buffer and media for microbiological culture

Table 5. Table of solutions, buffers and media for microbiological culture

Name	**Composition**
Ampicillin stock solution	100 mg/ml in 70% ethanol
Glycerol freezing solution	50% (v/v) glycerol
	in 1x LB medium
10x Luria-Bertani (LB) medium stock solution	10% NaCl
	5% peptone

	10% yeast extract
	in dH_2O, autoclaved
LB medium working solution	1% (w/v) NaCl
	0.5% (w/v) peptone
	1% (w/v) yeast extract
	in dH_2O
LB-Ampicilin working solution	0.1% ampicillin
	in 1x LB medium working solution
LB agar plate solution	1.5% Agar-agar
	in 1x LB medium
Transformation buffer for ultra-competent cells	10 mM PIPES
	15 mM $CaCl_2$
	250 mM KCl
	pH 6.7 (with 10 N KOH)
	55 mM $MnCl_2$
SOB medium for ultra-competent cells	0.05% NaCl (w/v)

	2% tryptone (w/v)
	0.5% yeast extract (w/v)
	deionized H_2O, to 950 ml
	1% 250 mM KCl (v/v)
	pH 7.0 (with 5 N NaOH)
	ad dH_2O to 1000 ml, autoclaved
	0.5% 2 M $MgCl_2$ (v/v) (sterile)

2.6 Solutions and buffers for molecular biology analyses

2.6.1 Gel electrophoresis

Table 6. Table of gel electrophoresis

Name	**Composition**
50x TAE buffer	2 M Tris base
	1 M pure acetic acid
	50 mM EDTA
	pH 8.5
	in dH_2O
1x TAE buffer	40 mM Tris base
	20 mM pure acetic acid

	1 mM EDTA
	pH 8.5
	in dH_2O
6x Loading buffer	40% Glycerol (v/v)
	2.5% (w/v) Xylene cyanol
	2.5% (w/v) Bromophenol blue
	in dH_2O

2.6.2 DNA precipitation

Table 7**.** Table of DNA precipitation

Name	**Composition**
Sodium acetate	3 M NaAc, pH 5.2
Ethanol (EtOH)	100% and 70%
Tris-EDTA (TE) buffer	10 mM Tris-HCl, pH 8.0
	1 mM EDTA, pH 8.0

2.6.3 Gibson assembly

Table 8. Table of Gibson assembly

Name	**Composition**
5x isothermal reaction buffer (6 ml)	3 ml 1 M Tris-HCl, pH 7.5
	150 µl 2 M $MgCl_2$
	60 µl each of 100 mM dGTP/dATP/dTTP/dCTP
	300 µl 1 M DTT
	1.5 g PEG-8000
	300 µl 100 nM NAD
	ad 6 ml dH_2O
Assembly master mixture (1.2 ml)	320 µl 5x isothermal reaction buffer
	0.64 µl 10U/µl T5 exonuclease
	20 µl 2U/µl Phusion DNA polymerase
	160 µl 40U/µl Taq DNA ligase
	ad 1.2 ml dH_2O

2.7 Media and solutions for cell biology experiments

2.7.1 *P. falciparum* in vitro culture

Table 9. Table of *P. falciparum* in vitro culture

Name	**Composition**
RPMI complete medium	1.587% (w/v) RPMI 1640
	12 mM $NaHCO_3$
	6 mM D-Glucose
	0.5% (v/v) Albumax II
	0.2 mM Hypoxanthine
	0.4 mM Gentamycin
	pH 7.2
	in dH_2O, sterile filtered
10% Giemsa solution	10 ml Giemsa’s azure, eosin
	methylene blue solution
	90 ml dH_2O
Transfection buffer	90 mM $NaPO_4$
	5 mM KCl
	0.15 mM $CaCl_2$

	50 mM HEPES
	pH 7.6, sterile filtered
Malaria freezing solution (MFS)	4.2% D-sorbitol
	0.9% NaCl
	28% Glycerol
	in dH2O, sterile filtered
Malaria thawing solution (MTS)	3.5% NaCl
	in dH_2O, sterile filtered
WR99210 stock solution	20 mM WR99210
	in 1 ml DMSO, sterile filtered
WR99210 working solution	1:1000 dilution of stock solution in RPMI complete medium, sterile filtered
G418 working solution	50 mg/ml in RPMI complete medium, sterile filtered
DHE stock solution (10x)	5 mg DHE

	in 1 ml DMSO
DHE working solution (1x)	0.5 mg DHE
	in 1 ml DMSO
DSM1 stock solution (50x)	187,5 mM DSM1
	in DMSO
DSM1 working solution	100 µl DSM1 stock solution
	ad 5 ml in 95% DMSO / 5% 1xPBS solution
Blasticidin S (BSD) working solution	5 mg/ml BSD in RPMI complete medium, sterile filtered
FACS stop solution	0.5 µl Glutaraldehyde (25%)
	in 40 ml RPMI complete medium
Hoechst 33342 stock solution (10x)	4.5 mg Hoechst 333442
	in 1 ml DMSO

Hoechst33342 working solution (1x)	0.45 mg Hoechst33342
	in 1 ml DMSO
Rapalog (AP21967) stock solution	500 mM in ethanol
Rapalog working solution	1:20 dilution of stock solution in RPMI complete medium, sterile filtered
Human red blood cells	sterile concentrate, blood group 0+,
	Blood bank, Universitäts-klinikum Eppendorf (UKE), Hamburg

2.7.2 Solutions for cell biology and biochemical assays

Table 10. Table of solutions for cell biology and biochemical assays

Name	**Composition**
Parasite lysis buffer	4% SDS
	0.5% Triton X-100
	0.5x PBS
	in H_2O
Percoll stock solution	90% (v/v) Percoll
	10% (v/v) 10x PBS

80% Percoll solution	8.9 ml 90% Percoll stock solution
	1.1 ml RPMI complete medium
	0.8 g Sorbitol
	sterile filtered
60% Percoll solution	6.7 ml 90% Percoll stock solution
	3.3 ml RPMI complete medium
	0.8 g Sorbitol
	sterile filtered
40% Percoll solution	4.4 ml 90% Percoll stock solution
	5.6 ml RPMI complete medium,
	0.8 g Sorbitol
	sterile filtered
Saponin solution	Saponin 0.03 % (w/v) in DPBS

2.8 Enzymes and antibodies

2.8.1 Polymerases

Table 11**.** Table of polymerases

Polymerase	**Manufacturer**
FirePol. DNA Polymerase [5 U/µl]	Solis Biodyne, Taipei, Taiwan
KAPA HiFi HotStart Polymerase [5 U/µl]	Roche, Mannheim

2.8.2 Enzymes

Table 12. Table of enzymes

Enzyme	**Manufacturer**
AgeI-HF®	NEB, Ipswich, USA
AvrII	NEB, Ipswich, USA
BamHI-HF®	NEB, Ipswich, USA
BclI-HF®	NEB, Ipswich, USA
BglI	NEB, Ipswich, USA
BslI	NEB, Ipswich, USA
DpnI	NEB, Ipswich, USA
EaeI	NEB, Ipswich, USA
HindIII-HF®	NEB, Ipswich, USA
KpnI-HF®	NEB, Ipswich, USA

MfeI-HF®	NEB, Ipswich, USA
MluI-HF®	NEB, Ipswich, USA
NaeI	NEB, Ipswich, USA
NotI-HF®	NEB, Ipswich, USA
PmeI	NEB, Ipswich, USA
PstI-HF®	NEB, Ipswich, USA
Sacl-HF®	NEB, Ipswich, USA
SalI-HF®	NEB, Ipswich, USA
SmaI	NEB, Ipswich, USA
SpeI-HF®	NEB, Ipswich, USA
XbaI	NEB, Ipswich, USA
XhoI	NEB, Ipswich, USA
XmaI	NEB, Ipswich, USA

2.8.3 Primary antibodies

Table 13. Table of primary antibodies

Antigen	**Organism**	**IFA dilution**	**Source**
GFP	mouse	1:500	ROCHE, Mannheim
HA	rat	1:500	ROCHE, Mannheim
RFP	rat	1:500	CHROMOTEK, Germany

2.8.4 Secondary antibodies

Table 14. Table of secondary antibodies

Antigen	Conjugate	Organism	IFA dilution	Source
mouse	Alexa 488	goat	1:2000	LIFE TECHNOL-OGIES, USA
mouse	Alexa 594	goat	1:2000	LIFE TECHNOL-OGIES, USA
Rabbit	Alexa 488	donkey	1:2000	INVITROGEN, Molecular probes Leiden
Rabbit	Alexa 594	donkey	1:2000	INVITROGEN, Molecular probes Leiden
Rabbit	Alexa 647	goat	1:2000	Life Technologies Cat. No. A-21244
rat	Alexa 594	goat	1:2000	INVITROGEN, Molecular probes Leiden

2.8.5 Streptavidin beads

Table 15. Table of streptavidin beads

Name	Antigen	Conjugate	Antibody	Source
GFP-Trap® Agarose	GFP	coupled agarose beads	GFP Nanobody/ VHH	Chromotek, Munich

2.9 Oligonucleotides and plasmids

2.9.1 Oligonucleotides

All oligonucleotides used in this thesis were synthetised by Sigma-Aldrich (Steinheim) (0.025 µmol, desalt, in TE, 100 µM). The stock solution was diluted 1:10 in Ampuwa® H_2O before its use for PCRs. The primer sequences are shown in Appendix 1.

2.9.2 General plasmids

Table 16. Table of general plasmids

General plasmids	**Source**
pSLI-2xFKBP-GFP-2xFKBP-T2A-Neo	(Birnbaum et al., 2017)
pSLI2-mSca-T2A-DHODH	(Cronshagen et al., 2024)
pARL_nmd3_1xNLS-FRB-mCherry-T2A-yDHODH	(Birnbaum et al., 2017)
pARL_*crt*-P40-mScarlet_*nmd3*-NLS-FRB-T2A-yDHODH	(Sabitzki et al., 2024)

2.10 Software, bioinformatic tools and data bases

2.10.1 Software

Table 17. Table of software

Software	**source/brand/distributor**
A plasmid Editor (ApE)	(http://biologylabs.utah.edu/ jorgensen/wayned/ape/)
Axio Vision 40 v4.7.0.0	Zeiss, Jena
Corel Draw 2021	Corel Corporation, Ottawa
Corel Photo Paint 2021	Corel Corporation, Ottawa
GraphPad Prism 8.0	GraphPad Software, La Jolla, USA
ImageJ 64 1.43u	Open Source (http://rsbweb.nih.gov/ij/)
ImageLab (version 5.2)	
Microsoft Office 2010	Microsoft Corporations, Redmond, USA

SnapGene	www.snapgene.com

2.10.2 Database and online sources

Table 18. Table of database and online sources

Program	**Address (URL)**
BLAST	http://blast.ncbi.nlm.nih.gov
ExPASy	http://myhits.isb-sib.ch
PlasmoDB	http://plasmodb.org
ToxoDB	https://toxodb.org/
FungiDB	https://fungidb.org/
Tair	https://www.arabidopsis.org/
HostDB	https://hostdb.org/
PubMed	http://www.ncbi.nlm.nih.gov
Clustal Omega	https://www.ebi.ac.uk/Tools/msa/clustalo/
Python3 (version 3.11.4)	
InterPro	https://www.ebi.ac.uk/interpro/
HHPred	https://toolkit.tuebingen.mpg.de/tools/hhpred
TMHMMv2.0	(https://services.healthtech.dtu.dk/services/TMHMM-2.0/)

2.11 Technical devices

Table 19. Table od technical devices

Device	**Article description**	**Manufacturer**
Agarose gel chamber	Sub Cell GT basic	Bio-Rad, München
Analytical Balance	870	Kern
Laboratory balance	Atilon	ACCULAB SARTORIUS, Göttingen
Centrifuge	Megafuge 1.0R	HERAUES, Hanover
Table centrifuge	Eppendorf 5415 D	Eppendorf, Hamburg
Cooling Unit Centrifuge	Rotor JA-12 Avanti J-26S XP Rotor JA-14	Beckman Coulter, Krefeld
Microcentrifuge	Butterfly	THERMO SCIENTIFIC, Schwerte
Electrophoresis chamber	Mini Protean 67s	Bio-Rad, München
Electroporator	Nucleofector II AAD-1001N	Amaxa Biosystems, Germany
Electroporator	Gene Pulser XCell	BIO-RAD, Munich
Flow cytometry cell analyser	LSR II	BECTON DICKINSON, Franklin Lakes/USA
Gel holder cassette	Mini Protean Tetra	Bio-Rad, München
Ice machine	EF 156 easy fit	Scotsman, Vernon Hills, USA

Bacterial incubator	Thermo function line	Heraeus, Hannover
Incubator for *P. falciparum* cell culture	Heratherm IGS400	Thermo Scientific, Langenselbold
Shaking incubator	MaxQ4000	Barnstead, Iowa, USA
Shaking incubator	Innova 40	NEW BRUNSWICK SCIENTIFIC, Edison/USA
Light microscope	Axio Lab A1	Zeiss, Jena
Fluorescence microscope	Axio Lab A1	Zeiss, Jena
Microscope digital camera	Orca C4742-95	HAMAMATSU PHOTONICS K. K., Japan
Microwave	Micro 750W	Whirlpool, China
Microwave	900 & Grill MW7869	SEVERIN, Sundern
Molecular imager	ChemiDocTM XRS+	BIO-RAD, Munich
Laboratory scale	Atilon	Acculab Sartorius, Göttingen
PCR Mastercycler	epgradient	Eppendorf, Hamburg
PCR Thermal cycler	C1000 Touch	BIO-RAD, Munich
pH-meter	SevenEasy	METTLER-TOLEDO, Giessen
Pipettes	0.2-2, 1-10, 100, 200, 1000 µl	Gilson, Middleton, USA
Pipettor	Pipetboy acu	IBS, USA
Pipettor	Cell Mate II”	THERMO SCIENTIFIC, Langenselbold

Power Supply	Power Source 300 V	VWR, Taiwan
Power Supply	E835 300 V	CONSORT, Belgium
Power Supply	EV231	CONSORT, Belgium
Roller Mixer	STR6	STUART, Staffordshire/UK
Roller Mixer	SU1400	SUN LAB, Germany
Sterile laminar flow bench	Sterilguard III Advance	Baker Company, Stanford, USA
Sterile laminar flow bench	Safe 2020”	THERMO SCIENTIFIC, Pinneberg
Thermoblock	Thermomixer compact	Eppendorf, Hamburg
Vacuum pump	BVC Control	Vacuubrand, Germany
Vortexer	Genie 2	Scientific Industries, USA
Waterbath	1083	GFL, Burgwedel

2.12 Labware and disposables

Table 20. Table of labware and disposables

Product	**Specification**	**Manufacturer**
Chromatography paper		Whatman, UK
Conical falcon tubes	15 ml, 50 ml	Sarstedt, Nümbrecht
Cryotubes	1.6 ml	Sarstedt, Nümbrecht
Culture bottles	50 ml	Sarstedt, Nümbrecht
Disposable pipette tips	1-10/20-200/100-1000 µl	Sarstedt, Nümbrecht

Eppendorf reaction tubes	1.5 ml/2 ml	Sarstedt, Nümbrecht/ Eppendorf, Hamburg
Flow cytometry tubes	55.1579: 5 ml, 75x 12 mm	Sarstedt, Nümbrecht/
Glass beads	2.85 – 3.45 mm	Roth, Karlsruhe
Glass cover slips	2.85 – 3.45 mm	Roth, Karlsruhe
Glass cover slips	24 x 65 mm thickness, 0.13-0.16 mm	R. Langenbrinck, Emmendingen
Glass slides		Engelbrecht, Edermünde
Gloves, latex EcoShield		Kimtech Science
Gloves, purple nitrile		BSN medical GmbH
Gloves, blue nitrile	35PLUS	BINGOLD, Hamburg
Leukosilk tape		BSN MEDICAL GmbH
Nitrocellulose blotting membrane	Amersham 0.45 µm	GE Healthcare, Germany
One way cannula		Braun, Melsungen
One way injection		Braun, Melsungen
Parafilm		Bemis, USA
Pasteur pipette		Brand, Wertheim
PCR reaction tubes	Multiply-µStrip Pro 8-Strip	Sarstedt, Nümbrecht
Pipette tips	1-10, 20-200, 100-1000 µl	SARSTEDT, Nümbrecht & EPPENDORF, Hamburg

Filter tips	1-10, 20-200, 100-1000 µl	SARSTEDT, Nümbrecht
Plastic pipettes	5 ml, 10 ml, 25 ml	SARSTEDT, Nümbrecht
Petri dishes	2 ml, 10x35 mm	THERMO SCIENTIFIC, Denmark
Petri dishes	5 ml, 15x60 mm; 10 ml, 14x90 mm	Sarstedt, Nümbrecht
reaction tubes	1.5 ml, 2 ml	SARSTEDT, Nümbrecht & EPPENDORF, Hamburg
Scalpel		BRAUN, Melsungen
Sterile filter	0.22 µm	SARSTEDT, Nümbrecht
TC-6-well plates	2-4 ml, 85.2x 127.8 mm	SARSTEDT, Nümbrecht
TC-12-well plates	2-4 ml, 85.2x 127.8 mm	SARSTEDT, Nümbrecht
Transfection cuvettes	0.2 cm	Bio-Rad, München

3. Methods

3.1 Microbiological methods

3.1.1 Preparation of competent *E. coli* cells

The preparation of the competent *E. coli* XL10-Gold cells was performed as described (Inoue et al., 1990). In order to perform this procedure, a scraping of glycerol stock of XL10-Gold *E. coli* bacteria (stored at -80°C) was inoculated into a 50 ml Falcon tube (lid not completely closed) containing 10 ml of LB medium supplemented with 34 µg/ml of chloramphenicol and was incubated while shaking at 37°C for overnight. On the following day, 200 ml of pre-warmed LB medium was inoculated with 5 ml of the overnight-grown bacteria culture and incubated at 18°C with shaking until the optical density (OD600) of the bacteria suspension reached between 0.5 and 0.6, indicating the proper growth density for harvesting.

The culture was then divided into four 50 Falcon tubes and rapidly chilled on ice for 10 minutes, followed by centrifugation at 2.600 g for 20 minutes at 4°C. The supernatant was discarded and the pelleted bacteria were gently resuspended in 20 ml of ice-cold TFBI solution, and incubated on ice for 10 minutes. After the incubation period, the suspension was centrifugated again at 2.600 g for 20 minutes at 4°C. The supernatant was discarded and the resultant pellet was resuspended in 4 ml of calcium chloride-containing solution (TBFII buffer). The resuspended pellet was gently mixed with 1.2 ml of DSMO, after which it was distributed in ~100 µl aliquots. These aliquots were immediately frozen in a mixture of dry ice or liquid nitrogen containing 100% ethanol. Subsequently, the frozen aliquots were stored at -80°C until they were required for the bacterial transformation process (see section 3.1.2).

3.1.2 Transformation of competent *E. coli* cells

An aliquot of 100 µl of competent *E. coli* cells was thawed on ice and mixed with 10 µl of plasmid that had been obtained by Gibson ligation (see section 3.2.4) and then incubated on ice for 10 minutes. Subsequent to the incubation period, the bacteria were subjected to heat shock

at 42°C for 30 seconds, and immediately placed back in ice for one minute. The suspension of transformed bacteria was centrifuged at 8000 x g for 2 minutes and half volume of the supernatant was discarded while the remanent volume was used to resuspend the pellet and the bacteria were plated onto a LB agar plate, which contained ampicillin as a drug selection marker. The plates were then incubated at 37°C for up to 20 hours.

3.1.3 Cultivation and storage of transformed *E. coli* cells

Bacteria that successfully carried the plasmid DNA (section 3.2.1) were cultured in LB liquid medium containing ampicillin and incubated while shaking at 37°C overnight. For Mini Pre (section 3.2.5), 2 ml of bacterial culture was incubated in a thermoblock, whereas for Midi Pre (section 3.2.5), 200 ml bacterial culture was incubated in an incubator. For long-term storage, an aliquot of bacteria containing the plasmid was mixed with the glycerol freezing suspension and stored at -80°C.

3.2 Molecular biology methods

3.2.1 Polymerase chain reaction (PCR)

The polymerase chain reaction (PCR) is a powerful *in vitro* molecular technique that is utilised for the amplification of specific DNA fragments (Mullis et al., 1986). The basis of this technique is the use of a thermostable DNA polymerase, which facilitates the amplification of a specific DNA fragment target at elevated temperatures (Mullis et al., 1986). To carry out this, it is necessary to use a pair of primers (forward and reverse) and a DNA template (e.g., parasite or plasmid DNA). In order to achieve this, the PCR reaction is categorised into different steps – denaturation, annealing and extension – to produce multiple copies of the desired DNA fragment. Firstly, the denaturation is required to separate the double-stranded DNA into single-stranded DNA by heating at up to 95°C. Subsequently, the annealing facilitates the binding of forward and reverse primers to specific regions of the single-stranded DNA template by complementarity, under a decreased temperature condition (48-68°C). Finally, the extension consists on the binding of the polymerase to the primers, which is followed by the elongation of the double-stranded DNA at 72°C. These steps are repeated in a serial sequence of 30 cycles to generate sufficient PCR product. Depending on the specific parameters of the PCR, the

annealing temperature of the primers was set within a range of 48 to 68°C, and the extension time was estimated on the basis of the size of the fragments to be amplified, considering that DNA polymerase extends the size of the PCR product by 1000 bp per minute. KAPA HiFi HotStart DNA Polymerase (Roche) was employed for the amplification of inserts for cloning (Tables 1 and 2). Conversely, Firepol® DNA Polymerase (Solis Biodyne) was utilised to amplify fragments for colony screening and integration check (Tables 3 and 4). The PCR reactions were performed using gDNA and cDNA from *P. falciparum* 3D7 parasites as well as plasmid DNA as template.

Table 21. PCR mix for KAPA HiFi HotStart DNA Polymerase (50 µl batch)

Reagent	**Volume [µl]**
Ampuwa® H_2O	33.5
5x Hifi Buffer	10
dNTPs (2 mM)	1.5
Forward primer (10 mM)	1.5
Reverse primer (10 mM)	1.5
KAPA HiFi HotStart DNA Polymerase	1
DNA template	1

Table 22. Conditions for cloning PCR

Steps	**Temperature [°C] for KAPA PCRs**	**Temperature range [°C] for gradient PCRs**	**Duration**	**Cycles**
Initial denaturation	95	95	2 minutes	1
Denaturation	95	95	20 seconds	

Annealing	52-68	48-68	20 seconds	30
Extension	70	70	1-2 minutes/kb	
Final extension	70	70	10 minutes	1

Table 23. PCR mix for Firepol® DNA Polymerase (10 µl batch)

Reagent	**Volume [µl]**
Ampuwa® H_2O	6.4
dNTPs (2 mM)	1
$MgCl_2$ (25 mM)	1
Forward primer (10 mM)	0.2
Reverse primer (10 mM)	0.2
10x Firepol Buffer	1
Firepol® DNA Polymerase	0.1
DNA template	0.1

Table 24. Conditions for screening PCR (colony and integration check)

Step	**Temperature [°C] for Firepol PCRs**	**Duration**	**Cycles**
Initial denaturation	95	3 minutes	1
Denaturation	95	40 seconds	
Annealing	48	1.5 minutes	30

Extension	61.5	1-2 minutes/kb	
Pause	10	∞	1

3.2.2 Restriction endonuclease digestion of DNA

The digestion of PCR products and plasmid vectors was carried out using a set of restriction enzymes from NEB (section 2.8.2) and its restriction buffer, CutSmart®, as described in the manufacturer's protocol. For the digestion of PCR products, the enzyme DpnI was used to cut the methylated DNA in vectors (Table 5). For the digestion of plasmid vectors, a pair of endonucleases were used to remove the original insert in the plasmid (Table 5). In both cases, the endonucleases were incubated at 37°C for 1-3 hours.

Table 25. Restriction digestion of DNA (100 µl)

Reagent	**PCR product digestion [µl]**	**Plasmid digestion [µl]**
Ampuwa® H_2O	59	85
10x CutSmart® Buffer	10	10
Endonuclease 1	1	1
Endonuclease 2	-	1
PCR product /Plasmid DNA	30	3

3.2.3 Purification of digested PCR products and plasmids

The purification of PCR-amplified DNA products (including those that were previously separated using agarose gel electrophoresis) and digested plasmid vectors was performed using the NucleoSpin® Gel and PCR Clean-up kit (Macherey-Nagel) in accordance with the manufacturer's protocol. The procedure is comprised of four sequential steps: clearance of lysate, binding, washing and elution. A column containing a silica membrane is used for the capture of negatively-charged double-stranded DNA, while reagents such as oligonucleotides,

salt-containing buffers, restriction enzymes and polymerases are removed. Finally, the DNA was eluted in TE-Buffer (30-40 µl).

3.2.4 Gibson assembly and transformation

The Gibson assembly method consists on the ligation of the digested plasmid vector and PCR products by the complementary sequences in the sticky ends of the inserts. The overlap between the inserts and the vector backbone is typically ~20-40bp (Gibson et al., 2009). This method facilitates the ligation in one-step isothermal DNA assembly of up to six different inserts. The Gibson ligation was performed by incubating the mixture at 50°C for 60 minutes. Subsequently, the ligated plasmid was used for transformation into competent XL10-gold *E. coli* cells by heat shock at 42°C for 30 seconds (section 3.1.2). Next, the transformed bacteria were transferred to a LB plate and incubated overnight at 37°C.

Table 26. Gibson assembly mix (10 µl)

Reagent	**Volume [µl]**
Assembly master mixture	8
Plasmid DNA	0.5-1
PCR product (insert)	1-1.5
Ampuwa® H_2O	Ad 10

3.2.5 Plasmid isolation

For Mini Preparation (Plasmid Mini Pre), the transformed *E. coli* clones, confirmed previously by screening PCR (section 3.2.1), were incubated in 2 ml LB medium at 37°C for ~16 hours while shaking. The plasmid was subsequently isolated by using the NucleoSpin Plasmid kit (Macherey-Nagel) following the instructions provided by the manufacturer. The plasmid was then eluted with 30 µl of Elution Buffer.

For Midi Preparation (Plasmid Midi Pre), clones that were confirmed by sequencing (section 3.2.7) were incubated in 200 ml LB medium at 37°C for ~20 hours while shaking. The plasmid was extracted using the QIAGEN Plasmid Midi Kit (QIAGEN) or PureYield™ Plasmid Midiprep (Promega) according to the manufacturer's protocol. The plasmid was then eluted with 200-600 µl of Elution Buffer (e.g., TE Buffer, dH_2O).

3.2.6 Nucleic acid quantification

A photometric analysis was performed to determine the DNA concentration of both Midi Pre and Midi Pre plasmid eluates using Nano Drop 2000c spectrophotometer (Thermo Scientific), with a ratio of absorbance at 260nm and 280nm (260/280).

3.2.7 Sequencing of plasmid DNA

Sanger sequencing was performed in order to examine possible mutations in the ligated plasmid DNA. The sample, containing 200-800ng of plasmid DNA and 3 µl of 10 mM sequencing primer (forward or reverse), was filled up to a final volume of 15 µl with Ampuwa® H_2O and sent to Seqlab (Microsynth Seqlab GmbH) for sequencing. The resulting sequencing was analysed with ApE – A Plasmid Editor or SnapGene, and the sequences subsequently compared using Clustal Omega.

3.2.8 DNA precipitation

For the precipitation of DNA, a concentration of 50-100 µg of plasmid DNA was mixed with 1/10 volume of 3M sodium acetate (pH 5.0) and three volumes of 100% ethanol. The suspension was centrifuged at maximum speed for 10 minutes at 4°C, followed by a disinfection step with 70-100% ethanol and subsequent centrifugation at maximum speed for 2 minutes. The plasmid DNA pellet was air dried and resuspended in 10 µl of TE buffer until its use. The disinfection and air-drying steps were performed under aseptic conditions (manipulating it in a culture hood).

3.2.9 Genomic DNA isolation

Genomic DNA isolation was used to obtain gDNA of 3D7 parasites for the purpose of amplifying a marker of interest template, as well as to confirm the correct integration of the plasmid into the targeted genomic locus of the parasite (section 3.2.1). To this end, 200 µl of blood from a parasite culture with at least 3 to 5% asynchronous parasitemia was used for the isolation of gDNA by using the QIAamp DNA Mini Kit following the manufacturer's protocol.

3.2.10 Agarose gel electrophoresis

Agarose gel electrophoresis was utilised to separate DNA fragments (PCR products and digested vectors) based on their size. Due to DNA is negatively charged by phosphate groups, it can be separated in an electric field, resulting in its migration towards the anode (+). To do this, 1% agarose gels were prepared by dissolving agarose powder (Invitrogen) in 1x TAE buffer, with boiling in a microwave. Once dissolved the agarose, 1 µg/ml ethidium bromide was added, and the suspension was transferred to a plastic carrier. After 30 minutes, the agarose had undergone solidification. The gel was then placed into a gel chamber that had been filled with 1x TAE buffer. The sample was mixed with 6x loading buffer and loaded into the wells next to the 1 kb DNA ladder (Fermentas). The gel was run a voltage of 150V for 30 minutes. The visualisation and photographic documentation of DNA bands was conducted using the ChemiDocTM XRS (Biorad) imager and the ImageLab software.

3.3 Cell biological methods

3.3.1 Continuous *in vitro* culture of *P. falciparum* (Trager and Jensen, 1976)

Plasmodium falciparum 3D7 parasites (Walliker et al., 1987) were cultured in human O+ RBCs (obtained from Universität Klinikum Eppendorf, Hamburg) at 5% haematocrit in RPMI-1640 complete medium containing 0.5% Albumax (Life Technologies), 20 mM glucose and 200 mM hypoxanthine. The culture was maintained in petri dishes with volumes of 2 ml, 5 ml and 10 ml at 37°C in an atmosphere consisting of 5% O_2, 5% CO_2, and 90% N_2 according to standard procedures (Trager & Jensen, 1976) and stored in plastic boxes. Transfected parasites were selected using either 4 nM WR99210 (Jacobus Pharmaceuticals), 0.9 µM DSM1 (Sigma-

Aldrich), or 2 µg/ml Blasticidin S (BSD, Life Technologies). To select integrant parasites, SLI was performed using either 400 µg/ml G418 (Sigma) or 0.9 µM DSM1, as previously described (Birnbaum et al., 2017; Cronshagen et al., 2024). After selection, the correct integration was verified by PCR using gDNA as described (section).

3.3.2 Blood smear and Giemsa staining

The estimation of parasitemia, differential stages and condition of the parasite cultures were monitored by Giemsa-stained thin blood smears. For thin blood smears, 0.5 – 1 µl of infected erythrocytes from parasite cultures were transferred to a glass slide, and the drop was extended in a monolayer by smearing with a second glass slide. The thin blood smear was air-dried, fixed with absolute methanol for 10 seconds and stained with 10% Giemsa solution (Merck) for 15 minutes. Immediately, the stained smears were then rinsed with tap water to remove the excess of Giemsa solution and air dried. The stained smears were then examined with a bright field microscope (Axio Lab A1) (section 3.4.1).

3.3.3 Freezing and thawing procedures for parasite cultures

3.3.3.1 Freezing

Parasites were stored as cryostabilates in liquid nitrogen for long-term storage or at -80°C. To achieve this, 5 ml of parasite culture enriched in ring stage (up to 15% ring parasitemia) was centrifuged at 1800xg for 3 minutes, and the supernatant discarded. The resultant pellet was then resuspended in 1 ml of malaria freezing solution (MFS) and transferred to a 2 ml cryotube. The tube was appropriately labelled and immediately frozen at -80°C and then transferred to a liquid nitrogen tank (as previous recorded in the software My Samples).

3.3.3.2 Thawing

When required, cryostabilates were thawed in a water bath at 37°C for 30 to 60 seconds, transferred to a 15 ml Falcon and centrifuged at 1800 x g for 3 minutes. The supernatant was removed and the pellet was gently resuspended in 1 ml of malaria thawing solution (MTS). Subsequently, the suspension was centrifuged again at 1800 x g for 3 minutes, and the

supernatant removed. The pellet containing ring stages was resuspended in pre-warmed RPMI medium without drugs, transferred to a petri dish, and ~200µl of fresh blood was added. On the following day, the dug selection was added to the parasite cultures, and the parasitemia was monitored by Giemsa-stained blood smears, generally checking 2- or 3-days post thawing.

3.3.4 Sorbitol synchronisation of *P. falciparum* parasites

The sorbitol synchronisation method was used to synchronise ring stages with an age ranging from 0 to 18 hours post-invasion (Lambros & Vanderberg, 1979) The basis of this successful synchronisation method is the establishment of new permeability pathways in parasites older than 18 hours. In the presence of sorbitol, it induces hypotonic lysis in trophozoite and schizont stages, while ring stages are unaffected (Ginsburg et al., 1983). For ring stage synchronisation, culture parasites were centrifugated at 1800 x g for 3 minutes at room temperature, and the supernatant discarded. Next, the pellet was resuspended in five-fold volume of pre-warmed 5% D-sorbitol solution. The solution was then incubated in water bath at 37°C for 7-10 minutes. After the incubation, the suspension was centrifugated at 1800 x g for 3 minutes, the supernatant discarded, and the resultant pellet was washed once with RPMI medium. Subsequently, the pellet containing uninfected RBCS as well as RBCs infected with ring stage parasites was transferred to a new petri dish for further cultivation. This synchronisation process was repeated once after 8 hours, in order to obtain a doubly synchronised ring population with an age of 8 to 18 hours post-invasion. Depending on the experiment, ring parasitemia was adjusted by diluting the synchronised ring-containing pellet with fresh blood.

3.3.5 Percoll gradient of *P. falciparum*-infected RBCs

The Percoll gradient method was used to isolate late trophozoite and schizont stage parasites based on their specific density, which was lower in comparison to uninfected RBCs and ring-infected RBCs (Rivadeneira et al., 1983). For the schizont transfection (see section 3.2.6), 4 ml of 60% Percoll was added to a 15 ml Falcon tube. Then 6-8 ml of parasite culture suspension with 5% haematocrit were gently layered on top of a the 60% Percoll, thereby forming two dense layers and centrifuged at 2000 x g for 5 minutes at RT with without brakes. Upon centrifugation, the top layer of RPMI supernatant was removed, whereas the purified fraction of late trophozoites and schizonts was collected and transferred to a new 15 ml Falcon tube.

The schizonts were washed with 10-14 ml of RPMI medium by centrifugation and the pellet was resuspended in RPMI medium for culture or used for transfection (section 3.3.6).

3.3.6 Transfection of *P. falciparum* schizonts by electroporation

In order to carry out the transfection by electroporation, the pellet of purified schizont stage parasites (section 3.3.5) was mixed with 90 µl of TB buffer, and then with 50-100 µg of purified plasmid DNA previously precipitated and dissolved with 10 µl of TE buffer (section 3.2.8). The mixture was transferred to an electroporation cuvette (Bio-Rad) and the parasites were electroporated using the Amaxa system Nucleofector™ 2b (program U-033, Lonza) according to the established protocol (Moon et al., 2013). The electroporated parasites were then transferred to a 2 ml tube containing 500 µl of RPMI medium and ~200 µl of fresh blood. The suspension was then incubated by shaking at 800 rpm for 30 minutes at 37°C to facilitate the invasion of merozoites into the RBCs. Following the induction of invasion by shaking, the suspension was transferred to a petri dish containing 5 ml of RPMI medium and parasite culture incubated overnight a 37°C. On the following day, the medium was replaced by fresh medium, and the selection drugs were added. The medium and drugs were changed on a daily basis for a period of five days. The culture of transfected parasites was monitored by Giemsa-stained blood smears (section 3.3.2).

3.3.7 Selection Linked Integration (SLI) system

The selection-linked integration (SLI) is a strategy used to induce the integration of episomal plasmids into the genome to endogenously express the protein of interest (POI) fused with the C-terminal 2xFKBP-GFP-2xFKBP tag using SLI (Birnbaum et al., 2017), or only with the C-terminal mScarlet tag using a modified version of SLI, termed SLI2 (Cronshagen et al., 2024). The SLI and SLI2 plasmids, which contain the homology region (800-1200 bp) of the gene of interest (GOI), were used to transfect 3D7 *P. falciparum* parasites. Once the parasites retained the episomal plasmids, the selection for integration into the genome was performed in a culture with a parasitemia of 4-10% using the selection drugs as follow: 400 µg/ml G418 (Sigma-Aldrich) for SLI plasmids, and 0.9 µM DSM1 (Sigma-Aldrich) for SLI2 plasmids. During the following seven days, medium was changed daily and the drugs added, and after one week every second day until parasites appeared. Giemsa-stained blood smears were done for monitoring the cultures (section 3.3.2). After parasites appeared in culture under the selective

pressure produced by the drugs, the gDNA was isolated as described (section 3.2.9) and the correct integration of the plasmid into the genomic locus of the GOI was confirmed by integration check PCR (section 3.2.1).

3.3.8 Flow cytometry growth assay

To monitor the growth of knock sideways parasites, cultures were analysed daily by flow cytometry measuring the parasitemia for five days as previously described (Malleret et al., 2011). On the day zero, the parasitemia of asynchronous parasite cultures was adjusted between 0.05 and 0.1% and the culture was split into two 2 petri dishes, one of which received rapalog to a final concentration of 250nM to induce knock sideways (see section 3.3.9), and the other served as a control without rapalog. The medium with and without rapalog was changed daily, and the parasitemia was measured every day for five consecutive days. For each flow cytometry sample, cultures were thoroughly resuspended and 20 µl of each culture was added to 80 µl of RPMI medium containing 0.5 mg/ml dihydroethidium (DHE) and 0.45 mg/ml Hoechst 33342, and incubated for 20 minutes in the dark at room temperature. Stained parasites were then inactivated by adding 400 µl of RPMI medium containing 0.003% glutaraldehyde. Parasitemia was measured by flow cytometry using an LSR-II flow cytometer, 100,000 events counted using the FACSDiva software (BD Biosciences).

3.3.9 Induction of knock sideways

In order to characterise the knock sideways phenotype and study protein function, the conditional inactivation via knock sideways was induced in integrated parasites that episomally co-express the mislocalizerN (Birnbaum et al., 2017). This strategy permits the rapid mislocalisation of a target protein away from its site of action (in this case to the nucleus) by rapalog-induced FRB-FKBP dimerisation (Figure 13). Depending on the purpose, knock sideways was induced in asynchronous parasite cultures (section 3.3.9.1), in ring parasite stages (section 3.3.9.2), or pre-segmented schizonts prior to cytokinesis (section 3.3.9.3).

3.3.9.1 Efficacy of knock sideways in asynchronous parasites

To determine the efficiency of knock sideways, asynchronous parasite culture containing 1-3% parasitemia were divided into two dishes, one of which was added 250nM rapalog to induce

the knock sideways, whereas the other dish served as a control. The kinetic of knock sideways was assessed in comparison to the control at varying time points – 2, 4, 8, 12 and 24 hours – by taking a small aliquot of the parasite cultures, and examined immediately by fluorescence microscopy.

3.3.9.2 Knock sideways induction in rings

For knock sideways induction in rings, parasite culture was doubly synchronised with 5% D-sorbitol to obtain rings aged 0-18 hours, followed by 8-18 hours (see section 3.3.4). In the first synchronisation, ring stage parasites were split in two petri dishes, one receiving 250 nM rapalog to induce the knock sideways, and other served as a control without rapalog. During the second synchronisation or when parasites were fed with fresh medium, both control and knock sideways conditions were conserved by adding or not rapalog. The control and rapalog cultures were smeared at different time points by monitoring the stage development of the parasite. Depending on the experiment and cell line, 500 µl of the control and rapalog parasite suspensions were collected and stained with 4.5 µg/ml Hoechst-33342 (Invitrogen) for 10 minutes at room temperature, and the mislocalisation of the protein of interest and mistargeting of protein markers were then assessed using live-cell fluorescence microscopy at different time points.

3.3.9.3 Knock sideways in schizonts (before cytokinesis)

For knock sideways induction in schizonts, parasite culture was doubly synchronised with 5% D-sorbitol to obtain rings aged 0-18 hours, followed by 8-18 hours and were then recultivated until the time point 28-36 hours before cytokinesis. At this time point (28-36 hours), parasite culture was split in two petri dishes, and the knock sideways was induced in one dish by adding 250nM rapalog, whereas the other dish was used as a control without rapalog. Depending on the purpose, 1 µM of compound 2 (C2), a PKG inhibitor that prevents schizont rupture to get comparably aged populations of late schizonts arrest the parasite egress (Taylor et al., 2010; Collins et al., 2013), was added at the 32-40 h time point. The control and rapalog cultures were monitored by Giemsa-stained smears to assess the stage development of the parasite at different time points. Furthermore, 500 µl of control and rapalog parasite suspensions were collected and stained with 4.5 µg/ml Hoechst-33342 (Invitrogen) for 10 minutes at room temperature, and the

mislocalisation of the protein of interest and mistargeting of protein markers were analysed using live-cell microscopy at different time points.

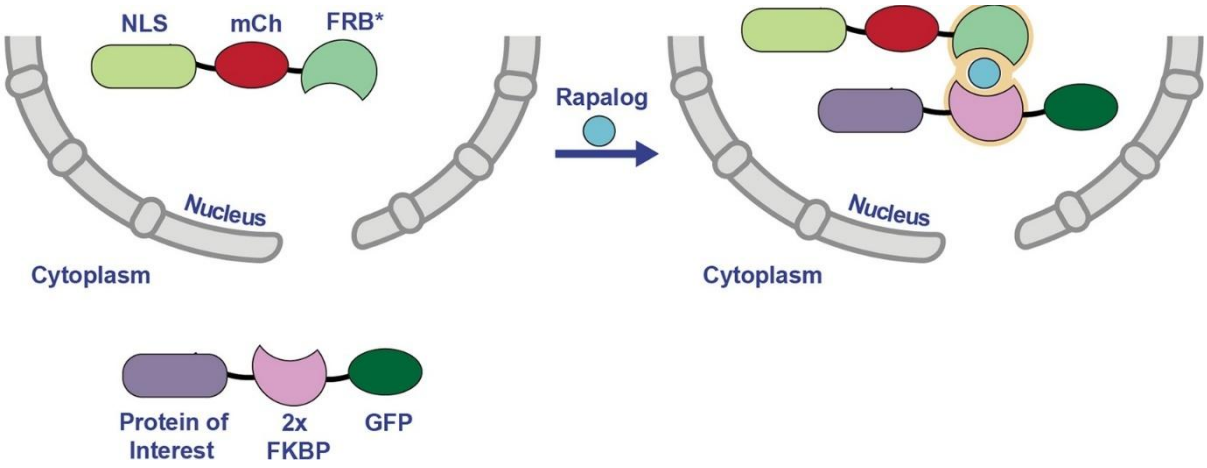

Figure 13. Knock sideways strategy.
The protein of interest is C-terminally fused with the 2xFKBP-GFP tag (POI-2xFKBP-GFP) and located in the cytoplasm, thereby mediating a specific function (e.g., vesicle trafficking); whereas the mislocaliser (NLS-mCh-FRB) is located in the nucleus. Upon the addition of rapalog, POI-2xFKBP-GFP is recruited to the nucleus and dimerises through the FKBP domain with the FRB domain of NLS-mCh-FRB, resulting in the conditional inactivation of the POI. NLS: nuclear localisation signal or nuclear mislocaliser; mCh: mCherry; GFP: green fluorescent protein; FRB: FKBP12-rapamycin binding domain; FKBP (from (Kudyba et al., 2021). Note that in this work the sandwich tag was used which includes 2 more FKBP domains (2xFKBP-GFP-2xFKBP) (Birnbaum et al., 2017).

3.3.10 DiQ-BioID of *P. falciparum* parasites

Dimerization-induced quantitative proximity-dependent biotin identification (DiQ-BioID) is a powerful tool used to identify the proxiome (interacting partners and compartment neighbours) of the protein of interest (POI) that are biotinylated in living parasites (Birnbaum et al., 2020). A notable advantage of DiQ-BioID is that background biotinylation in the same parasite culture can be subtracted, thereby resulting in highly specific proxiomes (Kimmel et al., 2022).

To do this, 200 ml of asynchronous culture of transgenic parasites expressing the product of SLI-integrated-tagged gene of interest (POI-2xFKBP-GFP-2xFKBP) and episomally co-expressing the biotin ligase mCherry-FRB-miniTurbo (miniTurbo-C^L) and miniTurbo-FRB-mCherry (miniTurbo-N^L) were grown in biotin-free RPMI medium (USBiological Life Sciences). The parasite culture was then split into two 100 ml flasks (parasitemia of 5 - 10%). The biotinylizer was recruited to the protein of interest in one culture by adding rapalog to 250 nM (+rapalog) and addition of biotin to 50 µM (Sigma-Aldrich), while the other culture without

rapalog (control) only received 50 µM biotin and both cultures were incubated for 30 minutes at 37°C. Parasites were harvested and washed twice in Dulbecco's Phosphate-Buffered Saline (DPBS). Subsequently, the pellet was resuspended in 10 pellet volumes of ice-cold, freshly prepared 0.03% saponin in DPBS (a detergent that selectively lyses the RBCs and the PVM, but retains the integrity of the PPM at low concentrations) and incubated on ice for 10 minutes. Upon incubation, the released parasites were centrifuged at 11.000 x g for 5 minutes at 4°C and washed with ice-cold DPBS until the supernatant remained clear of residual haemoglobin. The pellet was then lysed in 2 ml of BioID lysis buffer, and the lysate was frozen at -80°C.

In order to purify biotinylated proteins, lysates were subjected to two sequential freeze-thaw cycles and centrifuged at 16,000 x g for 10 minutes. The resulting supernatant was then split into two technical replicates for each experiment, diluted 1:2 in 50 mM Tris-HCl (pH 7.5) containing 2X PIC and 1 mM PMSF, and incubated with 25 µL of Streptavidin Sepharose (equilibrated in 50 mM Tris-HCl pH 7.5, GE Healthcare) by rotating overnight at 4°C. The beads were washed twice in lysis buffer, once in Ampuwa® H_2O, twice in 50 mM Tris-HCl pH 7.5 and three times in 100 mM Triethylammonium bicarbonate buffer pH 8.5 (TEAB, Sigma-Aldrich). Centrifugation of beads was performed after each step at 1600 x g for 2 minutes at room temperature, and each incubation step was carried out by horizontally rolling on a roller mixer for 2 minutes. After last washing step, the Sepharose beads were resuspended in 50 µl of 100 mM TEAB and sent on ice for mass spectrometry analysis in the Bartfai Laboratory at the Radboud Institute in Nijmegen, Netherlands. The mass-spectrometry analysis was performed by Gala Ramón-Zamorano at the Radboud University, NL (Bartfai lab) using the dimethyl labelling for quantification (Boersema et al., 2009).

3.4 Microscopy

3.4.1 Optical light microscopy

Giemsa-stained blood smears (section 3.3.2) were examined using a Zeiss Axio Lab A1 optical light microscope equipped with a Zeiss 1000x/1.4 oil immersion objective and a Zeiss Axio Cam ERC 5S C4742-95. The images were collected using the Zen2.3 software and processed using Corel Photo-Paint (version 2021).

3.4.2 Fluorescence microscopy

Imaging of live parasites endogenously expressing GFP fusion proteins and episomally expressing mCherry or mScarlet fusion proteins, as well as fixed parasites was performed as previously described (Grüring & Spielmann, 2012). If necessary, parasite nuclei were stained with 4.5 µg/ml Hoechst-33342 (Invitrogen) for 10 minutes at room temperature before imaging. Images were acquired using a Zeiss AxioImager M1 or M2 fluorescence microscope equipped with different filters (Zeiss cubes 44, 49, 64 and 50), Zeiss Plan-apochromat 63x/1.4 or 100x/1.4-numerical aperture oil immersion lenses, and a C4742-80 Hamamatsu Orca Digital camera. The images were acquired using the AxioVision software (version 4.7). The brightness and intensity of the images were manually adjusted, and the channels were merged in Corel Photo-Paint (version 2021). The preparation of figures was performed using Corel Draw (version 2021).

3.4.2.1 Immunofluorescence assay

Immunofluorescence assays were performed according to established protocols as described (Spielmann et al., 2003; Tonkin et al., 2004). For fixation in suspension, C2-arrested late schizonts (42-50 hpi) or trophozoites (24-32 hpi) were washed in PBS and incubated with 4% formaldehyde/0.0075% glutaraldehyde in PBS for 30 minutes at room temperature (Tonkin et al., 2004). Cells were permeabilised with 0.5% Triton X-100 in PBS, blocked with 3% BSA in PBS, and incubated overnight with primary antibodies: human α-MSP1$_{19}$ (PPM, 1:1,000, (Blackman et al., 1991)) and α-EXP2 (1:2000, The European Malaria Reagent Repository (http://www.malariaresearch.eu)) in 3% BSA in PBS. Thereafter the cells were washed three times with PBS and incubated for one hour with Alexa 488 nm, Alexa 546 nm or Alexa 594 nm conjugated secondary antibodies specific for human, mouse, rabbit, or rat IgG (Invitrogen) diluted 1:2,000 in 3% BSA in PBS and containing 1 µg/ml 4',6'-diamidine-2'-phenylindole dihydrochloride (DAPI). The cells were directly imaged after washing 3 times with PBS.

For acetone fixation, trophozoite parasites (24-32 hpi) were washed in PBS, air-dried as thin monolayers on 10-well slides (Thermo Fischer) and fixed in 100% acetone for 30 minutes at room temperature (Spielmann et al., 2003). Thereafter the cells were rehydrated with PBS, incubated with primary antibody solution containing rabbit α-SBP1 (Maurer's clefts, dilution 1:2,500, (Mesén-Ramírez et al., 2016)) and mouse α-MSRP6 (Maurer's clefts, dilution 1:500; (Heiber et al., 2013)) in 3% BSA in PBS. After three washes with PBS, secondary antibodies

(Molecular probes) were used at the same dilutions as for the IFA in suspension was carried out. The slides were mounted using mounting medium (Dako) and covered with a coverslip.

3.4.3 Transmission electron microscopy (TEM)

C2-arrested schizont (42-50 hpi) or trophozoite (24-32 hpi and 30-38 hpi) parasites after induction of knock sideways (and controls) were enriched with 60 or 80% Percoll respectively, and fixed with 2.5% glutaraldehyde (Electron Microscopy Science) in 50 mM cacodylate buffer pH7.2 for 30 minutes at room temperature. Parasites were post-fixed with 2% osmium tetroxide (OsO4, Electron Microscopy Sciences) in dH_2O for 40 minutes on ice in the dark, cell membranes contrasted with 0.5% uranyl acetate (Agar Scientific) in dH_20 for 30 minutes at room temperature and dehydrated through increasing concentrations of ethanol (from 50% to 100%). After that, the dehydrated samples were embedded in epoxy resin (EPON, Carl Roth GmbH & Co. KG), cut into 60 nm thick sections with an Ultracut UC7 (Leica) and examined with a Tecnai Spirit transmission electron microscope (FEI), equipped with a LaB6 filament and operated at an acceleration voltage of 80 kV. The EM image .emi/.ser-files were converted to 8-bit TIFF files using the TIA Reader Plugin for ImageJ. This section was kindly performed by Katharina Höhn (Electron Microscopy Department, BNITM).

4. Results

4.1 Studying the post-Golgi adaptors in malaria parasites

In this section the post-Golgi adaptors AP-1, AP-3 and AP-4 were studied.

4.1.1 SLI strategy

In order to investigate the subcellular localisation, function and proxiome of AP-1, AP-3 and AP-4 complexes, the SLI strategy (see schematic in Figure 14A) (Birnbaum et al., 2017) was used in 3D7 parasites to modify the genes encoding AP-1μ (PF3D7_1311400), AP-3μ (PF3D7_1440700) or AP-4μ (PF3D7_1119500) by homologous recombination and generate cell lines expressing C-terminally 2xFKBP-GFP-2xFKBP-tagged μ-subunits (see section 4.1.1.1). For co-localisation studies, a second strategy, SLI2 (see schematic in Figure 14B) (Cronshagen et al., 2024), was used in APμ-2xFKBP-GFP-2xFKBP^{endo} cell lines to modify the gene encoding the clathrin heavy chain (PF3D7_1219100) by homologous recombination, resulting in the generation of double integrant cell lines co-expressing C-terminally mScarlet-tagged CHC (see section 4.1.1.2). The correct integration of the pSLI_APμ-2xFKBP-GFP-2xFKBP into the genomic locus of each AP μ-subunit in 3D7 parasites, or the pSLI2_CHC-mScarlet into the locus of CHC in APμ-2xFKBP-GFP-2xFKBP parasite lines was confirmed by PCRs across the flanking 5'-, and 3'- plasmid integration junctions and by ensuring no parasites with original locus were present (see agarose gel images in Figure 14A and B), and the location of these proteins was assessed by fluorescence microscopy (see sections 4.1.1.1 and 4.1.1.2). The SLI and SLI2 plasmids, as well as the parental and double integrant cell lines, were kindly generated by Ulrike Fröhlke. The adaptor integration cell lines will in this thesis be referred to as AP-xμ^{endo} parasites (x standing for each adaptor).

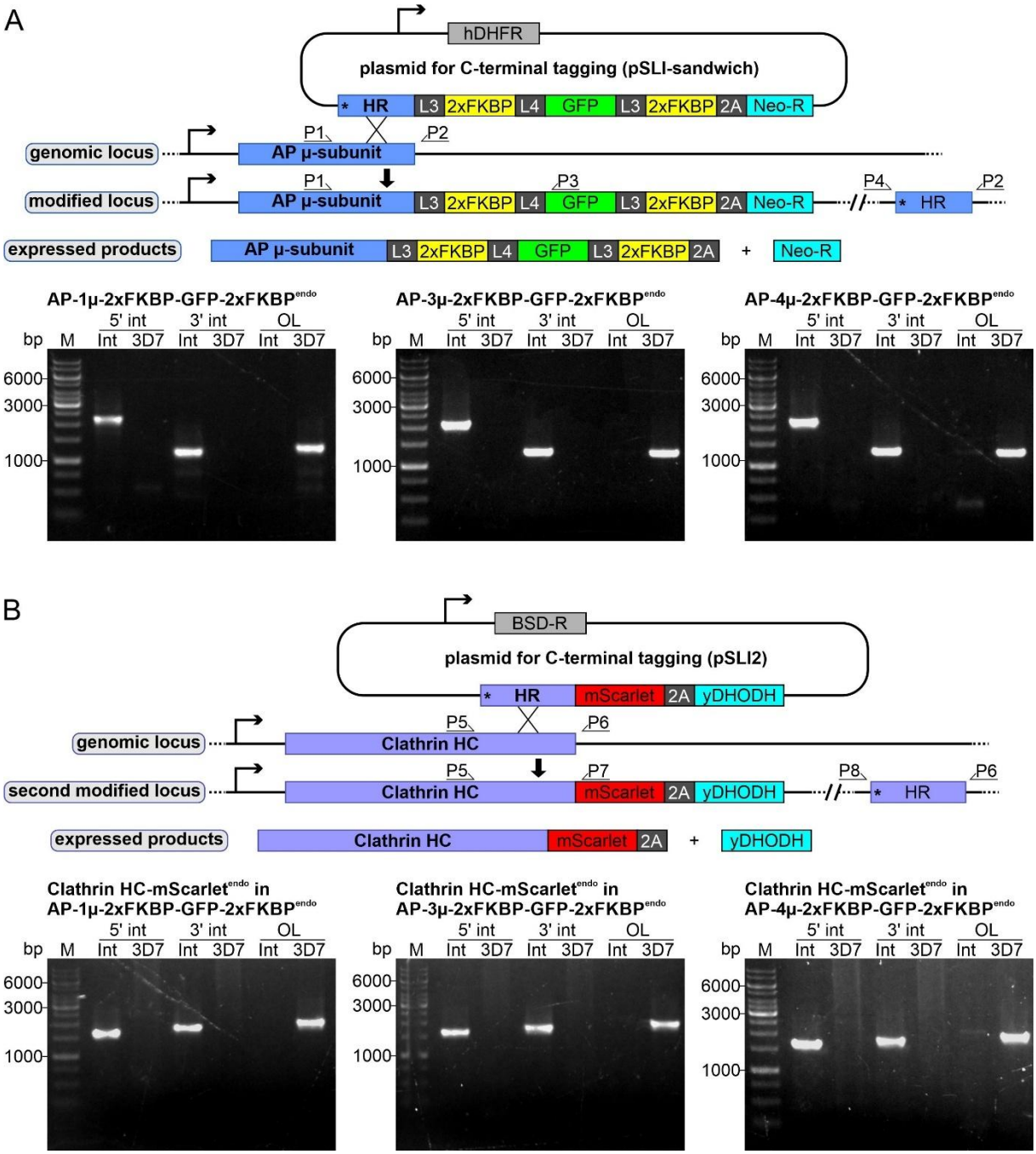

Figure 14. SLI strategies for AP µ subunits and CHC.
(A and B) Schematic of SLI (AP µ-subunits, A) and SLI2 (CHC, B) strategies to modify the genome to obtain C-terminal fusions of the targets. The SLI2 approach (Cronshagen et al., 2024) was used in parasite lines already modified by SLI. HR: homology region; L3 and L4: linkers (defined in (Birnbaum et al., 2017)); 2A: T2A skip peptide; Neo-R: G418-resistance; hDHFR: human dihydrofolate reductase; yDHODH: yeast dihydroorotate dehydrogenase; BSD-R: BSD-resistance; P1-P8 arrows: primers for PCR to assess the integration of the pSLI and pSLI2 plasmids. Agarose gels with PCR products showing correct integration of plasmids into AP-1µ, AP-3µ and AP-4µ encoding genes using pSLI_APµ-2xFKBP-GFP-2xFKBP in 3D7 parasites (SLI: **A**, bottom), and CHC using pSLI2_CHC-mScarlet in APµ integration parasites (SLI2: **B**, bottom). PCR products show 5' integration (5' int) using primers P1 and P3 (P5 and P7 for SLI2), 3' integration (3' int) using primers P4 and P2 (P8 and P6 for SLI2) or absence of the unmodified original locus (OL) using primers P1 and P2 (P5 and P6 for SLI2) in the SLI

integration parasites (int) compared to the 3D7 parent (3D7). M, marker. Primer positions are indicated in (A and B) and primer sequences in Appendix 1.2.

4.1.1.1 Localisation of the μ-subunit of the AP-1, AP-3 and AP-4 complexes

In order to determine the cellular localisation of the endogenously C-terminally 2xFKBP-GFP-2xFKBP-tagged versions of μ-subunits of the AP-1, AP-3 and AP-4 complexes, they were examined in living parasites by fluorescence microscopy. The results obtained revealed the presence of AP-1μ^{endo} (Figure 15) and AP-4μ^{endo} (Figure 17) foci in all asexual stages of the parasite, i.e., rings, trophozoites, schizonts and merozoites. In contrast, AP-3μ^{endo} (Figure 16) was detected in all asexual stages except for some merozoites and rings wherein no foci detected. All three adaptors were localised in foci in the proximity of the parasite nuclei, and the number of AP foci increased as the parasites replicated their nucleus and progressed through the erythrocytic cycle, from ring to schizont stages (Figures 15-17). This finding indicates that these adaptors are constitutively expressed throughout the erythrocytic development of the parasite and are associated with perinuclear compartments.

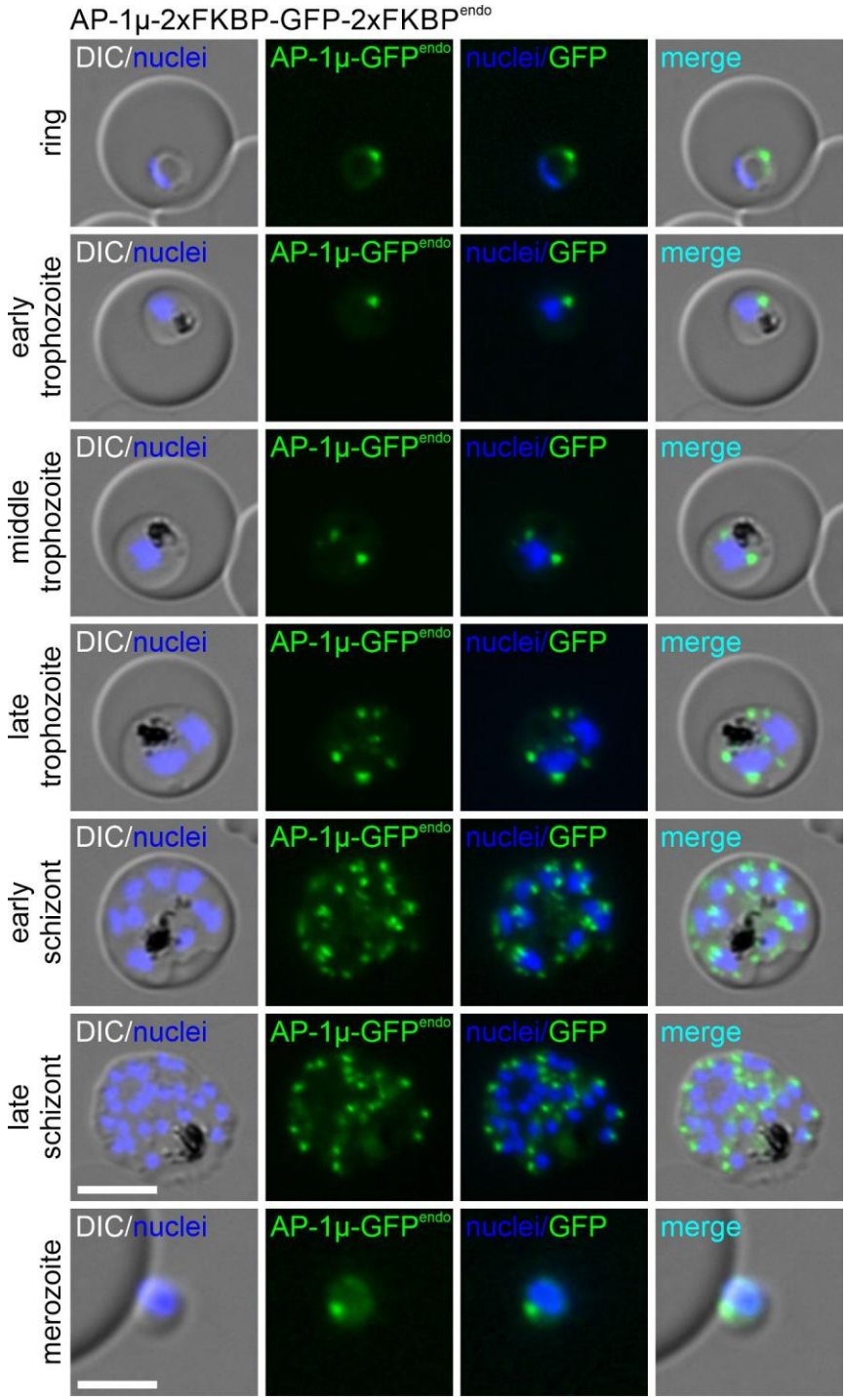

Figure 15. Localisation of endogenously tagged AP-1 µ-subunit.
Live-cell fluorescence microscopy images of AP-1µ-2xFKBP-GFP-2xFKBP^{endo} parasites at different stages during the erythrocytic cycle. Images are representative cells from at least three independent imaging sessions. Scale bar: 5µm for intracellular parasite stages and 2.5µm for merozoites. Nuclei were stained with Hoechst; merge, overlay of blue and green channels; DIC, differential interference contrast.

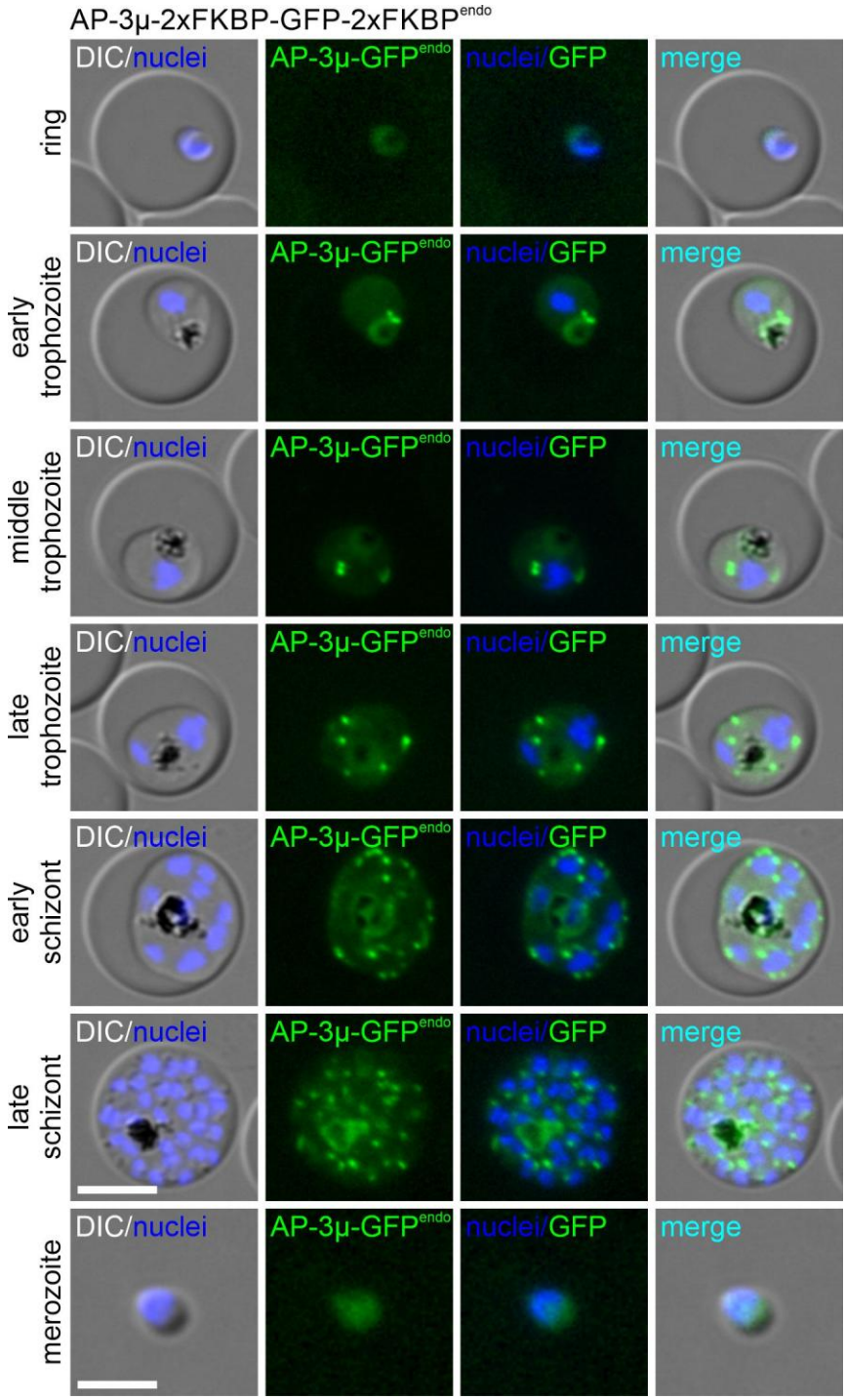

Figure 16. Localisation of endogenously tagged AP-3 µ-subunit.
Live-cell fluorescence microscopy images of AP-3µ-2xFKBP-GFP-2xFKBP^{endo} parasites at different stages during the erythrocytic cycle. Images are representative cells from at least three independent imaging sessions. Scale bar: 5µm for intracellular parasite stages and 2.5µm for merozoites. Nuclei were stained with Hoechst; merge, overlay of blue and green channels; DIC, differential interference contrast.

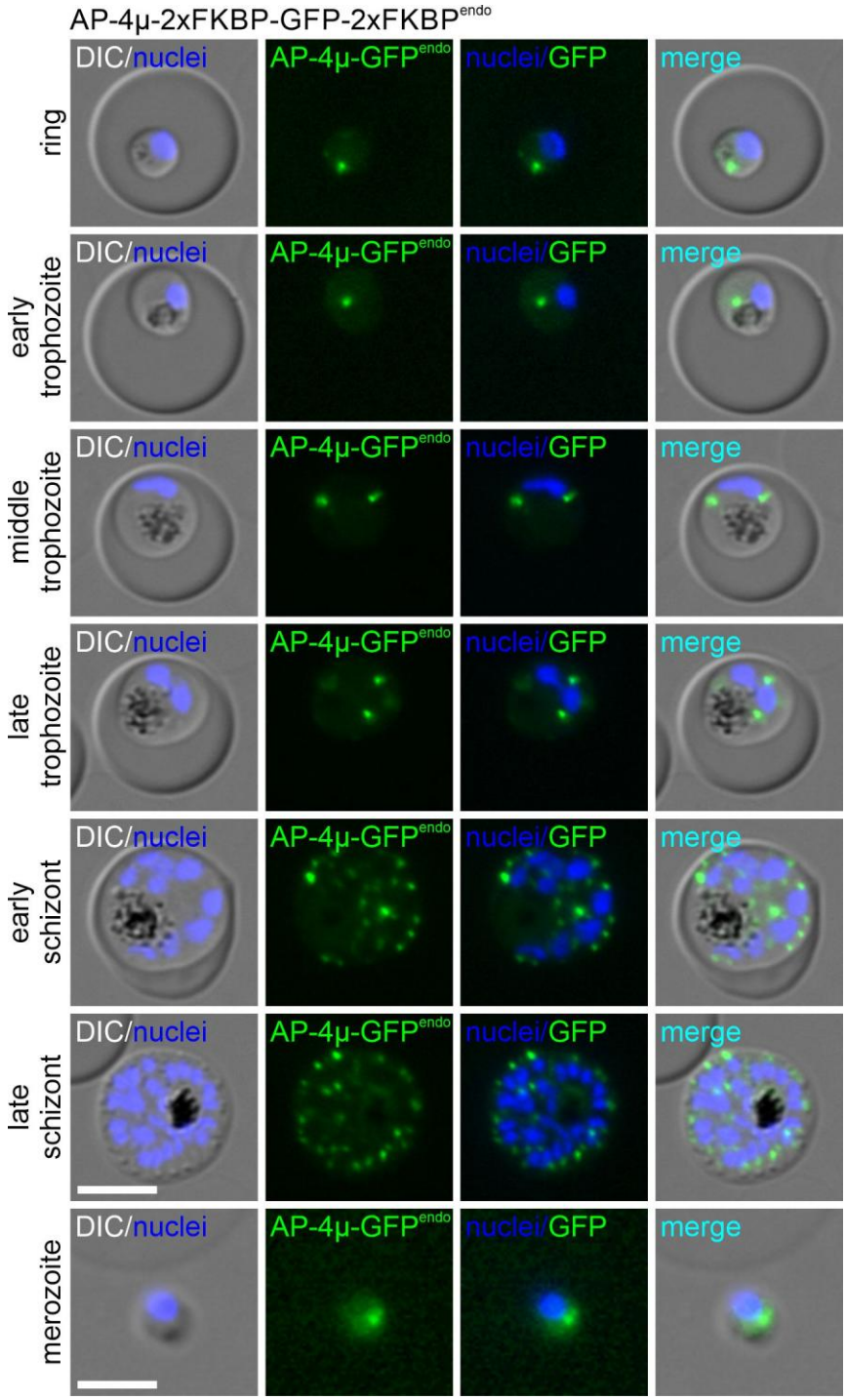

Figure 17. Localisation of endogenously tagged AP-4 µ-subunit.
Live-cell fluorescence microscopy images of AP-4µ-2xFKBP-GFP-2xFKBP^{endo} parasites at different stages during the erythrocytic cycle. Images are representative cells from at least three independent imaging sessions. Scale bar: 5µm for intracellular parasite stages and 2.5µm for merozoites. Nuclei were stained with Hoechst; merge, overlay of blue and green channels; DIC, differential interference contrast.

4.1.1.2 AP-1, AP-3 and AP-4 complexes localise at the trans-Golgi

As the adaptors exhibited a perinuclear pattern during the erythrocytic schizogony of the parasite (see Figures 15-17), the APμ^{endo} cell lines were co-transfected with a plasmid to episomally express GRASP-mScarlet (GRASP^{epi}), a cis-Golgi marker (Struck et al., 2005), to study the localisation of these adaptors. As shown in Figures 18-20, AP-1μ^{endo}, AP-3μ^{endo} and AP-4μ^{endo} foci were found to be in close proximity to the GRASP-marked Golgi compartment during the erythrocytic cycle of the parasite. Despite their proximity, the foci for all three adaptors appeared to be located in regions that were distinct from the GRASP foci (Figure 18-20), indicating that they are potentially residing in neighbour compartments. In subsequent experiments, each APμ^{endo} cell line was co-transfected with plasmids to enable endogenous expression of CHC-mScarlet (CHC^{endo}) (section 4.1.1; lines kindly provided by Ulrike Fröhlke) or to episomally express CLC fused to mScarlet (CLC^{epi}), as trans-Golgi marker, to study the localisation of these adaptors. The results showed that the foci of the three adaptors were found in close vicinity to, and overlapping with, the CHC- and CLC-defined foci during parasite development, indicating that these adaptors reside at the trans-Golgi (Figure 21-23).

In order to better describe the level of co-localisation of the adaptor foci with GRASP and clathrin foci, the Mander's overlap coefficient (Manders et al., 1993) was used. This analysis confirmed that all three adaptors showed comparable partial overlap with GRASP (Figure 24A), but when GRASP was assessed relative to each adaptor, AP-1 showed more overlap than AP-3 and AP-4 (Figure 24A). The difference between the two directions of comparison indicated that AP-1 foci cover more area of the GRASP foci than the AP-3 and AP-4 foci, while vice versa this was not the case. A similar approach, comparing the adaptor foci with CHC, showed more overlap than with GRASP, indicating that the foci of the three adaptins overlap more with the trans-Golgi than with the Golgi and were almost entirely encompassed in clathrin-positive areas (Figure 24B). Once more, AP-1 occupied a greater proportion of the CHC region than the other two adaptors (Figure 24B). These findings suggest that AP-1, AP-3 and AP-4 are located at or close to the trans-Golgi, overlapping with CHC-positive areas.

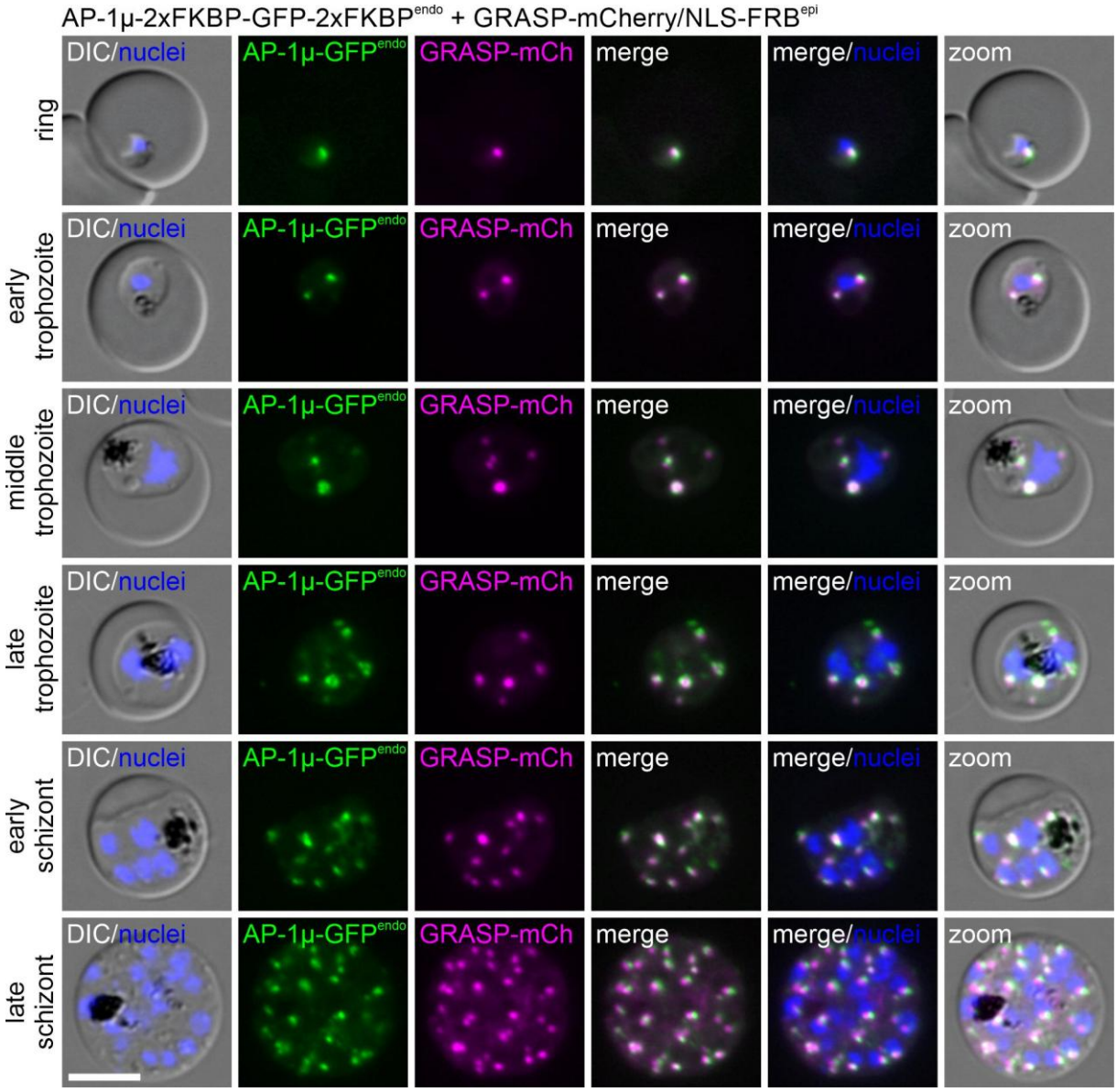

Figure 18. Co-localisation of AP-1 with GRASP.
Live-cell fluorescence microscopy images of AP-1μ^{endo} parasites co-expressing GRASP-mCherry. Images are representative cells from at least three independent imaging sessions. Scale bar: 5μm. Nuclei were stained with Hoechst; merge, overlay of green and magenta channels; DIC, differential interference contrast.

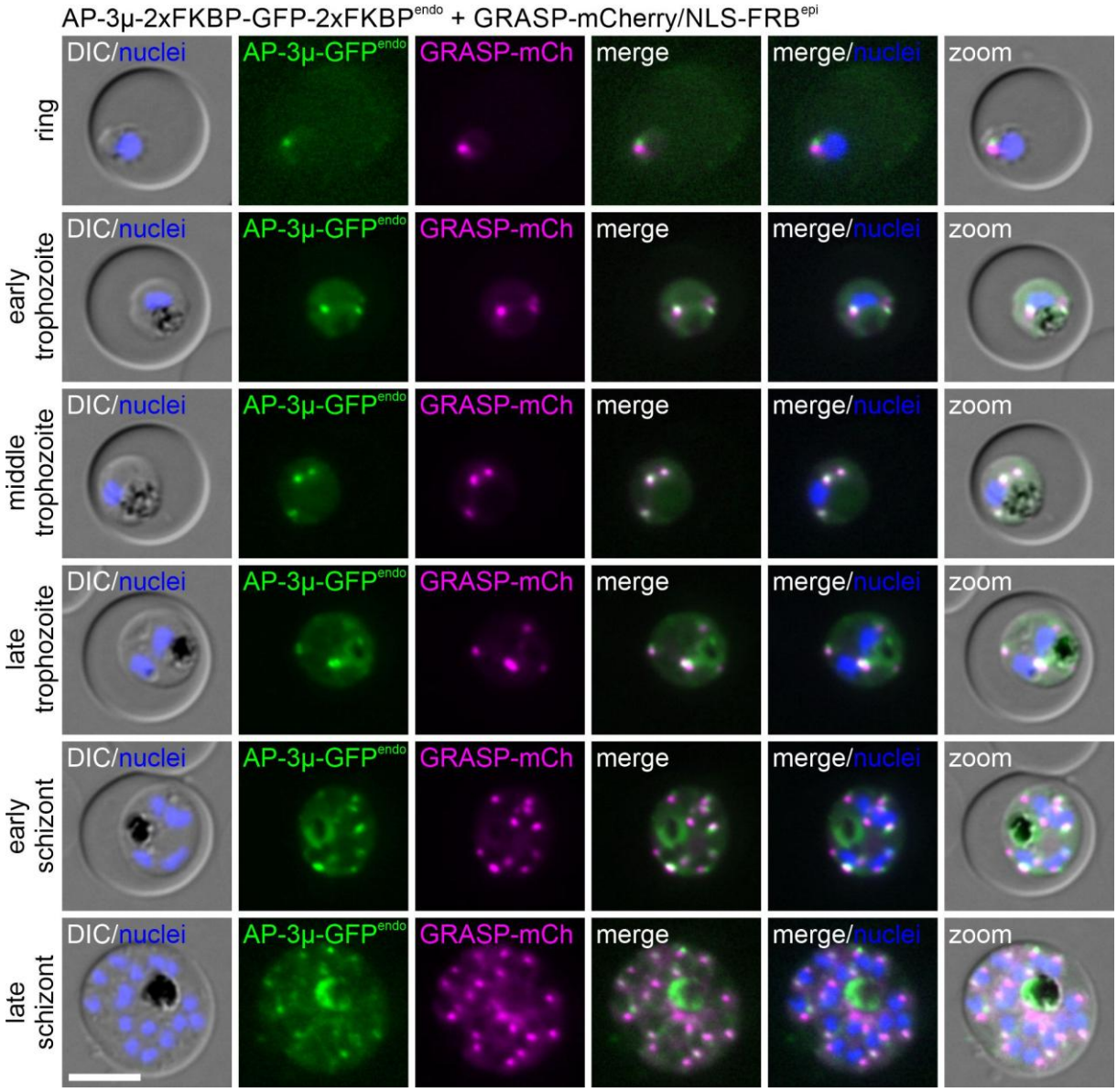

Figure 19. Co-localisation of AP-3 with GRASP.
Live-cell fluorescence microscopy images of AP-3µ^{endo} parasites co-expressing GRASP-mCherry. Images are representative cells from at least three independent imaging sessions. Scale bar: 5µm. Nuclei were stained with Hoechst; merge, overlay of green and magenta channels; DIC, differential interference contrast.

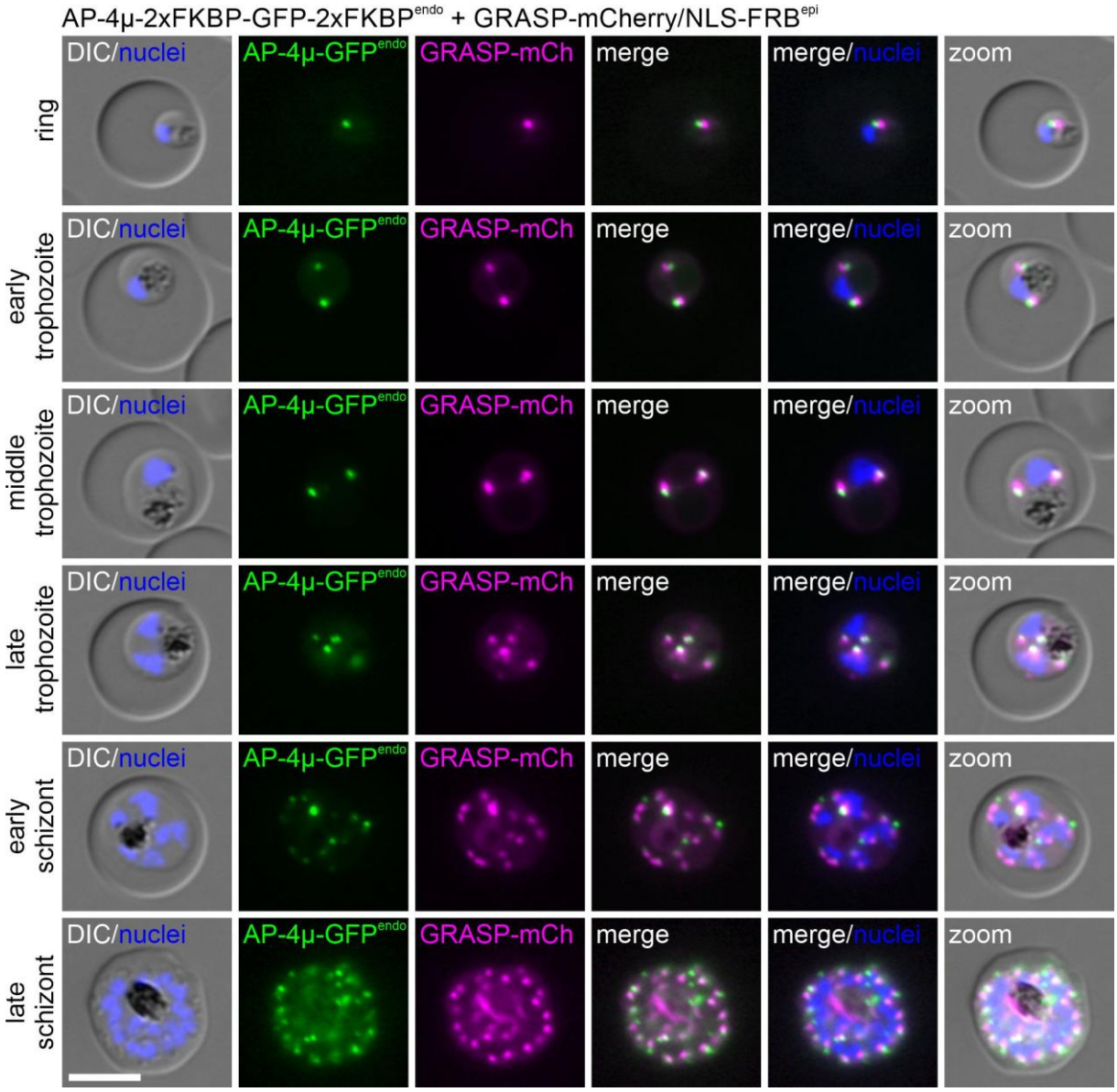

Figure 20. Co-localisation of AP-4 with GRASP.
Live-cell fluorescence microscopy images of AP-4μ^{endo} parasites co-expressing GRASP-mCherry. Images are representative cells from at least three independent imaging sessions. Scale bar: 5μm. Nuclei were stained with Hoechst; merge, overlay of green and magenta channels; DIC, differential interference contrast.

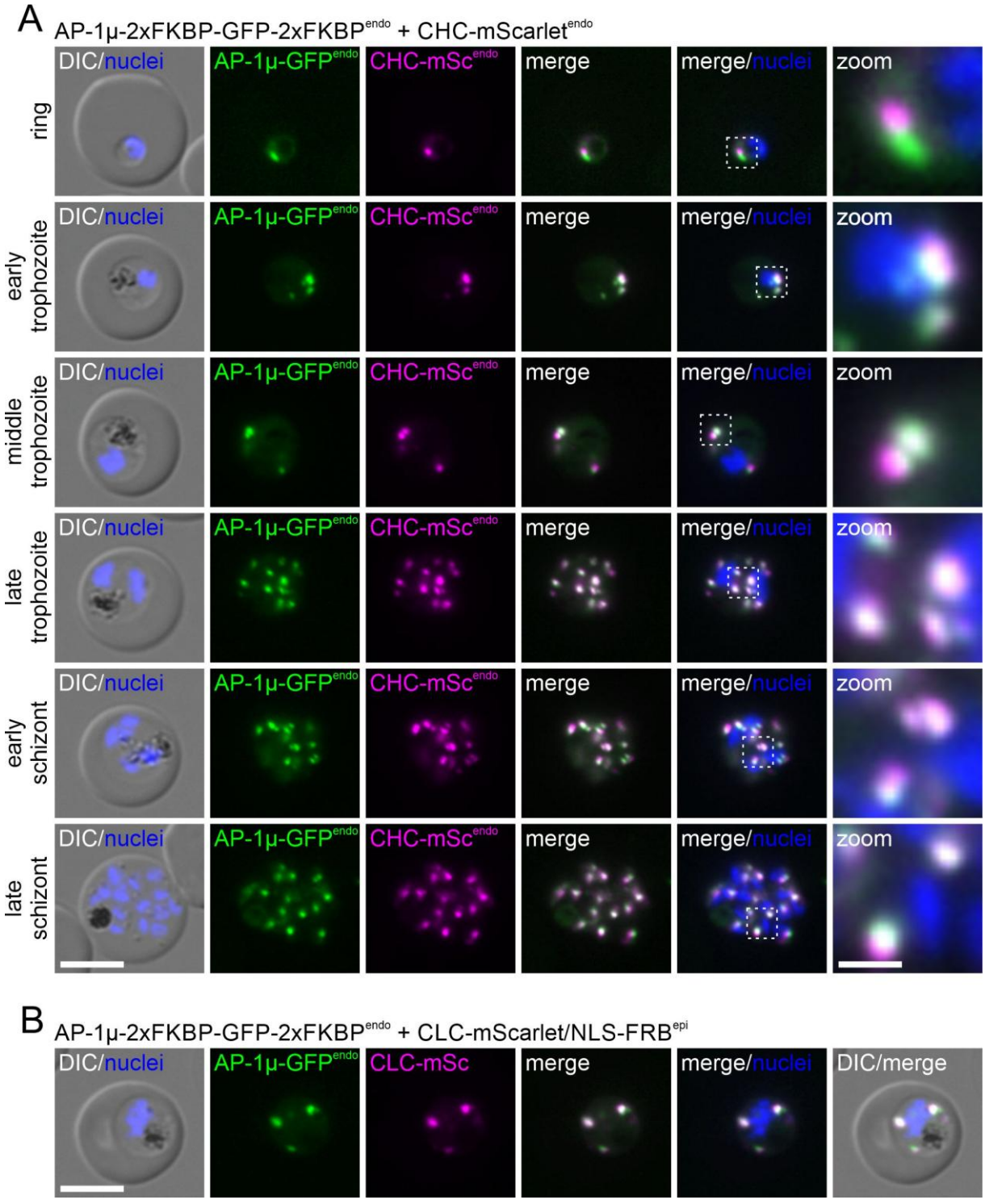

Figure 21. Co-localisation of AP-1 with clathrin.
(A and B) Live-cell fluorescence microscopy images of AP-1µ^{endo} parasites co-expressing CHC-mScarlet (A) or CLC-mScarlet (B). Images are representative cells from at least three independent imaging sessions. Boxed areas in A and B were enlarged (zoom). Scale bar: 5µm (1µm for zoomed section). Nuclei were stained with Hoechst; merge, overlay of green and magenta channels; DIC, differential interference contrast.

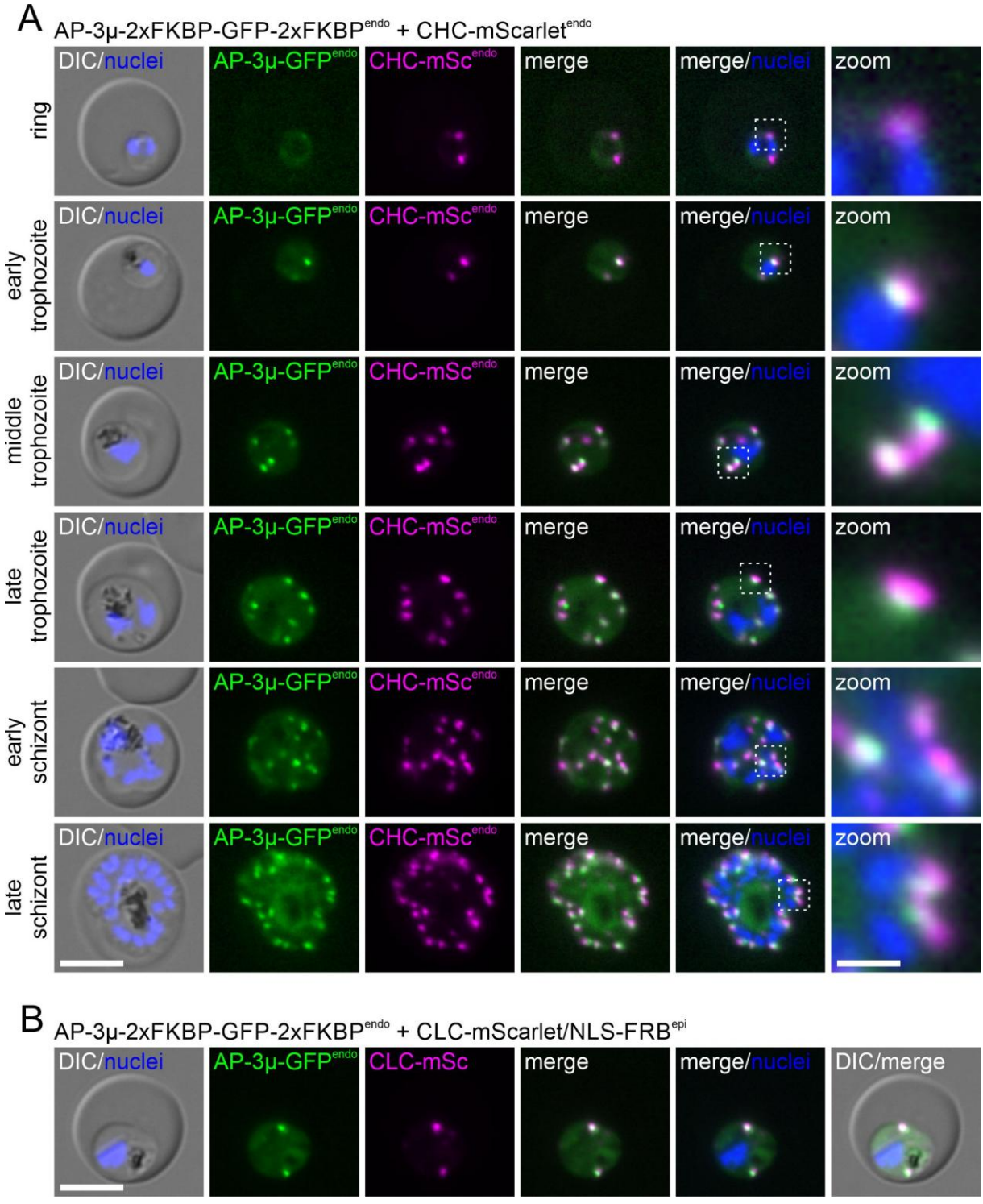

Figure 22. Co-localisation of AP-3 with clathrin.
(A and B) Live-cell fluorescence microscopy images of AP-3µ^{endo} parasites co-expressing CHC-mScarlet (A) or CLC-mScarlet (B). Images are representative cells from at least three independent imaging sessions. Boxed areas in A and B were enlarged (zoom). Scale bar: 5µm (1µm for zoomed section). Nuclei were stained with Hoechst; merge, overlay of green and magenta channels; DIC, differential interference contrast.

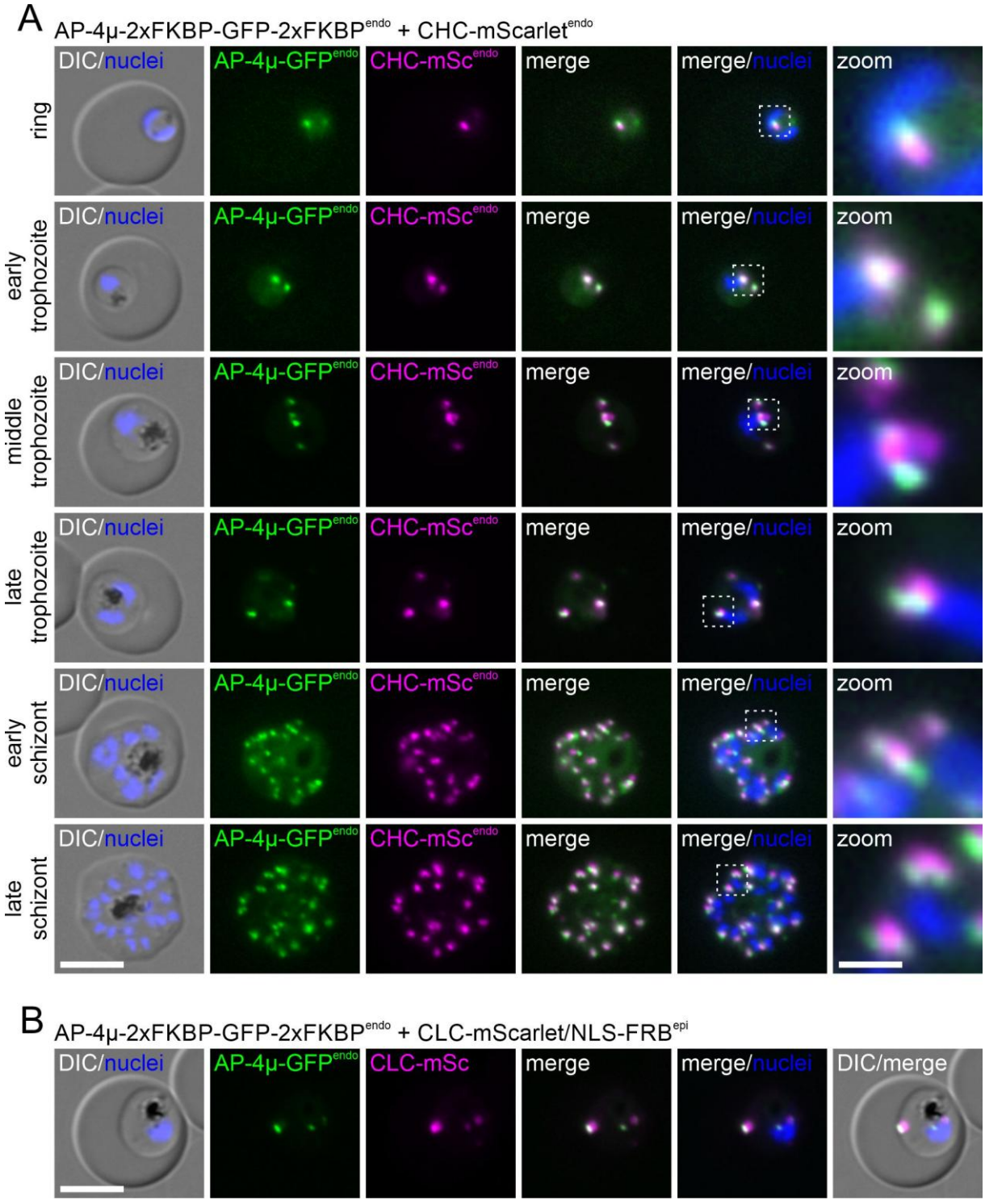

Figure 23. Co-localisation of AP-4 with clathrin.
(A and B) Live-cell fluorescence microscopy images of AP-4μ^{endo} parasites co-expressing CHC-mScarlet (A) or CLC-mScarlet (B). Images are representative cells from at least three independent imaging sessions. Boxed areas in A and B were enlarged (zoom). Scale bar: 5μm (1μm for zoomed section). Nuclei were stained with Hoechst; merge, overlay of green and magenta channels; DIC, differential interference contrast.

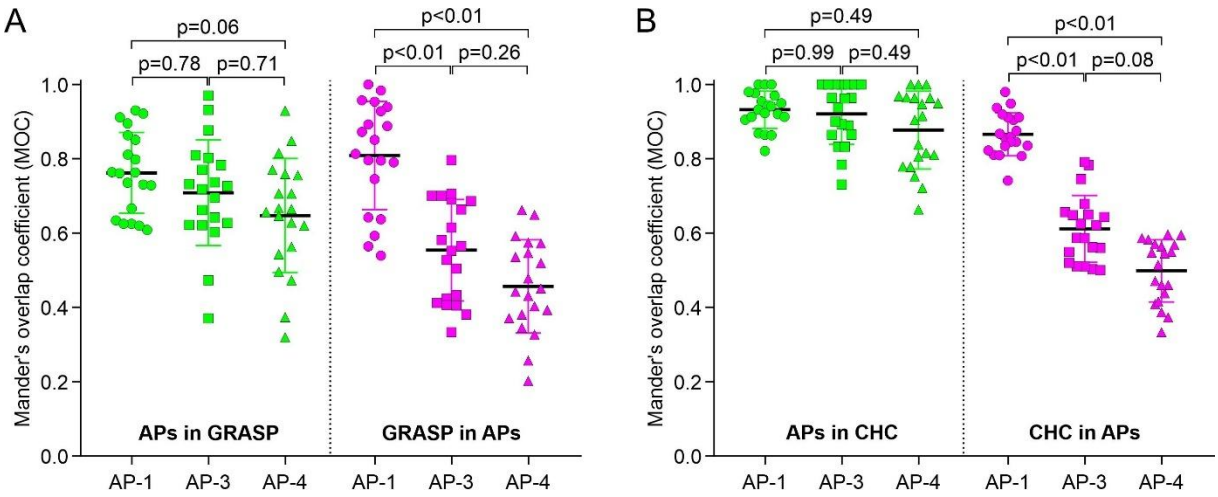

Figure 24. Mander's overlap coefficient.
(A and B) Mander's overlap coefficient of AP-1, AP-3 and AP-4 foci compared to GRASP- (A) and CHC- (B) foci in trophozoites. APs in GRASP or CHC: adaptor focus area overlapping with GRASP or CHC foci. GRASP or CHC in APs: area of GRASP or CHC foci overlapping with adaptor focus. Results from 20 foci per cell line. GRASP in AP-1: 7, 2, 2, 4, 4 and 1 foci; AP-3: 7, 2, 5 and 6 foci; and AP-4: 14, 3 and 3 foci taking cells from 6, 4 and 3 independent imaging sessions, respectively. CHC in AP-1: 15, 1, 2 and 2 foci; AP-3: 7, 7, 5 and 1 foci; and AP-4: 11, 7 and 2 foci taking cells from 4, 4 and 3 independent imaging sessions, respectively. One-way ANOVA (Kruskal-Wallis test) followed by a Dunn's multiple comparison test; p-values are indicated. Black lines, mean; green and magenta lines, error bars (SD).

4.1.2 Conditional inactivation of AP-1, AP-3 and AP-4 using knock sideways and efficiency of this approach

In order to conditionally inactivate AP-1, AP-3 and AP-4, the cell lines with the 2xFKBP-GFP-2xFKBP-tagged a APμ-subunits of these adaptors were transfected with a plasmid to episomally express a nuclear mislocaliser fused to FRB and mCherry (1xNLS-FRB-mCherry) under the control of the *nmd3* promoter (Birnbaum et al., 2017) (henceforth called APμ knock sideways parasites). This permits the conditional mislocalisation of the AP μ-subunits using the knock sideways strategy (Geda et al., 2008; Haruki et al., 2008; Robinson et al., 2010; Birnbaum et al., 2017). This strategy permits the rapid mislocalisation of a target protein away from its site of action (in this case to the nucleus) by rapalog-induced FRB-FKBP dimerization. Knock sideways has been previously found to be well suited to inactivate AP-1γ, AP-2α and AP-4ε1 in HeLa cells (Robinson et al., 2010; Hirst et al., 2012; Davies et al., 2018; Buser et al., 2018, 2022) and AP-2μ in *P. falciparum* parasites (Birnbaum et al., 2020).

To assess the efficiency of knock sideways, asynchronous APμ^{endo} parasite cultures expressing 1xNLS-FRB-mCherry were assessed at different time points upon addition of 250 nM rapalog

to induce the mislocalisation (Figure 25A-F). The results showed that the mislocalisation of AP-1μ (Figure 25A and D) and AP-3μ (Figure 25B and E) was more efficient, with these adaptors being recruited to the nucleus after 8 h and 4 h, respectively. In contrast, AP-4μ inactivation (Figure 25C and F) was less efficient and showed only a partial mislocalisation to the nucleus, even after a 24 h incubation with rapalog, with additional reverse localisation of the mislocaliser to the target foci (arrow, Figure 25C and F). Taken together, these findings indicate that conditional inactivation of adaptors is a suitable strategy to study the function of adaptors in the parasite.

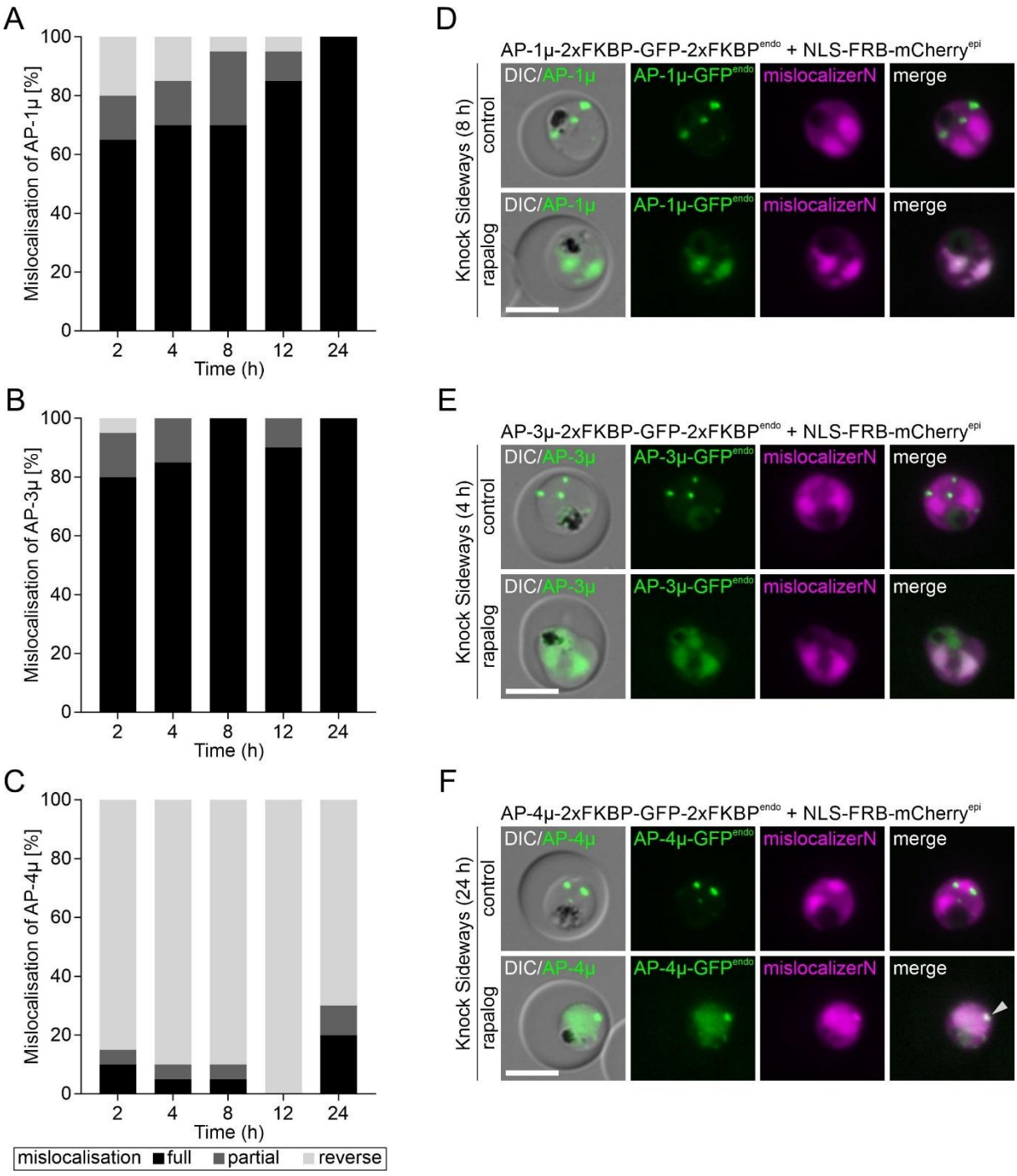

Figure 25. Kinetics of mislocalisation of AP-1µ, AP-3µ and AP-4µ.
(A-C) AP-1µ^{endo} (A), AP-3µ^{endo} (B) and AP-4µ^{endo} (C) parasites expressing 1xNLS-FRB-mCherry (Birnbaum et al., 2017) were analysed at different time points after addition of rapalog (2h, 4h, 8h, 12h and 24h) and percent of cells with the indicated mislocalisation is shown. Mislocalisation was classified as follows: full mislocalisation (black): no APµ focus detectable outside the nucleus; partial mislocalisation (dark grey): some APµ fluorescence focus remaining outside of the nucleus; reverse mislocalisation (light grey): detectable adaptor focus colocalising with mislocaliserN outside the nucleus; n = 20 cells per time point per cell line in two independent experiments (see second replicate in Appendix 3). **(D-F)** Live-cell fluorescence microscopy images of A, B and C at 8h (D), 4h (E) and 24h (F) after addition of rapalog (knock sideways), respectively. Arrow indicates reverse

mislocalisation. Scale bar: 5µm; merge, overlay of green and magenta channels; DIC, differential interference contrast.

4.1.2.1 Characterisation of AP-1 knock sideways phenotype

With the aim to investigate the importance of AP-1, asynchronous parasites with the endogenously 2xFKBP-GFP-2xFKBP tagged AP-1µ and expressing 1xNLS-FRB-mCherry were used to conditionally inactivate AP-1 by knock sideways and growth was monitored over 5 days by flow cytometry (Figure 26A and Appendix 4). The results showed that AP-1 inactivation resulted in a drastic growth defect (~4% growth compared to control) (Figure 26A and Appendix 4), suggesting an essential role of this adaptor for parasite blood stage development.

To gain more insight into and characterise the knock sideways phenotype, AP-1 was conditionally inactivated in highly synchronous ring stage parasites (obtained through consecutive synchronisations 10 h apart, see Methods 3.3.4) and the development stage was analysed at different time points during the erythrocytic cycle (Figure 26B). While control AP-1 parasites developed normally and completed the erythrocytic cycle, with the formation of newly-formed rings in the second cycle, the inactivation of this adaptor resulted in delayed trophozoite development and failure to progress to late stages (Figure 26B and Appendix 5). Giemsa smears of parasites with inactivated AP-1 revealed that few of the cells reached the stage with six nuclei or more and close to half of the parasites exhibited large white areas ("vacuolated" parasites) (Figure 26B and C). To explore whether AP-1 was also required in later stage parasites, this adaptor was inactivated late in the cycle, during cytokinesis and prior to egress (induction of knock sideways at 32-40 hours post invasion (hpi)). This resulted in the formation of aberrant schizonts and a failure to produce new rings, indicating an important function of AP-1 also during parasite schizogony (Figure 26D). Taken together, these findings suggest that AP-1 is indispensable for parasite development in trophozoites and in schizonts.

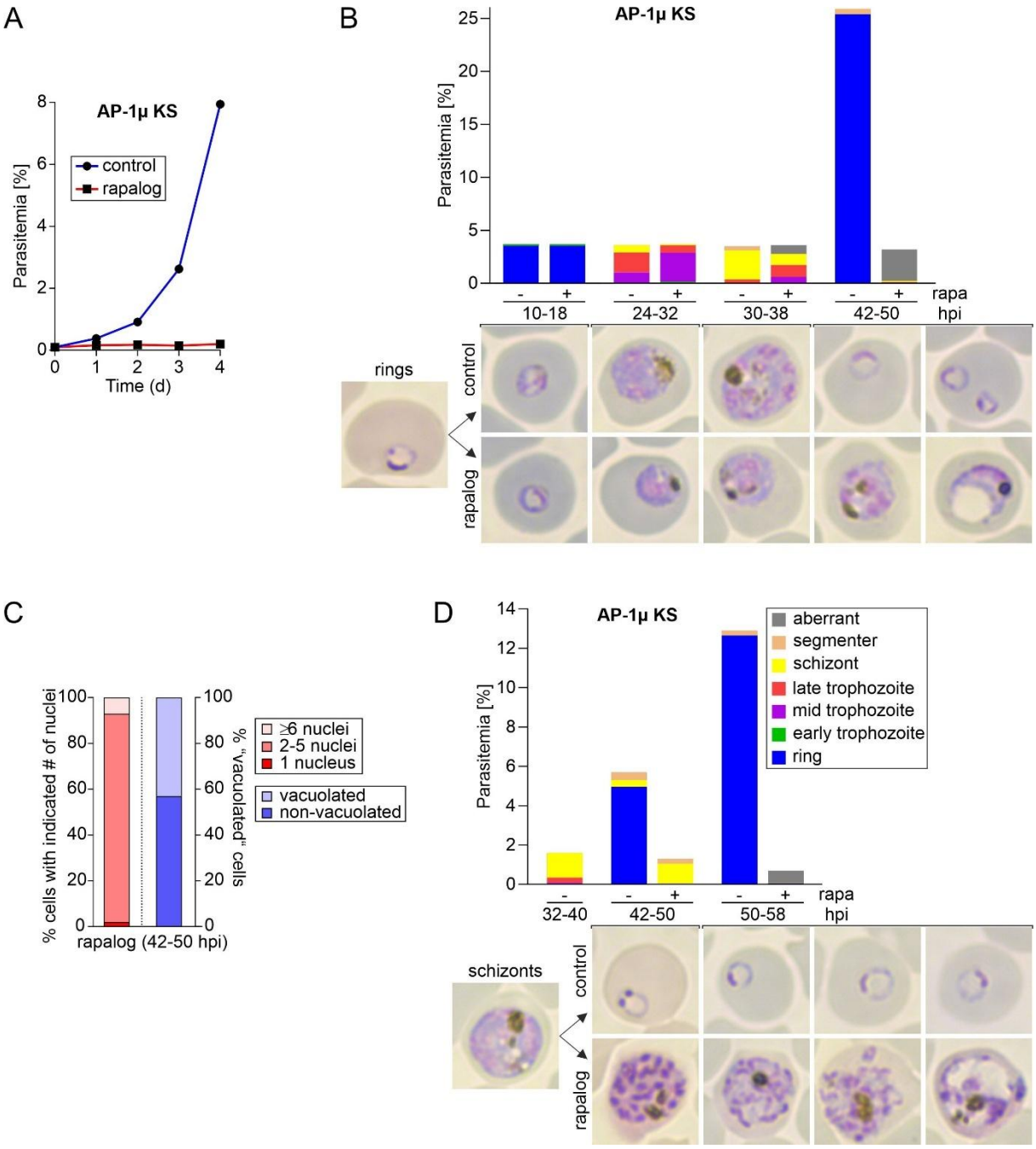

Figure 26. Stage-specific importance of AP-1 for growth of blood stage parasites.
(A) Growth curves of AP-1µ^{endo} parasites expressing 1xNLS-FRB-mCherry after induction of knock sideways with rapalog compared to control over 5 days (day 0 to 4; parasitemia measured by flow cytometry). One representative experiment, replicates are shown in Appendix 4. **(B)** Parasite stages and parasitemia based on Giemsa smears of AP-1µ^{endo} knock sideways parasites compared to controls at the indicated time points after rapalog (rapa) addition starting with synchronous ring stage (n = 2, second and third independent experiments are shown in Appendix 5). Giemsa smear images show representative parasites at the indicated time points. **(C)** Percentage of AP-1 knock sideways parasites with number of nuclei and vacuolated phenotype of the 42-50 hpi time point from Figure 17B (n = 100 parasites per analysis in one replicate). **(D)** Parasite stage distribution and parasitemia based on Giemsa smears of AP-1µ^{endo} knock sideways parasites compared to controls at the indicated time points after rapalog (rapa) addition starting in synchronous late stages (n = 2, second independent experiment are shown in Appendix 5). Giemsa smear images show representative parasites at the indicated time points.

4.1.2.2 Characterisation of AP-3 and AP-4 knock sideways phenotypes

Using the same strategy employed for AP-1 (see section 4.1.2.1), asynchronous parasites with the endogenously 2xFKBP-GFP-2xFKBP tagged AP-3μ and AP-4μ and expressing 1xNLS-FRB-mCherry were used to conditionally inactivate these adaptors. After induction of the knock sideways growth of the parasites was monitored over 5 days by flow cytometry (Figure 27A and B). The results showed that AP-3μ^{endo} and AP-4μ^{endo} were also crucial for parasite growth, although the effect was less pronounced, with ~15% and ~11% growth compared to their controls, respectively (Figure 27A and B and Appendix 4). Given the evidence that the AP-4 recruitment to the nucleus was likely less efficient than for AP-1 and AP-3 (Figure 25C and F), an incomplete inactivation of AP-4 might contribute to the residual parasite growth after knock sideways of this adaptor. These results show the importance of AP-3 and AP-4 for parasite blood stage development.

To assess the importance of these adaptors for the development of specific stages, the inactivation of AP-3μ^{endo} and AP-4μ^{endo} was induced in synchronous ring stage parasites, and the development of the parasites was assessed at different time points during the erythrocytic cycle (Figure 27C and D). In these experiments, the intraerythrocytic development of control and knock sideways AP-3 and AP-4 parasites showed no substantial difference compared to controls (Figure 27C and D). However, when the knock sideways AP-3 and AP-4 parasites were progressing to the next erythrocytic cycle, a notable reduction in the parasitemia of new rings was observed at the 42-50 hpi time point (Figure 27C and D). This difference in ring stage parasitemia compared to control was more pronounced when knock sideways AP-3 and AP-4 parasites were examined at the 50-58 hpi time point (Figure 27C and D), suggesting that in the control more schizonts had produced daughter merozoites that had invaded new RBCs compared to the knock sideways parasites. Overall, these results indicated that inactivation of these adaptors resulted in defective invasion (Figure 27C and D and Appendix 5).

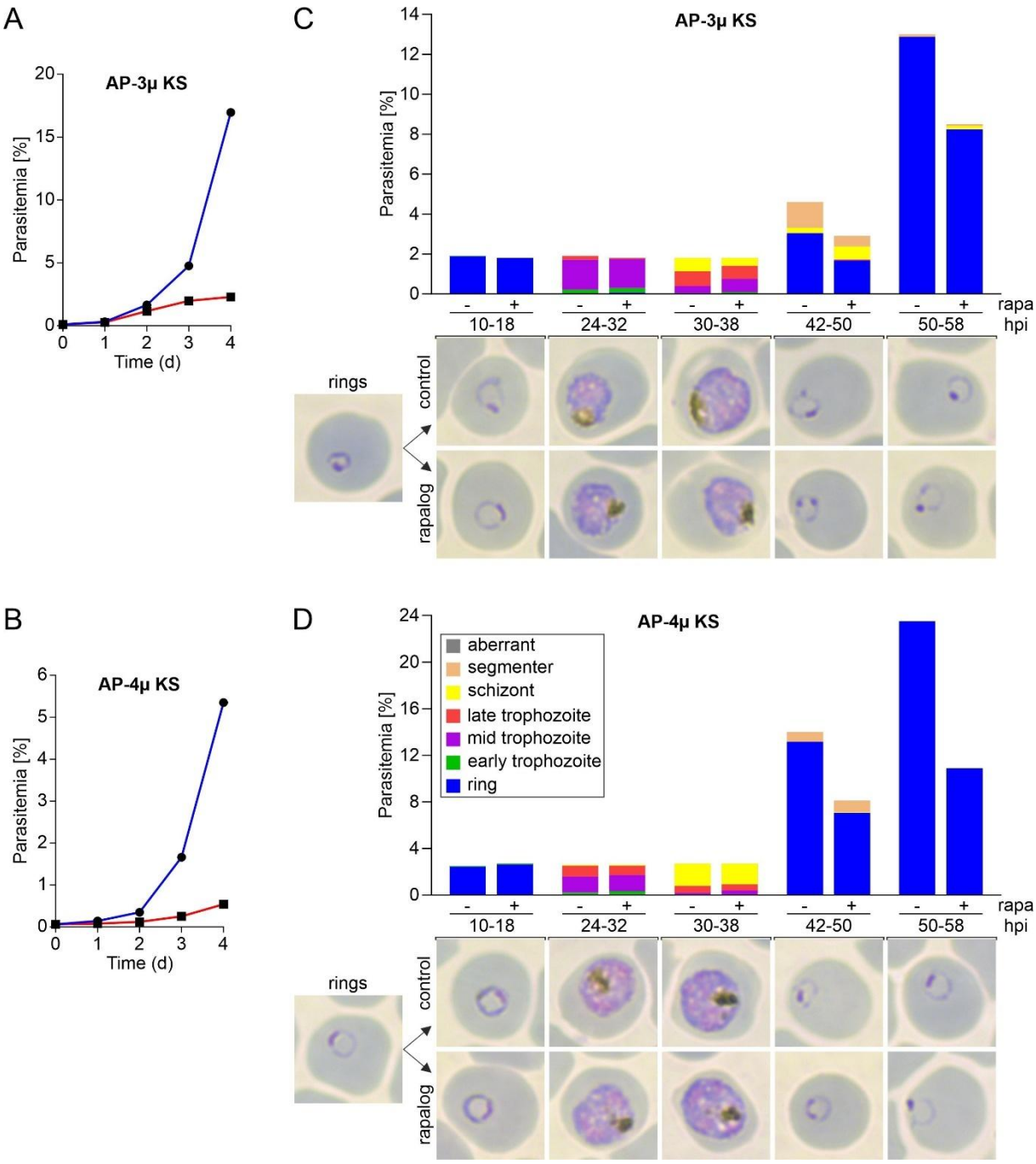

Figure 27. Stage-specific importance of AP-3 and AP-4 for growth of blood stage parasites.
(A and B) Growth curves of AP-3µ^{endo} (A) and AP-4µ^{endo} (B) parasites expressing 1xNLS-FRB-mCherry after induction of knock sideways with rapalog compared to control over 5 days (day 0 to 4; parasitemia measured by flow cytometry). One representative of two experiments (replicates are shown in Appendix 4). **(C and D)** Parasite stages and parasitemia based on Giemsa smears of AP-3µ^{endo} (C) and AP-4µ^{endo} (D) knock sideways parasites compared to controls at the indicated time points after rapalog (rapa) addition starting with synchronous ring stage (n = 3, second and third independent experiments are shown in Appendix 5). Giemsa smear images show representative parasites at the indicated time points.

4.1.2.3 Conditional inactivation of AP-3 and AP-4 negatively impacts the invasion of RBCs

In an effort to corroborate the impact of AP-3 and AP-4 knock sideways on invasion, additional experiments were carried out to measure the difference in number of rings between control and knock sideways parasites. The conditional inactivation of these adaptors was induced in early-stage parasites and the quantification of newly formed ring stage parasites was performed at the 50-58 hpi time window, when all previous cycle schizonts had progressed to new cycle ring stages (Figure 28A and B). The examination of Giemsa smears confirmed a significant reduction of newly formed rings by ~37% and ~65% after inactivation of AP-3μ^{endo} or AP-4μ^{endo} compared to controls, respectively (Figure 28A and B). As free merozoites were detectable (arrows, Figure 28A and B) and no schizont parasites remained from the previous cycle (Figure 28A and B), this was not due to a failure to egress but pointed to a requirement of AP-3μ^{endo} and AP-4μ^{endo} for erythrocyte invasion. Of note, AP-4 knock sideways had a more profound impact on new ring formation in comparison to the AP-3 knock sideways.

Collectively, these observations illustrated that AP-1μ^{endo} has a critical function in both trophozoite and schizont development, whereas AP-3μ^{endo} and AP-4μ^{endo} are crucial for the transition to the next erythrocytic cycle, likely for invasion.

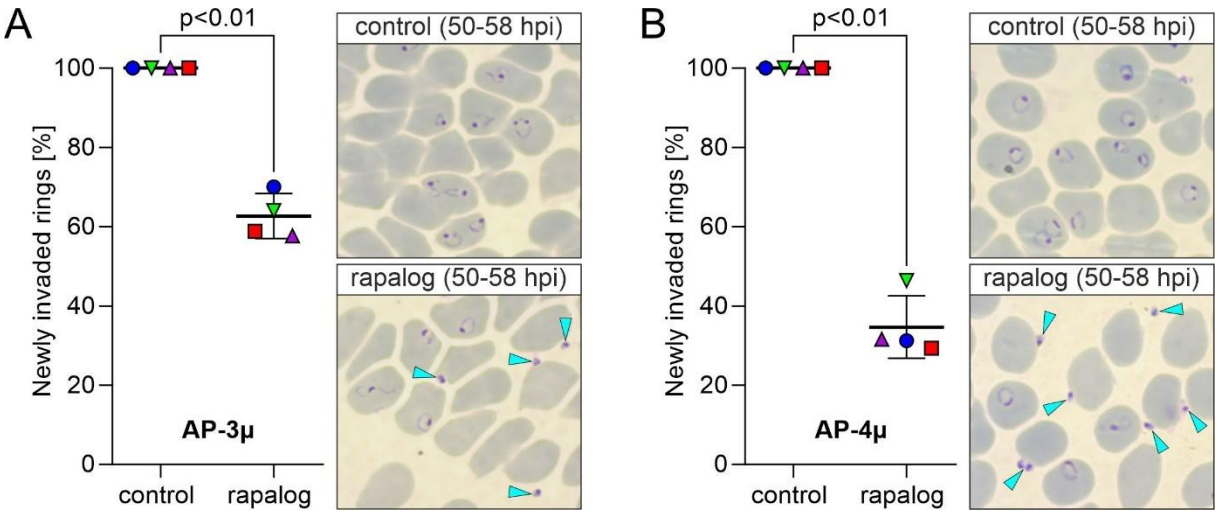

Figure 28. AP-3 and AP-4 inactivation impacts erythrocyte invasion.
(A and B) Newly invaded rings after AP-3 (A) and AP-4 (B) knock sideways as percent of control (n = 4 independent experiments, counting rings per 2000 RBCs per condition per experiment). Error bars represent mean ± SD. P-value determined by paired t-test. Images show representative example areas of Giemsa smears at 50-58 hpi time point for AP-3μ^{endo} and AP-4μ^{endo}. Arrows show free merozoites (indicator for invasion defectiveness).

4.1.3 Conditional inactivation of AP-1 partially disrupts the trans-Golgi but not ER and cis-Golgi

As the inactivation of AP-1μ^{endo} had a significant effect on trophozoite-to-schizont development, the function of this adaptor was investigated in trophozoites to understand its role in the secretory system of malaria parasites. To explore this, AP-1μ^{endo} parasites were co-transfected with plasmids to episomally overexpress STEVOR$_{1-30}$-mScarlet-SDEL (ER, (Külzer et al., 2009; Birnbaum et al., 2020)), GRASP-mScarlet (cis-Golgi, (Struck et al., 2005)) and mScarlet-Rab6 (trans-Golgi, (Struck et al., 2008)) under the control of the *crt* promoter (Heiber et al., 2013). Next, knock sideways was carried out by conditionally inactivating synchronous ring stage parasites and the resultant effect was analysed in the trophozoite stage (24-32hpi) by fluorescence microscopy (see schematic of inactivation in Figure 29A).

Images of control parasites revealed that AP-1μ^{endo} localised distal to the ER (Figure 29B), close to the cis-Golgi (Figure 29C; as described in section 4.1.1.2) and overlapped with the Rab6 foci at the trans-Golgi (Figure 29E), supporting the interpretation that AP-1μ^{endo} is located at the trans-Golgi (Figure 29E; of note, no co-localisation with the perinuclear pool of Rab6 corresponding to the ER was observed). Upon inactivation of AP-1μ^{endo}, no effect on the morphology of the ER and cis-Golgi was apparent (Figure 29B and C). A modest, yet statistically significant, reduction in the number of GRASP foci per single-nucleus trophozoite was likely due to a delay in parasite development rather than an effect on the integrity of the cis-Golgi (Figure 29D). Conversely, AP-1μ^{endo} inactivation affected the trans-Golgi compartment, as most cells (~87%) showed a diffuse cytosolic pool of Rab6 that was not present in the control (Figure 29E and F). The presence of some of the Rab6 remaining in trans-Golgi-like foci may be indicative of a partially functional trans-Golgi (Figure 29E). The results suggest that AP-1μ^{endo} inactivation does not visibly influence the secretory pathway up to the cis-Golgi, but leads to a partial dispersal of Rab6, pointing to partial disorganisation of the trans-Golgi compartment.

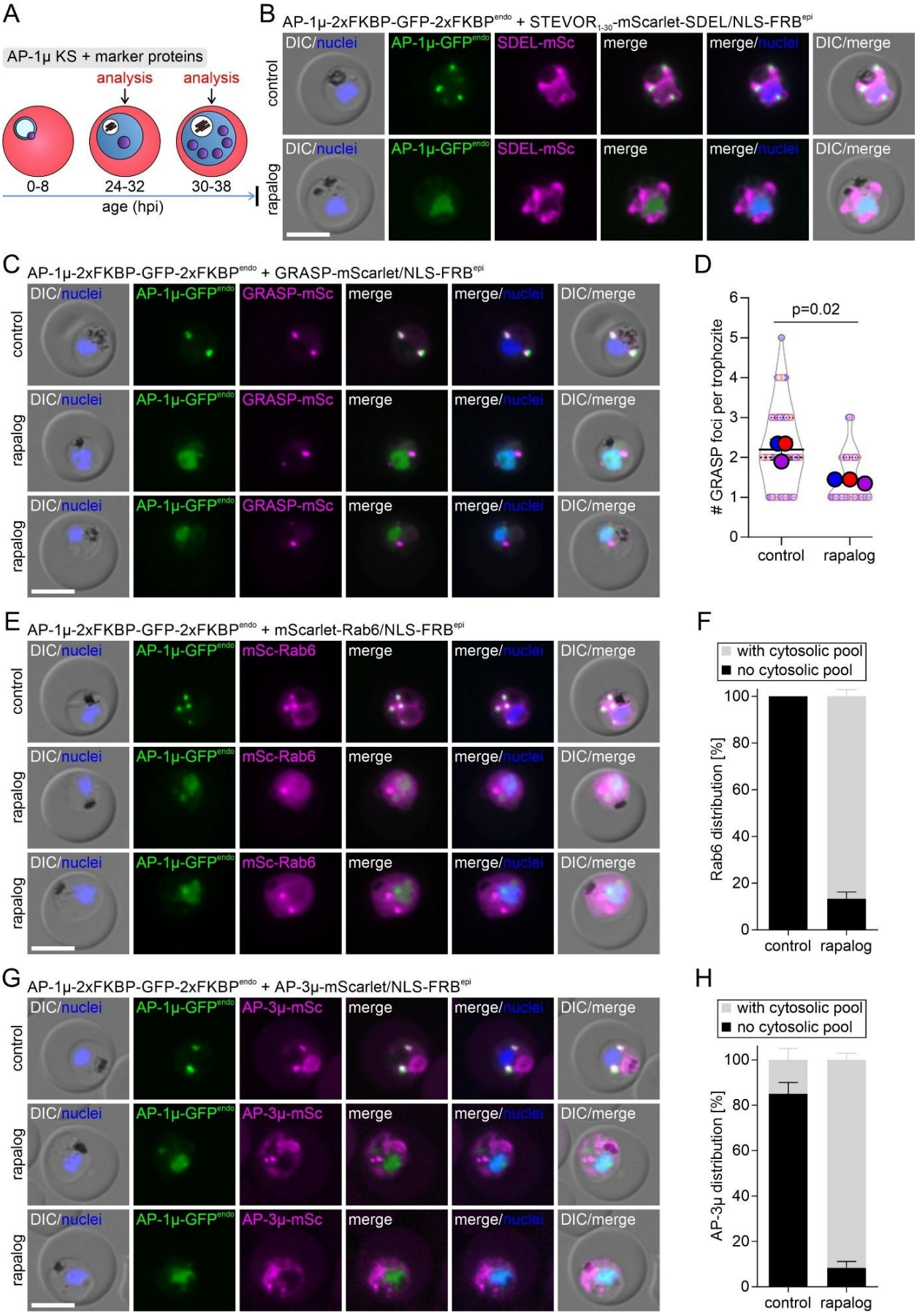

Figure 29. Effect of AP-1 inactivation on ER, Golgi, and trans-Golgi.

(A) Scheme showing timing of AP-1 inactivation used for the experiments in this figure. **(B and C)** Live-cell microscopy images of knock sideways (rapalog) and control AP-1μ^{endo} parasites episomally expressing STEVOR$_{1-30}$-mScarlet-SDEL (B) or GRASP-mScarlet (C). Scale bar: 5μm. Nuclei: Hoechst; DIC, differential interference contrast; merge, overlay of green and magenta channels. **(D)** Quantification of GRASP foci per one-nucleus trophozoite after AP-1 knock sideways with each 20 parasites per condition per replicate in 3 independent experiments; large dots, mean of each experiment; small dots, individual data points; data presented following SuperPlot guidelines (Lord et al., 2020); error bars, mean ± SD; P-value, paired t-test. **(E)** Live cell microscopy images as in B, but with AP-1μ^{endo} parasites episomally expressing mScarlet-Rab6. **(F)** Quantification of percent of cell showing Rab6 dispersal phenotype after AP-1 knock sideways with each 20 parasites per condition per replicate in three independent experiments. Coloured error bars represent mean ± SD. **(G)** Live cell microscopy images as in (B), but with AP-1μ^{endo} parasites episomally expressing AP-3μ-mScarlet. **(H)** Quantification of percent of cell showing AP-3μ dispersal phenotype after AP-1 knock sideways with each 20 parasites per condition per replicate in three independent experiments. Coloured error bars represent mean ± SD.

In order to determine whether this was a general or AP-1μ^{endo} -restricted effect on the integrity of the trans-Golgi, the impact of AP-1μ^{endo} inactivation was assessed using AP-3, an adaptor which resides in the trans-Golgi (see section 4.1.1.2) but is unlikely to contribute to the same vesicle sorting pathway as the one mediated by AP-1. To carry out this experiment, AP-1μ^{endo} parasites were co-transfected with a plasmid to episomally overexpress AP-3μ-mScarlet (Mesén-Ramírez et al., 2025). The results showed that AP-1μ^{endo} only partially overlapped with AP-3 (Figure 29G), indicating that both adaptins may reside in different sub-compartments of the trans-Golgi. However, upon AP-1 inactivation, AP-3 exhibited a dispersed pool in the parasite cytosol (~92%), along with foci that likely corresponded to AP-3 remaining at the trans-Golgi (Figure 29G and H), indicating that the effect of AP-1 inactivation was not restricted to Rab6. Taken together, these findings suggest that AP-1 inactivation results in a partial disruption of the trans-Golgi compartment beyond the areas directly involved in AP-1-dependent vesicle trafficking.

4.1.4 AP-1 inactivation does not impact endocytosis and protein export

In view of the effect of AP-1 inactivation on the trans-Golgi, general protein trafficking was assessed when AP-1 was inactivated. In the context of malaria parasites, a classical N-terminal signal peptide (SP) is sufficient for a protein to enter the default secretory pathway, and the addition of a SP to a fluorescent protein leads to the transport to the PV lumen (Adisa et al., 2003) which surrounds the intracellular parasite. To test whether this transport route was still

operational, AP-1µ^{endo} parasites episomally expressing SP-mScarlet (Mesén-Ramírez et al., 2019) were conditionally inactivated in early-stage parasites and the effect was monitored in trophozoite stage (24-32 hpi) (Figure 29A). No discernible difference in the distribution of SP-mScarlet was observed between control and knock sideways parasites, as SP-mScarlet was transported to the PV lumen and re-internalised to the FV (Figure 30A). This finding indicated that both general secretion and endocytosis processes were not affected. The conclusion that endocytosis was not impaired was also supported by the fact that hemozoin was still found in the FV (Figure 30A).

In order to assess endocytosis, AP-1µ^{endo} parasites episomally expressing 1xNLS-FRB-mCherry were used to conditionally inactivate AP-1µ^{endo} in the ring stage by adding rapalog and examined in the trophozoite stage (24-32 hpi) (Figure 29A). Subsequent IFAs were then performed by fixing the parasites with 4% FA + 0.0075% GA and using antibodies raised against the 19 KDa C-terminal fragment of MSP1 (MSP1$_{19}$ (Dluzewski et al., 2008)), a marker that is internalised from the PPM to the FV membrane during haemoglobin endocytosis (Dluzewski et al., 2008). The results of the control and knock sideways parasites showed no gross detrimental impact on endocytosis, as MSP1$_{19}$ was internalised from the PPM to the FV (Figure 30B).

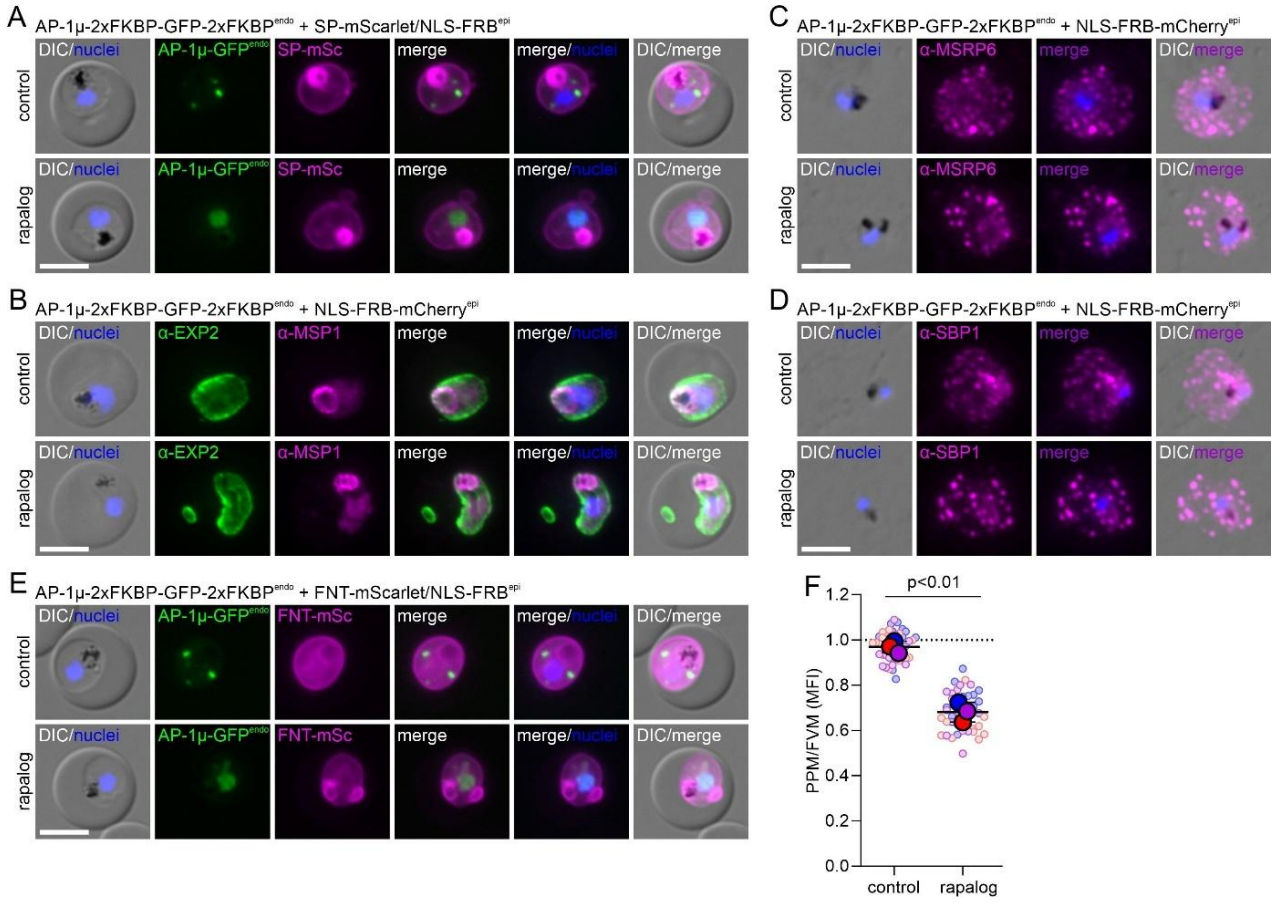

Figure 30. Effect of AP-1 inactivation on general secretion and protein export.
(A) Live-cell microscopy images of knock sideways (rapalog) and control AP-1µ^{endo} parasites overexpressing SP-mScarlet. **(B)** Microscopy images of IFA with FA/GA-fixed knock sideways (rapalog) and control AP-1µ^{endo} parasites detecting EXP2 (green) and MSP1$_{19}$ (magenta). Results from one replicate with 20 inspected cells. A second IFA experiment using acetone fixed parasites to detect EXP2 showed similar results. **(C and D)** Microscopy images of IFA with acetone-fixed knock sideways (rapalog) and control AP-1µ^{endo} parasites detecting MSRP6 (C) and SBP1 (D). Results from two independent replicates. **(E)** Live-cell microscopy images of knock sideways (rapalog) and control AP-1µ^{endo} parasites expressing FNT-mScarlet. Scale bars, 5µm; nuclei were stained with Hoechst; DIC, differential interference contrast; merge, overlay of green and magenta channels. **(F)** Relative fluorescence of FNT signal at the PPM compared to FV membrane in AP-1 knock sideways with each 15 parasites per condition per replicate in 3 independent experiments; mean of each experiment indicated by large circle, individual measurements by small circles). Data presented following SuperPlot guidelines (Lord et al., 2020), error bars, mean ± SD; P-value determined by paired t-test.

Given the finding that knock sideways of AP-1µ^{endo} had not impact on general secretion and endocytosis, trafficking beyond the boundaries of the parasite was assessed. In order to test this, the same fixed parasites used for detection of MSP1$_{19}$ (Figure 30B), were also used for IFAs using antibodies raised against EXP2, a PTEX component that is located in the PVM (De Koning-Ward et al., 2009). The results of the control and knock sideways parasites showed no defect on transport to the PVM, as EXP2 was trafficked to the PVM (Figure 30B). In addition,

protein export was assessed. AP-1µ^{endo} parasites expressing 1xNLS-FRB-mCherry were used to inactivate AP1µ in early-stage parasites and analysed in the trophozoite stage (24-32 hpi) upon fixation with acetone (Figure 29A). IFAs using antibodies specific against the Maurer's cleft markers SBP1 (an exported protein with transmembrane domain) (Blisnick et al., 2000) and MSRP6 (an exported protein without transmembrane domain) (Heiber et al., 2013) revealed no differences in the export of these proteins into the host cell between control and knock sideways parasites (Figure 30C and D), indicating that protein export remains functional in parasites with inactivated AP-1. These observations suggest that default transport through the secretory system to deliver proteins to the PPM and beyond the confines of the parasite does not depend on the AP-1 sorting pathway at the trans-Golgi.

To understand whether secretory trafficking of transmembrane proteins to the PPM was affected, AP-1µ^{endo} parasites episomally overexpressing the multipass PPM protein formate-nitrate transporter FNT-mScarlet (Wu et al., 2015) were used to inactivate AP-1µ^{endo} in early-stage parasites and examined in the trophozoite stage (Figure 29A). In both control and knock sideways AP-1µ^{endo} parasites, FNT-mScarlet was localised at the PPM and FV membrane (Figure 30E), thereby supporting the notion that there was no significant impact on default secretion. However, inactivation of AP-1 resulted in a relative increase of the FNT signal in the FV membrane compared to the PPM (Figure 30E and F), indicating that this could either be due to a decreased outward vesicular trafficking while endocytosis is maintained at an unchanged rate or due to impaired recycling of internalised FNT.

4.1.5 AP-1 partially impacts the distribution of Rab7

In order to assess the impact of AP-1 inactivation on the organellar integrity and trafficking to the FV, AP-1µ^{endo} parasites were co-transfected to episomally express P40PX-mScarlet, a PI(3)P reporter which labels the FV membrane and FV-adjacent circular structures (Tawk et al., 2010), and Plasmepsin II-(fused to mScarlet), a protease involved in haemoglobin degradation that reaches the FV via endocytic re-internalisation (Klemba et al., 2004a). An analysis of control and knock sideways parasites showed that the localisation of P40PX and Plasmepsin II remained seemingly unaltered, as both markers exhibited association with the FV (Figure 31A and B), indicating no detrimental effects on transport to this organelle or its integrity. It also further (in addition to the results from section 4.1.4) indicated no negative impact on endocytic processes.

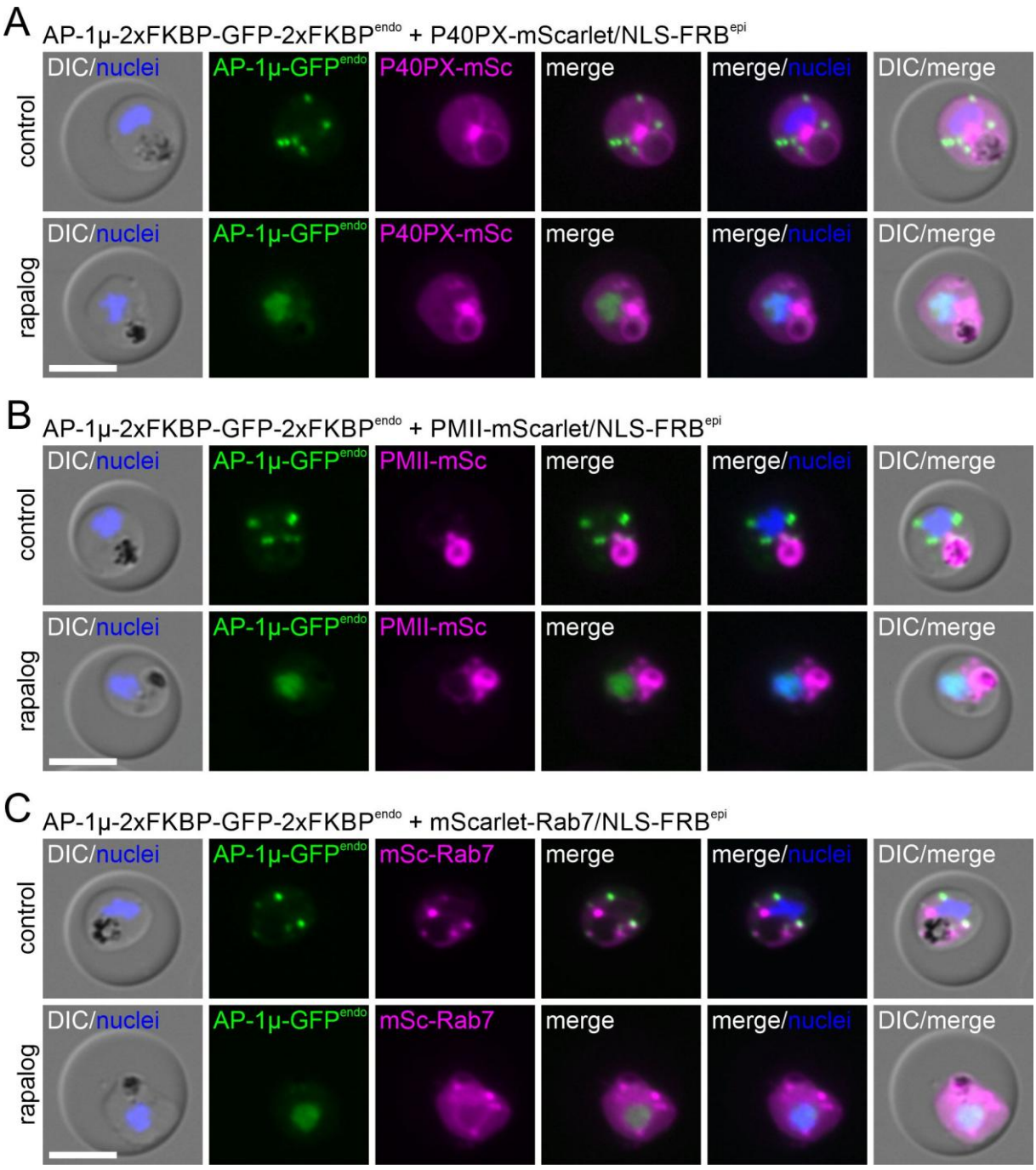

Figure 31. Effect of AP-1 inactivation on integrity and trafficking to the FV, and endosomes.
(A-C) Live-cell microscopy images of knock sideways (rapalog) and control AP-1μ^{endo} parasites episomally expressing P40PX-mScarlet (A), Plasmepsin II-mScarlet (B) and mScarlet-Rab7 (C). Results from three independent replicates with at least 20 parasites per replicate. Scale bar: 5μm. Nuclei were stained with Hoechst. DIC, differential interference contrast. Merge, overlay of green and magenta channels.

The distribution of Rab7, a marker of late endosomes in other organisms (Borchers et al., 2021) and proposed to be at endosomes in the parasite (Krai et al., 2014) was also studied. AP-1 parasites episomally expressing mScarlet-Rab7 were used to inactivate AP-1 in early-stage

parasites and assessed in trophozoites (Figure 29A). In control parasites, AP-1 was found in proximity to some but not all Rab7 foci, indicating that they reside in different compartments. Conditional inactivation of AP-1 resulted in an increased cytosolic pool of Rab7, while another pool appeared to be associated with accumulations that may constitute its original location and might correspond to endosomal compartments (Figure 31C). As AP-1 knock sideways had no apparent impact on endocytosis, this finding might indicate an effect on trans-Golgi to endosome trafficking, a role previously proposed for Rab7 (Krai et al., 2014).

4.1.6 Conditional inactivation of AP-1 leads to ultrastructural alterations in the parasite

Examination of Giemsa-stained smears inactivation of AP-1 in early-stage parasites revealed the presence of parasites with vacuole-like structures (Figure 26B). On the basis of this finding, AP-1 parasites expressing 1xNLS-FRB-mCherry were conditionally inactivated early in the cycle, and the knock sideways phenotype was analysed at the ultrastructural level by electron microscopy either at the trophozoite stage (24-32 hpi) or during schizont development (30-38 hpi) (see schematic in Figure 29A). Control parasites typically underwent the trophozoite-to-schizont transition, displaying normal FV, haemoglobin-filled vesicular structures, as well as apical organelles in segmented schizonts (Figure 32). However, inactivation of AP-1 resulted in the presence of unusual compartments with a translucent lumen in the parasite cytosol (24-32 hpi) that grew more prominent at the 30-38 hpi time point (Figure 32, purple arrows). These large translucent areas may correspond to the “vacuolization” phenotype detected in Giemsa smears (Figure 26B). Furthermore, an increase in ribosome-positive membranes was detected (turquoise arrows, Figure 32).

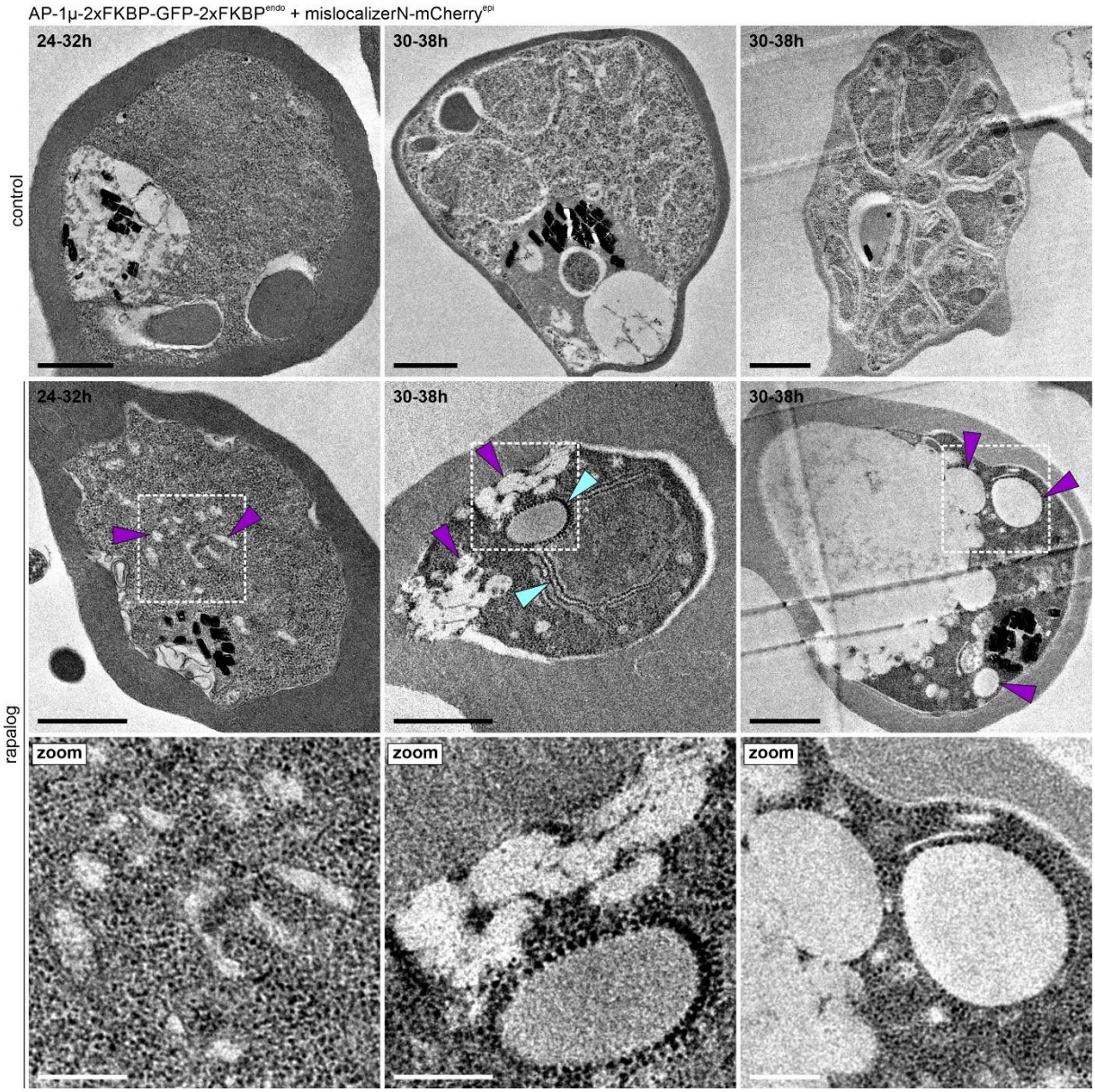

Figure 32. Effect of AP-1 inactivation on the ultrastructural level.
EM micrographs of knock sideways (rapalog) and control AP-1µ^{endo} parasites induced in ring stage and analysed at the indicated 24-32 hpi and 30-38 hpi time points (see schematic in Figure 20A). Boxed areas were enlarged (zoom). Arrows show vacuole-like vesicular structures (purple) and ER-attached ribosomes (turquoise). Scale bars, 1µm (black) and 300 nm in enlargements (white).

The presence of ribosome-studded membranes might indicate a backlog and stalling of ER protein import, possibly due to reduced post-Golgi trafficking. Additionally, there also appears to be an accumulation of intracellular membranes and vesicular structures (Figure 32), which may result from a reduced outgoing vesicular transport or a failure to recycle material back to the trans-Golgi. Overall, inactivation of AP-1 rapidly leads to profound ultrastructural

alterations in the parasite and a severe phenotype within a short timeframe (hours) in the parasite.

4.1.7 Proxiome of AP-1

With the aim to define the components of the AP-1-mediated vesicle trafficking machinery in the parasite, a conditional version of proximity labelling, DiQ-BioID (Birnbaum et al., 2020; Kimmel et al., 2022), was used to identify the proxiome (interactors and compartment neighbours) of AP-1 in living parasites. A key advantage of the DiQ-BioID is that background biotinylation in the same parasite culture can be subtracted, resulting in highly specific proxiomes (Kimmel et al., 2022). The replacement of the classical biotin ligase BirA* (requiring 18-24 h biotinylation time) for miniTurbo (30 minutes biotinylation time) for DiQ-BioID was here done based on previous reports which showed that the use of miniTurbo reduced incubation times of biotin labelling (Branon et al., 2018; Kimmel et al., 2022).

To explore this, AP-1^{endo} parasites were co-transfected with plasmids to episomally express miniTurbo-FRB-mCherry (miniTurbo-N^{L}) or mCherry-FRB-miniTurbo (miniTurbo-C^{L}) (both of which were kindly provided by Gala Ramón-Zamorano and corresponded to the DiQ-BioID plasmids from (Birnbaum et al., 2020) where the sequence encoding BirA* had been replaced with miniTurbo) under the control of the *sf3a2* promoter. Using asynchronous parasite cultures (5 – 10% parasitemia), either the N- or the C-terminal miniTurbo-FRB versions were conditionally recruited to the endogenously FKBP-tagged AP-1µ subunit (by adding rapalog), where they biotinylated AP-1 proximal proteins (Figure 33A). Fluorescence microscopy images of control parasites (only biotin) showed the biotinylizer being distributed in the parasite cytosol, whereas parasites with rapalog (rapa and biotin) exhibited a recruitment of the biotinylizer to the AP-1 foci (Figure 33A). A quantitative mass spectrometry analysis of biotinylated proteins was then performed to compare rapalog (miniTurbo recruited to target) over control (miniTurbo cytoplasmic) (Figure 33B and Appendices 6 and 9). Mass spectrometry analysis (kindly carried out by Gala Ramón-Zamorano in the Bartfai lab, Radboud University, Nijmegen, The Netherlands) resulted in a list of high-confidence hits (Figure 33B and C and Appendices 6).

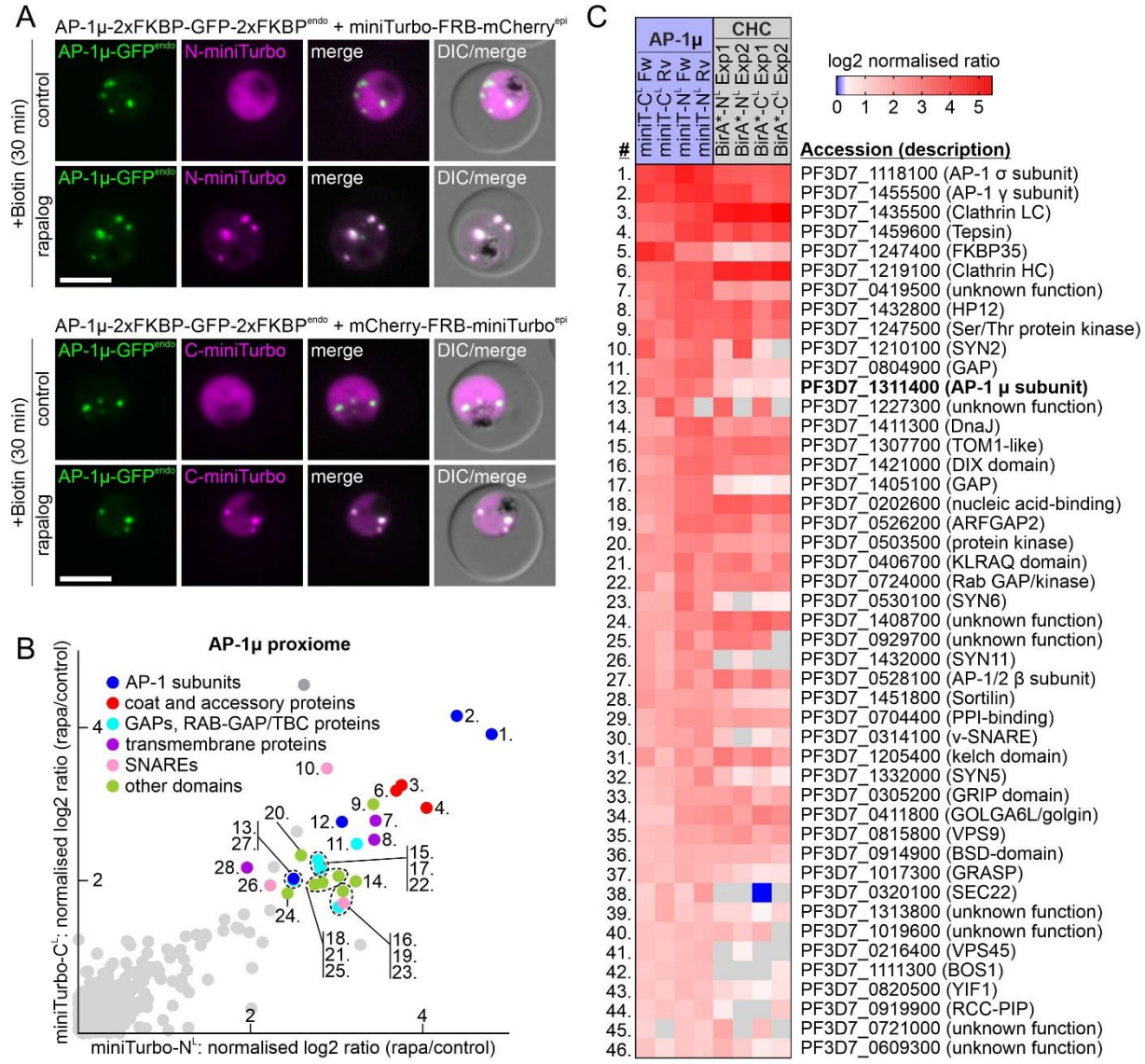

Figure 33. Proxiome of AP-1.

(A) Live-cell microscopy images of AP-1μ^{endo} parasites expressing miniTurbo-N^{L} or miniTurbo-C^{L} grown in the presence of rapalog (miniTurbo recruited to AP-1 foci) or not (miniTurbo cytoplasmic) for 30 minutes. Scale bar: 5μm. Nuclei were stained with Hoechst; merge, overlay of green and magenta channels; DIC, differential interference contrast. **(B)** Top-right quadrant of scatter plot of AP-1 DiQ-BioID showing proteins enriched (log2 ratio) on rapalog (biotinylizer on target) compared with control (biotinylizer free in cytoplasm) from the miniTurbo-N^{L} (fw technical replicate) and miniTurbo-C^{L} (fw technical replicate) expressing cell lines. Full plots of fw and rv technical replicates are shown in Appendix 9. Significantly enriched proteins (log2 fold change >2) are coloured into general groups; proteins below the threshold, light grey; known contaminants, dark grey. IDs of numbered proteins are indicated in (C). **(C)** Heatmap comparing AP-1 (this study) and CHC (Birnbaum et al., 2020) DiQ-BioIDs, including the proteins enriched in at least three of four experiments with an FDR of 0.05 or smaller, corrected p-value <0.1 and log-2 enrichment >1 for the AP-1μ dataset. No value obtained (NaN), grey; bold font, DiQ-BioID bait.

The AP-1 proxiome included all subunits of the AP-1 complex and the clathrin heavy and light chains (Figure 33B and C and Appendices 6 and 9). The γ and σ AP-1 subunits as well as the clathrin chains were even more highly enriched than the μ subunit, which had served as bait. The presence of clathrin was consistent with the previously published CHC DiQ-BioID (Birnbaum et al., 2020), indicating that, as in model organisms, AP-1 functions in a clathrin-dependent manner in malaria parasites. A comparison of the AP-1 DiQ-BioID results of this study and the CHC DiQ-BioID (Birnbaum et al., 2020) showed that the vesicle fusion machinery (Syntaxins, SNAREs and SEC22) and one highly enriched GAP were less consistently or not enriched in the clathrin proxiome (Figure 33C). This might indicate functions in vesicle fusion when the clathrin coat has already been lost, although it should be noted that some SNAREs can also be cargo of AP-1 and may therefore be present in coated vesicles (Peden et al., 2001; Hirst et al., 2012; Shimizu et al., 2021; Dahhan et al., 2022; Robinson et al., 2024). Sortilin, a multi-ligand sorting receptor (Malik & Willnow, 2020; Mitok et al., 2022), was also enriched (Figure 33B and C). Unexpectedly, tepsin (PF3D7_1459600), an ENTH domain-containing protein considered an accessory factor exclusive to the AP-4 complex (Borner et al., 2012; Mattera et al., 2015; Frazier et al., 2016), was one of the most enriched proteins (Figure 33B and C and Appendices 6 and 9). Conversely, the sole epsin-like protein (EpsL) (Kibria et al., 2016) of the parasite was not enriched. The AP-1 proxiome thus appears to comprise a plausible set of proteins necessary for vesicle coat assembly, cargo selection, and membrane fusion. This finding suggests that the AP-1 complex in malaria parasites functions in clathrin-dependent vesicular trafficking. Furthermore, a VHS domain containing TOM1-like protein was identified, which has also been previously found to be highly enriched in the clathrin BioID and pulldowns (Birnbaum et al., 2020; Henrici et al., 2020). The presence of typical Golgi proteins in the AP-1 proxiome, such as GRASP, indicated that the less highly enriched proteins also included general Golgi and resident trans-Golgi proteins (Figure 33B and C and Appendices 6 and 9).

4.1.7.1 Validation of interacting partners of AP-1 sortilin, tepsin and CLC

Based on the evidence provided by the AP-1 proxiome, three candidate interacting partners (sortilin, tepsin and clathrin) were selected for validation and further analysed for co-localisation and knock sideways studies. To investigate these candidates, AP-1μ^{endo} parasites episomally overexpressing sortilin-mScarlet (receptor for cargo proteins), tepsin-mScarlet

(accessory protein) and CLC-mScarlet (coat protein) were used to conditionally inactivate AP-1 at the ring stage and analysed at the trophozoite stage (24-32hpi) (Figure 29A).

Images of control trophozoites showed that sortilin colocalised with AP-1 at the trans-Golgi (Figure 34A). In contrast, when AP-1 was inactivated, all cells exhibited a mistargeting of sortilin to the PPM and FV membrane, which was evident in addition to the foci in the proximity of the nucleus, indicating that there was also a pool of sortilin remaining at the trans-Golgi (Figure 34A and B). The PPM pool of sortilin suggested that in the absence of AP-1, sortilin escaped to (or was not returned from) the PPM. The FV location was likely due to internalisation via endocytosis but may also be due to a failure to retrieve it from a trans-Golgi to FV route, although the AP-1 BioID did not give any indication for involvement in such a pathway (Figure 33B and C and Appendices and 9). Moreover, it was observed that the sortilin remaining in areas near the nuclei appeared less defined (Figure 34A and B), potentially indicating alterations of the distribution of this receptor at the trans-Golgi due to the absence of AP-1.

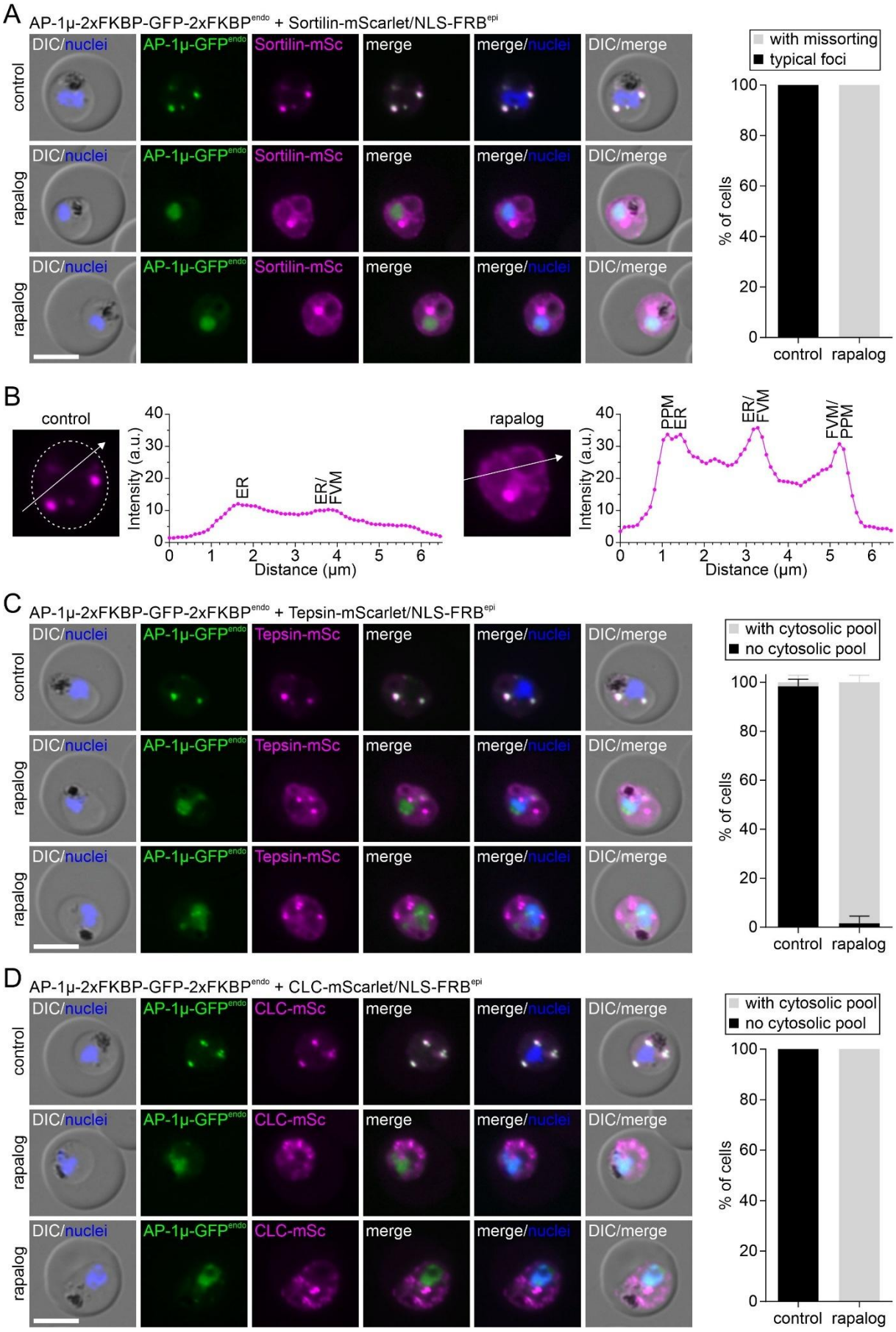
A
AP-1μ-2xFKBP-GFP-2xFKBP^endo + Sortilin-mScarlet/NLS-FRB^epi
DIC/nuclei
AP-1μ-GFP^endo
Sortilin-mSc
merge
merge/nuclei
DIC/merge
control
rapalog
with missorting
typical foci
% of cells
control
rapalog
B
control
rapalog
Intensity (a.u.)
Distance (μm)
ER
ER/FVM
PPM ER
FVM/PPM
C
AP-1μ-2xFKBP-GFP-2xFKBP^endo + Tepsin-mScarlet/NLS-FRB^epi
Tepsin-mSc
with cytosolic pool
no cytosolic pool
D
AP-1μ-2xFKBP-GFP-2xFKBP^endo + CLC-mScarlet/NLS-FRB^epi
CLC-mSc

Figure 34. Validation of AP-1 DiQ-BioID candidates.
(A) Live-cell microscopy images of knock sideways (rapalog) and control AP-1μ^{endo} parasites episomally expressing sortilin-mScarlet. Graph shows quantification of % cells with indicated sortilin phenotype; n = 3 independent experiments with each 20 parasites per condition per replicate. **(B)** Example intensity plot of sortilin signal (arbitrary units, a.u.) in the cells from (D). Dotted circle: PPM in control parasites. **(C and D)** Live-cell microscopy images of knock sideways (rapalog) and control AP-1μ^{endo} parasites episomally expressing tepsin-mScarlet (F) or CLC-mScarlet (G). Graphs show quantification of % cells with the indicated phenotype of tepsin (C) or CLC (D); n = 3 independent experiments with each 20 parasites per condition per replicate per cell line. All scale bars: 5 μm; nuclei were stained with Hoechst; DIC, differential interference contrast; merge, merged green and magenta channels.

The unanticipated identification of tepsin in the AP-1 proxiome suggested a marked discrepancy in the configuration of the AP-1 vesicle machinery of the parasite in comparison to that observed in model organisms. Consequently, tepsin was investigated. In control parasites, this accessory factor overlapped with AP-1 at the trans-Golgi (Figure 34C), congruent with the results of the AP-1 proxiome. Upon conditional inactivation of AP-1, the distribution of tepsin was altered, resulting in a cytoplasmic pool (Figure 34C). This finding indicates that in the absence of functional AP-1, tepsin was released from the trans-Golgi, pointing to a direct function with AP-1. Similar to sortilin, a proportion of tepsin remained in nucleus-proximal areas, however, in this case, the foci appeared similar to controls (Figure 34C).

As clathrin was also identified in the AP-1 proxiome, this coat protein was investigated. In control parasites, the episomally expressed CLC colocalised with AP-1 at the trans-Golgi (Figure 34D), in a similar localisation to sortilin and tepsin (Figure 34A and C) and matching the initial localisation analysis (Figure 21). After the inactivation of AP-1, a dispersed pattern of CLC was observed, with some clathrin remaining in nuclear proximity likely constituting its original location (Figure 34D). The profound effect on CLC when AP-1 was inactivated supports the hypothesis that AP-1-dependent vesicle trafficking machinery functions with a clathrin coat.

Taken together, these findings imply that the inactivation of AP-1 leads to a partial loss of sortilin, tepsin and clathrin at the trans-Golgi, with sortilin being missorted to the PPM and FV. As general secretory transport beyond the parasite boundaries was not inhibited (Figure 30), these effects are not due to a general disintegration of the trans-Golgi compartment, but are specific for AP-1, providing support for a function of these proteins in AP-1 sorting, as indicated by the BioID results.

4.1.8 AP-1 is needed for the biogenesis of rhoptries and micronemes

The preliminary characterisation of AP-1 indicated that this adaptor complex plays a significant important role during the schizont stage of parasite development (Figure 26D). Schizonts with inactivated AP-1 appeared to be "segmented" in some way, but never progressed to form ring stage parasites in the next cycle. In light of this evidence, AP-1 parasites were co-transfected to episomally express ARO-mCherry (cytosolic face of the rhoptry bulb), RON12-mCherry (luminal face of the rhoptry neck) (plasmid kindly provided by Guilherme B. Farias) and AMA1-mCherry (micronemes) under the control of the *ama1* promoter.

AP-1 was conditionally inactivated in synchronous parasites before they started cytokinesis (28-36 hpi) and the integrity of the apical secretory organelles was examined in late schizonts (42-50 hpi) (see schematic in Figure 35A). In order to obtain a comparable population of schizonts in the rapalog and control conditions, an important step consisted in the addition of compound 2 (C2), a PKG inhibitor that irreversibly arrests the segmented schizonts at the end of erythrocytic schizogony, thus preventing the egress of daughter merozoites (Taylor et al., 2010; Collins et al., 2013) (Figure 35A).

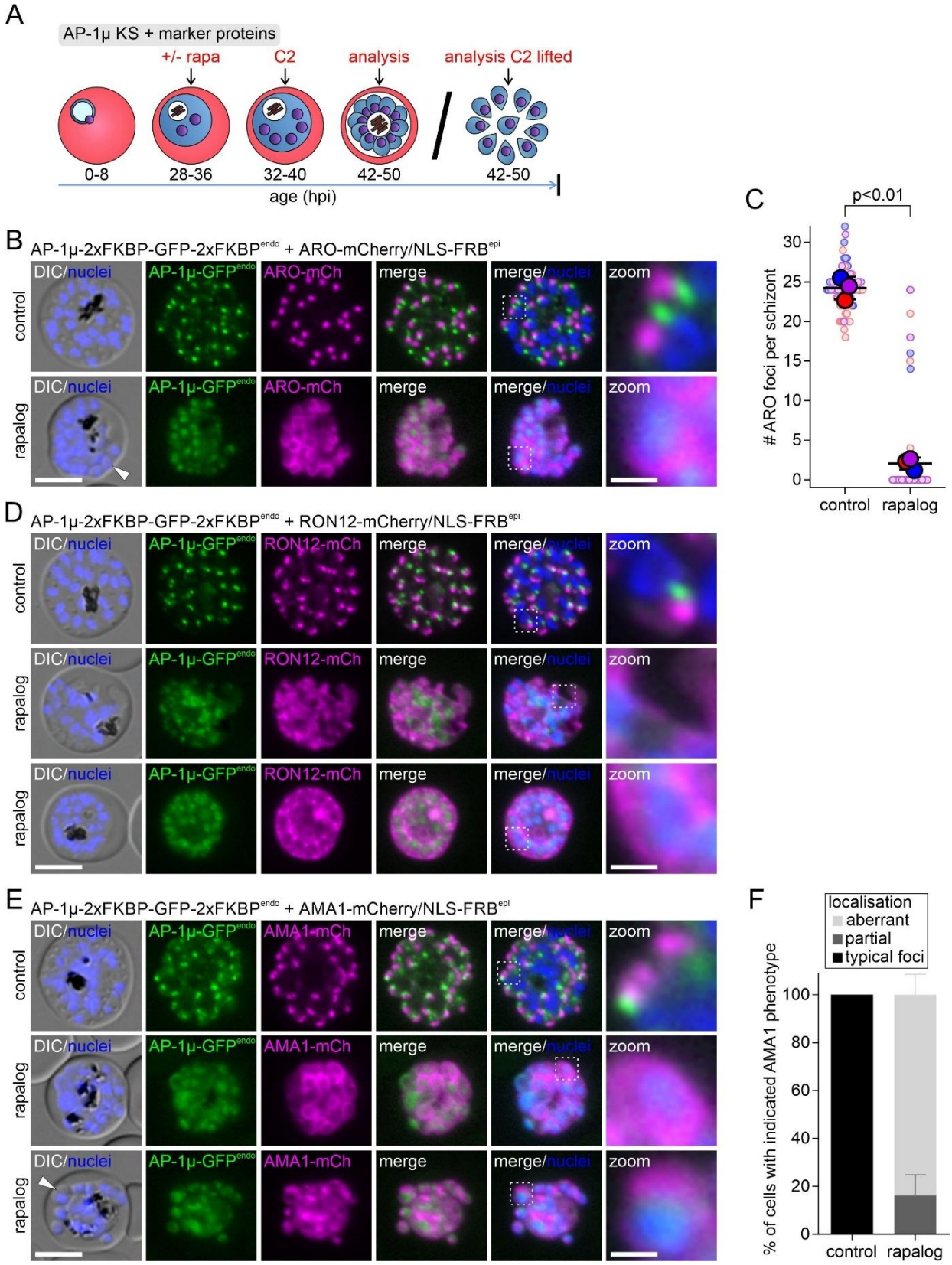

Figure 35. Effect of AP-1 inactivation on the biogenesis of rhoptries and micronemes.
(A) Schematic of AP-1 inactivation late in the cycle used for the experiments in this figure. C2, compound 2. **(B)** Live-cell microscopy images of knock sideways (rapalog) and control AP-1µ^{endo} parasites episomally expressing ARO-mCherry, representative images from 3 independent experiments quantified in (C). **(C)** Quantification of number of ARO foci per schizont, n = 25, 25 and 25 rapalog and

25, 25 and 17 control parasites in three independent experiments. Mean of each experiment is indicated by coloured large circle and individual data points per cell by coloured small circle. Data is presented following the SuperPlot guidelines (Lord et al., 2020), error bars represent mean ± SD. P-value is determined by paired t-test. **(D and E)** Live-cell microscopy images of knock sideways (rapalog) and control AP-1μ^{endo} parasites episomally expressing RON12-mCherry (D) or AMA1-mCherry (E), representative images from 2 (D) and 4 (E) independent experiments. (E) is quantified in (F). Boxed areas in B, D and E were enlarged (zoom). Scale bar: 5 μm (1 μm for zoomed section). Nuclei were stained with Hoechst; merge, overlay of green and magenta channels; DIC, differential interference contrast. **(F)** Quantification of number of cells with indicated AMA1 phenotype from (E), n = 20 parasites per condition per replicate in four independent experiments. Coloured error bars represent mean ± SD.

In control C2-arrested schizont parasites, AP-1 was localised in proximity to, but not overlapping with, the rhoptries (ARO and RON12) and micronemes (AMA1) (see Figure 35B, D and E), which is consistent with its trans-Golgi localisation. However, the inactivation of this adaptor resulted in a drastic alteration in the localisation of ARO with a peripheral distribution around the nuclei (Figure 35B). Quantification showed an almost complete loss of detectable ARO foci per schizont (Figure 35C). Given that ARO is attached to the cytosolic face of rhoptries and therefore is not expected to require vesicular trafficking to reach this site (A. Cabrera et al., 2012), this indicated that the integrity of the rhoptries was severely compromised or that they were missing altogether. In agreement with a loss of the rhoptries, RON12 was found to be diffusely distributed in the cytosol or transported to the PV space (Figure 35D). A drastic phenotype of AP-1 inactivation was also observed for AMA1 with the signal surrounding the nuclei (classified as “aberrant” in Figure 35E and F) or in a cytosolic distribution with poorly defined foci (classified as “partial” in Figure 35E and F), indicating either mistargeting of AMA1 or absence of the micronemes.

4.1.9 AP-1 is needed for the biogenesis of dense granules and IMC

As the integrity of the invasion organelles, rhoptries and micronemes, was affected, the characterisation of the schizont phenotype was extended to the dense granules/PVM and the IMC. AP-1 parasites episomally expressing EXP2 were used to conditionally inactivate AP-1, and the phenotype was analysed after lifting C2 to obtain merozoites or in C2-arrested schizonts as described for the analysis of the rhoptry and microneme markers (section 4.1.8 and schematic in Figure 35A).

The results showed that AP-1 was found in proximity but not overlapping with dense granule-associated EXP2 in merozoites (Figure 36A) and surrounded by PVM-associated EXP2 in schizonts (Figure 36B). Conversely, AP-1 inactivation caused a diffuse distribution pattern in merozoites (Figure 36A) and an accumulation of EXP2 in foci in the cytosol of the aberrantly segmented parasites (Figure 36B), indicating a negative impact on the dense granules.

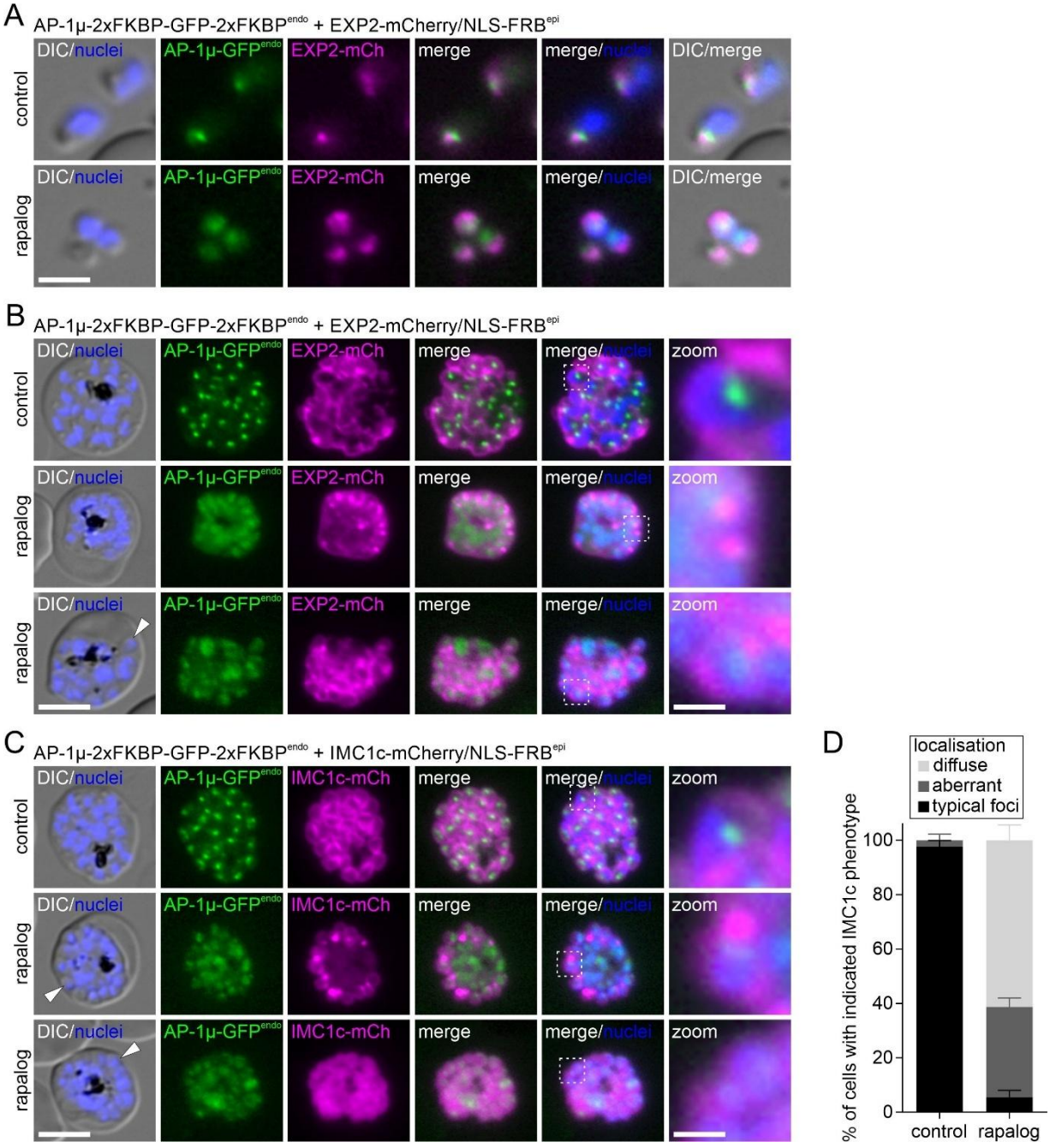

Figure 36. Effect of AP-1 inactivation on the biogenesis of dense granules and IMC.
(A-C) Live-cell microscopy images of knock sideways (rapalog) and control AP-1µ^{endo} parasites episomally expressing EXP2-mCherry without (A, merozoites) or with C2 (B, segmented schizonts) or

IMC1c-mCherry (C), n = at least 3 independent experiments analysing at least 25 parasites per condition per replicate. Boxed areas in B and C were enlarged (zoom). Scale bar: 5 μm (1 μm for zoomed section). Nuclei were stained with Hoechst; merge, overlay of green and magenta channels; DIC, differential interference contrast. **(D)** Quantification of number of cells with the indicated IMC1c phenotype from (C); n = 40, 34, 37 and 37 rapalog and 40, 18, 39 and 23 control schizonts in four independent experiments. Coloured error bars represent mean ± SD.

Next, the IMC, a flattened membrane organelle underlying the PPM that is formed during the late schizogony, was inspected. AP-1 parasites were co-transfected with a plasmid episomally expressing the IMC marker IMC1c-mCherry under the control of the *ama1* promoter (Schmidt et al., 2023) and AP-1 inactivated by knock sideways (see schematic in Figure 35A). As expected, in control parasites, AP-1 was observed to be surrounded by IMC1c (Figure 36C). After inactivation of AP-1, IMC1c showed a diffuse pattern within the parasite cytosol (classified as "diffuse" in Figure 36C and D), while in other parasites evidenced a partially or aberrantly formed (classified as "aberrant" in Figure 36C and D). The data presented here indicates that AP-1 plays an important role in the biogenesis of apical secretory organelles and the IMC.

4.1.10 AP-1 plays a role in the cytokinesis process

The examination of the DIC images showed that AP-1 knock sideways schizonts appeared to form at least some nascent merozoites (white arrows in Figure 35 and 36), raising the question of whether the cytokinesis process was disrupted or not. Therefore, the PPM (which will engulf the newly formed merozoites once segmentation is complete) was used as a reference to assess the level of segmentation. AP-1 parasites expressing the 1xNLS-FRB-mCherry were used to conditionally inactivate AP-1 before the onset of segmentation (28-36 hpi) and evaluated in C2-treated late schizonts (42-50 hpi) after fixation with FA/GA (see schematic in Figure 35A).

Subsequently, IFA was performed using antibodies raised against $MSP1_{19}$, a protein expressed on the parasite surface connected to the PPM via a GPI anchor (Dluzewski et al., 2008). In control parasites, it was observed that each daughter merozoite was surrounded by $MSP1_{19}$ (Figure 37A), indicating that they were properly segmented. By contrast, in knock sideways parasites, a small proportion of fully-segmented cells were noticed, whereas most of the parasites displayed partial (only some segmented areas per schizont, defined as "aberrant", Figure 37A and B) or no segmentation (Figure 37A and B), suggesting that loss of the adaptor partially impaired cytokinesis.

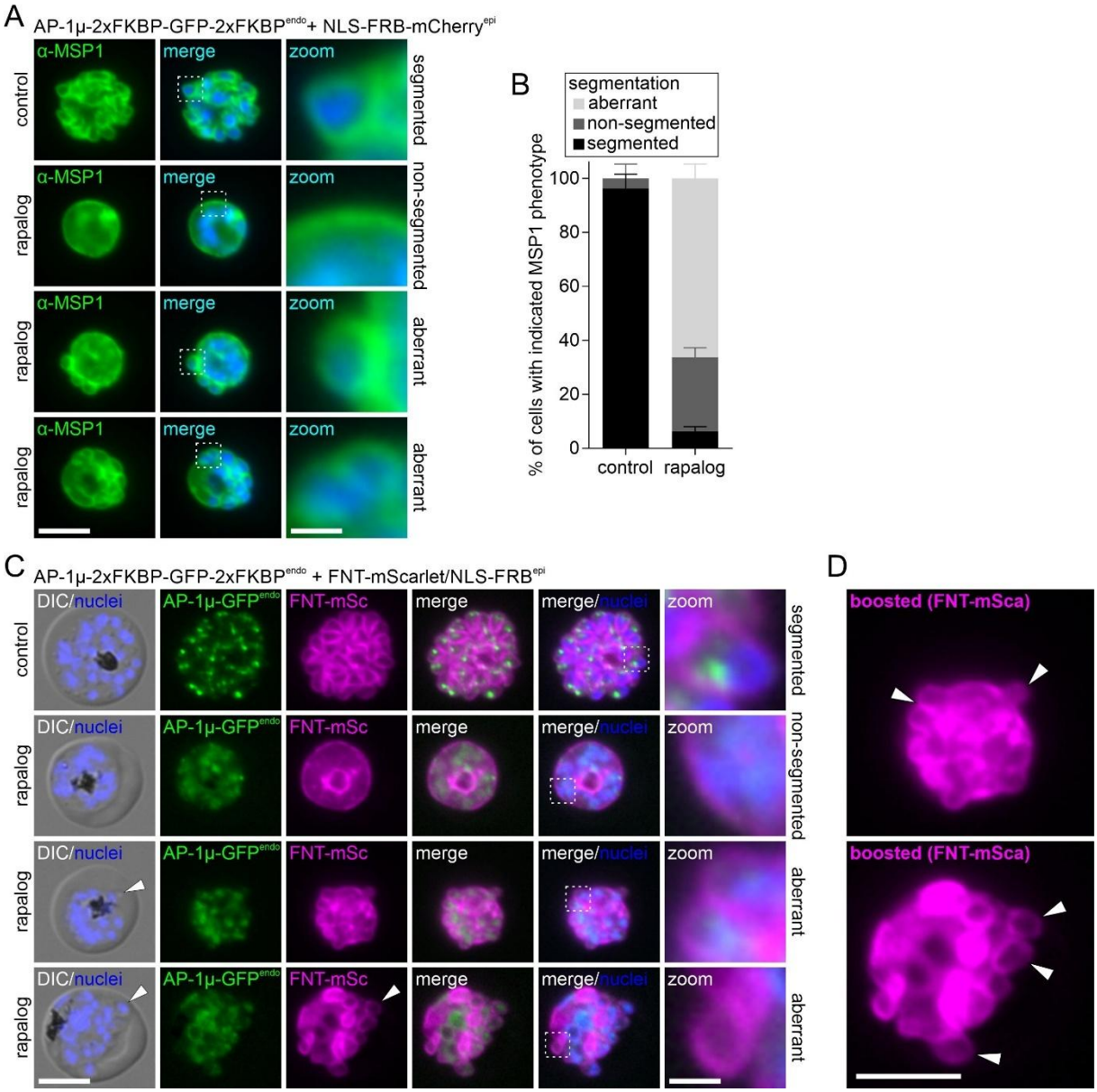

Figure 37. Effect of AP-1 inactivation on cytokinesis.
(A) Microscopy images of IFA with FA/GA-fixed knock sideways (rapalog) and control AP-1μ^{endo} parasites detecting MSP1$_{19}$. **(B)** Quantification of MSP1 phenotype; n = 40 and 40 rapalog and 40 and 20 control schizonts in two independent experiments. Coloured error bars represent mean ± SD. **(C)** Live-cell microscopy images of knock sideways (rapalog) and control AP-1μ^{endo} parasites episomally expressing FNT-mScarlet, n = 2 independent experiments analysing at least 25 parasites per condition per replicate. **(D)** Boosted and enlarged images of knock sideways (rapalog) AP-1μ^{endo} parasites episomally expressing FNT-mScarlet from C. Arrows, PPM surrounded areas indicative of segmentation. Boxes, enlarged image area (zoom). Scale bar: 5 μm (1 μm for zoomed section). Nuclei were stained with Hoechst; merge, overlay of blue and green or green and magenta channels; DIC, differential interference contrast.

Similar results were obtained when AP-1 parasites episomally expressing FNT-mScarlet were used to conditionally inactivate AP-1 (see schematic in Figure 35A): again, these parasites

exhibited aberrant segmentation during schizont development compared to controls (Figure 37C). In these parasites, membrane indentations were surrounded by FNT (also detected by DIC, white arrows in Figure 35 and 36) and contained a nucleus, indicating that they correspond to merozoite-like structures (arrows in Figure 37D, which shows enlarged overexposed images illustrating PPM segments from Figure 37C). Overall, these findings suggest that AP-1 plays a role in the cytokinesis at the end of erythrocytic schizogony of the parasite.

4.1.11 AP-1 inactivation impacts the ultrastructure of schizonts

As parasites with AP-1 inactivated exhibited a profound defect in schizont development, this phenotype was analysed further by EM. AP-1μ^{endo} parasites expressing 1xNLS-FRB-mCherry were inactivated prior to cytokinesis, incubated with C2 to arrest the egress, and assessed at the 42-50 hpi time point (as shown in Figure 35A). The analysis of EM micrographs of control schizonts revealed the presence of properly segmented merozoites with a well-defined apical pole, rhoptries, and dense granules (Figure 38, control). Conversely, knock sideways schizonts were only partially segmented and showed dispersed hemozoin foci and an absence of apical secretory organelles (Figure 38, rapalog). Despite this, individual merozoite-like structures were frequently discernible, which likely correspond to the DIC visible indentations with nuclei surrounded by PPM (white arrows in Figures 35-37) but these structures lacked the typical apical organelles seen in control merozoites (Figure 38, rapalog).

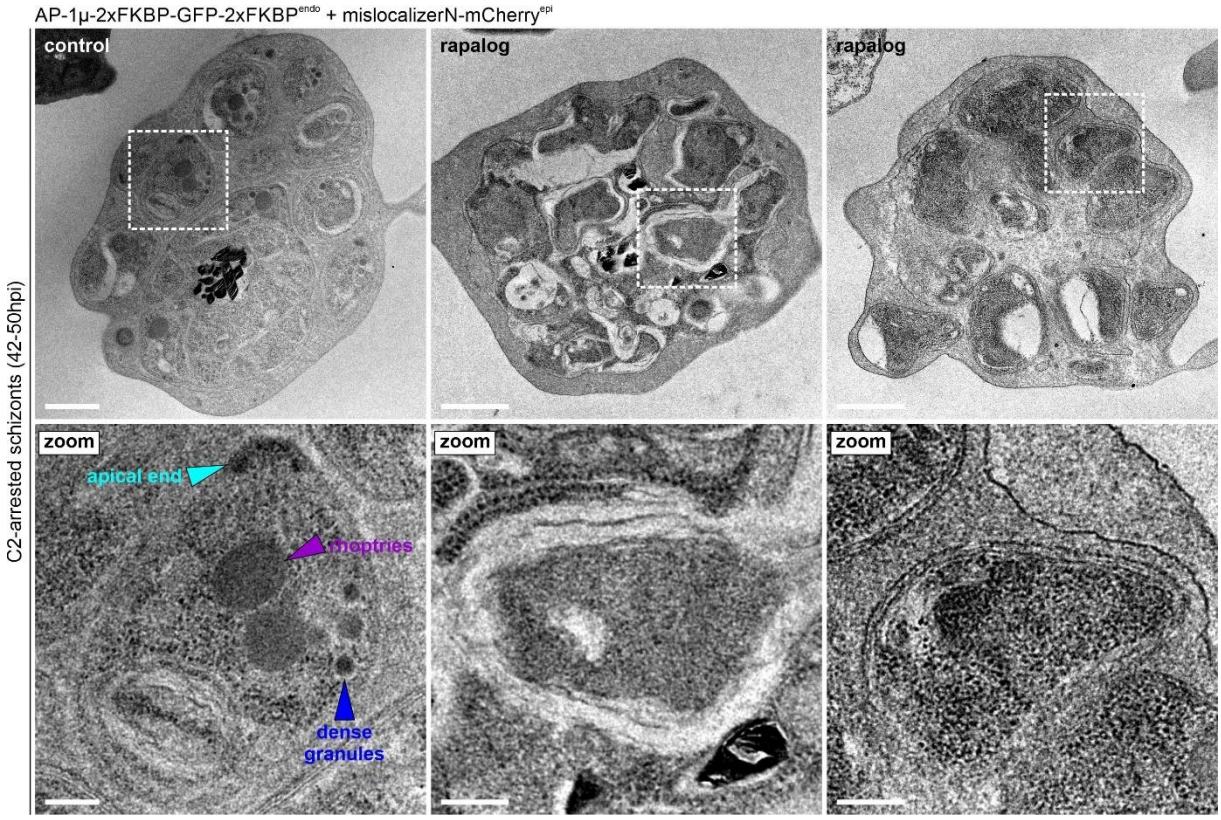

Figure 38. Effect of AP-1 inactivation on the architecture of schizonts.
EM micrographs of knock sideways (rapalog) and control AP-1µ parasites induced before cytokinesis, n = 2 independent experiments analysing at least 35 parasites per condition per replicate. Boxed areas are enlarged (zoom). Arrows show rhoptries (purple), dense granules (blue) and apical pole (turquoise). Scale bars: 1 µm and 300 nm in enlargements.

Collectively, these data show that AP-1 function is central for late schizont and merozoite development. This adaptor is required for the biogenesis of apical secretory organelles and the IMC, and its loss also partially impairs cytokinesis process.

4.1.12 Inactivation of AP-3 inactivation does not affect the integrity of invasion-related organelles

In sections 4.1.2.2 and 4.1.2.3, examination of Giemsa smears demonstrated that conditional inactivation of AP-3 led to a defective invasion phenotype, as indicated by a reduction in newly formed ring stages and the presence of free merozoites when progressing to the next development cycle in RBCs. In an attempt to find a reason for this phenotype, the integrity and trafficking to rhoptries and micronemes after AP-3 inactivation were inspected. For this, AP-3μ^{endo} parasites were co-transfected with plasmids to episomally express the apical secretory

markers ARO-mCherry, RON12-mCherry and AMA1-mCherry. Early-stage parasites were then used to inactivate AP-3, the schizonts arrested before rupture by adding C2, and the parasites analysed at the 42-50 hpi time point (see schematic in Figure 39A).

In control parasites, AP-3 was located in proximity to, although not overlapping with, rhoptries and micronemes (Figure 39B, D and E), in a similar manner as described for AP-1 (Figure 35). Surprisingly, the inactivation of this adaptor showed no detectable effect on the integrity of rhoptries (ARO and RON12) and micronemes (AMA1) (Figure 39B, D and E), and no significant impact on the number of ARO foci per schizont detected between control and rapalog conditions (Figure 39C).

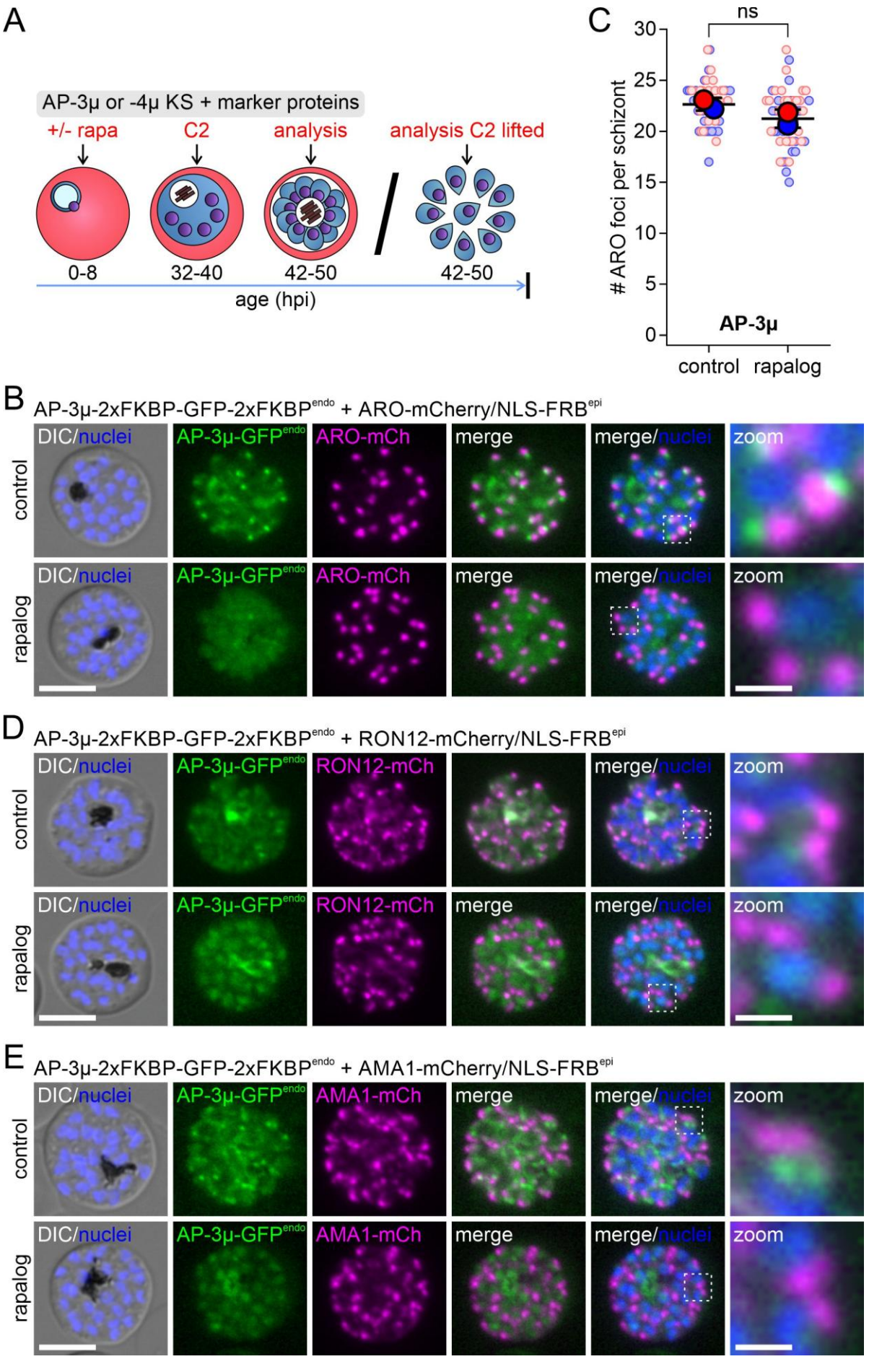
A
AP-3μ or -4μ KS + marker proteins
+/- rapa
C2
analysis
analysis C2 lifted
0-8
32-40
42-50
42-50
age (hpi)
C
ns
ARO foci per schizont
AP-3μ
control
rapalog
B
AP-3μ-2xFKBP-GFP-2xFKBP^endo + ARO-mCherry/NLS-FRB^epi
DIC/nuclei
AP-3μ-GFP^endo
ARO-mCh
merge
merge/nuclei
zoom
control
rapalog
D
AP-3μ-2xFKBP-GFP-2xFKBP^endo + RON12-mCherry/NLS-FRB^epi
RON12-mCh
E
AP-3μ-2xFKBP-GFP-2xFKBP^endo + AMA1-mCherry/NLS-FRB^epi
AMA1-mCh

Figure 39. Inactivation of AP-3 does not visibly affect rhoptries and micronemes.
(A) Schematic of AP inactivation late in the cycle used for the experiments in this Figure and Figures 40-42. C2, compound 2. **(B)** Live-cell microscopy images of knock sideways (rapalog) and control AP-3μ^{endo} parasites episomally expressing ARO-mCherry in C2-arrested schizonts, n = 2 independent experiments analysing at least 25 parasites per condition per replicate. **(C)** Quantification of number of ARO foci per schizont after AP-3 knock sideways (rapalog) compared to control, n = 25 parasites per condition per replicate per cell line in two independent experiments. Mean of each experiment is indicated by coloured large circle and individual data by coloured small circle. Data is presented following the SuperPlot guidelines (Lord et al., 2020), error bars represent mean ± SD. P-value is determined by paired t-test. **(D and E)** Live-cell microscopy images of knock sideways (rapalog) and control AP-3μ^{endo} parasites episomally expressing RON12-mCherry (D) or AMA1-mCherry (E), n = 2 independent experiments analysing at least 25 parasites per condition per replicate. Boxes show enlarged areas (zoom). Scale bars: 5 μm and 1 μm for enlarged sections; DIC, differential interference contrast; merge, overlay of green and magenta channels.

To further understand the importance of other invasion-related organelles, the analysis of the invasion phenotype of AP-3 knock sideways was extended to the dense granules and the IMC. To evaluate this, AP-3μ^{endo} parasites expressing EXP2-mCherry and IMC1c-mCherry from episomal plasmids were used to inactivate AP-3 early in the cycle and examined at the 42-50 hpi time point (see schematic in Figure 39A). In control parasites, AP-3 was located in proximity to, but not overlapping with, the dense granules (EXP2) in merozoites (Figure 40A), and was surrounded by PVM-associated EXP2 (Figure 40B) and IMC (Figure 40C) in C2-arrested schizonts, as seen with AP-1 (Figure 36). The inactivation of this adaptor did not result in obvious alterations in the localisation of EXP2 in merozoites and schizonts (Figure 40A and B), as well as of IMC1c in schizonts (Figure 40C), indicating that the invasion-related functions of AP-3 may be due to effects on specific cargoes rather than affecting the integrity of the apical secretory organelles and the IMC.

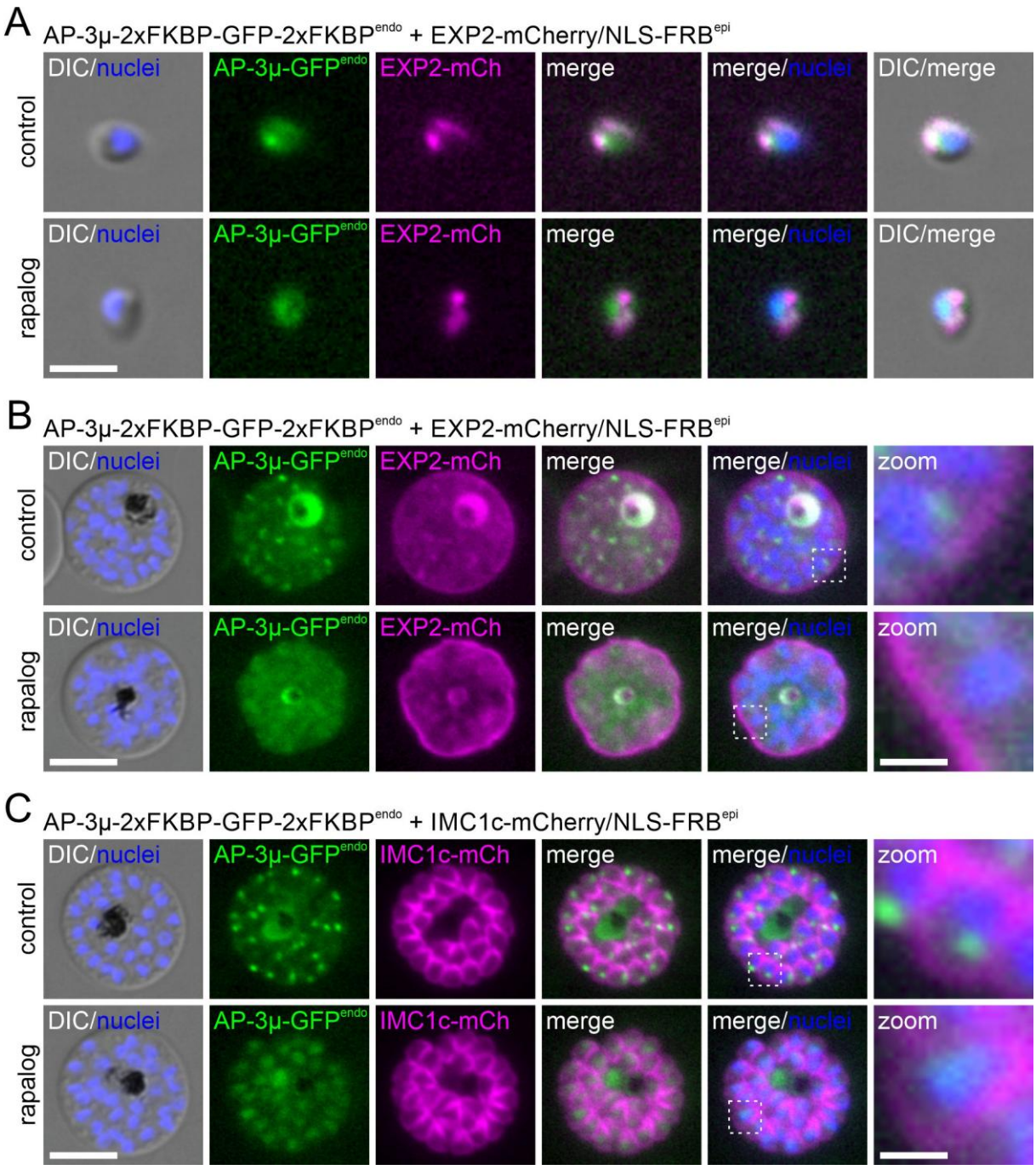

Figure 40. Inactivation of AP-3 does not visibly affect dense granules and IMC.
(A-C) Live-cell microscopy images of knock sideways (rapalog) and control AP-3µ^{endo} parasites episomally expressing EXP2-mCherry in merozoites after lifting C2 (A) and in C2-arrested schizonts (B) or IMC1c-mCherry in C2-arrested schizonts (C), n = 2 independent experiments analysing at least 25 parasites per condition per replicate. Boxes show enlarged areas (zoom). Scale bars: 5µm and 1µm for enlarged sections; DIC, differential interference contrast; merge, overlay of green and magenta channels.

4.1.13 AP-4 inactivation has no major effect on the integrity of invasion-related organelles

In a similar approach to that those performed for AP-3, the integrity of invasion-related organelles and the IMC was further examined in AP-4 knock sideways parasites. As demonstrated in sections 4.1.2.2 and 4.1.2.3, Giemsa smears had indicated an invasion defect after AP-4 knock sideways that was evident from a decline in newly formed ring stages and the presence of free merozoites (Figure 28B). In order to test whether this was due to an effect on invasion-related organelles or not, AP-4μ^{endo} parasites expressing ARO-mCherry, RON12-mCherry and AMA1-mCherry from episomal plasmids were used to inactivate AP-4 in early stages and analysed in C2-arrested schizonts (see schematic in Figure 39A).

In control parasites, AP-4 foci were located adjacent to, but did not overlap with, rhoptries (ARO and RON12, see Figure 41A and C) and micronemes (AMA1, see Figure 41D). When inactivation of AP-4 was induced, the localisation of ARO and RON12 appeared to be intact (Figure 41A and C), and no significant impact on the number of ARO foci per schizont was observed between the control and rapalog conditions (Figure 41B), indicating no effect on the integrity of rhoptries in AP-4 knock sideways parasites. Instead, micronemes appeared to be partially affected, as an increase in the cytosolic pool of AMA1 was detected (Figure 41D). The quantification of the intensity of microneme-associated AMA1 and cytosolic AMA1 showed a significant difference between control and knock sideways parasites (Figure 41E), as also evident by an intensity plot of AMA1 (Figure 41F). This finding indicated that either the micronemes were mildly impaired or that the trafficking of AMA1 to these organelles was to some extent negatively affected.

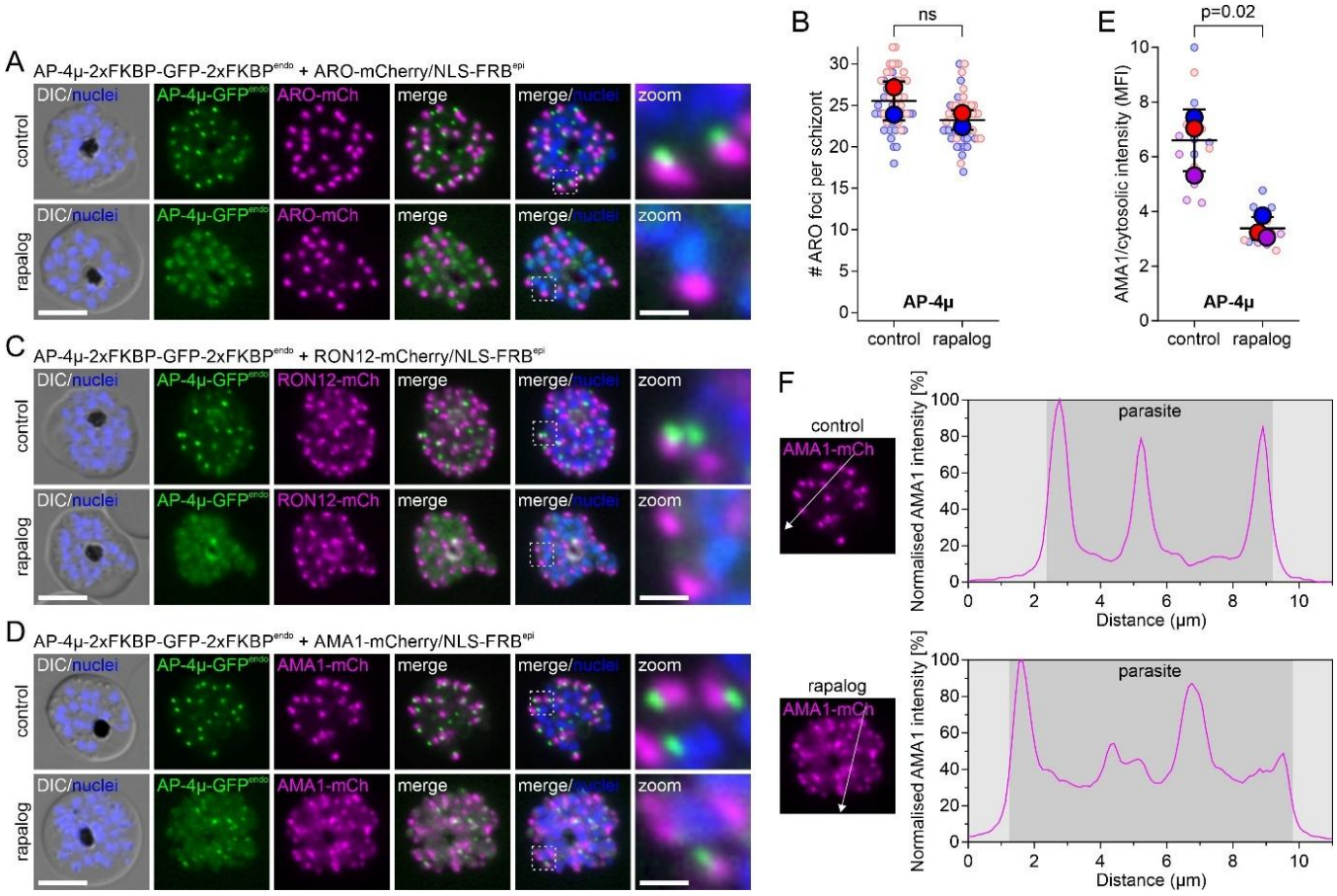

Figure 41. Inactivation of AP-4 may have a minor effect on trafficking to the micronemes but not the rhoptries.

(A) Live-cell microscopy images of knock sideways (rapalog) and control AP-4μ^{endo} parasites episomally expressing ARO-mCherry in C2-arrested schizonts, n = 3 independent experiments analysing at least 25 parasites per condition per replicate. **(B)** Quantification of number of ARO foci per schizont after AP-4 knock sideways (rapalog) compared to control, n = 25 parasites per condition per replicate per cell line in two independent experiments. Mean of each experiment is indicated by coloured large circle and data for individual cells by coloured small circles. Data is presented following the SuperPlot guidelines (Lord et al., 2020), error bars represent mean ± SD. P-value is determined by paired t-test. **(C and D)** Live-cell microscopy images of knock sideways (rapalog) and control AP-4μ^{endo} parasites episomally expressing RON12-mCherry (C) or AMA1-mCherry (D), n = at least 2 independent experiments analysing at least 25 parasites per condition per replicate. Boxes show enlarged areas (zoom). Scale bars: 5 μm and 1 μm for enlarged sections; DIC, differential interference contrast; merge, overlay of green and magenta channels. **(E)** Relative fluorescence of individual AMA1 foci compared to cytosolic background in inactivated (rapa) and control AP-4μ^{endo} parasites, n = 5 parasites per condition from three independent replicates, where values per parasite were averaged between 2 to 5 higher or lower fluorescence intensity peaks. Mean of each experiment is indicated by coloured large circle and individual data by coloured small circle. Data is presented following the SuperPlot guidelines (Lord et al., 2020), error bars represent mean ± SD. P-value is determined by paired t-test. **(F)** Fluorescence intensity plot of AMA1 signals of images in (D) from AP-4μ^{endo} schizonts illustrating the presence of the cytosolic pool of AMA1-mCherry. Dark grey, signal in the parasite; light grey, signal outside the parasite.

The trafficking and integrity of the dense granules/PVM and the IMC was also tested using AP-4 parasites expressing EXP2-mCherry and IMC1c-mCherry from episomal plasmids, respectively (see schematic in Figure 39A). In control parasites, AP-4 was found to be localised in proximity to, but not colocalising with, dense granules in merozoites (Figure 42A) and was surrounded by PVM-associated EXP2 (Figure 42B) and IMC1c-marked IMC (Figure 42C) in schizonts, similar to the results obtained with AP-1 (Figure 36) and AP-3 (Figure 40). In the case of knock sideways AP-4 parasites, no alteration in the localisation of EXP2 and IMC1c was observed (Figure 42A-C), indicating that these organelles and the trafficking of these markers were not compromised after AP-4 inactivation. Taken together, these findings imply that the invasion defect is not due to a major disturbance of the invasion-related organelles, although AP-4 inactivation may exert a minor effect on the trafficking to or integrity of the micronemes.

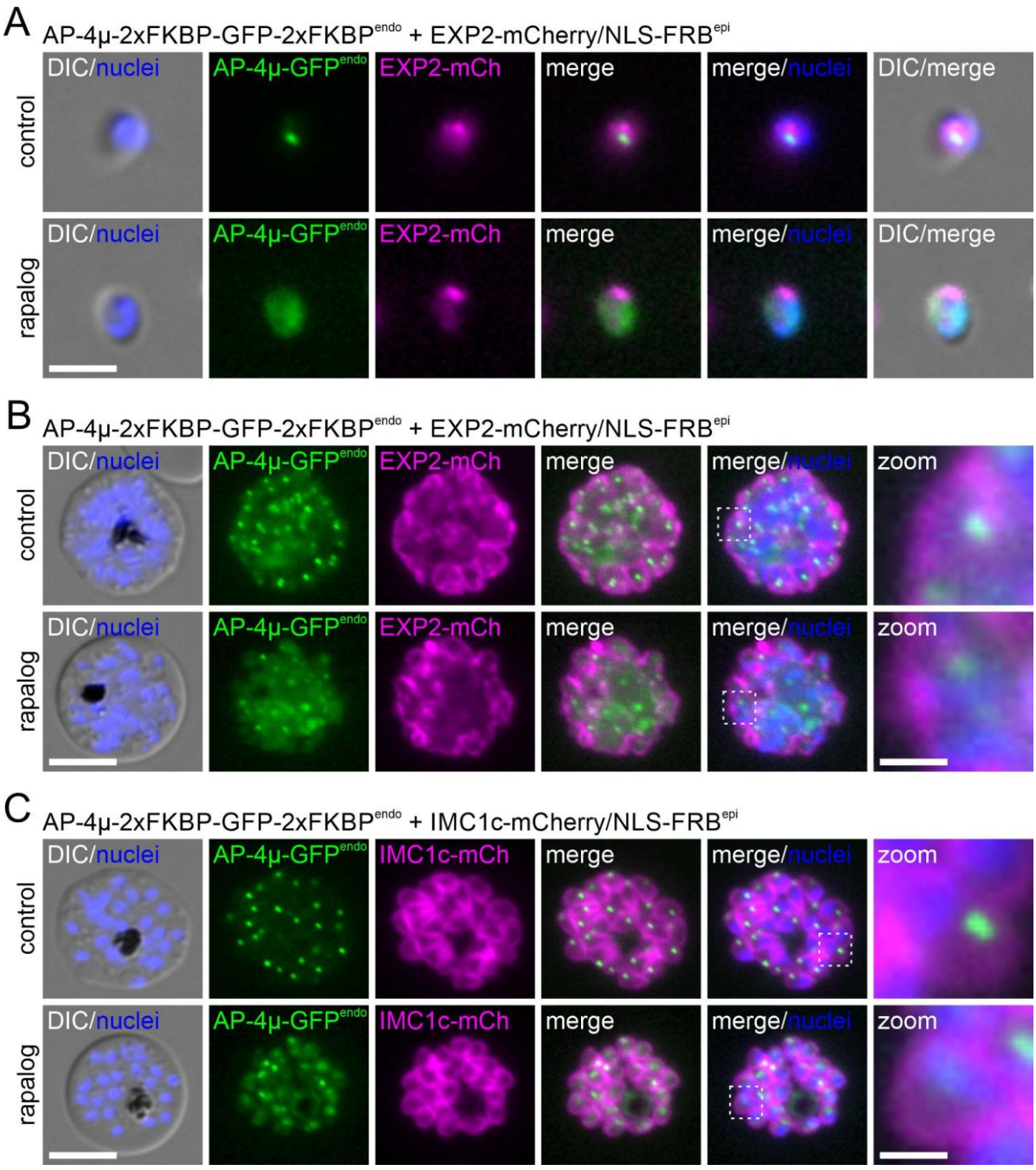

Figure 42. Inactivation of AP-4 does not visibly affect dense granules and IMC.
(A-C) Live-cell microscopy images of knock sideways (rapalog) and control AP-4μ^{endo} parasites episomally expressing EXP2-mCherry in merozoites after lifting C2 (A) and in C2-arrested schizonts (B) or IMC1c-mCherry in C2-arrested schizonts (C), n = 3 independent experiments analysing at least 25 parasites per condition per replicate. Boxes show enlarged areas (zoom). Scale bars: 5 μm and 1 μm for enlarged sections; DIC, differential interference contrast; merge, overlay of green and magenta channels.

4.1.14 Proxiome of AP-3

With the intention to identify the composition of the AP-3-mediated vesicle trafficking machinery in the parasite, DiQ-BioID was carried out with this adaptor, as previously described for AP-1 (section 4.1.7). To investigate this, AP-3µ^{endo} parasites were co-transfected with plasmids to episomally express either miniTurbo-N^{L} or miniTurbo-C^{L} under the control of the *sf3a2* promoter. Asynchronous parasite cultures (5 – 10% parasitemia) were used, and either the N- or C-terminal miniTurbo-FRB versions were conditionally recruited to the endogenously FKBP-tagged AP-3µ subunit (upon addition of rapalog), where they can biotinylate AP-3 proximal proteins (Figure 43A). Live-cell fluorescence microscopy images of control AP-3 parasites (only biotin) showed that the miniTurbo was located in the parasite cytosol, whereas parasites with rapalog (rapa and biotin) showed a recruitment of the biotin ligase to the AP-3 foci (Figure 43A). Quantitative mass spectrometry analysis (kindly carried out by Gala Ramón-Zamorano in the Bartfai lab, Radboud University, Nijmegen, The Netherlands) of biotinylated proteins comparing rapalog (miniTurbo recruited to target) over control (miniTurbo cytoplasmic) (Figure 43B and Appendices 7 and 10) resulted in a list of high-confidence hits (Figure 43B and C and Appendix 7 and 10), representing potential interactors and compartment neighbours of AP-3 in living parasites.

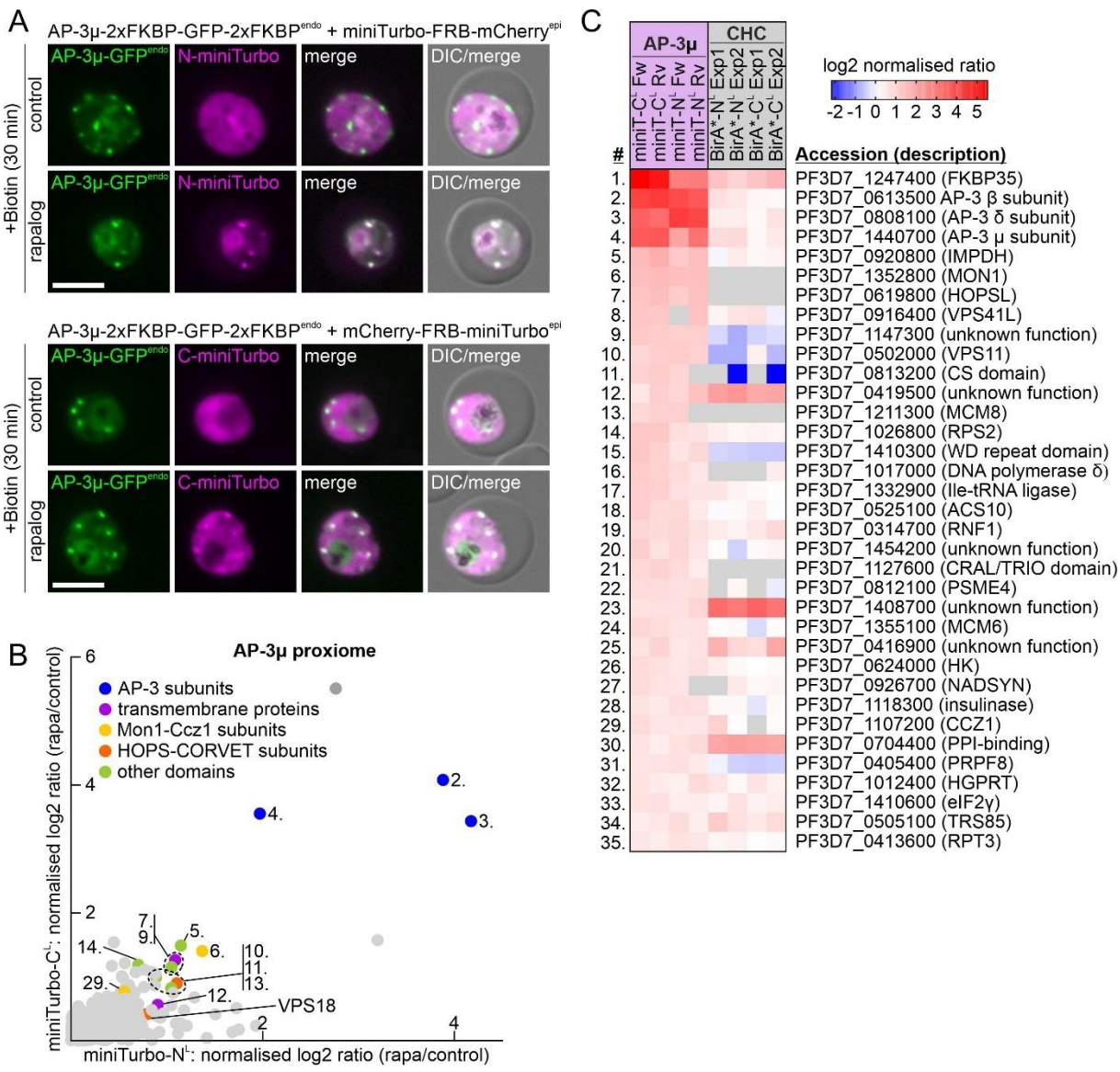

Figure 43. Proxiome of AP-3.

(A) Live-cell microscopy images of AP-3µ^{endo} parasites expressing miniTurbo-N^{L} or miniTurbo-C^{L} grown in the presence of rapalog (miniTurbo recruited to AP-3 foci) or not (miniTurbo cytoplasmic) for 30 minutes show rapalog-dependent recruitment of the biotinylating enzymes. Scale bar: 5 µm. Nuclei were stained with Hoechst; merge, overlay of green and magenta channels; DIC, differential interference contrast. **(B)** Top-right quadrant of scatter plots of AP-3 DiQ-BioID showing proteins enriched (log2 ratio) on rapalog (biotinylizer on target) compared with control (biotinylizer free in cytoplasm) from the miniTurbo-N^{L} (fw technical replicate) and miniTurbo-C^{L} (fw technical replicate) expressing cell lines. Full plots of fw and rv technical replicates are shown in Appendix 10. Significantly enriched proteins (log2 fold change >0.9) are coloured into general groups; proteins below the threshold, light grey; known contaminants, dark grey. IDs of numbered proteins are indicated in (C). **(C)** Heatmap comparing AP-3µ (this study) and CHC (Birnbaum et al., 2020) DiQ-BioIDs including the proteins enriched in at least three of four experiments of the AP-3µ dataset with an FDR of 0.05 or better, corrected p-value <0.1 and log2 enrichment >0.5. NaN, grey; bold font, DiQ-BioID bait.

In the AP-3 proxiome, the dominantly enriched proteins were restricted to the AP-3 complex itself, including the bait (μ) and both large (β, δ) subunits, but not the small (σ) subunit (Figure 43B and C and Appendices 7 and 10). Notably, no obvious coat and accessory proteins were found to be enriched (Figure 43B and C and Appendices 7 and 10), suggesting that AP-3 vesicle trafficking is clathrin-independent in malaria parasites, a conclusion supported by previous clathrin interaction analyses (Birnbaum et al., 2020; Henrici et al., 2020). Instead, the core subunits MON1/Sand1 and Ccz1 (significantly but less enriched compared to MON1) of the MON1-Ccz1 complex were detected, a guanine nucleotide exchange factor (GEF) for Rab7, which in other organisms is present in the destination compartment for AP-3 vesicle transport (Rehling et al., 1999; Bröcker et al., 2012; Balderhaar & Ungermann, 2013). Further hits were the subunits VPS11 (significant) and VPS18 (enrichment not statistically significant) of the HOPS-CORVET complex, which, in other organisms, function as multi-subunit endosomal tethering complexes, including for AP-3 vesicles (Bröcker et al., 2012; Schoppe et al., 2020). In yeast (mostly studied) and mammals, the HOPS component VPS41 plays a central role in AP-3 trafficking, by capturing AP-3 vesicles at the destination compartment (Angers & Merz, 2009; M. Cabrera et al., 2010; Asensio et al., 2013; Schoppe et al., 2020). Interestingly, HHPred searches (Zimmermann et al., 2018) with the unknown proteins in the top ten hits of the AP3-BioID revealed that PF3D7_0916400 is likely the parasite's VPS41 or VPS8, whereas PF3D7_0619800 contains a PEP3/VPS18 domain in its N-terminus (top HHPred hit), indicating that the most enriched proteins contained further HOPS/CORVET components besides VPS11, including the parasite's potential VPS41 or possibly VPS8 (here designated VPS41/VPS8). GAPs such as yeast Age2 (AGAP1 in humans) that have been linked with AP-3 trafficking (Nie et al., 2003; Schoppe et al., 2020) or SNAREs, were not detected (Figure 43B and C and Appendices 7 and 10).

A further comparison with the clathrin DiQ-BioID showed only minor overlap between the clathrin and AP-3 BioIDs (Fig. 43C), further indicating that AP-3 vesicle machinery functions independently of clathrin.

4.1.15 Proxiome of AP-4

In a similar strategy described for AP-1 (section 4.1.7) and AP-3 (section 4.1.14), the proxiome of AP-4 was determined in order to identify the AP-4-mediated vesicle trafficking machinery in the parasite. AP-4 parasites were transfected with episomal plasmids mediating the

expression of miniTurbo-N^L or miniTurbo-C^L. In asynchronous parasite cultures at high parasitemia (5 – 10%), the conditional recruitment of N- or C-terminal miniTurbo-FRB versions to the endogenously FKBP-tagged AP-4 μ subunit (by adding rapalog) was carried out to biotinylate AP-4 proximal proteins (Figure 44A). The results demonstrated that control parasites (only biotin) showed the miniTurbo uniformly distributed in the parasite cytosol, whereas parasites with rapalog (rapa and biotin) showed a recruitment of this biotin ligase to the AP-4 foci (Figure 44A). A quantitative mass spectrometry analysis (kindly carried out by Gala Ramón-Zamorano in the Bartfai lab, Radboud University, Nijmegen, The Netherlands) of biotinylated proteins comparing rapalog (miniTurbo recruited to target) over control (miniTurbo cytoplasmic) (Figure 44B and Appendices 8 and 11) resulted in a list of high-confidence hits (Figure 44B and C and Appendices 8 and 11).

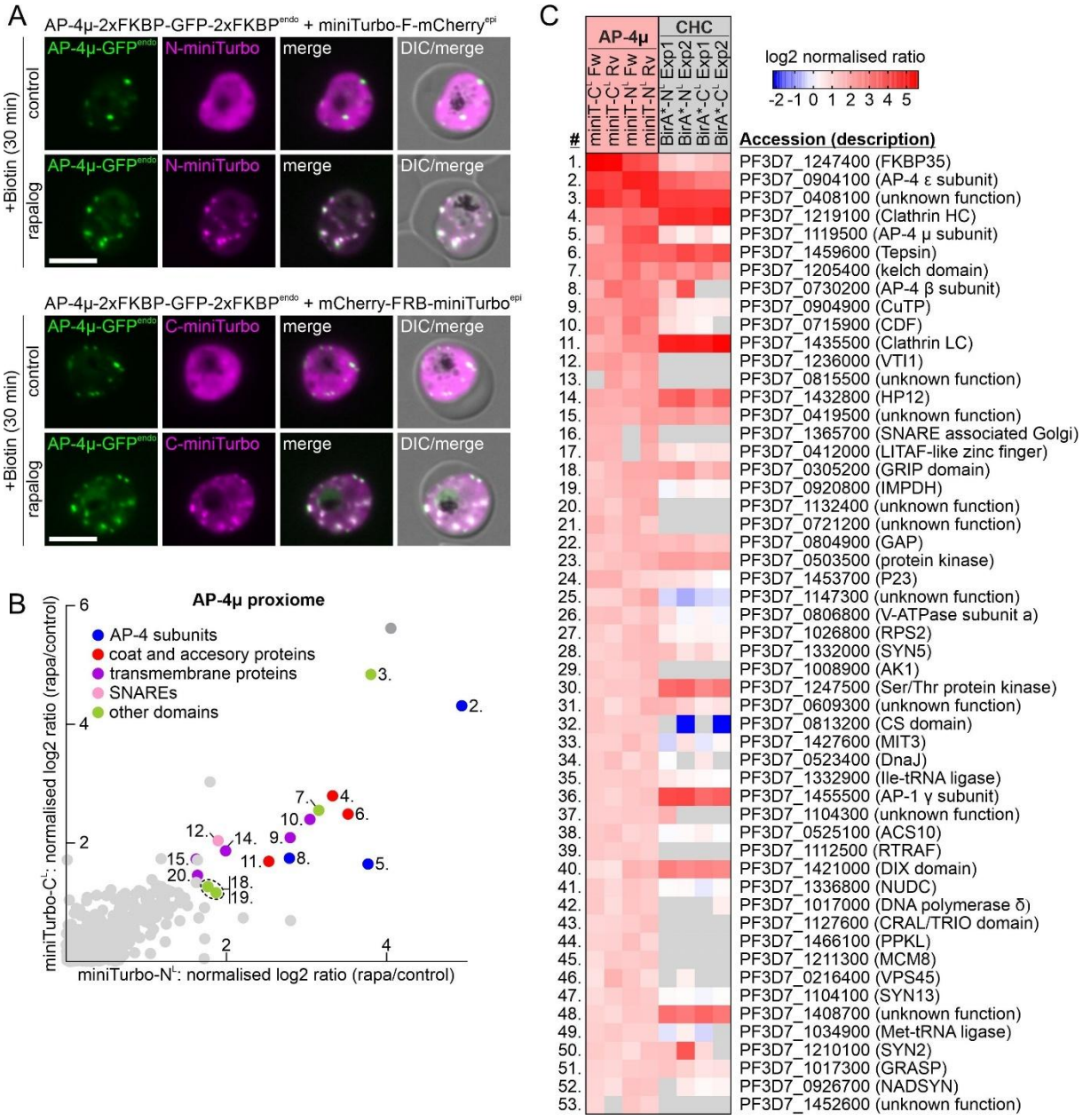

Figure 44. Proxiome of AP-4.

(A) Live-cell microscopy images of AP-4μ^{endo} parasites expressing miniTurbo-N^{L} or miniTurbo-C^{L} grown in the presence of rapalog (miniTurbo recruited to AP-4 foci) or not (miniTurbo cytoplasmic) for 30 minutes. Scale bar: 5μm. Nuclei were stained with Hoechst; merge, overlay of green and magenta channels; DIC, differential interference contrast. **(B)** Top-right quadrant of scatter plots of AP-4 DiQ-BioID showing proteins enriched (log2 ratio) on rapalog (biotinylizer on target) compared with control (biotinylizer free in cytoplasm) from the miniTurbo-N^{L} (fw technical replicate) and miniTurbo-C^{L} (fw technical replicate) expressing cell lines. Full plots of fw and rv technical replicates are shown in Appendix 11. Significantly enriched proteins (log2 fold change >1.5) are coloured into general groups; proteins below the threshold, light grey; known contaminants, dark grey. IDs of numbered proteins are indicated in (C). **(C)** Heatmap comparing AP-4μ (this study) and CHC (Birnbaum et al., 2020) DiQ-BioIDs including the proteins enriched in at least three of four experiments of the AP-4μ dataset with an FDR of 0.05 or better, corrected p-value <0.1 and log2 enrichment >1. NaN, grey; bold font, DiQ-BioID bait.

The AP-4 proxiome data identified subunits of its own adaptor complex, including both large subunits ε and β, the bait μ, but again not σ (Figure 44B and C and Appendices 8 and 11). The list also included tepsin, and interestingly, the clathrin heavy and light chains (Figure 44B and C), as described for the AP-1 proxiome (Figure 33B and C). Further hits were SNAREs, GAPs and several transporters, including the copper-transporting ATPase (CuTP, (Kenthirapalan et al., 2014)), cation diffusion facilitator (CDF, (Wichers et al., 2022)), PF3D7_1132400 (CRT-like domain, (Sayers et al., 2018; Behrens & Spielmann, 2024)), PF3D7_1427600 (MIT3), and vacuolar iron transporter (VIT, enriched in only 3 out of 4 replicates (Appendices 8 and 11) and therefore not listed in Figure 44C). Lower in the list were an AP-1 subunit and GRASP, indicating more general Golgi and trans-Golgi hits among the lower enriched proteins. The prominent detection of clathrin in the AP-4 proxiome was unexpected considering data from model systems (Hirst et al., 1999; Stockhammer et al., 2024b) but agreed with the previous *P. falciparum* clathrin DiQ-BioID (Birnbaum et al., 2020). Furthermore, a comparison with the clathrin DiQ-BioID showed considerable overlap with proteins enriched in the AP-4 BioID (Fig. 44B and C).

4.1.15.1 AP-4 foci overlap with tepsin foci

The AP-4 proxiome identified clathrin and tepsin with a high degree of confidence (Figure 44B and C), indicating that AP-4-coated vesicle machinery requires clathrin. In order to assess whether these proteins are located in similar areas to this adaptor, AP-4μ^{endo} parasites were co-transfected with plasmids to episomally express tepsin-mScarlet and CLC-mScarlet, inactivated in early stages and examined in trophozoite stage (see schematic in Figure 45A). In control parasites, AP-4 partially localised in tepsin- and clathrin-positive regions (Figure 45B-E).

It was further attempted to assess whether AP-4 knock sideways would affect the location of clathrin or tepsin as done for AP-1 (see section 4.1.7.1). Upon induction of knock sideways (see schematic in Figure 45A), parasites with inactivated AP-4 did not show differences in the trans-Golgi localisation of tepsin and clathrin foci compared to controls (Figure 45B-E). While these findings do not seem to support the BioID results, it needs to be considered that the limited efficiency of removal of AP-4μ from the trans-Golgi after knock sideways and the fact that AP-1 also occupies tepsin and clathrin molecules, likely precludes a proper validation of the tepsin- and clathrin-mediated functional connection to this adaptor in the manner done for AP-1 (Figure

34). A more efficient means to inactivate AP-4 may therefore be needed to validate this interaction.

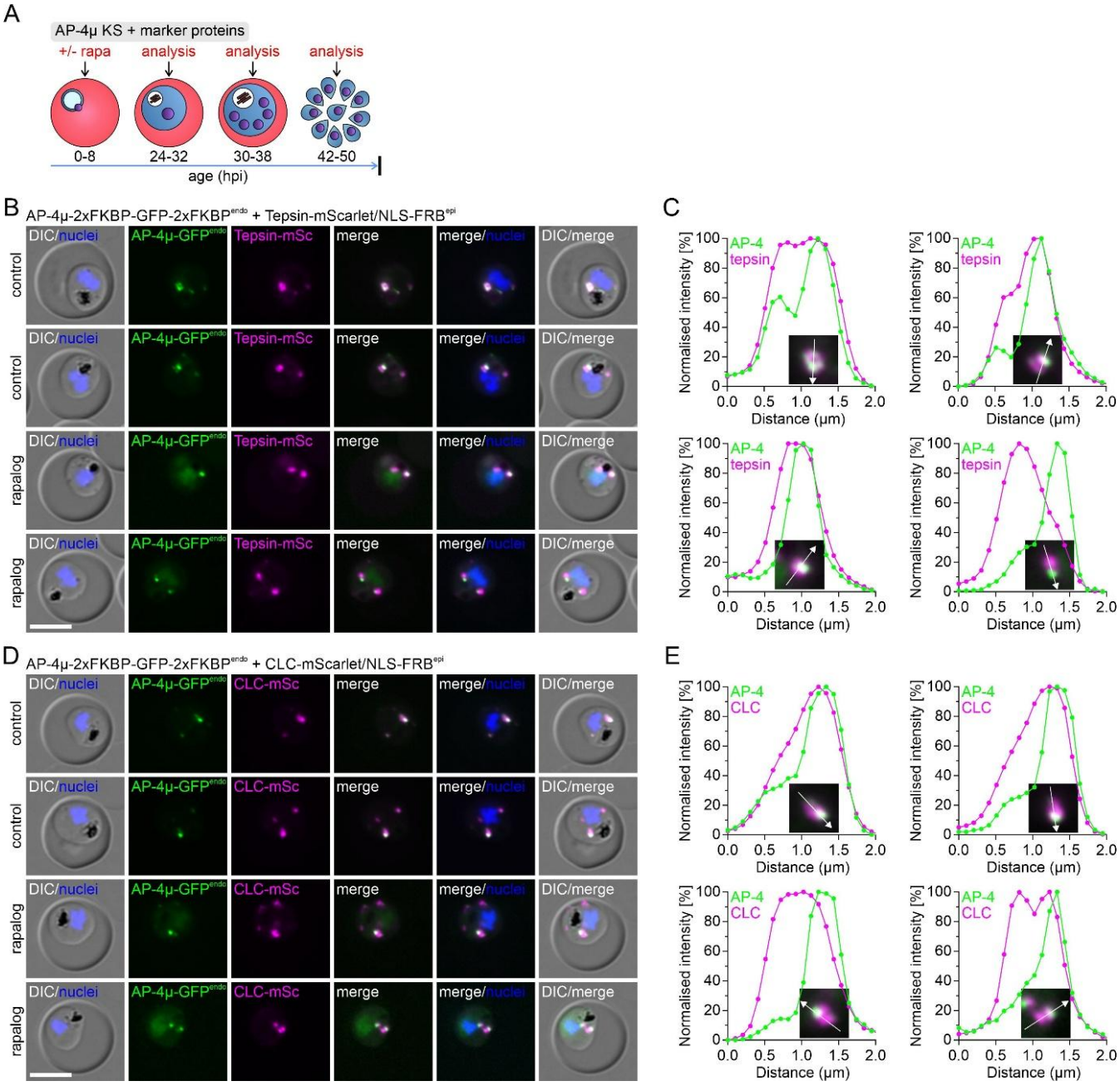

Figure 45. AP-4 partially overlaps with tepsin and clathrin areas.
(A) Schematic of AP-4μ inactivation used for the following panels if not otherwise indicated. C2, compound 2. **(B)** Live-cell fluorescent microscopy images of AP-4μ^{endo} parasites episomally overexpressing tepsin fused to mScarlet in trophozoite stage (24-32h), n = 4 independent experiments analysing at least 25 parasites per condition per replicate. **(C)** Examples of normalised intensity plots of (B); in 2 representative example parasites per condition (control: top plots, and rapalog: bottom plots) from four independent imaging session. **(D and E)**, as in (B) and (C) using CLC fused to mScarlet. Scale bar: 5 μm. Nuclei were stained with Hoechst. DIC, differential interference contrast. Merge, overlay of green and magenta channels.

4.1.15.2 Inactivation of AP-4 affects the localisation of CDF and VIT

In view of the presence of numerous transporters identified in the AP-4 proxiome, two of them were selected for validation as potential cargoes. AP-4μ^{endo} parasites were co-transfected with plasmids to episomally express either CDF-mScarlet or VIT-mScarlet under the control of the *crt* promoter. Next, synchronous parasites were used to inactivate AP-4 in early stages, and the fate of the potential cargoes was examined at 30-38 and 42-50 hpi (free merozoites) (see schematic in Figure 45A).

Fluorescence microscopy images of control pre-segmented schizonts (30-38 hpi) showed that CDF was located in the FV membrane and in foci in the cytosol of the parasite (Figure 46A), whereas VIT was distributed only in cytosolic foci (Figure 47A), in agreement with the previously reported locations of these proteins (Wichers et al., 2022; Wunderlich et al., 2024). The majority of the CDF and VIT foci did not overlap with AP-4, indicating that they do not correspond to Golgi-related compartments (Figures 46A and 47A). In schizonts with inactivated AP-4, CDF maintained its localisation at the FV membrane and in cytosolic foci (although less abundant compared to controls), but also showed a location at the PPM (Figure 46A and B), whereas most of VIT was redistributed to the PPM (Figure 47A and B), suggesting a loss of sorting of these transporters to their target compartments and escape via the default transport to the PPM. This finding indicates that CDF and VIT, but likely also more of the putative transporters in the AP-4 DiQ-BioID (Figure 44B and C), are sorted by AP-4.

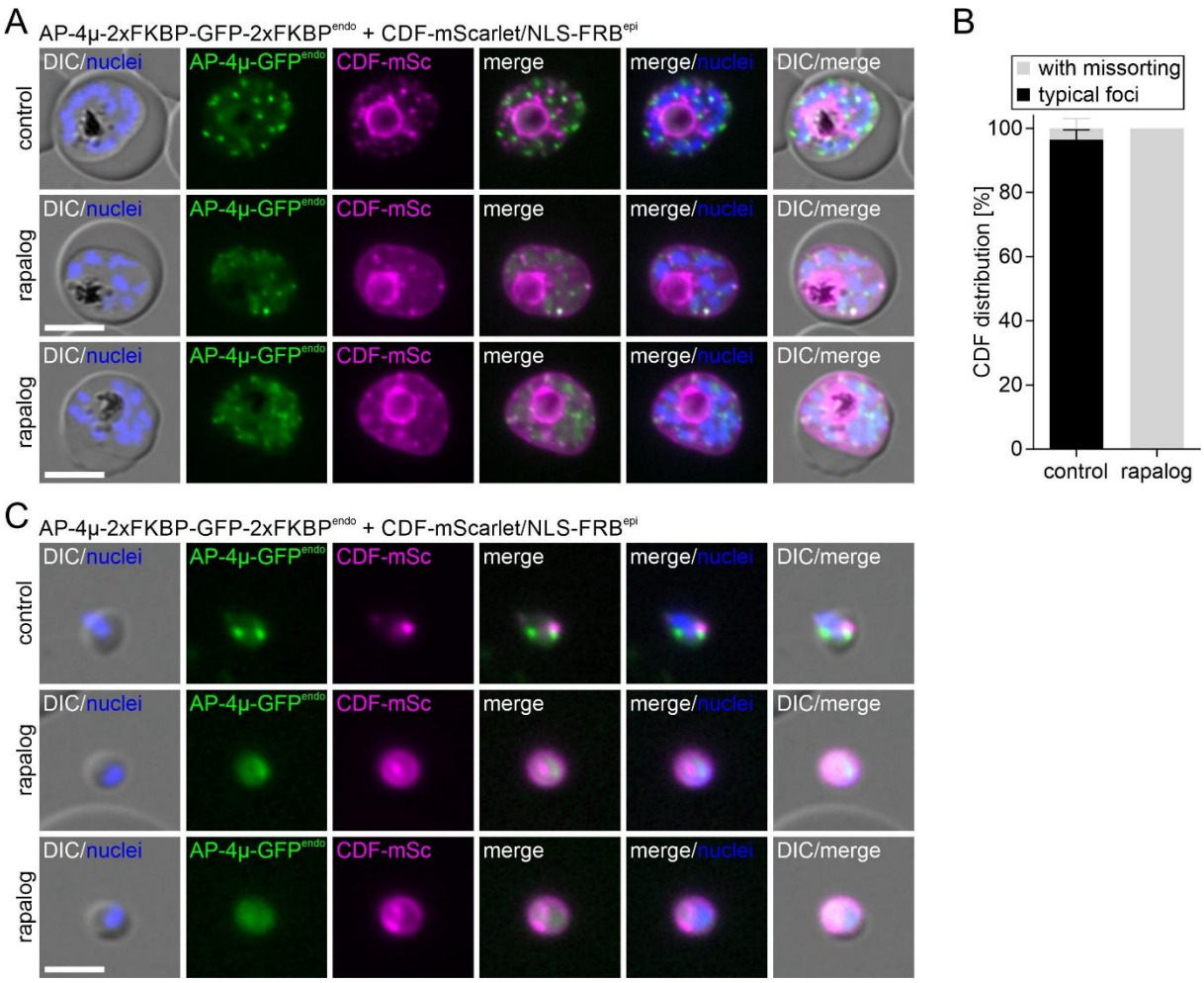

Figure 46. Inactivation of AP-4 affects the localisation of CDF.
(A) Live-cell microscopy images of knock sideways (rapalog) and control AP-4μ^{endo} parasites episomally expressing CDF-mScarlet in early schizonts. **(B)** Quantification of number of cells with indicated CDF phenotype from (A), n = 20 parasites per condition per replicate in three independent experiments. **(C)** Live-cell microscopy images of knock sideways (rapalog) and control AP-4μ^{endo} merozoite parasites episomally expressing CDF-mScarlet. Scale bar: 5 μm for intracellular parasite stages and 2.5 μm for merozoites. Nuclei were stained with Hoechst. DIC, differential interference contrast. Merge, overlay of green and magenta channels.

Interestingly, daughter merozoites with inactivated AP-4 retained both CDF and VIT in their PPM, in contrast to the localisation of these transporters in cytosolic foci in control merozoites (Figures 46C and 47C). Taken together, these results suggest that a redistribution of these transporters, as well as other AP-4 vesicle-trafficked transporters, may result in defective invasion of RBCs by merozoites, thereby providing a potential explanation for the AP-4 inactivation phenotype.

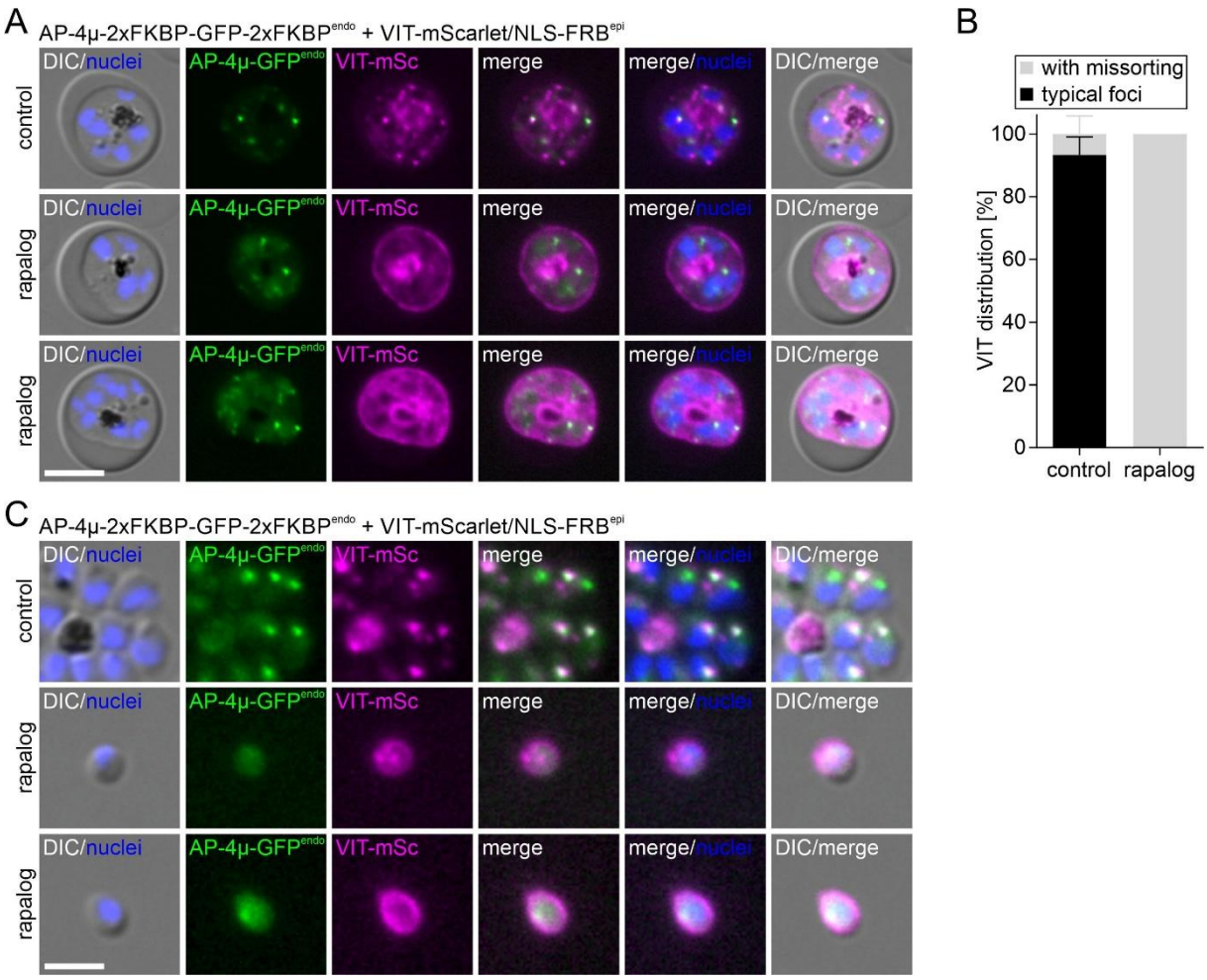

Figure 47. Inactivation of AP-4 affects the localisation of VIT.
(A) Live-cell microscopy images of knock sideways (rapalog) and control AP-4μ^{endo} parasites episomally expressing VIT-mScarlet in early schizonts. **(B)** Quantification of number of cells with indicated VIT phenotype from (A), n = 20 parasites per condition per replicate in three independent experiments. **(C)** Live-cell microscopy images of knock sideways (rapalog) and control AP-4μ^{endo} merozoite parasites episomally expressing VIT-mScarlet. Scale bar: 5 μm for intracellular parasite stages and 2.5 μm for merozoites. Nuclei were stained with Hoechst. DIC, differential interference contrast. Merge, overlay of green and magenta channels.

4.1.16 Comparison of adaptors and clathrin proxiomes

The proxiome of AP-1, AP-3 and AP-4 in the malaria parasite *P. falciparum* provided in this work (see sections 4.1.7, 4.1.14 and 4.1.15, respectively) was compared to the clathrin proxiome (Birnbaum et al., 2020) that had also been generated by DiQ-BioID (although with BirA* instead of miniTurbo). For this comparison a hierarchically-clustered heatmap was generated (Figure 48). The results emphasised the unique configuration of AP-3 with a seeming lack of a typical coat and association with HOPS/CORVET components and the Rab7 effector Mon1 (Figure 48). In contrast, both AP-1 and AP-4 clustered with clathrin and tepsin and a

number of adaptor-type specific SNAREs and small GTPase controlling proteins (Figure 48). AP-1 was found to cluster with sortilin, while AP-4 was found to cluster with several transporters that, based on the results obtained here (see section 4.1.15.2 and Figures 46 and 47), are likely to be cargoes (Figure 48). Furthermore, proteins were identified that clustered with specific subsets of adaptors, which may correspond to accessory vesicle transport machinery, sub-compartment-specific trans-Golgi proteins, cargo or destination compartment proteins such as e.g., PF3D7_0408100, a coiled-coil domain-containing protein that was found to be highly enriched with AP-4 and clathrin; or HP12 and a kelch domain-containing protein that were highly enriched with AP-1, AP-4 and clathrin (Figure 48).

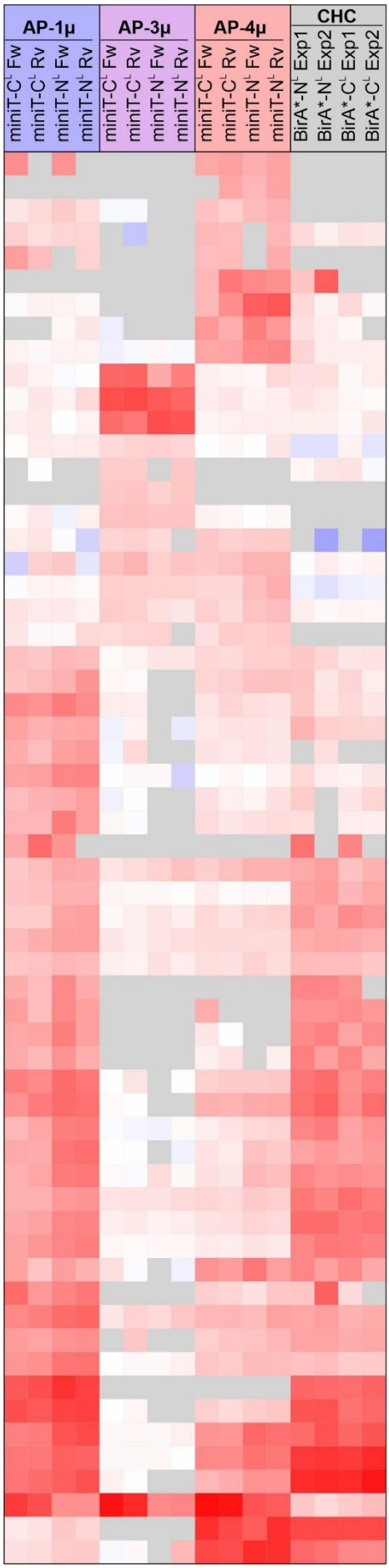
AP-1µ
AP-3µ
AP-4µ
CHC
miniT-C^{L} Fw
miniT-C^{L} Rv
miniT-N^{L} Fw
miniT-N^{L} Rv
BirA*-N^{L} Exp1
BirA*-N^{L} Exp2
BirA*-C^{L} Exp1
BirA*-C^{L} Exp2
log2 normalised ratio
-2 -1 0 1 2 3 4 5
Accession (description)
PF3D7_1236000 (VTI1)
PF3D7_0815500 (unknown function)
PF3D7_1132400 (transporter)
PF3D7_0412000 (LITAF-like zinc finger)
PF3D7_1365700 (SNARE associated Golgi)
PF3D7_0730200 (AP-4 β subunit)
PF3D7_1119500 (AP-4 µ subunit)
PF3D7_0715900 (CDF)
PF3D7_0904900 (CuTP)
PF3D7_1440700 (AP-3 µ subunit)
PF3D7_0613500 (AP-3 β subunit)
PF3D7_0808100 (AP-3 δ subunit)
PF3D7_0502000 (VPS11)
PF3D7_0916400 (VPS41L)
PF3D7_0619800 (HOPS)
PF3D7_1352800 (MON1)
PF3D7_0813200 (CS domain)
PF3D7_0920800 (IMPDH)
PF3D7_1147300 (unknown function)
PF3D7_1026800 (RPS2)
PF3D7_1211300 (MCM8)
PF3D7_1017300 (GRASP)
PF3D7_1332000 (SYN5)
PF3D7_1311400 (AP-1 µ subunit)
PF3D7_1451800 (Sortilin)
PF3D7_1432000 (SYN11)
PF3D7_1405100 (GAP)
PF3D7_0314100 (v-SNARE)
PF3D7_0530100 (SYN6)
PF3D7_1227300 (unknown function)
PF3D7_0305200 (GRIP domain)
PF3D7_0815800 (VPS9)
PF3D7_0411800 (unknown function)
PF3D7_0704400 (PPI-binding)
PF3D7_0914900 (BSD-domain)
PF3D7_0929700 (unknown function)
PF3D7_0724000 (Rab GAP/kinase)
PF3D7_0406700 (KLRAQ domain)
PF3D7_0528100 (AP-1/2 β subunit)
PF3D7_1247500 (Ser/Thr protein kinase)
PF3D7_1432800 (HP12)
PF3D7_0526200 (ARFGAP2)
PF3D7_1411300 (DnaJ)
PF3D7_1421000 (DIX domain)
PF3D7_1408700 (unknown function)
PF3D7_0202600 (nucleic acid-binding)
PF3D7_1307700 (TOM1-like)
PF3D7_1205400 (kelch domain)
PF3D7_1210100 (SYN2)
PF3D7_0419500 (unknown function)
PF3D7_0503500 (protein kinase)
PF3D7_0804900 (GAP)
PF3D7_1118100 (AP-1 σ subunit)
PF3D7_1455500 (AP-1 γ subunit)
PF3D7_1459600 (Tepsin)
PF3D7_1219100 (Clathrin HC)
PF3D7_1435500 (Clathrin LC)
PF3D7_1247400 (FKBP35)
PF3D7_0408100 (unknown function)
PF3D7_0904100 (AP-4 ε subunit)

Figure 48. Comparison of proxiome of AP-1, AP-3, AP-4 and CHC.
Hierarchical clustering heatmap of AP-1, AP-3, AP-4 (this study) and CHC (Birnbaum et al., 2020) DiQ-BioID experiments (including proteins enriched in at least three out of four experiments for each target with an FDR of 0.05 or better and corrected p-value <0.1 and a log2 enrichment of at least 1.5 (AP-1, AP-4 and CHC) or 0.9 (AP-3)). Ordering according to hierarchical clustering using the Ward clustering method and Euclidean distance. NaN, grey. Bold, DiQ-BioID baits from this study.

Overall, the obtained results illustrate a model (see a proposed model in Discussion, Figure 51) of the core set up for vesicle sorting at the trans-Golgi of the parasite with a clathrin-independent AP-3 pathway, and AP-1 and AP-4 pathways both functioning in a tepsin- and clathrin-dependent manner, while the sole epsin of the parasite, EpsL, was absent (Figure 48). These findings highlight differences to model organisms, wherein AP-1 does not function with tepsin (but epsinR or epsin) and AP-4 is considered as clathrin independent (Figure 48), suggesting that these elements are to some extent interchangeable over evolutionary distances. Other aspects recapitulate the situation in other organisms, such as the HOPS/CORVET association and the clathrin-independence of AP-3.

4.2 AP-1, AP-3 and AP-4 complexes

In eukaryotic model organisms, the AP complexes are constituted of two large subunits (one each of γ/α/δ/ε/ζ and β1-5) complexed with one medium subunit (μ1-5) and one small subunit (σ1-5) (see section 1.4.2). The properties to interact with coat and accessory proteins have been demonstrated to occur predominantly within the hinge region and ear domains (Dell'Angelica et al., 1998; Owen et al., 2000; Mattera et al., 2015). An analysis performed with AlphaFold2- and AlphaFold3-predicted structures (Abramson et al., 2024) of the large adaptor subunits in *P. falciparum* (illustrated in schematic representations in Figure 49A) showed that in AP-1, the γ appendage contained the structure resembling the sandwich subdomain, and that the β1/2 appendage contained the entire ear domain (platform and sandwich subdomains), similar to AP-1 of *Toxoplasma*, plants and humans but differing to yeast (Figure 49B and C). Instead, in AP-3, the δ appendage contained the entire ear domain (sandwich and platform) matching *Toxoplasma* and humans but not yeast and plants (Figure 49B and C). In contrast, the β3 appendage was completely lost in *P. falciparum*, similar to *Toxoplasma* and yeast but differing from plants and humans (Figure 49B and C). Finally, in AP-4, both the ε and β4 appendages showed contained the platform subdomains, but not the sandwich subdomains, displaying

structural similarity with *Toxoplasma*, and partial similarity with plants and humans in their β4 platform subdomain (Figure 49B and C).

These results show similarity of the setup of appendices in the post-Golgi adaptors with *Toxoplasma gondii*, indicating conservation in apicomplexans. In contrast there were different degrees of variation in the appendage composition (platform and sandwich subdomains) compared to different organisms of the eukaryotic kingdom (yeast, plants, human), overall indicating only partial conservation of the adaptors in this parasite and common model organisms.

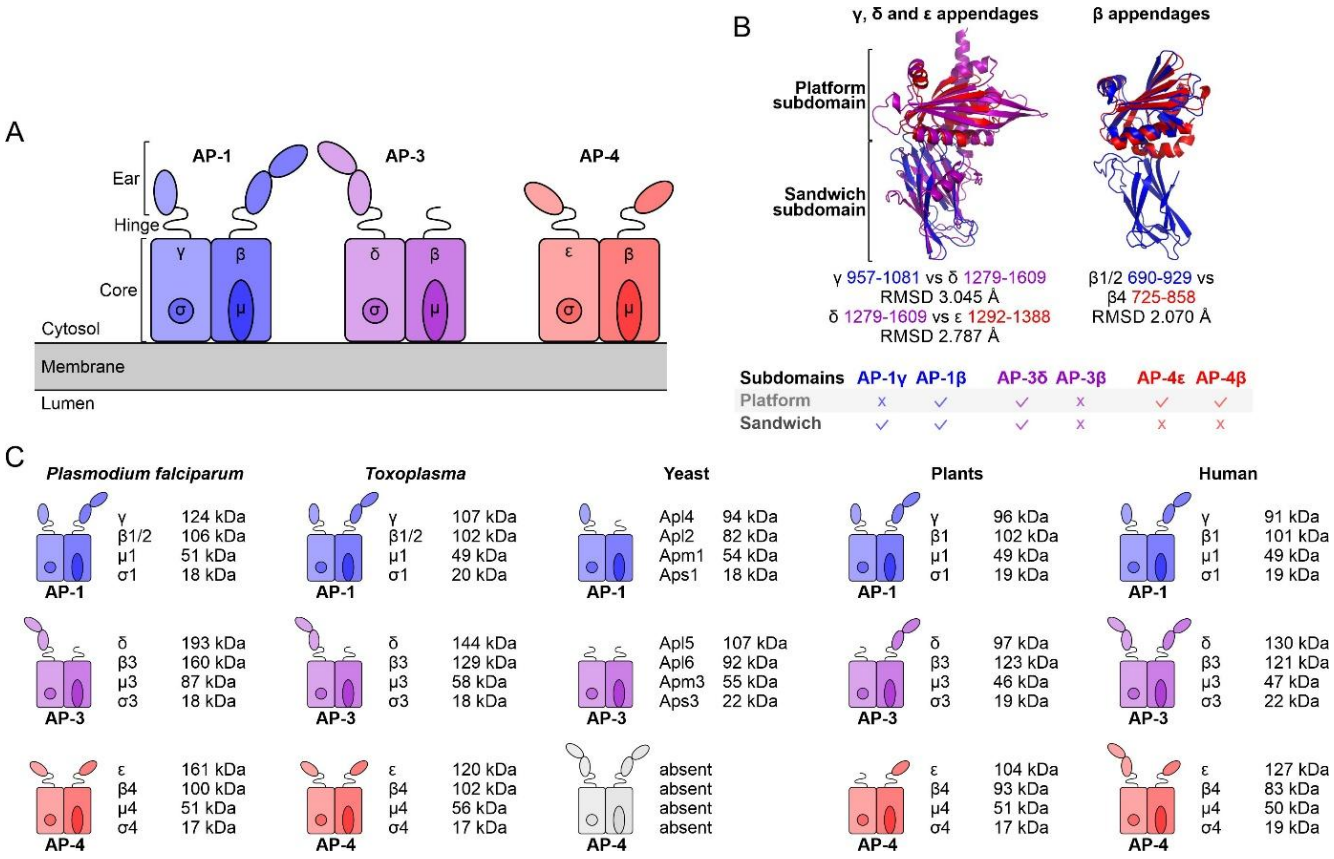

Figure 49. Comparison of AP-1, AP-3 and AP-4 complexes with those of selected other organisms. **(A)** Schematic of AP-1 (blue), AP-3 (purple) and AP-4 (red) complexes in the malaria parasite *P. falciparum*. **(B)** γ, δ and ε appendages or β1/2, β3 and β4 appendages of AP-1, A-3 and AP-4 were structurally predicted by Alphafold3 (Abramson et al., 2024) and aligned by PyMOL. **(C)** Schematic of composition and domains of AP-1, AP-3 and AP-4 complexes in *P. falciparum*, *Toxoplasma gondii*, *Saccharomyces cerevisiae* (yeast), *Arabidopsis thaliana* (plant) and *Homo sapiens* (human). All the subunits are shown, with special detail on ear subdomains, as corroborated by Alphafold2 (Varadi et al., 2024) and Alphafold3 (Abramson et al., 2024). Molecular weight (kDa) is showed for each subunit.

4.3 Sequence analysis of tepsin

As tepsin was found to be highly enriched in the AP-1 and AP-4 BioIDs in this study, as well as in the clathrin BioID and pulldowns (Birnbaum et al., 2020; Henrici et al., 2020), a thorough investigation of the N-terminal part and the C-terminal unstructured segment of this accessory protein was conducted in *P. falciparum*, *T. gondii*, *A. thaliana* and *H. sapiens* to identify motifs that may explain the association with AP-1, AP-4 and clathrin. The sequence analysis showed that PfTepsin and TgTepsin contained the ENTH- and VHS/ENTH-like domains in their N-terminal regions, in accordance with other model organisms (Figure 50A). Both domains were further apart in *Plasmodium* and *Toxoplasma* tepsin than in tepsin from plants or humans (Figure 50A). When the C-terminal unstructured region was examined, all the tepsins showed the ε- and β4-ear binding motifs as previously described (Mattera et al., 2015), with some degree of variability in the consensus sequence (Figure 50A), supporting the capability of tepsins and tepsin-like proteins in general to bind the AP-4 complex (Mattera et al., 2015). However, the unstructured C terminal segment of apicomplexan (*Plasmodium* and *Toxoplasma*) and plant (*Arabidopsis*) tepsins displayed atypical binding motifs that were absent in human (*Homo*) tepsin (Figure 50A). This included the presence of potential clathrin-binding boxes and appendage-binding motifs (Figure 50A).

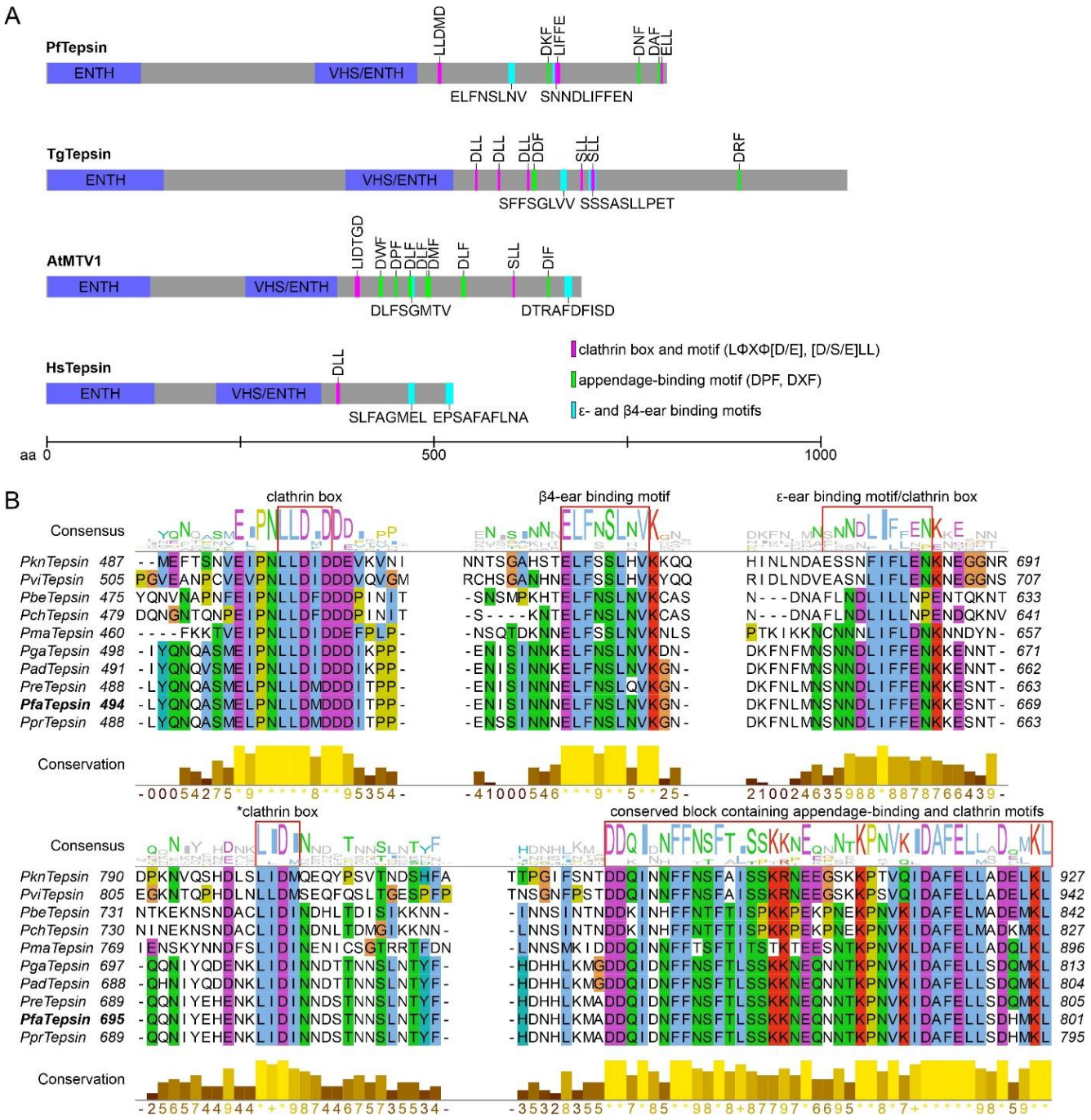

Figure 50. Sequence analysis of tepsin.

(A) Schematic representation of domains and motifs detected in Pftepsin compared to *Toxoplasma*, plant and human tepsins. ENTH and VHS/ENTH domains are shown in blue, ε-ear (ELFNSLN) and β4-ear (SNNLDLIFFEN) binding motifs for AP-4 complex in turquoise, clathrin box (LφXφD/E] and [D/S/E]LL) motifs in magenta, and appendage (DPF and DXF) binding motifs in green. Appendage-binding motifs and clathrin boxes are distributed in the unstructured C-terminal tail (downstream of the VHS/ENTH domain). The ε-ear and β4-ear biding motifs in Pftepsin correspond to the positions of the motifs detected in *P. knowlesi* (Mattera et al., 2015). Clathrin box 1 (LφXφD/E], where φ represents any hydrophobic amino acid and X any amino acid) (Dell'Angelica et al., 1998; Ter Haar et al., 2000) and clathrin box variations ([D/S/E]LL) (Morgan et al., 2000; Legendre-Guillemin et al., 2005), as well as the appendage-biding motifs (DPF and DXF) (Owen et al., 1999, 2000; Mills et al., 2003) were searched in the tepsin sequences. **(B)** Sequence comparison of unstructured C-terminal segment of tepsin of

different species of *Plasmodium* by Clustal Omega. Blocks represent the most conserved areas across the unstructured C-terminus of a full alignment (Full alignment shown in Appendix 12) and contain the ε-ear and β4-ear binding motifs for the AP-4 complex, clathrin box motifs, and appendage binding motifs. Top of aligned sequences, consensus sequence; bottom of aligned sequences: conservation of amino acids. Asterisk represents potential clathrin box.

An examination of tepsin in different *Plasmodium* species revealed the presence of highly conserved blocks distributed in the unstructured C-terminal parts with non-conserved areas flaking these blocks (Figure 50B and Appendix 12). The first block was represented by the presence of the first clathrin box (LLD[MIF]D), which showed five amino acids also conserved upstream of this motif (Figure 50A and B). The second block contained the β4-ear binding motif (ELF[NS]SL[NHQ]V), followed by the third block, which had the ε-ear domain motif ([SEFC][NSAL][NS][DN][LF]I[FL][FL][END][NP]) (Figure 50A and B). These two AP-4 appendage binding motifs were identified in the *P. knowlesi* tepsin sequence as previously described (Mattera et al., 2015). Interestingly, a second clathrin box (LIFFE) was identified in the ε-ear domain motif (Figure 50A and B), indicating that this motif (in third block) may have a dual function to bind to both AP-4 ε subunit and clathrin. A fourth conserved block showed the LIDI sequence (Figure 50B), which is very similar to the LID[LI] peptide sequences found in yeast epsins, and recently described to interact with clathrin NTD (Defelipe et al., 2024). Finally, the last block, a compact sequence of ~40 amino acids, was highly conserved in *Plasmodium* species and contained appendage (DPF and DXF)- and clathrin (ELL)-binding motifs (Figure 50A and B). Overall, these results suggest that these conserved blocks may play critical functional roles in AP-1 and AP-4 vesicles. These motifs might mediate interaction to both, adaptors (AP-1 and AP-4) as well as clathrin, thereby bridging the adaptor complex with clathrin, providing a possible explanation for the BioID findings.

5 Discussion

The present thesis investigated the function of the post-Golgi adaptors AP-1, AP-3 and AP-4 in the human malaria parasite *P. falciparum*, a unicellular organism belonging to the apicomplexans, a lineage of alveolates that includes many of the medically most important eukaryotic pathogens (Votýpka et al., 2017). The malaria parasite displays a relatively simple organisation of the secretory system, and towards the end of each round of replication in RBCs, it generates highly specialised organelles that are required for host cell invasion. The findings presented here demonstrate that all three adaptors are critical for the propagation of blood stage parasites which contrasts with many other organisms. An example for this is yeast, where none of the adaptor complexes is essential for survival under standard growth conditions (Huang et al., 1999; Yeung et al., 1999). One potential explanation for the strong dependence on adaptors in malaria parasites may lie in the importance of the specialised apical secretory system which is believed to have evolved for host cell invasion and is a defining feature of apicomplexan parasites. As invasion was either directly or indirectly compromised by the conditional inactivation of each of the adaptors, sorting events needed for the biogenesis of this system or for the delivery of its proteins are likely to be important for parasite propagation. A further reason for the importance of all adaptors in malaria parasites could be the lack of other adaptors – such as GGAs – which, in other organisms, contribute to the post-Golgi protein sorting (Boman, 2001). Another reason could be the use of a rapid inactivation system – known as "knock sideways" or "anchor away" – which has been previously demonstrated to avoid compensatory effects when analysing vesicle adaptors (Robinson et al., 2010; Hirst et al., 2012; Davies et al., 2018; Buser et al., 2018, 2022).

5.1 Localisation of post-Golgi adaptors AP-1 AP-3 and AP-4

Plasmodium falciparum parasites contain the genes encoding the post-Golgi trafficking machinery mediated by AP-1, AP-3 and AP-4, whereas AP-5 is a pseudogene (Hirst et al., 2011). During blood-stage development of the parasite, these adaptors were localised in close proximity to the cis-Golgi, and colocalised even more closely with clathrin-positive regions. The number of AP foci increased when the parasites progressed to the end of the erythrocytic

cycle (Figures 15-23). Given that AP-1 foci covered more clathrin-positive regions than AP-3 and AP-4 (Figure 24B), and that AP-1 colocalised with the trans-Golgi marker Rab6 (Figure 29E), the data suggests that AP-1 localises at the trans-Golgi compartment. Based on these results, the trans-Golgi, which is spatially separated from the cis-Golgi (Van Wye et al., 1996; Adisa et al., 2007; Struck et al., 2008), also harbours AP-3 and AP-4, likely located in distinct regions specific for these adaptors. Consequently, other cytosolic factors present in the parasite, such as the retromer complex, may be involved in the retrieval of adaptor-sorted cargoes to the trans-Golgi (Krai et al., 2014).

5.2 AP-1 knock sideways

The knock sideways approach was used to conditionally inactivate the post-Golgi adaptors and to study protein function in the parasite. To inactivate the adaptors, the μ subunit was chosen because its function by recognising sorting signals in the cytosolic tail of transmembrane cargoes, a critical step in the recruitment of the adaptors onto the membrane and the formation of adaptor-coated vesicles. In addition, studies have demonstrated that the knockout of any adaptor subunit leads to a full inactivation of the entire complex when missing from the complex (Meyer et al., 2000; Peden et al., 2002). The subunits have been observed to assemble in both heterodimers or heterotrimers, however, in most of cases, these assemblies are not functional (Meyer et al., 2000; Peden et al., 2002). In the context of the parasite, the conditional inactivation via knock sideways takes the adaptors away from their site of action (recruited to the nucleus), leading to a functional deactivation of the entire complex. The data presented in this thesis showed that the inactivation of AP-1 significantly impacted the blood-stage development of the parasite, suggesting that this adaptor plays a critical role in trafficking functions. During the characterisation of the knock sideways phenotype, inactivating at different parasite stages, it was observed that AP-1 was required for the late trophozoite-to-pre-segmented schizont transition (inactivation in ring stage parasites; discussed in 5.2.1), and before parasite egress (inactivation prior to cytokinesis, discussed in 5.2.2).

5.2.1 Conditional inactivation of AP-1 in ring parasites shows impact of AP-1 in trophozoites and for sorting

The first phenotype was characterised by a progressive impact on the endomembrane system, as evidenced by the formation of translucent vesicles that grew in size and then likely fused to the large translucent vacuole observed after longer inactivation times (Figure 32). The inactivation did not appear to affect the ring stage (0-18 hours) and the main activity of this stage, protein export, was not apparently affected. Rings also endocytose early after invasion and inactivating this activity arrests the parasite at the transition to the trophozoite stage (Birnbaum et al., 2020). As endocytosis was in later stages not affected after AP-1 inactivation, this again is in conform with the lacking effect on progression to the trophozoite stage. The lacking impact on endocytosis after AP-1 inactivation was based on a number of findings: (i) the presence of haemozoin crystals in the FV in trophozoites (24-32 hours post-invasion), (ii) the internalisation of the FV biogenesis marker $MSP1_{19}$ to the FV membrane, and (iii) the trafficking of Plasmepsin II to FV. All of this suggested that endocytosis processes and the function of the FV machinery are functional up to early/middle trophozoites and indicate that endocytosis and post-Golgi trafficking are conducted by independent routes and mechanisms. This idea is reasonable, considering that the clathrin-independent endocytosis process is coordinated by AP-2 (Birnbaum et al., 2020; Henrici et al., 2020). Despite the fact that the sole β1/2 subunit exhibits dual functionality for both AP-1 (post-Golgi) and AP-2 (endocytosis) adaptors (Birnbaum et al., 2020; Henrici et al., 2020; Sabitzki, 2022), it is likely that the conditional inactivation of the µ1 subunit of the AP-1 complex did not influence the β1/2 subunit-mediated endocytic role.

Furthermore, the data demonstrated that the default secretion pathway and protein export remained functional in parasites with AP-1 inactivated (Figure 30A-D), indicating that default transport through the secretory pathway to deliver proteins beyond the confines of the PPM does not depend on AP-1 sorting at the trans-Golgi. A comparable finding was described for the knockdown of sortilin (Hallée et al., 2018b), a canonical cargo receptor, thereby supporting the hypothesis that general secretion and protein export use AP-1- and sortilin-independent trafficking routes. Since default pathway leads to the secretion of proteins to the PV lumen and subsequent internalisation to the FV via endocytosis in malaria parasites (Figure 30A), the panorama seems slightly different regarding to the related apicomplexan parasite, *T. gondii*. In these coccidian parasites, the dense granules (and the plasma membrane) constitute the default constitutive pathway for soluble proteins (Karsten et al., 1998; Striepen et al., 1998, 2001;

Chaturvedi et al., 1999). It is noteworthy that the ablation of TgSORTLR and TgAP-1 using an inducible knock-out (KO) system did not compromise the biogenesis of dense granules, as microneme and rhoptry proteins were rerouted to this organelle and discharged to the vacuolar space (Sloves et al., 2012; Venugopal et al., 2017). These findings contrast to the malaria parasite, in which the dense granules are formed very late during the schizogony (Vallintine & van Ooij, 2023).

The early inactivation of AP-1 did not impact the architecture of the ER and the cis-Golgi on the fluorescence microscopy level (Figure 29B and C). With regard to the cis-Golgi, this finding is consistent with the simple and rudimentary sub-compartmentalisation of the Golgi apparatus in malaria parasites, where it cooperates with the trans-Golgi platform for secretory functions (see section 5.1). In contrast, the integrity of the trans-Golgi – as determined by the presence of markers such as Rab6 and AP-3 – was partially affected, indicating that AP-1 inactivation impairs the integrity of the exit face of the Golgi apparatus. Similar finding has been described for the knock down of sortilin using the cis-Golgi marker ERD2 and the trans-Golgi marker Rab6 (Hallée et al., 2018b), suggesting that this adaptor controls the AP-1-dependent protein sorting and vesicular trafficking, as well as the organellar integrity downstream of the trans-Golgi compartment. However, it should also be noted that the membranes of the trans-Golgi were not directly visualised and the exact nature of this disturbance remains unknown.

In order to further understand the impact of the AP-1 inactivation on protein sorting and vesicle trafficking in malaria parasites, two proteins were studied: clathrin and sortilin. In eukaryotic organism models, clathrin is a scaffolding protein that is recruited during the formation of AP-1 vesicles by interacting with a clathrin box present in the hinge region of large subunits of this adaptor complex (Shih et al., 1995; Doray & Kornfeld, 2001). Sortilin is a multiligand receptor that possesses tyrosine- and dileucine-based sorting motifs in its C-terminal cytosolic tail which are recognised by AP-1, AP-2, AP-5, GGAs and the retromer complex (Nielsen et al., 2001; Seaman, 2007; Canuel et al., 2008; Hirst et al., 2018; Mitok et al., 2022).

In the context of malaria parasites, only the γ subunit hinge of the AP-1 complex contains a clathrin binding box (DLLDLD, residues 822 and 827) which may recruit the clathrin triskelion, but not the β1/2 subunit hinge of the subunit incorporated into the AP-1 and AP-2 complexes. This may explain why the AP-2 complex does not recruit clathrin and mediates clathrin-independent endocytosis in *P. falciparum* parasites (Birnbaum et al., 2020; Henrici et al., 2020) and *T. gondii* (Pieperhoff et al., 2013; Wan et al., 2023). With regards to sortilin, its C-terminal cytosolic tail contains the tyrosine (YSVI, between residues 813 and 816)- and dileucine

(DVPTLL, between residues 845 and 850)-based sorting motifs, which may be recognised by the μ and β1/2 subunits of the AP-1 complex. Evidence for a function of certain tyrosine-based sorting motifs in apicomplexan parasites has previously been provided (Hoppe et al., 2000; Ngô et al., 2003) but potential substrates can be trafficked without the tail containing the motifs (Treeck et al., 2006), leaving the relevance of these motifs for sorting in the parasite an open question. The results of this study illustrate a highly conserved association between AP-1, clathrin and sortilin in malaria parasites.

An analysis of control trophozoite-stage parasites (24–32-hour post-invasion) showed that AP-1 colocalised with clathrin- and sortilin-positive regions, suggesting that both clathrin and sortilin are interaction partners of AP-1 (see AP-1 proxiome, sections 5.5 and 5.6), whose interaction is conserved in other organisms (Ter Haar et al., 2000; Canuel et al., 2008). In agreement with a functional connection of these interactions, the inactivation of AP-1 resulted in an impaired clathrin and sortilin localisation, with clathrin being dispersed in the parasite cytosol and sortilin being missorted to the PPM and internalised via endocytosis to the FV (Figure 34A, B and D). Furthermore, it was evident that sortilin accumulated in trans-Golgi-like foci, suggesting that remnants of this cargo receptor might be retained at the trans-Golgi compartment due to the absence of proper sorting adaptors. These results are intriguing because sortilin is potentially trafficked to the PPM via the default pathway, indicative of a failure to sort it into the correct pathway. From the PPM, it is then internalised to the FV using the endocytic machinery, which is apparently functional up to the trophozoite stage when AP-1 is not functional. These results contrast with those observed in *Toxoplasma*, where the inducible ablation of TgAP-1 does not appear to disrupt the trans-Golgi localisation of TgSORTLR (Venugopal et al., 2017). The disparities in the default pathways of *Plasmodium* and *Toxoplasma* may provide an explanation for these incongruences, although TgSORTLR was not missorted to the dense granules (Venugopal et al., 2017). A different explanation could be that *Toxoplasma* possesses an "elaborated" endosomal system (Tomavo, 2014), which is responsible for the recycling of missorted SORTLR back to the trans-Golgi compartment in the absence of TgAP-1. In more detail, the retromer complex is the endosomal player involved in the retrieval of SORTLR from Rab7-positive endosome-like compartments (ELCs) to the trans-Golgi compartment (Sangaré et al., 2016). The inducible knockout of VPS35, a component of the retromer complex, led to the accumulation of SORTLR in Rab5A- and Rab7-positive ELCs (Sangaré et al., 2016).

Whether such a pathway exists in malaria parasites is not clear. The existence of ELCs in malaria parasites remains a subject of debate due to the lack of reliable endosomal markers for their identification. Assuming it does not exist or is more limited in function in malaria parasites than in *T. gondii*, the endosomal system machinery may not be sufficient to recycle sortilin back to the trans-Golgi compartment, permitting a part of the population of this receptor to escape to the PPM via the default pathway. Interestingly, the retromer complex has been investigated in the parasite, and their subunits – VPS26, VPS29 and VPS35 – have been described as localising in endosome-like membrane structures and colocalising with a limited number of punctate structures with Rab7 (Krai et al., 2014). Based on this evidence, AP-1 may facilitate the delivery of cargoes (e.g., sortilin) from the trans-Golgi compartment to the retromer complex-associated compartments (anterograde trafficking). In turn, the retromer complex may act as a mediator in the retrieval of cargoes from its resident compartments to the trans-Golgi (retrograde trafficking). Nevertheless, it is conceivable that the parasite may possess a variety of endosome-like membrane structures, which could function as intermediate platforms for the specific sorting to different destinations. A hypothetical outgoing function for AP-1 in malaria parasites reflects marked differences compared to classical model organisms, where AP-1 has been proposed to mediate a retrograde trafficking from endosomes to the TGN (see section 1.4.2.1; (Robinson et al., 2024)). However, the absence of GGAs in the parasite genome – except by the presence of a hybrid GGA-like protein (KIC4) localised at the kelch13 compartment and involved in endocytosis (Birnbaum et al., 2020; Schmidt et al., 2023) – underscores the potential involvement of AP-1 in the anterograde trafficking process in malaria parasites. If AP-1 retained a retrieval function as described in model organisms (Robinson et al., 2024), the phenotype may be similar, with a failure to return sortilin to the trans-Golgi, and then leading to its escape to the PPM.

In eukaryotic model organisms, Rab7 is a small GTPase located in early and late endosomes and lysosomes, and is involved in multiple functions such as the maturation of early endosomes to late endosomes, trafficking from late endosomes to lysosomes, biogenesis of lysosomes, and fusion of late endosomes and lysosomes (Guerra & Bucci, 2016; Borchers et al., 2021). In the context of malaria parasites, Rab7 has been identified as a potential endosomal marker that colocalises with the retromer complex in specific foci (Krai et al., 2014), and delimits circular compartments associated with the FV (Flemming, 2015; Sabitzki, 2022). As shown in the result section 4.1.5, the conditional inactivation of AP-1 resulted in an increased cytosolic pool of Rab7, whilst other Rab7-positive compartments remained unaffected. Since AP-1 knock

sideways exerted no discernible effect on endosomal transport to the FV, this finding might indicate an effect on the trans-Golgi to endosome trafficking of secretory cargoes, a role previously suggested to Rab7, with possible participation of the retromer complex (Krai et al., 2014). This agrees with the lack of endocytosis function of the Rab7 GEF PfMon1/Sand1 (Sven thesis, (Birnbaum et al., 2017; Sabitzki et al., 2024) and the repurposing of endosomal components for the formation of secretory organelles in apicomplexan parasites (Tomavo, 2014).

Moreover, the inactivation of AP-1 resulted in a marked defect at ultrastructural levels in trophozoites (24-32 hpi) or during schizont development (30-38 hpi), which showed the appearance of unusual compartments with a translucent lumen in the parasite cytosol that increased in size with continued inactivation time (within hours), in a similar manner as described for the knockdown of sortilin in certain *P. falciparum* parasites (Hallée et al., 2018b), as well as the knockout of TgAP-1 in *Toxoplasma* parasites (Venugopal et al., 2017). Overall, the findings indicate an impairment of the secretory pathway downstream to the trans-Golgi that is specific to AP-1 but does not affect general secretion but leads to the build-up of unknown membranous structures. The findings also show that the involved trafficking routes are essential for the development and transition from trophozoites to schizonts.

5.2.2 Conditional inactivation of AP-1 in pre-segmented schizont parasites affects the biogenesis of invasion-related organelles

The knock sideways of AP-1 also showed a defective schizont development when it was inactivated prior to cytokinesis. The present section will focus on the role of AP-1 sorting for the invasion-related organelles formed at the end of schizogony, represented by the apical secretory organelles – rhoptries, micronemes, and dense granules – and the scaffold structure for assembly of daughter merozoites, the IMC. The data presented in this thesis provide compelling evidence that AP-1 does not colocalise with any apical secretory organelles and the IMC.

For instance, while AP-1 was found in close proximity to rhoptries using specific markers for the cytosolic (ARO) and luminal (RON12) faces of the rhoptry bulbs, the markers did not overlap (Figures 35B and D). These findings contrast with the apparent overlap between AP-1 and the resident rhoptry proteins RAP1 and Clag3.1, as previously described (Kaderi Kibria et al., 2015). One possible explanation for this discrepancy is the close vicinity of these organelles

(Bannister et al., 2000b), which could result in overlap in merozoites. Considering that AP-1 is localised at the trans-Golgi (data based on this thesis) and that the secretory trafficking is highly polarised during schizogony (Cowman et al., 2017), it is expected that organelles such as rhoptries, lie in close proximity to the Golgi cisternae (Bannister et al., 2000b; Hanssen et al., 2013). Studies in *Toxoplasma* have suggested that the trafficking of apical cargoes from the trans-Golgi platform – for example, rhoptry proteins – is preceded by their delivery to ELCs, followed by precursor compartments, and ultimately to their apical destination compartments (Sakura et al., 2016).

The inactivation of AP-1 affected the biogenesis of apical secretory organelles, as ARO was found diffuse in the parasite cytosol, and RON12 and AMA1 were diffuse in the parasite cytosol, accumulated in the ER or secreted to the PV lumen, most probably via the default pathway. Similar findings showing a defect in the biogenesis of apical secretory organelles were observed in the knockdown of sortilin in malaria parasites (Hallée et al., 2018b), as well as in the knockout or ablation of TgAP-1, clathrin and SORTLR in *T. gondii* (Sloves et al., 2012; Pieperhoff et al., 2013; Venugopal et al., 2017). In addition, the biogenesis of the IMC was also affected in parasites with inactivated AP-1, indicating that this adaptor is essential for the formation of, and trafficking of specific cargoes to, these specialised organelles during schizogony. Based on this evidence, AP-1 selects cargoes at the trans-Golgi, packages them into clathrin-coated vesicles and subsequently transports them, either directly or indirectly, to these invasion-related organelles. Interestingly, sortilin/SORTLR, which is recognised by AP-1, has been described as acting as a multiligand receptor and as a single escorter for specific cargoes destined for rhoptries, micronemes, dense granules and the IMC in apicomplexan parasites (Ngô et al., 2003; Sloves et al., 2012; Venugopal et al., 2017; Hallée et al., 2018a; Honfozo et al., 2023; Li et al., 2024). How the function in the biogenesis of these organelles is related to the sorting function is not clear, but likely the biogenesis depends on cargo proteins and membrane material from the AP-1 transport pathway (Ngô et al., 2003). In addition, the trans-Golgi compartment plays a pivotal role in the biogenesis of apical secretory organelles and the IMC, as earlier studies have suggested that rhoptries, micronemes and dense granules are formed from Golgi-derived vesicles or the ER (Bannister et al., 2000b, 2003; Counihan et al., 2013).

5.3 AP-3 knock sideways

The findings of this thesis showed that the inactivation of AP-3 starting in early parasite stages did not have any effect on the development of the parasite during intracellular growth but led to a defective invasion, characterised by a detection of free merozoites in Giemsa smears and reduced rate of newly formed ring-stage parasites in comparison to controls. Although a subsequent examination revealed that the integrity of the apical secretory organelles – rhoptries, micronemes and dense granules – and the IMC remined unaffected, the finding suggests that AP-3 mediates the traffic of specific cargoes to the invasion-related organelles rather than contributing to the biogenesis or integrity of them. However, it cannot be excluded that the effect is indirect, for instance due to mis-sorting of proteins that impair invasion through unrelated negative effects. AP-3, located in clathrin-positive areas at the trans-Golgi compartment (see section 5.1), did not colocalise with any apical secretory organelles and the IMC. These results are consistent with sorting roles at the trans-Golgi.

In organisms such as mammals, yeast and plants, AP-3 has been described to mediate the transport of cargoes to lysosomes, lysosome-related organelles or vacuoles (Simpson et al., 1996, 1997; Cowles et al., 1997; Ooi et al., 1997; Stepp et al., 1997; Peden et al., 2004; Zwiewka et al., 2011). In contrast, malaria parasites lack these classical organelles, but instead possess the FV, a specialised lysosome-like organelle that is exclusive to the genus *Plasmodium* (Klemba et al., 2004a). Nonetheless, it is unlikely that AP-3 traffics cargoes to the FV, as the knock sideways AP-3 parasites did not show an impact on the morphology or content (hemozoin) of this organelle.

5.4 AP-4 knock sideways

The inactivation of AP-4 early in the parasite cycle did not impair intracellular development of the parasite but resulted in a defective invasion, with the presence of non-invaded free daughter merozoites apparent in Giemsa smears and a reduced rate of newly-formed ring-stage parasites, which was more pronounced in comparison to the AP-3 phenotype. At first glance, these findings indicate that AP-4 has trafficking functions related to invasion.

AP-4 did not colocalise with any apical secretory organelles and the IMC, suggesting transport functions associated with the trans-Golgi compartment and its inactivation did not show differences in the integrity of the invasion-related organelles, except for a minor impact on the microneme protein AMA-1 of unknown relevance, which suggest that this adaptor may play a

role in the trafficking to this organelle. However, based on the identification of likely cargoes for AP-4 in this work (discussed further in section 5.7) that all consisted of membrane transporters, it seems more likely that the impairment of invasion after AP-4 inactivation was due to an indirect effect. Further work will be needed to understand the exact trafficking routes this adaptor sorts proteins into.

5.5 AP-1 and AP-4 proxiomes – coat and accessory proteins

DiQ-BioID is a powerful tool used to identify the proxiome of the protein of interest in living parasites (Birnbaum et al., 2020). Based on the well-established FKBP-FRB dimerisation system (Banaszynski et al., 2006), the DiQ-BioID has the advantage that background biotinylation in the same parasite culture can be subtracted, thereby resulting in highly specific proxiomes (Kimmel et al., 2022).

In this section, the proxiomes of AP-1 and AP-4 are discussed with emphasis on the coat and accessory proteins. The findings for the proxiomes of AP-1 and AP-4 showed some unexpected disparities, with the detection of tepsin and clathrin, which were highly enriched with both adaptors with similar values when compared to the adaptor subunits. Tepsin, an accessory factor exclusive for AP-4 (Borner et al., 2012), was found to function with AP-1 in this study, indicating that both AP-1 and AP-4 require tepsin in *P. falciparum* parasites. Interestingly, recent studies have identified this accessory protein to be significantly enriched in the DiQ-BioID and Co-IP of clathrin (Birnbaum et al., 2020; Henrici et al., 2020), a canonical scaffold protein for AP-1 vesicles (see section 1.4.3.1).

In agreement with these findings, neither the BioIDs with AP-1 in this study nor previous clathrin BioID and Co-IP experiments (Birnbaum et al., 2020; Henrici et al., 2020) detected the sole epsin-like ENTH protein EpsinL but instead detected tepsin. These results contrast with those previously obtained in *T. gondii*, where TgAP-1 was shown to interact with TgEpsinL (Venugopal et al., 2017), indicating that the association between tepsin and AP-1 in malaria parasites is not an ancestral state, but likely a secondary taxa-specific adaptation. Considering that AP-1 requires an ENTH protein (Clint1/EpsinR in mammals, Ent5 in yeast, Epsin1 in plants, EpsL in *Toxoplasma*) as an accessory vesicular factor (Duncan et al., 2003; Mills et al., 2003; Song et al., 2006; Venugopal et al., 2017), these results might point to tepsin as an accessory component with shared functions for the AP-1 and AP-4 vesicles in malaria parasites.

Irrespective of the evolutionary origin, the data shows that the type of ENTH domain protein is not necessarily hard-wired to a specific type of adaptor.

A further distinguishing feature from common model organisms was the association of clathrin with AP-4. While the functional link between AP-4 and clathrin could not be validated in the same way as it was done with AP-1, previous BioIDs with clathrin provide support for this connection (Birnbaum et al., 2020). An association of AP-4 with clathrin-coated vesicles has also been described in plants and Trypanosomes (Kalb et al., 2016; Dahhan et al., 2022), indicating that this occurs in diverse other taxa and may be conserved in apicomplexans.

Bioinformatic analysis performed here identified potential clathrin-binding (LφXφ[D/E], ELL) and appendage-binding (DxF) motifs (Dell'Angelica et al., 1998; Owen et al., 1999; Ter Haar et al., 2000) in the unstructured C-terminus of tepsin (Figure 50A). These motifs were found in conserved blocks of C-terminus between different *Plasmodium* species (Figure 50B). Based on these findings, the existence of clathrin- and appendage-binding motifs could serve as a linkage between tepsin, clathrin and AP-1 as well as AP-4. This would be reminiscent to the situation in plants, wherein the tepsin-like AP-4 interacting protein MTV1 has been shown to interact with clathrin (Sauer et al., 2013; Heinze et al., 2020). This result indicates that in malaria parasites, tepsin contributes to the recruitment of clathrin during AP-1 and AP-4 vesicle coat formation.

Besides tepsin, AP-4 vesicles in mammals also incorporate the FHF complex (Mattera et al., 2020) and RUSC1/2 (Davies et al., 2018) as accessory components. Despite the parasite expressing HOOK and FTS, which are components of the FHF complex, both were undetectable in the AP-4 BioID, suggesting that they are not components of AP-4 vesicles in the parasite. The AP-4 proxiome, however, identified a coiled coil protein (PF3D7_0408100) with a high degree of confidence, which was also observed in the clathrin BioID (Birnbaum et al., 2020). A search by HHpred and InterPro revealed that this protein, which is conserved across *Plasmodium* species, showed partial similarity with dynein and myosin, suggesting that it may be an accessory or tethering component for AP-4 vesicles. However, as these similarities were in a region predicted to form coiled coils which frequently result in similarities to dyneins and myosins, they likely are protein-protein interaction regions rather than actually having functions related to these proteins.

Interestingly, the DiQ-BioID of AP-1, as well as the DiQ-BioID and Co-IP of clathrin (Birnbaum et al., 2020; Henrici et al., 2020) identified a VHS-domain protein, named TOM1L

in PlasmoDB. The presence of TOM1L in the AP-1 proxiome might indicate a cooperativity for the AP-1- and clathrin-coated vesicles. In model organisms, TOM1, a member of the subfamily of VHS domain (T. Wang et al., 2010), is involved in the initial steps of endosomal cargo sorting (T. Wang et al., 2010). It interacts with ubiquitinated protein cargoes via its VHS and GAT domains, as well as with clathrin through its C-terminus (Yamakami et al., 2003; Roach et al., 2021). Based on this, it is also possible that this protein version in the parasite might mediate independent functions via the VHS domain (as TOM1L lacks the GAT domain), thereby contributing to the post-Golgi vesicular trafficking. More studies are required to elucidate the function of this protein.

5.6 AP-1 proxiome – cargoes and destination compartments

The proxiome of AP-1 also identified sortilin (Krai et al., 2014; Hallée et al., 2018a) as the major receptor of the AP-1 complex in malaria parasites. Pfsortilin – and its *Toxoplasma* ortholog, TgSORTLR – are multiligand receptors (Willnow et al., 2008; Mitok et al., 2022) that interact with a vast repertoire of apical proteins via the luminal VPS10-domain (Sloves et al., 2012; Hallée et al., 2018a; Honfozo et al., 2023; Li et al., 2024).

In both of these apicomplexan parasites, this receptor is needed for the transport of proteins destined for invasion-related organelles (Sloves et al., 2012; Hallée et al., 2018a, b). The single receptor-dependent sorting functions align with the AP-1 inactivation phenotype observed in this work. In a similar manner, the absence of alternative multiligand receptors in malaria parasites, such as the hydrolase receptor MPRs (Krai et al., 2014), suggests a high degree of dependence of AP-1 on sortilin for trafficking of luminal cargoes to invasion-related organelles. This is further supported by the absence of AP-5 and GGAs in the *P. falciparum* parasite genome, both of which recognise sortilin in mammalian cells (Nielsen et al., 2001; Hirst et al., 2018).

The AP-1 proxiome also identified VPS9, in agreement with the findings of the clathrin BioID and pull-down (Birnbaum et al., 2020; Henrici et al., 2020), suggesting that this Rab5 GEF might localise in VPS9-positive compartments, which function as intermediate stations for AP-1- and clathrin-coated vesicles (Sakura et al., 2016). Interestingly, the VPS9 ortholog in *Toxoplasma*, TgVPS9, has been described as localising in the ELCs, colocalising with TgRab5A and TgSORTLR, and its ablation by knocking out impaired the biogenesis of apical secretory organelles (Sakura et al., 2016). Equally, inactivation of PfRab5a has a schizont

phenotype, which might be due to a similar function (Flemming, 2015; Birnbaum et al., 2017). Furthermore, the detection of multiple SNAREs in the AP-1 proxiome indicates that AP-1 is involved in multiple pathways, although in other organisms some of the SNAREs have been reported to also be cargo (Peden et al., 2001; Hirst et al., 2012; Shimizu et al., 2021; Dahhan et al., 2022; Robinson et al., 2024) and thus the presence of multiple SNAREs are not necessarily indicators for different destinations.

5.7 AP-3 proxiome

The dependence on clathrin for AP-3 varies between organisms and is still debated, with some studies indicating an interaction (Dell'Angelica et al., 1998; Drake et al., 2000; Zwiewka et al., 2011), or no interaction (Simpson et al., 1996; Zlatic et al., 2013; Schoppe et al., 2020) with this coat protein in mammalian cells, plants and yeast (see section 1.4.3.1). Recent studies in yeast have shown a cargo-dependent recruitment of AP-3 onto membranes and subsequent formation of AP-3 lattices capable of inducing membrane curvature to generate vesicles or tubules without an outer scaffold protein (Schoppe et al., 2021; Begley et al., 2024). This recruitment is facilitated by the amphipathic helices present in the AP-3 subunits, which are capable to insert into the membrane (Begley et al., 2024). This may also apply to malaria parasites, for which the proxiome of AP-3 did not include any evidence for a coat such as clathrin.

Furthermore, the AP-3 proxiome failed to detect other accessory proteins or transmembrane cargoes. However, components of the Mon1-Ccz1 complex (Rab7 GEF) (Nordmann et al., 2010) and subunits of the HOPS/CORVET complexes were detected, albeit with enrichment levels that were lower relative to the AP-3 subunits than that of typical accessory or coat proteins in the AP-1 and AP-4 proxiomes. In other organisms, both Mon1-Ccz1 and HOPS/CORVET complexes are involved in vacuolar fusion and trafficking for AP-3 vesicles (Balderhaar & Ungermann, 2013). The list of enriched proteins included two previously unannotated HOPS-like proteins: a possible parasite VPS41 designated PfVPS41L (Mesén-Ramírez et al., 2025) and another termed PfHOPS-L. Additionally, the HOPS/CORVET subunits VPS11 and VPS18 were identified. In other organisms, Rab7 interacts with HOPS subunits, promoting the recruitment of this heterocomplex onto the target membrane (Brett et al., 2008; Plemel et al., 2011; Ungermann & Moeller, 2025).

Recently, it was described that AP-3 colocalised with VPS11, a subunit of the HOPS and CORVET complex in *P. falciparum* (Mesén-Ramírez et al., 2025). Interestingly, the conditional inactivation of certain subunits of this complex – VPS11, VPS16 or VPS18 – showed an effect on endocytosis and invasion (Mesén-Ramírez et al., 2025). The invasion phenotype was characterised by the mistrafficking of microneme and rhoptry proteins (Mesén-Ramírez et al., 2025). As the HOPS-CORVET complex – via the VPS41 subunit – is involved in the tethering of uncoated AP-3 vesicles in model organisms (Rehling et al., 1999; Angers & Merz, 2009; Cabrera et al., 2010; Asensio et al., 2013; Schoppe et al., 2020), and form different hybrid complexes based on the composition of its VPS subunits (Balderhaar & Ungermann, 2013; Van Der Beek et al., 2019; Ungermann & Moeller, 2025), it is conceivable that one of these hybrid complexes not yet determined might be specific for AP-3 vesicles in malaria parasites. The knock sideways phenotypes of VPS11, VPS16 and VPS18 (Mesén-Ramírez et al., 2025) differed to the knock sideways phenotype described here for AP-3 (see section 4.1.12). Based on the above, one explanation may be the presence of the distinct hybrid HOPS-CORVET complexes in the parasite, which mediate a variety of functions, with one of them being specific for AP-3 vesicles. Another explanation may be that these HOPS and CORVET-positive compartments – potentially ELCs – receive cargo vesicles via alternative adaptors (e.g., AP-1).

Overall, the proxiome data is congruent with an emerging model (mostly from yeast) suggesting that clathrin-free AP-3 vesicles bud from the trans-Golgi platform and subsequently fuse with a Rab7-positive endosomal target compartment via interaction with VPS41 of the HOPS-CORVET complex (Rehling et al., 1999; Angers & Merz, 2009; Cabrera et al., 2010; Balderhaar & Ungermann, 2013; Asensio et al., 2013; Schoppe et al., 2020). Hence, in malaria parasites AP-3 likely is needed for transport to an endosomal compartment involved in secretion and this may be similar to metazoan cells where VPS41 and AP-3 function in regulated secretion (Asensio et al., 2010, 2013; Sirkis et al., 2013). A repurposed secretory function of the AP-3 target compartment in the parasite is supported by PfMon1/Sand1, one of the highest enriched proteins in the AP-3 proxiome, which is dispensable for endosomal trafficking in trophozoites, yet essential for schizont stages (Birnbaum et al., 2017; Sabitzki et al., 2024), supporting an important function related to the invasion phenotype observed in parasites with inactivated AP-3. Overall, this indicates that AP-3 is needed for protein transport to an endosomal compartment repurposed for secretory functions (Tomavo, 2014) that likely is distinct from that AP-1 transports cargo to.

The BioID data did not reveal SNAREs (and regulators), indicating that AP-3 had already left the vesicle when SNAREs mediate fusion, or alternatively, that the HOPS/CORVET complex itself mediates fusion. The absence of potential cargoes could be due to the low expression of AP-3 (based on its transcript expression compared to AP-1 and AP-4 in PlasmoDB) or low affinity of AP-3 to bind its cargo.

5.8 AP-4 proxiome - cargoes

In contrast to the evidence for multi-ligand receptor-mediated sorting of AP-1, no obvious cargo receptor was detected in the AP-4 proxiome of the parasite. Instead, a number of multi-pass transmembrane proteins were found to be enriched, thereby providing evidence that they are cargoes for the AP-4 sorting pathway (see Figures 46 and 47). Interestingly, works in mammalian cells and plants started to reveal AP-4 cargoes. These included the lipid scramblase ATG9A (Mattera et al., 2017; Davies et al., 2018; De Pace et al., 2018), the carrier proteins SERINC1 and SERINC3 (Davies et al., 2018), and the diacylglycerol lipase beta (DAGLB, (Davies et al., 2022)) in mammals, or the borate transporter 1 (BOR1, (Yoshinari et al., 2024)), and the metal transporters NRAMP3 and NRAMP4 (Müdsam et al., 2018) in plants. It is therefore possible that AP-4 preferably sorts multi-pass membrane proteins and that this is conserved across wide evolutionary distances although single-pass type-I transmembrane cargoes such as e.g., APP (Burgos et al, 2010), VSR1 (Fuji et al, 2016) or ApoER2 (Caracci et al., 2024) are also known. Despite the fact that ATG9A – the sole transmembrane protein in the autophagy machinery and the best-studied AP-4 cargo (Mattera et al., 2017; Davies et al., 2018) – has been identified in various groups of eukaryotes, including *Toxoplasma* (Smith et al., 2021; Zhang et al., 2021), it is not present in malaria parasites (Brennand et al., 2011; Hain & Bosch, 2013; Cervantes et al., 2014). This raises the question of the panorama of cargoes for AP-4 and their similarities or differences compared to other organisms.

The potential cargoes identified in the proxiome of AP-4 in the malaria parasite included proteins such as CDF, CuTP, CRT-like transporter and VIT. These transporters were previously reported to localise mostly in cytosolic vesicles that for VIT were considered to be acidocalcisomes (Kenthirapalan et al., 2014; Sayers et al., 2018; Wichers et al., 2022; Wunderlich, 2022; Wunderlich et al., 2024). Acidocalcisomes – defined as lysosome-like organelles present in a wide range of evolutionarily distant organisms – were in *Trypanosomes* shown to be rich in transporters, including TbVIT, TbZnT2 (corresponds to PfCDF) and

TbCuTP (Huang et al., 2014; Docampo & Huang, 2016; Huang & Docampo, 2024) and contain V-ATPase (Vercesi et al., 1994), which was also detected in the AP-4 proxiome (Figure 44B and C). The match between the likely AP-4 cargoes and typical acidocalcisome proteins lends support to the idea that this is a destination compartment for the AP-4 vesicle transport pathway. Significantly, the AP-4 proxiome only detected the multi-transmembrane subunit a of the PfV-ATPase. It is noteworthy that this subunit is also an AP-4 cargo rather than a protein coincidentally detected upon fusion of the AP-4 vesicle with the destination compartment. Of note, PfV-ATPase is not only located at the FV but also in smaller vesicular structures within the cytosol (Alder et al., 2023) which might correspond to the location of the AP-4-trafficked transporters. Furthermore, the AP-4 proxiome identified a type I membrane protein (PF3D7_0815500), which might correspond to a further cargo.

Taken together, AP-4 functions in the transport of different transmembrane cargoes to structures that may be acidocalcisomes (Wunderlich et al., 2024), a compartment belonging to the endosomal system. The AP-4 proxiome may help define the protein composition of acidocalcisomes which in malaria parasites have not been systematically studied to date. While different studies have shown that the knockout of transporters, such as CuTP, CDF and VIT, are not essential for asexual blood development of the parasite and invasion functions (Kenthirapalan et al., 2014; Wichers et al., 2022; Wunderlich et al., 2024), some explanations for these results may be due to the single knockout for each transporter is not enough to induce an invasion phenotype, or functional redundancy with other transporters. However, the effect might also be indirect as a consequence of the mistargeting of these transporters to the PPM of the parasite, altering the homeostasis of copper (CuTP), zinc (CDF) and iron (VIT) and impacting the invasion capacity of merozoites. In the case of AMA1 phenotype, the observed mild effect might also point to more direct effects (see section 4.1.13).

5.9 A proposed model for post-Golgi trafficking mediated by AP-1, AP-3 and AP-4 in malaria parasites

The findings of this thesis provide evidence for a unique configuration of the post-Golgi adaptors in *P. falciparum* parasites. Conditional inactivation demonstrated the critical functions of AP-1 for trophozoite and schizont development, and of AP-3 and AP-4 for invasion. The AP proxiomes revealed striking similarities conform with much of the literature on adaptors from other organisms, but at the same time, some key elements appear to be different, suggesting

exchangeability of certain elements. The proposed model posits AP-1 and AP-4 vesicles functioning with clathrin and tepsin, whereas AP-3 vesicles are without any coat and accessory proteins. Further, AP-1 recognises sortilin as a major cargo receptor, and sorts vesicles to repurposed endosomal compartments that are associated with secretory organelles, whereas AP-3 traffics unknown cargoes to HOPS/CORVET positive repurposed endosomal compartments. Instead, AP-4 sorts transporters to acidocalcisome-like compartments (Figure 51).

In summary, the findings of this thesis show indispensable functions of all three post-Golgi adaptors in malaria parasites, indicating a strong reliance of the parasite for specific protein sorting to compartments of endosomal origin. This includes functions critical for the generation of invasion organelles but also in sorting of multi-transmembrane proteins within the parasite. A remarkable conservation of the sorting pathways compared to those in distantly grouped organisms was found, but also unexpected differences, even to the more closely related apicomplexan *T. gondii*, indicating that elements of the vesicle sorting machinery are exchangeable over evolutionary distances.

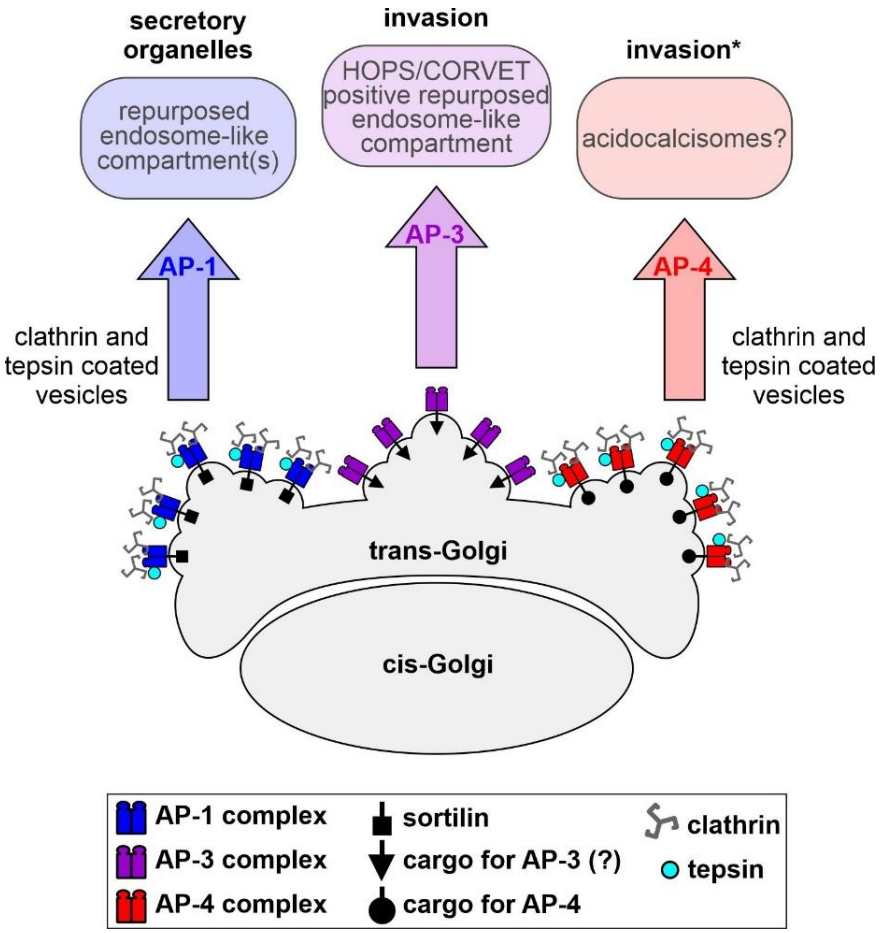

Figure 51. A proposed model for post-Golgi vesicular trafficking mediated by AP-1, AP-3, and AP-4 in *P. falciparum* parasites.

Model of AP-1 (blue), AP-3 (purple) and AP-4 (red)-mediated sorting pathways in malaria parasites with key components, functionalities and potential destination compartments. Asterisk indicates that the invasion phenotype likely is indirect.

6 References

Abramson, J., Adler, J., Dunger, J., Evans, R., Green, T., Pritzel, A., Ronneberger, O., Willmore, L., Ballard, A. J., Bambrick, J., Bodenstein, S. W., Evans, D. A., Hung, C.-C., O'Neill, M., Reiman, D., Tunyasuvunakool, K., Wu, Z., Žemgulytė, A., Arvaniti, E., … Jumper, J. M. (2024). Accurate structure prediction of biomolecular interactions with AlphaFold 3. *Nature*, *630*(8016), 493–500. https://doi.org/10.1038/s41586-024-07487-w

Abu Bakar, N., Klonis, N., Hanssen, E., Chan, C., & Tilley, L. (2010). Digestive-vacuole genesis and endocytic processes in the early intraerythrocytic stages of Plasmodium falciparum. *Journal of Cell Science*, *123*(Pt 3), 441–450. https://doi.org/10.1242/jcs.061499

Adams, T., Ennuson, N. A. A., Quashie, N. B., Futagbi, G., Matrevi, S., Hagan, O. C. K., Abuaku, B., Koram, K. A., & Duah, N. O. (2018). Prevalence of Plasmodium falciparum delayed clearance associated polymorphisms in adaptor protein complex 2 mu subunit (pfap2mu) and ubiquitin specific protease 1 (pfubp1) genes in Ghanaian isolates. *Parasites & Vectors*, *11*(1), 175. https://doi.org/10.1186/s13071-018-2762-3

Adisa, A., Frankland, S., Rug, M., Jackson, K., Maier, A. G., Walsh, P., Lithgow, T., Klonis, N., Gilson, P. R., Cowman, A. F., & Tilley, L. (2007). Re-assessing the locations of components of the classical vesicle-mediated trafficking machinery in transfected Plasmodium falciparum. *International Journal for Parasitology*, *37*(10), 1127–1141. https://doi.org/10.1016/j.ijpara.2007.02.009

Adisa, A., Rug, M., Klonis, N., Foley, M., Cowman, A. F., & Tilley, L. (2003). The Signal Sequence of Exported Protein-1 Directs the Green Fluorescent Protein to the Parasitophorous Vacuole of Transfected Malaria Parasites. *Journal of Biological Chemistry*, *278*(8), 6532–6542. https://doi.org/10.1074/jbc.M207039200

Alder, A., Sanchez, C. P., Russell, M. R. G., Collinson, L. M., Lanzer, M., Blackman, M. J., Gilberger, T.-W., & Matz, J. M. (2023). The role of Plasmodium V-ATPase in vacuolar physiology and antimalarial drug uptake. *Proceedings of the National Academy of Sciences of the United States of America*, *120*(30), e2306420120. https://doi.org/10.1073/pnas.2306420120

Allen, S. J., O'Donnell, A., Alexander, N. D., Alpers, M. P., Peto, T. E., Clegg, J. B., & Weatherall, D. J. (1997). Alpha+-Thalassemia protects children against disease caused by other infections as well as malaria. *Proceedings of the National Academy of Sciences of the United States of America*, *94*(26), 14736–14741. https://doi.org/10.1073/pnas.94.26.14736

Amino, R., Thiberge, S., Martin, B., Celli, S., Shorte, S., Frischknecht, F., & Ménard, R. (2006). Quantitative imaging of Plasmodium transmission from mosquito to mammal. *Nature Medicine*, *12*(2), 220–224. https://doi.org/10.1038/nm1350

Angers, C. G., & Merz, A. J. (2009). HOPS interacts with Apl5 at the vacuole membrane and is required for consumption of AP-3 transport vesicles. *Molecular Biology of the Cell*, *20*(21), 4563–4574. https://doi.org/10.1091/mbc.e09-04-0272

Ansari, H. R., Templeton, T. J., Subudhi, A. K., Ramaprasad, A., Tang, J., Lu, F., Naeem, R., Hashish, Y., Oguike, M. C., Benavente, E. D., Clark, T. G., Sutherland, C. J., Barnwell, J. W., Culleton, R., Cao, J., & Pain, A. (2016). Genome-scale comparison of expanded gene families in Plasmodium ovale wallikeri and Plasmodium ovale curtisi with Plasmodium malariae and with other Plasmodium species. *International Journal for Parasitology*, *46*(11), 685–696. https://doi.org/10.1016/j.ijpara.2016.05.009

Appenzeller-Herzog, C., & Hauri, H.-P. (2006). The ER-Golgi intermediate compartment (ERGIC): In search of its identity and function. *Journal of Cell Science*, *119*(Pt 11), 2173–2183. https://doi.org/10.1242/jcs.03019

Archuleta, T. L., Frazier, M. N., Monken, A. E., Kendall, A. K., Harp, J., McCoy, A. J., Creanza, N., & Jackson, L. P. (2017). Structure and evolution of ENTH and VHS/ENTH-like domains in tepsin. *Traffic (Copenhagen, Denmark)*, *18*(9), 590–603. https://doi.org/10.1111/tra.12499

Aridor, M., Bannykh, S. I., Rowe, T., & Balch, W. E. (1995). Sequential coupling between COPII and COPI vesicle coats in endoplasmic reticulum to Golgi transport. *The Journal of Cell Biology*, *131*(4), 875–893. https://doi.org/10.1083/jcb.131.4.875

Arisue, N., Hashimoto, T., Mitsui, H., Palacpac, N. M. Q., Kaneko, A., Kawai, S., Hasegawa, M., Tanabe, K., & Horii, T. (2012). The Plasmodium apicoplast genome: Conserved structure and close relationship of P. ovale to rodent malaria parasites. *Molecular Biology and Evolution*, *29*(9), 2095–2099. https://doi.org/10.1093/molbev/mss082

Asensio, C. S., Sirkis, D. W., & Edwards, R. H. (2010). RNAi screen identifies a role for adaptor protein AP-3 in sorting to the regulated secretory pathway. *The Journal of Cell Biology*, *191*(6), 1173–1187. https://doi.org/10.1083/jcb.201006131

Asensio, C. S., Sirkis, D. W., Maas, J. W., Egami, K., To, T.-L., Brodsky, F. M., Shu, X., Cheng, Y., & Edwards, R. H. (2013). Self-Assembly of VPS41 Promotes Sorting Required for Biogenesis of the Regulated Secretory Pathway. *Developmental Cell*, *27*(4), 425–437. https://doi.org/10.1016/j.devcel.2013.10.007

Baer, K., Klotz, C., Kappe, S. H. I., Schnieder, T., & Frevert, U. (2007). Release of hepatic Plasmodium yoelii merozoites into the pulmonary microvasculature. *PLoS Pathogens*, *3*(11), e171. https://doi.org/10.1371/journal.ppat.0030171

Balderhaar, H. J. kleine, & Ungermann, C. (2013). CORVET and HOPS tethering complexes—Coordinators of endosome and lysosome fusion. *Journal of Cell Science*, *126*(Pt 6), 1307–1316. https://doi.org/10.1242/jcs.107805

Banaszynski, L. A., Chen, L.-C., Maynard-Smith, L. A., Ooi, A. G. L., & Wandless, T. J. (2006). A rapid, reversible, and tunable method to regulate protein function in living cells using synthetic small molecules. *Cell*, *126*(5), 995–1004. https://doi.org/10.1016/j.cell.2006.07.025

Band, G., Leffler, E. M., Jallow, M., Sisay-Joof, F., Ndila, C. M., Macharia, A. W., Hubbart, C., Jeffreys, A. E., Rowlands, K., Nguyen, T., Gonçalves, S., Ariani, C. V., Stalker, J., Pearson, R. D., Amato, R., Drury, E., Sirugo, G., d'Alessandro, U., Bojang, K. A., … Kwiatkowski, D. P. (2022). Malaria protection due to sickle haemoglobin depends on parasite genotype. *Nature*, *602*(7895), 106–111. https://doi.org/10.1038/s41586-021-04288-3

Bannister, L. H., Hopkins, J. M., Dluzewski, A. R., Margos, G., Williams, I. T., Blackman, M. J., Kocken, C. H., Thomas, A. W., & Mitchell, G. H. (2003). Plasmodium falciparum apical membrane antigen 1 (PfAMA-1) is translocated within micronemes along subpellicular microtubules during merozoite development. *Journal of Cell Science*, *116*(Pt 18), 3825–3834. https://doi.org/10.1242/jcs.00665

Bannister, L. H., Hopkins, J. M., Fowler, R. E., Krishna, S., & Mitchell, G. H. (2000a). A brief illustrated guide to the ultrastructure of Plasmodium falciparum asexual blood stages. *Parasitology Today (Personal Ed.)*, *16*(10), 427–433. https://doi.org/10.1016/s0169-4758(00)01755-5

Bannister, L. H., Hopkins, J. M., Fowler, R. E., Krishna, S., & Mitchell, G. H. (2000b). Ultrastructure of rhoptry development in Plasmodium falciparum erythrocytic schizonts. *Parasitology*, *121 (Pt 3)*, 273–287. https://doi.org/10.1017/s0031182099006320

Bannister, L. H., Hopkins, J. M., Margos, G., Dluzewski, A. R., & Mitchell, G. H. (2004). Three-dimensional ultrastructure of the ring stage of Plasmodium falciparum: Evidence for export pathways. *Microscopy and Microanalysis: The Official Journal of Microscopy Society of America, Microbeam Analysis Society, Microscopical Society of Canada*, *10*(5), 551–562. https://doi.org/10.1017/S1431927604040917

Beacham, G. M., Partlow, E. A., & Hollopeter, G. (2019). Conformational regulation of AP1 and AP2 clathrin adaptor complexes. *Traffic (Copenhagen, Denmark)*, *20*(10), 741–751. https://doi.org/10.1111/tra.12677

Begley, M., Aragon, M., & Baker, R. W. (2024). A structure-based mechanism for initiation of AP-3 coated vesicle formation. *Proceedings of the National Academy of Sciences of the United States of America*, *121*(52), e2411974121. https://doi.org/10.1073/pnas.2411974121

Behrens, H. M., & Spielmann, T. (2024). Identification of domains in Plasmodium falciparum proteins of unknown function using DALI search on AlphaFold predictions. *Scientific Reports*, *14*(1), 10527. https://doi.org/10.1038/s41598-024-60058-x

Ben Mamoun, C., Gluzman, I. Y., Hott, C., MacMillan, S. K., Amarakone, A. S., Anderson, D. L., Carlton, J. M., Dame, J. B., Chakrabarti, D., Martin, R. K., Brownstein, B. H., &

Goldberg, D. E. (2001). Co-ordinated programme of gene expression during asexual intraerythrocytic development of the human malaria parasite Plasmodium falciparum revealed by microarray analysis. *Molecular Microbiology*, *39*(1), 26–36. https://doi.org/10.1046/j.1365-2958.2001.02222.x

Bennink, S., Kiesow, M. J., & Pradel, G. (2016). The development of malaria parasites in the mosquito midgut. *Cellular Microbiology*, *18*(7), 905–918. https://doi.org/10.1111/cmi.12604

Billker, O., Dechamps, S., Tewari, R., Wenig, G., Franke-Fayard, B., & Brinkmann, V. (2004). Calcium and a calcium-dependent protein kinase regulate gamete formation and mosquito transmission in a malaria parasite. *Cell*, *117*(4), 503–514. https://doi.org/10.1016/s0092-8674(04)00449-0

Billker, O., Lindo, V., Panico, M., Etienne, A. E., Paxton, T., Dell, A., Rogers, M., Sinden, R. E., & Morris, H. R. (1998). Identification of xanthurenic acid as the putative inducer of malaria development in the mosquito. *Nature*, *392*(6673), 289–292. https://doi.org/10.1038/32667

Birnbaum, J., Flemming, S., Reichard, N., Soares, A. B., Mesén-Ramírez, P., Jonscher, E., Bergmann, B., & Spielmann, T. (2017). A genetic system to study Plasmodium falciparum protein function. *Nature Methods*, *14*(4), 450–456. https://doi.org/10.1038/nmeth.4223

Birnbaum, J., Scharf, S., Schmidt, S., Jonscher, E., Hoeijmakers, W. A. M., Flemming, S., Toenhake, C. G., Schmitt, M., Sabitzki, R., Bergmann, B., Fröhlke, U., Mesén-Ramírez, P., Blancke Soares, A., Herrmann, H., Bártfai, R., & Spielmann, T. (2020). A Kelch13-defined endocytosis pathway mediates artemisinin resistance in malaria parasites. *Science*, *367*(6473), 51–59. https://doi.org/10.1126/science.aax4735

Blisnick, T., Morales Betoulle, M. E., Barale, J. C., Uzureau, P., Berry, L., Desroses, S., Fujioka, H., Mattei, D., & Braun Breton, C. (2000). Pfsbp1, a Maurer's cleft Plasmodium falciparum protein, is associated with the erythrocyte skeleton. *Molecular and Biochemical Parasitology*, *111*(1), 107–121. https://doi.org/10.1016/s0166-6851(00)00301-7

Boersema, P. J., Raijmakers, R., Lemeer, S., Mohammed, S., & Heck, A. J. R. (2009). Multiplex peptide stable isotope dimethyl labeling for quantitative proteomics. *Nature Protocols*, *4*(4), 484–494. https://doi.org/10.1038/nprot.2009.21

Boman, A. L. (2001). GGA proteins: New players in the sorting game. *Journal of Cell Science*, *114*(Pt 19), 3413–3418. https://doi.org/10.1242/jcs.114.19.3413

Bonifacino, J. S. (2014a). Adaptor proteins involved in polarized sorting. *The Journal of Cell Biology*, *204*(1), 7–17. https://doi.org/10.1083/jcb.201310021

Bonifacino, J. S. (2014b). Vesicular transport earns a Nobel. *Trends in Cell Biology*, *24*(1), 3–5. https://doi.org/10.1016/j.tcb.2013.11.001

Bonifacino, J. S., & Glick, B. S. (2004). The mechanisms of vesicle budding and fusion. *Cell*, *116*(2), 153–166. https://doi.org/10.1016/s0092-8674(03)01079-1

Borchers, A.-C., Langemeyer, L., & Ungermann, C. (2021). Who's in control? Principles of Rab GTPase activation in endolysosomal membrane trafficking and beyond. *Journal of Cell Biology*, *220*(9), e202105120. https://doi.org/10.1083/jcb.202105120

Borner, G. H. H., Antrobus, R., Hirst, J., Bhumbra, G. S., Kozik, P., Jackson, L. P., Sahlender, D. A., & Robinson, M. S. (2012). Multivariate proteomic profiling identifies novel accessory proteins of coated vesicles. *Journal of Cell Biology*, *197*(1), 141–160. https://doi.org/10.1083/jcb.201111049

Boucrot, E., Saffarian, S., Zhang, R., & Kirchhausen, T. (2010). Roles of AP-2 in clathrin-mediated endocytosis. *PloS One*, *5*(5), e10597. https://doi.org/10.1371/journal.pone.0010597

Boyle, M. J., Wilson, D. W., Richards, J. S., Riglar, D. T., Tetteh, K. K. A., Conway, D. J., Ralph, S. A., Baum, J., & Beeson, J. G. (2010). Isolation of viable Plasmodium falciparum merozoites to define erythrocyte invasion events and advance vaccine and drug development. *Proceedings of the National Academy of Sciences of the United States of America*, *107*(32), 14378–14383. https://doi.org/10.1073/pnas.1009198107

Bozdech, Z., Llinás, M., Pulliam, B. L., Wong, E. D., Zhu, J., & DeRisi, J. L. (2003). The transcriptome of the intraerythrocytic developmental cycle of Plasmodium falciparum. *PLoS Biology*, *1*(1), E5. https://doi.org/10.1371/journal.pbio.0000005

Branon, T. C., Bosch, J. A., Sanchez, A. D., Udeshi, N. D., Svinkina, T., Carr, S. A., Feldman, J. L., Perrimon, N., & Ting, A. Y. (2018). Efficient proximity labeling in living cells and organisms with TurboID. *Nature Biotechnology*, *36*(9), 880–887. https://doi.org/10.1038/nbt.4201

Brasil, P., Zalis, M. G., de Pina-Costa, A., Siqueira, A. M., Júnior, C. B., Silva, S., Areas, A. L. L., Pelajo-Machado, M., de Alvarenga, D. A. M., da Silva Santelli, A. C. F., Albuquerque, H. G., Cravo, P., Santos de Abreu, F. V., Peterka, C. L., Zanini, G. M., Suárez Mutis, M. C., Pissinatti, A., Lourenço-de-Oliveira, R., de Brito, C. F. A., … Daniel-Ribeiro, C. T. (2017). Outbreak of human malaria caused by Plasmodium simium in the Atlantic Forest in Rio de Janeiro: A molecular epidemiological investigation. *The Lancet. Global Health*, *5*(10), e1038–e1046. https://doi.org/10.1016/S2214-109X(17)30333-9

Brennand, A., Gualdrón-López, M., Coppens, I., Rigden, D. J., Ginger, M. L., & Michels, P. A. M. (2011). Autophagy in parasitic protists: Unique features and drug targets. *Molecular and Biochemical Parasitology*, *177*(2), 83–99. https://doi.org/10.1016/j.molbiopara.2011.02.003

Brett, C. L., Plemel, R. L., Lobingier, B. T., Vignali, M., Fields, S., & Merz, A. J. (2008). Efficient termination of vacuolar Rab GTPase signaling requires coordinated action by a GAP and a protein kinase. *The Journal of Cell Biology*, *182*(6), 1141–1151. https://doi.org/10.1083/jcb.200801001

Bröcker, C., Kuhlee, A., Gatsogiannis, C., Kleine Balderhaar, H. J., Hönscher, C., Engelbrecht-Vandré, S., Ungermann, C., & Raunser, S. (2012). Molecular architecture of the

multisubunit homotypic fusion and vacuole protein sorting (HOPS) tethering complex. *Proceedings of the National Academy of Sciences*, *109*(6), 1991–1996. https://doi.org/10.1073/pnas.1117797109

Bullen, H. E., Charnaud, S. C., Kalanon, M., Riglar, D. T., Dekiwadia, C., Kangwanrangsan, N., Torii, M., Tsuboi, T., Baum, J., Ralph, S. A., Cowman, A. F., De Koning-Ward, T. F., Crabb, B. S., & Gilson, P. R. (2012). Biosynthesis, Localization, and Macromolecular Arrangement of the Plasmodium falciparum Translocon of Exported Proteins (PTEX). *Journal of Biological Chemistry*, *287*(11), 7871–7884. https://doi.org/10.1074/jbc.M111.328591

Burgos, P. V., Mardones, G. A., Rojas, A. L., daSilva, L. L. P., Prabhu, Y., Hurley, J. H., & Bonifacino, J. S. (2010). Sorting of the Alzheimer's Disease Amyloid Precursor Protein Mediated by the AP-4 Complex. *Developmental Cell*, *18*(3), 425–436. https://doi.org/10.1016/j.devcel.2010.01.015

Buser, D. P., Bader, G., & Spiess, M. (2022). Retrograde transport of CDMPR depends on several machineries as analyzed by sulfatable nanobodies. *Life Science Alliance*, *5*(7), e202101269. https://doi.org/10.26508/lsa.202101269

Buser, D. P., Schleicher, K. D., Prescianotto-Baschong, C., & Spiess, M. (2018). A versatile nanobody-based toolkit to analyze retrograde transport from the cell surface. *Proceedings of the National Academy of Sciences*, *115*(27). https://doi.org/10.1073/pnas.1801865115

Cabrera, A., Herrmann, S., Warszta, D., Santos, J. M., John Peter, A. T., Kono, M., Debrouver, S., Jacobs, T., Spielmann, T., Ungermann, C., Soldati-Favre, D., & Gilberger, T. W. (2012). Dissection of Minimal Sequence Requirements for Rhoptry Membrane Targeting in the Malaria Parasite. *Traffic*, *13*(10), 1335–1350. https://doi.org/10.1111/j.1600-0854.2012.01394.x

Cabrera, M., Langemeyer, L., Mari, M., Rethmeier, R., Orban, I., Perz, A., Bröcker, C., Griffith, J., Klose, D., Steinhoff, H.-J., Reggiori, F., Engelbrecht-Vandré, S., & Ungermann, C. (2010). Phosphorylation of a membrane curvature-sensing motif switches function of the HOPS subunit Vps41 in membrane tethering. *The Journal of Cell Biology*, *191*(4), 845–859. https://doi.org/10.1083/jcb.201004092

Caminade, C., Kovats, S., Rocklov, J., Tompkins, A. M., Morse, A. P., Colón-González, F. J., Stenlund, H., Martens, P., & Lloyd, S. J. (2014). Impact of climate change on global malaria distribution. *Proceedings of the National Academy of Sciences of the United States of America*, *111*(9), 3286–3291. https://doi.org/10.1073/pnas.1302089111

Canuel, M., Lefrancois, S., Zeng, J., & Morales, C. R. (2008). AP-1 and retromer play opposite roles in the trafficking of sortilin between the Golgi apparatus and the lysosomes. *Biochemical and Biophysical Research Communications*, *366*(3), 724–730. https://doi.org/10.1016/j.bbrc.2007.12.015

Caracci, M. O., Pizarro, H., Alarcón-Godoy, C., Fuentealba, L. M., Farfán, P., De Pace, R., Santibañez, N., Cavieres, V. A., Pástor, T. P., Bonifacino, J. S., Mardones, G. A., &

Marzolo, M.-P. (2024). The Reelin receptor ApoER2 is a cargo for the adaptor protein complex AP-4: Implications for Hereditary Spastic Paraplegia. *Progress in Neurobiology*, *234*, 102575. https://doi.org/10.1016/j.pneurobio.2024.102575

Cervantes, S., Bunnik, E. M., Saraf, A., Conner, C. M., Escalante, A., Sardiu, M. E., Ponts, N., Prudhomme, J., Florens, L., & Le Roch, K. G. (2014). The multifunctional autophagy pathway in the human malaria parasite, Plasmodium falciparum. *Autophagy*, *10*(1), 80–92. https://doi.org/10.4161/auto.26743

Chaturvedi, S., Qi, H., Coleman, D., Rodriguez, A., Hanson, P. I., Striepen, B., Roos, D. S., & Joiner, K. A. (1999). Constitutive calcium-independent release of Toxoplasma gondii dense granules occurs through the NSF/SNAP/SNARE/Rab machinery. *The Journal of Biological Chemistry*, *274*(4), 2424–2431. https://doi.org/10.1074/jbc.274.4.2424

Chu, C. S., Bancone, G., Moore, K. A., Win, H. H., Thitipanawan, N., Po, C., Chowwiwat, N., Raksapraidee, R., Wilairisak, P., Phyo, A. P., Keereecharoen, L., Proux, S., Charunwatthana, P., Nosten, F., & White, N. J. (2017). Haemolysis in G6PD Heterozygous Females Treated with Primaquine for Plasmodium vivax Malaria: A Nested Cohort in a Trial of Radical Curative Regimens. *PLoS Medicine*, *14*(2), e1002224. https://doi.org/10.1371/journal.pmed.1002224

Chugh, M., Sundararaman, V., Kumar, S., Reddy, V. S., Siddiqui, W. A., Stuart, K. D., & Malhotra, P. (2013). Protein complex directs hemoglobin-to-hemozoin formation in Plasmodium falciparum. *Proceedings of the National Academy of Sciences of the United States of America*, *110*(14), 5392–5397. https://doi.org/10.1073/pnas.1218412110

Collins, C. R., Hackett, F., Strath, M., Penzo, M., Withers-Martinez, C., Baker, D. A., & Blackman, M. J. (2013). Malaria Parasite cGMP-dependent Protein Kinase Regulates Blood Stage Merozoite Secretory Organelle Discharge and Egress. *PLoS Pathogens*, *9*(5), e1003344. https://doi.org/10.1371/journal.ppat.1003344

Counihan, N. A., Kalanon, M., Coppel, R. L., & de Koning-Ward, T. F. (2013). Plasmodium rhoptry proteins: Why order is important. *Trends in Parasitology*, *29*(5), 228–236. https://doi.org/10.1016/j.pt.2013.03.003

Cowles, C. R., Odorizzi, G., Payne, G. S., & Emr, S. D. (1997). The AP-3 adaptor complex is essential for cargo-selective transport to the yeast vacuole. *Cell*, *91*(1), 109–118. https://doi.org/10.1016/s0092-8674(01)80013-1

Cowman, A. F., Berry, D., & Baum, J. (2012). The cellular and molecular basis for malaria parasite invasion of the human red blood cell. *The Journal of Cell Biology*, *198*(6), 961–971. https://doi.org/10.1083/jcb.201206112

Cowman, A. F., Tonkin, C. J., Tham, W.-H., & Duraisingh, M. T. (2017). The Molecular Basis of Erythrocyte Invasion by Malaria Parasites. *Cell Host & Microbe*, *22*(2), 232–245. https://doi.org/10.1016/j.chom.2017.07.003

Cox, F. E. (2010). History of the discovery of the malaria parasites and their vectors. *Parasites & Vectors*, *3*(1), 5. https://doi.org/10.1186/1756-3305-3-5

Cronshagen, J., Allweier, J., Mesén-Ramírez, P., Stäcker, J., Vaaben, A. V., Ramón-Zamorano, G., Naranjo-Prado, I., Ofori, S., Jansen, P. W., Hornebeck, J., Kieferle, F., Murk, A., Martin, E., Castro-Peña, C., Bártfai, R., Lavstsen, T., Bruchhaus, I., & Spielmann, T. (2024). *A system for functional studies of the major virulence factor of malaria parasites*. https://doi.org/10.7554/eLife.103542.1

Dacks, J. B., & Robinson, M. S. (2017). Outerwear through the ages: Evolutionary cell biology of vesicle coats. *Current Opinion in Cell Biology*, *47*, 108–116. https://doi.org/10.1016/j.ceb.2017.04.001

Dahhan, D. A., Reynolds, G. D., Cárdenas, J. J., Eeckhout, D., Johnson, A., Yperman, K., Kaufmann, W. A., Vang, N., Yan, X., Hwang, I., Heese, A., De Jaeger, G., Friml, J., Van Damme, D., Pan, J., & Bednarek, S. Y. (2022). Proteomic characterization of isolated Arabidopsis clathrin-coated vesicles reveals evolutionarily conserved and plant-specific components. *The Plant Cell*, *34*(6), 2150–2173. https://doi.org/10.1093/plcell/koac071

Daily, J. P., & Parikh, S. (2025). Malaria. *The New England Journal of Medicine*, *392*(13), 1320–1333. https://doi.org/10.1056/NEJMra2405313

Dash, M., Sachdeva, S., Bansal, A., & Sinha, A. (2022). Gametogenesis in Plasmodium: Delving Deeper to Connect the Dots. *Frontiers in Cellular and Infection Microbiology*, *12*, 877907. https://doi.org/10.3389/fcimb.2022.877907

Davies, A. K., Alecu, J. E., Ziegler, M., Vasilopoulou, C. G., Merciai, F., Jumo, H., Afshar-Saber, W., Sahin, M., Ebrahimi-Fakhari, D., & Borner, G. H. H. (2022). AP-4-mediated axonal transport controls endocannabinoid production in neurons. *Nature Communications*, *13*(1), 1058. https://doi.org/10.1038/s41467-022-28609-w

Davies, A. K., Itzhak, D. N., Edgar, J. R., Archuleta, T. L., Hirst, J., Jackson, L. P., Robinson, M. S., & Borner, G. H. H. (2018). AP-4 vesicles contribute to spatial control of autophagy via RUSC-dependent peripheral delivery of ATG9A. *Nature Communications*, *9*(1), 3958. https://doi.org/10.1038/s41467-018-06172-7

De Craene, J.-O., Ripp, R., Lecompte, O., Thompson, J. D., Poch, O., & Friant, S. (2012). Evolutionary analysis of the ENTH/ANTH/VHS protein superfamily reveals a coevolution between membrane trafficking and metabolism. *BMC Genomics*, *13*, 297. https://doi.org/10.1186/1471-2164-13-297

De Koning-Ward, T. F., Gilson, P. R., Boddey, J. A., Rug, M., Smith, B. J., Papenfuss, A. T., Sanders, P. R., Lundie, R. J., Maier, A. G., Cowman, A. F., & Crabb, B. S. (2009). A newly discovered protein export machine in malaria parasites. *Nature*, *459*(7249), 945–949. https://doi.org/10.1038/nature08104

De Niz, M., Burda, P.-C., Kaiser, G., Del Portillo, H. A., Spielmann, T., Frischknecht, F., & Heussler, V. T. (2017). Progress in imaging methods: Insights gained into Plasmodium biology. *Nature Reviews. Microbiology*, *15*(1), 37–54. https://doi.org/10.1038/nrmicro.2016.158

De Pace, R., Skirzewski, M., Damme, M., Mattera, R., Mercurio, J., Foster, A. M., Cuitino, L., Jarnik, M., Hoffmann, V., Morris, H. D., Han, T.-U., Mancini, G. M. S., Buonanno, A., & Bonifacino, J. S. (2018). Altered distribution of ATG9A and accumulation of axonal aggregates in neurons from a mouse model of AP-4 deficiency syndrome. *PLoS Genetics*, *14*(4), e1007363. https://doi.org/10.1371/journal.pgen.1007363

Defelipe, L. A., Veith, K., Burastero, O., Kupriianova, T., Bento, I., Skruzny, M., Kölbel, K., Uetrecht, C., Thuenauer, R., & García-Alai, M. M. (2024). Subtleties in Clathrin heavy chain binding boxes provide selectivity among adaptor proteins of budding yeast. *Nature Communications*, *15*(1), 9655. https://doi.org/10.1038/s41467-024-54037-z

Dell'Angelica, E. C., & Bonifacino, J. S. (2019). Coatopathies: Genetic Disorders of Protein Coats. *Annual Review of Cell and Developmental Biology*, *35*, 131–168. https://doi.org/10.1146/annurev-cellbio-100818-125234

Dell'Angelica, E. C., Klumperman, J., Stoorvogel, W., & Bonifacino, J. S. (1998). Association of the AP-3 Adaptor Complex with Clathrin. *Science*, *280*(5362), 431–434. https://doi.org/10.1126/science.280.5362.431

Dell'Angelica, E. C., Mullins, C., & Bonifacino, J. S. (1999). AP-4, a Novel Protein Complex Related to Clathrin Adaptors. *Journal of Biological Chemistry*, *274*(11), 7278–7285. https://doi.org/10.1074/jbc.274.11.7278

Deponte, M., Hoppe, H. C., Lee, M. C. S., Maier, A. G., Richard, D., Rug, M., Spielmann, T., & Przyborski, J. M. (2012). Wherever I may roam: Protein and membrane trafficking in P. falciparum-infected red blood cells. *Molecular and Biochemical Parasitology*, *186*(2), 95–116. https://doi.org/10.1016/j.molbiopara.2012.09.007

Dluzewski, A. R., Ling, I. T., Hopkins, J. M., Grainger, M., Margos, G., Mitchell, G. H., Holder, A. A., & Bannister, L. H. (2008). Formation of the Food Vacuole in Plasmodium falciparum: A Potential Role for the 19 kDa Fragment of Merozoite Surface Protein 1 (MSP119). *PLoS ONE*, *3*(8), e3085. https://doi.org/10.1371/journal.pone.0003085

Docampo, R., & Huang, G. (2016). Acidocalcisomes of eukaryotes. *Current Opinion in Cell Biology*, *41*, 66–72. https://doi.org/10.1016/j.ceb.2016.04.007

Doray, B., & Kornfeld, S. (2001). Gamma subunit of the AP-1 adaptor complex binds clathrin: Implications for cooperative binding in coated vesicle assembly. *Molecular Biology of the Cell*, *12*(7), 1925–1935. https://doi.org/10.1091/mbc.12.7.1925

Douki, J.-B. L., Sterkers, Y., Lépolard, C., Traoré, B., Costa, F. T. M., Scherf, A., & Gysin, J. (2003). Adhesion of normal and Plasmodium falciparum ring-infected erythrocytes to endothelial cells and the placenta involves the rhoptry-derived ring surface protein-2. *Blood*, *101*(12), 5025–5032. https://doi.org/10.1182/blood-2002-12-3710

Drake, M. T., Zhu, Y., & Kornfeld, S. (2000). The assembly of AP-3 adaptor complex-containing clathrin-coated vesicles on synthetic liposomes. *Molecular Biology of the Cell*, *11*(11), 3723–3736. https://doi.org/10.1091/mbc.11.11.3723

Drew, M. E., Banerjee, R., Uffman, E. W., Gilbertson, S., Rosenthal, P. J., & Goldberg, D. E. (2008). Plasmodium food vacuole plasmepsins are activated by falcipains. *The Journal*

of Biological Chemistry, *283*(19), 12870–12876. https://doi.org/10.1074/jbc.M708949200

Duncan, M. C. (2022). New directions for the clathrin adaptor AP-1 in cell biology and human disease. *Current Opinion in Cell Biology*, *76*, 102079. https://doi.org/10.1016/j.ceb.2022.102079

Duncan, M. C., Costaguta, G., & Payne, G. S. (2003). Yeast epsin-related proteins required for Golgi-endosome traffic define a gamma-adaptin ear-binding motif. *Nature Cell Biology*, *5*(1), 77–81. https://doi.org/10.1038/ncb901

Egan, T. J. (2008). Haemozoin formation. *Molecular and Biochemical Parasitology*, *157*(2), 127–136. https://doi.org/10.1016/j.molbiopara.2007.11.005

Eggleson, K. K., Duffin, K. L., & Goldberg, D. E. (1999). Identification and characterization of falcilysin, a metallopeptidase involved in hemoglobin catabolism within the malaria parasite Plasmodium falciparum. *The Journal of Biological Chemistry*, *274*(45), 32411–32417. https://doi.org/10.1074/jbc.274.45.32411

Escalante, A. A., Cepeda, A. S., & Pacheco, M. A. (2022). Why Plasmodium vivax and Plasmodium falciparum are so different? A tale of two clades and their species diversities. *Malaria Journal*, *21*(1), 139. https://doi.org/10.1186/s12936-022-04130-9

Fanello, C. I., Karema, C., Avellino, P., Bancone, G., Uwimana, A., Lee, S. J., d'Alessandro, U., & Modiano, D. (2008). High risk of severe anaemia after chlorproguanil-dapsone+artesunate antimalarial treatment in patients with G6PD (A-) deficiency. *PloS One*, *3*(12), e4031. https://doi.org/10.1371/journal.pone.0004031

Faust, C., & Dobson, A. P. (2015). Primate malarias: Diversity, distribution and insights for zoonotic Plasmodium. *One Health (Amsterdam, Netherlands)*, *1*, 66–75. https://doi.org/10.1016/j.onehlt.2015.10.001

Flammersfeld, A., Lang, C., Flieger, A., & Pradel, G. (2018). Phospholipases during membrane dynamics in malaria parasites. *International Journal of Medical Microbiology: IJMM*, *308*(1), 129–141. https://doi.org/10.1016/j.ijmm.2017.09.015

Flemming, S. (2015). *Visualization and characterization of endocytic processes in the human Malaria parasite P. falciparum (Welch, 1897).* University Hamburg.

Flint, J., Hill, A. V., Bowden, D. K., Oppenheimer, S. J., Sill, P. R., Serjeantson, S. W., Bana-Koiri, J., Bhatia, K., Alpers, M. P., & Boyce, A. J. (1986). High frequencies of alpha-thalassaemia are the result of natural selection by malaria. *Nature*, *321*(6072), 744–750. https://doi.org/10.1038/321744a0

Foote, C., & Nothwehr, S. F. (2006). The clathrin adaptor complex 1 directly binds to a sorting signal in Ste13p to reduce the rate of its trafficking to the late endosome of yeast. *The Journal of Cell Biology*, *173*(4), 615–626. https://doi.org/10.1083/jcb.200510161

Ford, M. G. J., Mills, I. G., Peter, B. J., Vallis, Y., Praefcke, G. J. K., Evans, P. R., & McMahon, H. T. (2002). Curvature of clathrin-coated pits driven by epsin. *Nature*, *419*(6905), 361–366. https://doi.org/10.1038/nature01020

Ford, M. G., Pearse, B. M., Higgins, M. K., Vallis, Y., Owen, D. J., Gibson, A., Hopkins, C. R., Evans, P. R., & McMahon, H. T. (2001). Simultaneous binding of PtdIns(4,5)P2 and clathrin by AP180 in the nucleation of clathrin lattices on membranes. *Science (New York, N.Y.), 291*(5506), 1051–1055. https://doi.org/10.1126/science.291.5506.1051

Fotin, A., Cheng, Y., Sliz, P., Grigorieff, N., Harrison, S. C., Kirchhausen, T., & Walz, T. (2004). Molecular model for a complete clathrin lattice from electron cryomicroscopy. *Nature*, *432*(7017), 573–579. https://doi.org/10.1038/nature03079

Francis, S. E., Sullivan, D. J., & Goldberg, D. E. (1997). Hemoglobin metabolism in the malaria parasite Plasmodium falciparum. *Annual Review of Microbiology*, *51*, 97–123. https://doi.org/10.1146/annurev.micro.51.1.97

Frazier, M. N., Davies, A. K., Voehler, M., Kendall, A. K., Borner, G. H. H., Chazin, W. J., Robinson, M. S., & Jackson, L. P. (2016). Molecular Basis for the Interaction Between AP4 β4 and its Accessory Protein, Tepsin. *Traffic (Copenhagen, Denmark)*, *17*(4), 400–415. https://doi.org/10.1111/tra.12375

Fréville, A., Moreira-Leite, F., Roussel, C., Russell, M. R. G., Fricot, A., Carret, V., Sissoko, A., Hayes, M. J., Diallo, A. B., Kerkhoven, N. C., Ressurreição, M., Dokmak, S., Blackman, M. J., Collinson, L. M., Buffet, P. A., Vaughan, S., Ndour, P. A., & van Ooij, C. (2025). Malaria parasites undergo a rapid and extensive metamorphosis after invasion of the host erythrocyte. *EMBO Reports*. https://doi.org/10.1038/s44319-025-00435-3

Fuji, K., Shirakawa, M., Shimono, Y., Kunieda, T., Fukao, Y., Koumoto, Y., Takahashi, H., Hara-Nishimura, I., & Shimada, T. (2016). The Adaptor Complex AP-4 Regulates Vacuolar Protein Sorting at the trans-Golgi Network by Interacting with VACUOLAR SORTING RECEPTOR1. *Plant Physiology*, *170*(1), 211–219. https://doi.org/10.1104/pp.15.00869

Gaidarov, I., & Keen, J. H. (1999). Phosphoinositide-AP-2 interactions required for targeting to plasma membrane clathrin-coated pits. *The Journal of Cell Biology*, *146*(4), 755–764. https://doi.org/10.1083/jcb.146.4.755

Galen, S. C., Borner, J., Martinsen, E. S., Schaer, J., Austin, C. C., West, C. J., & Perkins, S. L. (2018). The polyphyly of Plasmodium: Comprehensive phylogenetic analyses of the malaria parasites (order Haemosporida) reveal widespread taxonomic conflict. *Royal Society Open Science*, *5*(5), 171780. https://doi.org/10.1098/rsos.171780

Gardner, M. J., Hall, N., Fung, E., White, O., Berriman, M., Hyman, R. W., Carlton, J. M., Pain, A., Nelson, K. E., Bowman, S., Paulsen, I. T., James, K., Eisen, J. A., Rutherford, K., Salzberg, S. L., Craig, A., Kyes, S., Chan, M.-S., Nene, V., … Barrell, B. (2002). Genome sequence of the human malaria parasite Plasmodium falciparum. *Nature*, *419*(6906), 498–511. https://doi.org/10.1038/nature01097

Garten, M., Nasamu, A. S., Niles, J. C., Zimmerberg, J., Goldberg, D. E., & Beck, J. R. (2018). EXP2 is a nutrient-permeable channel in the vacuolar membrane of Plasmodium and is

essential for protein export via PTEX. *Nature Microbiology*, *3*(10), 1090–1098. https://doi.org/10.1038/s41564-018-0222-7

Geda, P., Patury, S., Ma, J., Bharucha, N., Dobry, C. J., Lawson, S. K., Gestwicki, J. E., & Kumar, A. (2008). A small molecule-directed approach to control protein localization and function. *Yeast*, *25*(8), 577–594. https://doi.org/10.1002/yea.1610

Gibson, D. G., Young, L., Chuang, R.-Y., Venter, J. C., Hutchison, C. A., & Smith, H. O. (2009). Enzymatic assembly of DNA molecules up to several hundred kilobases. *Nature Methods*, *6*(5), 343–345. https://doi.org/10.1038/nmeth.1318

Gilson, P. R., & Crabb, B. S. (2009). Morphology and kinetics of the three distinct phases of red blood cell invasion by Plasmodium falciparum merozoites. *International Journal for Parasitology*, *39*(1), 91–96. https://doi.org/10.1016/j.ijpara.2008.09.007

Ginsburg, H., Krugliak, M., Eidelman, O., & Cabantchik, Z. I. (1983). New permeability pathways induced in membranes of Plasmodium falciparum infected erythrocytes. *Molecular and Biochemical Parasitology*, *8*(2), 177–190. https://doi.org/10.1016/0166-6851(83)90008-7

Griffiths, G., & Simons, K. (1986). The trans Golgi network: Sorting at the exit site of the Golgi complex. *Science (New York, N.Y.)*, *234*(4775), 438–443. https://doi.org/10.1126/science.2945253

Grüring, C., Heiber, A., Kruse, F., Ungefehr, J., Gilberger, T.-W., & Spielmann, T. (2011). Development and host cell modifications of Plasmodium falciparum blood stages in four dimensions. *Nature Communications*, *2*(1), 165. https://doi.org/10.1038/ncomms1169

Grüring, C., & Spielmann, T. (2012). Imaging of live malaria blood stage parasites. *Methods in Enzymology*, *506*, 81–92. https://doi.org/10.1016/B978-0-12-391856-7.00029-9

Guardia, C. M., De Pace, R., Mattera, R., & Bonifacino, J. S. (2018). Neuronal functions of adaptor complexes involved in protein sorting. *Current Opinion in Neurobiology*, *51*, 103–110. https://doi.org/10.1016/j.conb.2018.02.021

Guerra, F., & Bucci, C. (2016). Multiple Roles of the Small GTPase Rab7. *Cells*, *5*(3), 34. https://doi.org/10.3390/cells5030034

Hain, A. U. P., & Bosch, J. (2013). Autophagy in Plasmodium, a multifunctional pathway? *Computational and Structural Biotechnology Journal*, *8*, e201308002. https://doi.org/10.5936/csbj.201308002

Hallée, S., Boddey, J. A., Cowman, A. F., & Richard, D. (2018a). Evidence that the Plasmodium falciparum Protein Sortilin Potentially Acts as an Escorter for the Trafficking of the Rhoptry-Associated Membrane Antigen to the Rhoptries. *mSphere*, *3*(1), e00551-17. https://doi.org/10.1128/mSphere.00551-17

Hallée, S., Counihan, N. A., Matthews, K., de Koning-Ward, T. F., & Richard, D. (2018b). The malaria parasite Plasmodium falciparum Sortilin is essential for merozoite formation

and apical complex biogenesis. *Cellular Microbiology*, *20*(8), e12844. https://doi.org/10.1111/cmi.12844

Hanssen, E., Dekiwadia, C., Riglar, D. T., Rug, M., Lemgruber, L., Cowman, A. F., Cyrklaff, M., Kudryashev, M., Frischknecht, F., Baum, J., & Ralph, S. A. (2013). Electron tomography of Plasmodium falciparum merozoites reveals core cellular events that underpin erythrocyte invasion. *Cellular Microbiology*, *15*(9), 1457–1472. https://doi.org/10.1111/cmi.12132

Hao, W., Luo, Z., Zheng, L., Prasad, K., & Lafer, E. M. (1999). AP180 and AP-2 interact directly in a complex that cooperatively assembles clathrin. *The Journal of Biological Chemistry*, *274*(32), 22785–22794. https://doi.org/10.1074/jbc.274.32.22785

Haruki, H., Nishikawa, J., & Laemmli, U. K. (2008). The Anchor-Away Technique: Rapid, Conditional Establishment of Yeast Mutant Phenotypes. *Molecular Cell*, *31*(6), 925–932. https://doi.org/10.1016/j.molcel.2008.07.020

Hawass, Z., Gad, Y. Z., Ismail, S., Khairat, R., Fathalla, D., Hasan, N., Ahmed, A., Elleithy, H., Ball, M., Gaballah, F., Wasef, S., Fateen, M., Amer, H., Gostner, P., Selim, A., Zink, A., & Pusch, C. M. (2010). Ancestry and pathology in King Tutankhamun's family. *JAMA*, *303*(7), 638–647. https://doi.org/10.1001/jama.2010.121

Hawryluk, M. J., Keyel, P. A., Mishra, S. K., Watkins, S. C., Heuser, J. E., & Traub, L. M. (2006). Epsin 1 is a polyubiquitin-selective clathrin-associated sorting protein. *Traffic (Copenhagen, Denmark)*, *7*(3), 262–281. https://doi.org/10.1111/j.1600-0854.2006.00383.x

Healer, J., Crawford, S., Ralph, S., McFadden, G., & Cowman, A. F. (2002). Independent translocation of two micronemal proteins in developing Plasmodium falciparum merozoites. *Infection and Immunity*, *70*(10), 5751–5758. https://doi.org/10.1128/IAI.70.10.5751-5758.2002

Heiber, A., Kruse, F., Pick, C., Grüring, C., Flemming, S., Oberli, A., Schoeler, H., Retzlaff, S., Mesén-Ramírez, P., Hiss, J. A., Kadekoppala, M., Hecht, L., Holder, A. A., Gilberger, T.-W., & Spielmann, T. (2013). Identification of New PNEPs Indicates a Substantial Non-PEXEL Exportome and Underpins Common Features in Plasmodium falciparum Protein Export. *PLoS Pathogens*, *9*(8), e1003546. https://doi.org/10.1371/journal.ppat.1003546

Heiny, S. R., Pautz, S., Recker, M., & Przyborski, J. M. (2014). Protein Traffic to the Plasmodium falciparum apicoplast: Evidence for a sorting branch point at the Golgi. *Traffic (Copenhagen, Denmark)*, *15*(12), 1290–1304. https://doi.org/10.1111/tra.12226

Heinze, L., Freimuth, N., Rößling, A.-K., Hahnke, R., Riebschläger, S., Fröhlich, A., Sampathkumar, A., McFarlane, H. E., & Sauer, M. (2020). EPSIN1 and MTV1 define functionally overlapping but molecularly distinct *trans* -Golgi network subdomains in *Arabidopsis*. *Proceedings of the National Academy of Sciences*, *117*(41), 25880–25889. https://doi.org/10.1073/pnas.2004822117

Heldwein, E. E., Macia, E., Wang, J., Yin, H. L., Kirchhausen, T., & Harrison, S. C. (2004). Crystal structure of the clathrin adaptor protein 1 core. *Proceedings of the National Academy of Sciences of the United States of America*, *101*(39), 14108–14113. https://doi.org/10.1073/pnas.0406102101

Henrici, R. C., Edwards, R. L., Zoltner, M., van Schalkwyk, D. A., Hart, M. N., Mohring, F., Moon, R. W., Nofal, S. D., Patel, A., Flueck, C., Baker, D. A., Odom John, A. R., Field, M. C., & Sutherland, C. J. (2020). The Plasmodium falciparum Artemisinin Susceptibility-Associated AP-2 Adaptin μ Subunit is Clathrin Independent and Essential for Schizont Maturation. *mBio*, *11*(1), e02918-19. https://doi.org/10.1128/mBio.02918-19

Henriques, G., van Schalkwyk, D. A., Burrow, R., Warhurst, D. C., Thompson, E., Baker, D. A., Fidock, D. A., Hallett, R., Flueck, C., & Sutherland, C. J. (2015). The Mu subunit of Plasmodium falciparum clathrin-associated adaptor protein 2 modulates in vitro parasite response to artemisinin and quinine. *Antimicrobial Agents and Chemotherapy*, *59*(5), 2540–2547. https://doi.org/10.1128/AAC.04067-14

Hirst, J., Barlow, L. D., Francisco, G. C., Sahlender, D. A., Seaman, M. N. J., Dacks, J. B., & Robinson, M. S. (2011). The fifth adaptor protein complex. *PLoS Biology*, *9*(10), e1001170. https://doi.org/10.1371/journal.pbio.1001170

Hirst, J., Borner, G. H. H., Antrobus, R., Peden, A. A., Hodson, N. A., Sahlender, D. A., & Robinson, M. S. (2012). Distinct and Overlapping Roles for AP-1 and GGAs Revealed by the "Knocksideways" System. *Current Biology*, *22*(18), 1711–1716. https://doi.org/10.1016/j.cub.2012.07.012

Hirst, J., Bright, N. A., Rous, B., & Robinson, M. S. (1999). Characterization of a Fourth Adaptor-related Protein Complex. *Molecular Biology of the Cell*, *10*(8), 2787–2802. https://doi.org/10.1091/mbc.10.8.2787

Hirst, J., Irving, C., & Borner, G. H. H. (2013). Adaptor protein complexes AP-4 and AP-5: New players in endosomal trafficking and progressive spastic paraplegia. *Traffic (Copenhagen, Denmark)*, *14*(2), 153–164. https://doi.org/10.1111/tra.12028

Hirst, J., Itzhak, D. N., Antrobus, R., Borner, G. H. H., & Robinson, M. S. (2018). Role of the AP-5 adaptor protein complex in late endosome-to-Golgi retrieval. *PLoS Biology*, *16*(1), e2004411. https://doi.org/10.1371/journal.pbio.2004411

Hirst, J., Motley, A., Harasaki, K., Peak Chew, S. Y., & Robinson, M. S. (2003). EpsinR: An ENTH domain-containing protein that interacts with AP-1. *Molecular Biology of the Cell*, *14*(2), 625–641. https://doi.org/10.1091/mbc.e02-09-0552

Holloway, Z. G., Velayos-Baeza, A., Howell, G. J., Levecque, C., Ponnambalam, S., Sztul, E., & Monaco, A. P. (2013). Trafficking of the Menkes copper transporter ATP7A is regulated by clathrin-, AP-2–, AP-1–, and Rab22-dependent steps. *Molecular Biology of the Cell*, *24*(11), 1735–1748. https://doi.org/10.1091/mbc.e12-08-0625

Honfozo, A., Ghouil, R., Alayi, T. D., Ouldali, M., Arteni, A.-A., Atindehou, C. M., Fanou, L. A., Hathout, Y., Zinn-Justin, S., & Tomavo, S. (2023). The luminal domain of

Toxoplasma gondii sortilin adopts a ring-shaped structure exhibiting motifs specific to apicomplexan parasites. *Frontiers in Parasitology*, *2*, 1103772. https://doi.org/10.3389/fpara.2023.1103772

Hoppe, H. C., Ngô, H. M., Yang, M., & Joiner, K. A. (2000). Targeting to rhoptry organelles of Toxoplasma gondii involves evolutionarily conserved mechanisms. *Nature Cell Biology*, *2*(7), 449–456. https://doi.org/10.1038/35017090

Huang, G., & Docampo, R. (2024). Acidocalcisome localization of membrane transporters and enzymes in Trypanosoma brucei. *Microbiology Spectrum*, *12*(11), e0112824. https://doi.org/10.1128/spectrum.01128-24

Huang, G., Ulrich, P. N., Storey, M., Johnson, D., Tischer, J., Tovar, J. A., Moreno, S. N. J., Orlando, R., & Docampo, R. (2014). Proteomic analysis of the acidocalcisome, an organelle conserved from bacteria to human cells. *PLoS Pathogens*, *10*(12), e1004555. https://doi.org/10.1371/journal.ppat.1004555

Huang, K. M., D'Hondt, K., Riezman, H., & Lemmon, S. K. (1999). Clathrin functions in the absence of heterotetrameric adaptors and AP180-related proteins in yeast. *The EMBO Journal*, *18*(14), 3897–3908. https://doi.org/10.1093/emboj/18.14.3897

Huang, Y., Ma, T., Lau, P. K., Wang, J., Zhao, T., Du, S., Loy, M. M. T., & Guo, Y. (2019). Visualization of Protein Sorting at the Trans-Golgi Network and Endosomes Through Super-Resolution Imaging. *Frontiers in Cell and Developmental Biology*, *7*, 181. https://doi.org/10.3389/fcell.2019.00181

Inoue, H., Nojima, H., & Okayama, H. (1990). High efficiency transformation of Escherichia coli with plasmids. *Gene*, *96*(1), 23–28. https://doi.org/10.1016/0378-1119(90)90336-p

Institute of Medicine (US) Committee on the Economics of Antimalarial Drugs. (2004). *Saving Lives, Buying Time: Economics of Malaria Drugs in an Age of Resistance* (K. J. Arrow, C. Panosian, & H. Gelband, Eds.). National Academies Press (US). http://www.ncbi.nlm.nih.gov/books/NBK215624/

Ismail, H. M., Barton, V., Phanchana, M., Charoensutthivarakul, S., Wong, M. H. L., Hemingway, J., Biagini, G. A., O'Neill, P. M., & Ward, S. A. (2016). Artemisinin activity-based probes identify multiple molecular targets within the asexual stage of the malaria parasites Plasmodium falciparum 3D7. *Proceedings of the National Academy of Sciences of the United States of America*, *113*(8), 2080–2085. https://doi.org/10.1073/pnas.1600459113

Jani, D., Nagarkatti, R., Beatty, W., Angel, R., Slebodnick, C., Andersen, J., Kumar, S., & Rathore, D. (2008). HDP-a novel heme detoxification protein from the malaria parasite. *PLoS Pathogens*, *4*(4), e1000053. https://doi.org/10.1371/journal.ppat.1000053

Jeyaprakasam, N. K., Liew, J. W. K., Low, V. L., Wan-Sulaiman, W.-Y., & Vythilingam, I. (2020). Plasmodium knowlesi infecting humans in Southeast Asia: What's next? *PLoS Neglected Tropical Diseases*, *14*(12), e0008900. https://doi.org/10.1371/journal.pntd.0008900

Jonscher, E. (2018). *Identification of proteins involved in host cell cytosol uptake in the human Malaria parasite Plasmodium falciparum.* University Hamburg.

Josling, G. A., & Llinás, M. (2015). Sexual development in Plasmodium parasites: Knowing when it's time to commit. *Nature Reviews. Microbiology*, *13*(9), 573–587. https://doi.org/10.1038/nrmicro3519

Joy, D. A., Feng, X., Mu, J., Furuya, T., Chotivanich, K., Krettli, A. U., Ho, M., Wang, A., White, N. J., Suh, E., Beerli, P., & Su, X. (2003). Early origin and recent expansion of Plasmodium falciparum. *Science (New York, N.Y.)*, *300*(5617), 318–321. https://doi.org/10.1126/science.1081449

Kaderi Kibria, K. M., Rawat, K., Klinger, C. M., Datta, G., Panchal, M., Singh, S., Iyer, G. R., Kaur, I., Sharma, V., Dacks, J. B., Mohmmed, A., & Malhotra, P. (2015). A role for adaptor protein complex 1 in protein targeting to rhoptry organelles in Plasmodium falciparum. *Biochimica Et Biophysica Acta*, *1853*(3), 699–710. https://doi.org/10.1016/j.bbamcr.2014.12.030

Kalb, L. C., Frederico, Y. C. A., Boehm, C., Moreira, C. M. D. N., Soares, M. J., & Field, M. C. (2016). Conservation and divergence within the clathrin interactome of Trypanosoma cruzi. *Scientific Reports*, *6*(1), 31212. https://doi.org/10.1038/srep31212

Kalthoff, C., Groos, S., Kohl, R., Mahrhold, S., & Ungewickell, E. J. (2002). Clint: A novel clathrin-binding ENTH-domain protein at the Golgi. *Molecular Biology of the Cell*, *13*(11), 4060–4073. https://doi.org/10.1091/mbc.e02-03-0171

Kang, B.-H., Nielsen, E., Preuss, M. L., Mastronarde, D., & Staehelin, L. A. (2011). Electron tomography of RabA4b- and PI-4Kβ1-labeled trans Golgi network compartments in Arabidopsis. *Traffic (Copenhagen, Denmark)*, *12*(3), 313–329. https://doi.org/10.1111/j.1600-0854.2010.01146.x

Kariuki, S. N., & Williams, T. N. (2020). Human genetics and malaria resistance. *Human Genetics*, *139*(6–7), 801–811. https://doi.org/10.1007/s00439-020-02142-6

Karsten, V., Qi, H., Beckers, C. J., Reddy, A., Dubremetz, J. F., Webster, P., & Joiner, K. A. (1998). The protozoan parasite Toxoplasma gondii targets proteins to dense granules and the vacuolar space using both conserved and unusual mechanisms. *The Journal of Cell Biology*, *141*(6), 1323–1333. https://doi.org/10.1083/jcb.141.6.1323

Kelly-Hope, L. A., Hemingway, J., & McKenzie, F. E. (2009). Environmental factors associated with the malaria vectors Anopheles gambiae and Anopheles funestus in Kenya. *Malaria Journal*, *8*, 268. https://doi.org/10.1186/1475-2875-8-268

Kenthirapalan, S., Waters, A. P., Matuschewski, K., & Kooij, T. W. A. (2014). Copper-transporting ATPase is important for malaria parasite fertility. *Molecular Microbiology*, *91*(2), 315–325. https://doi.org/10.1111/mmi.12461

Kibria, K. M. K., Hossain, M. U., Oany, A. R., & Ahmad, S. A. I. (2016). Novel insights on ENTH domain-containing proteins in apicomplexan parasites. *Parasitology Research*, *115*(6), 2191–2202. https://doi.org/10.1007/s00436-016-4961-1

Kimmel, J., Kehrer, J., Frischknecht, F., & Spielmann, T. (2022). Proximity-dependent biotinylation approaches to study apicomplexan biology. *Molecular Microbiology*, *117*(3), 553–568. https://doi.org/10.1111/mmi.14815

Kirchhausen, T., & Harrison, S. C. (1981). Protein organization in clathrin trimers. *Cell*, *23*(3), 755–761. https://doi.org/10.1016/0092-8674(81)90439-6

Kirchhausen, T., Owen, D., & Harrison, S. C. (2014). Molecular structure, function, and dynamics of clathrin-mediated membrane traffic. *Cold Spring Harbor Perspectives in Biology*, *6*(5), a016725. https://doi.org/10.1101/cshperspect.a016725

Klaus, S., Binder, P., Kim, J., Machado, M., Funaya, C., Schaaf, V., Klaschka, D., Kudulyte, A., Cyrklaff, M., Laketa, V., Höfer, T., Guizetti, J., Becker, N. B., Frischknecht, F., Schwarz, U. S., & Ganter, M. (2022). Asynchronous nuclear cycles in multinucleated Plasmodium falciparum facilitate rapid proliferation. *Science Advances*, *8*(13), eabj5362. https://doi.org/10.1126/sciadv.abj5362

Klemba, M., Beatty, W., Gluzman, I., & Goldberg, D. E. (2004a). Trafficking of plasmepsin II to the food vacuole of the malaria parasite Plasmodium falciparum. *The Journal of Cell Biology*, *164*(1), 47–56. https://doi.org/10.1083/jcb200307147

Klemba, M., Gluzman, I., & Goldberg, D. E. (2004b). A Plasmodium falciparum dipeptidyl aminopeptidase I participates in vacuolar hemoglobin degradation. *The Journal of Biological Chemistry*, *279*(41), 43000–43007. https://doi.org/10.1074/jbc.M408123200

Kono, M., Heincke, D., Wilcke, L., Wong, T. W. Y., Bruns, C., Herrmann, S., Spielmann, T., & Gilberger, T. W. (2016). Pellicle formation in the malaria parasite. *Journal of Cell Science*, *129*(4), 673–680. https://doi.org/10.1242/jcs.181230

Kono, M., Herrmann, S., Loughran, N. B., Cabrera, A., Engelberg, K., Lehmann, C., Sinha, D., Prinz, B., Ruch, U., Heussler, V., Spielmann, T., Parkinson, J., & Gilberger, T. W. (2012). Evolution and architecture of the inner membrane complex in asexual and sexual stages of the malaria parasite. *Molecular Biology and Evolution*, *29*(9), 2113–2132. https://doi.org/10.1093/molbev/mss081

Koreny, L., Mercado-Saavedra, B. N., Klinger, C. M., Barylyuk, K., Butterworth, S., Hirst, J., Rivera-Cuevas, Y., Zaccai, N. R., Holzer, V. J. C., Klingl, A., Dacks, J. B., Carruthers, V. B., Robinson, M. S., Gras, S., & Waller, R. F. (2023). Stable endocytic structures navigate the complex pellicle of apicomplexan parasites. *Nature Communications*, *14*(1), 2167. https://doi.org/10.1038/s41467-023-37431-x

Kovtun, O., Dickson, V. K., Kelly, B. T., Owen, D. J., & Briggs, J. A. G. (2020). Architecture of the AP2/clathrin coat on the membranes of clathrin-coated vesicles. *Science Advances*, *6*(30), eaba8381. https://doi.org/10.1126/sciadv.aba8381

Krai, P., Dalal, S., & Klemba, M. (2014). Evidence for a Golgi-to-Endosome Protein Sorting Pathway in Plasmodium falciparum. *PLoS ONE*, *9*(2), e89771. https://doi.org/10.1371/journal.pone.0089771

Kudyba, H. M., Cobb, D. W., Vega-Rodríguez, J., & Muralidharan, V. (2021). Some conditions apply: Systems for studying Plasmodium falciparum protein function. *PLoS Pathogens*, *17*(4), e1009442. https://doi.org/10.1371/journal.ppat.1009442

Külzer, S., Gehde, N., & Przyborski, J. M. (2009). Return to sender: Use of Plasmodium ER retrieval sequences to study protein transport in the infected erythrocyte and predict putative ER protein families. *Parasitology Research*, *104*(6), 1535–1541. https://doi.org/10.1007/s00436-009-1397-x

Kwiatkowski, D. P. (2005). How malaria has affected the human genome and what human genetics can teach us about malaria. *American Journal of Human Genetics*, *77*(2), 171–192. https://doi.org/10.1086/432519

Kyes, S. A., Kraemer, S. M., & Smith, J. D. (2007). Antigenic variation in Plasmodium falciparum: Gene organization and regulation of the var multigene family. *Eukaryotic Cell*, *6*(9), 1511–1520. https://doi.org/10.1128/EC.00173-07

Lamarque, M., Besteiro, S., Papoin, J., Roques, M., Vulliez-Le Normand, B., Morlon-Guyot, J., Dubremetz, J.-F., Fauquenoy, S., Tomavo, S., Faber, B. W., Kocken, C. H., Thomas, A. W., Boulanger, M. J., Bentley, G. A., & Lebrun, M. (2011). The RON2-AMA1 interaction is a critical step in moving junction-dependent invasion by apicomplexan parasites. *PLoS Pathogens*, *7*(2), e1001276. https://doi.org/10.1371/journal.ppat.1001276

Lambros, C., & Vanderberg, J. P. (1979). Synchronization of Plasmodium falciparum erythrocytic stages in culture. *The Journal of Parasitology*, *65*(3), 418–420.

Legendre-Guillemin, V., Metzler, M., Lemaire, J.-F., Philie, J., Gan, L., Hayden, M. R., & McPherson, P. S. (2005). Huntingtin interacting protein 1 (HIP1) regulates clathrin assembly through direct binding to the regulatory region of the clathrin light chain. *The Journal of Biological Chemistry*, *280*(7), 6101–6108. https://doi.org/10.1074/jbc.M408430200

Legendre-Guillemin, V., Wasiak, S., Hussain, N. K., Angers, A., & McPherson, P. S. (2004). ENTH/ANTH proteins and clathrin-mediated membrane budding. *Journal of Cell Science*, *117*(1), 9–18. https://doi.org/10.1242/jcs.00928

Leih, M., Plemel, R. L., West, M., Angers, C. G., Merz, A. J., & Odorizzi, G. (2024). Disordered hinge regions of the AP-3 adaptor complex promote vesicle budding from the late Golgi in yeast. *Journal of Cell Science*, *137*(21), jcs262234. https://doi.org/10.1242/jcs.262234

Lemgruber, L., Kudryashev, M., Dekiwadia, C., Riglar, D. T., Baum, J., Stahlberg, H., Ralph, S. A., & Frischknecht, F. (2013). Cryo-electron tomography reveals four-membrane architecture of the Plasmodium apicoplast. *Malaria Journal*, *12*, 25. https://doi.org/10.1186/1475-2875-12-25

Li, C., Jiang, N., Liu, Y., Zhang, Y., Chen, R., Feng, Y., Sang, X., & Chen, Q. (2024). Toxoplasma sortilin interacts with secretory proteins and it is critical for parasite

proliferation. *Parasites & Vectors*, *17*(1), 105. https://doi.org/10.1186/s13071-024-06207-7

Liffner, B., Balbin, J. M., Wichers, J. S., Gilberger, T.-W., & Wilson, D. W. (2021). The Ins and Outs of Plasmodium Rhoptries, Focusing on the Cytosolic Side. *Trends in Parasitology*, *37*(7), 638–650. https://doi.org/10.1016/j.pt.2021.03.006

Liffner, B., Cepeda Diaz, A. K., Blauwkamp, J., Anaguano, D., Frolich, S., Muralidharan, V., Wilson, D. W., Dvorin, J. D., & Absalon, S. (2023). Atlas of Plasmodium falciparum intraerythrocytic development using expansion microscopy. *eLife*, *12*, RP88088. https://doi.org/10.7554/eLife.88088

Lim, L., & McFadden, G. I. (2010). The evolution, metabolism and functions of the apicoplast. *Philosophical Transactions of the Royal Society of London. Series B, Biological Sciences*, *365*(1541), 749–763. https://doi.org/10.1098/rstb.2009.0273

Liu, W., Li, Y., Learn, G. H., Rudicell, R. S., Robertson, J. D., Keele, B. F., Ndjango, J.-B. N., Sanz, C. M., Morgan, D. B., Locatelli, S., Gonder, M. K., Kranzusch, P. J., Walsh, P. D., Delaporte, E., Mpoudi-Ngole, E., Georgiev, A. V., Muller, M. N., Shaw, G. M., Peeters, M., … Hahn, B. H. (2010). Origin of the human malaria parasite Plasmodium falciparum in gorillas. *Nature*, *467*(7314), 420–425. https://doi.org/10.1038/nature09442

Liu, W., Li, Y., Shaw, K. S., Learn, G. H., Plenderleith, L. J., Malenke, J. A., Sundararaman, S. A., Ramirez, M. A., Crystal, P. A., Smith, A. G., Bibollet-Ruche, F., Ayouba, A., Locatelli, S., Esteban, A., Mouacha, F., Guichet, E., Butel, C., Ahuka-Mundeke, S., Inogwabini, B.-I., … Sharp, P. M. (2014). African origin of the malaria parasite Plasmodium vivax. *Nature Communications*, *5*, 3346. https://doi.org/10.1038/ncomms4346

Lohi, O., Poussu, A., Mao, Y., Quiocho, F., & Lehto, V. P. (2002). VHS domain—A longshoreman of vesicle lines. *FEBS Letters*, *513*(1), 19–23. https://doi.org/10.1016/s0014-5793(01)03287-2

Lord, S. J., Velle, K. B., Mullins, R. D., & Fritz-Laylin, L. K. (2020). SuperPlots: Communicating reproducibility and variability in cell biology. *Journal of Cell Biology*, *219*(6), e202001064. https://doi.org/10.1083/jcb.202001064

Loy, D. E., Liu, W., Li, Y., Learn, G. H., Plenderleith, L. J., Sundararaman, S. A., Sharp, P. M., & Hahn, B. H. (2017). Out of Africa: Origins and evolution of the human malaria parasites Plasmodium falciparum and Plasmodium vivax. *International Journal for Parasitology*, *47*(2–3), 87–97. https://doi.org/10.1016/j.ijpara.2016.05.008

Macro, L., Jaiswal, J. K., & Simon, S. M. (2012). Dynamics of clathrin-mediated endocytosis and its requirement for organelle biogenesis in Dictyostelium. *Journal of Cell Science*, *125*(Pt 23), 5721–5732. https://doi.org/10.1242/jcs.108837

Mai, X., Wang, Y., Wang, X., Liu, M., Teng, F., Liu, Z., Su, M.-Y., & Stjepanovic, G. (2025). Structural basis for membrane remodeling by the AP5-SPG11-SPG15 complex. *Nature Structural & Molecular Biology*. https://doi.org/10.1038/s41594-025-01500-0

Makowski, S. L., Kuna, R. S., & Field, S. J. (2020). Induction of membrane curvature by proteins involved in Golgi trafficking. *Advances in Biological Regulation*, *75*, 100661. https://doi.org/10.1016/j.jbior.2019.100661

Malik, A. R., & Willnow, T. E. (2020). VPS10P Domain Receptors: Sorting Out Brain Health and Disease. *Trends in Neurosciences*, *43*(11), 870–885. https://doi.org/10.1016/j.tins.2020.08.003

Malleret, B., Claser, C., Ong, A. S. M., Suwanarusk, R., Sriprawat, K., Howland, S. W., Russell, B., Nosten, F., & Rénia, L. (2011). A rapid and robust tri-color flow cytometry assay for monitoring malaria parasite development. *Scientific Reports*, *1*, 118. https://doi.org/10.1038/srep00118

Manders, E. M. M., Verbeek, F. J., & Aten, J. A. (1993). Measurement of co-localization of objects in dual-colour confocal images. *Journal of Microscopy*, *169*(3), 375–382. https://doi.org/10.1111/j.1365-2818.1993.tb03313.x

Marti, M., Good, R. T., Rug, M., Knuepfer, E., & Cowman, A. F. (2004). Targeting malaria virulence and remodeling proteins to the host erythrocyte. *Science (New York, N.Y.)*, *306*(5703), 1930–1933. https://doi.org/10.1126/science.1102452

Martinez, M., Chen, W. D., Cova, M. M., Molnár, P., Mageswaran, S. K., Guérin, A., John, A. R. O., Lebrun, M., & Chang, Y.-W. (2022). Rhoptry secretion system structure and priming in Plasmodium falciparum revealed using in situ cryo-electron tomography. *Nature Microbiology*, *7*(8), 1230–1238. https://doi.org/10.1038/s41564-022-01171-3

Matsuda, S., Miura, E., Matsuda, K., Kakegawa, W., Kohda, K., Watanabe, M., & Yuzaki, M. (2008). Accumulation of AMPA receptors in autophagosomes in neuronal axons lacking adaptor protein AP-4. *Neuron*, *57*(5), 730–745. https://doi.org/10.1016/j.neuron.2008.02.012

Mattera, R., Boehm, M., Chaudhuri, R., Prabhu, Y., & Bonifacino, J. S. (2011). Conservation and diversification of dileucine signal recognition by adaptor protein (AP) complex variants. *The Journal of Biological Chemistry*, *286*(3), 2022–2030. https://doi.org/10.1074/jbc.M110.197178

Mattera, R., Guardia, C. M., Sidhu, S. S., & Bonifacino, J. S. (2015). Bivalent Motif-Ear Interactions Mediate the Association of the Accessory Protein Tepsin with the AP-4 Adaptor Complex. *Journal of Biological Chemistry*, *290*(52), 30736–30749. https://doi.org/10.1074/jbc.M115.683409

Mattera, R., Park, S. Y., De Pace, R., Guardia, C. M., & Bonifacino, J. S. (2017). AP-4 mediates export of ATG9A from the trans-Golgi network to promote autophagosome formation. *Proceedings of the National Academy of Sciences of the United States of America*, *114*(50), E10697–E10706. https://doi.org/10.1073/pnas.1717327114

Mattera, R., Williamson, C. D., Ren, X., & Bonifacino, J. S. (2020). The FTS-Hook-FHIP (FHF) complex interacts with AP-4 to mediate perinuclear distribution of AP-4 and its cargo ATG9A. *Molecular Biology of the Cell*, *31*(9), 963–979. https://doi.org/10.1091/mbc.E19-11-0658

McFadden, G. I., & Yeh, E. (2017). The apicoplast: Now you see it, now you don't. *International Journal for Parasitology*, *47*(2–3), 137–144. https://doi.org/10.1016/j.ijpara.2016.08.005

McManus, K. F., Taravella, A. M., Henn, B. M., Bustamante, C. D., Sikora, M., & Cornejo, O. E. (2017). Population genetic analysis of the DARC locus (Duffy) reveals adaptation from standing variation associated with malaria resistance in humans. *PLoS Genetics*, *13*(3), e1006560. https://doi.org/10.1371/journal.pgen.1006560

McMillan, P. J., Millet, C., Batinovic, S., Maiorca, M., Hanssen, E., Kenny, S., Muhle, R. A., Melcher, M., Fidock, D. A., Smith, J. D., Dixon, M. W. A., & Tilley, L. (2013). Spatial and temporal mapping of the PfEMP1 export pathway in Plasmodium falciparum. *Cellular Microbiology*, *15*(8), 1401–1418. https://doi.org/10.1111/cmi.12125

Mesén-Ramírez, J. P., Fuchs, G., Burmester, J., Farias, G. B., Alape-Flores, A. M., Singla, S., Alder, A., Cubillán-Marín, J., Castro-Peña, C., Lemcke, S., Sondermann, H., Prado, M., Spielmann, T., Wilson, D., & Gilberger, T.-W. (2025). HOPS/CORVET tethering complexes are critical for endocytosis and protein trafficking to invasion related organelles in malaria parasites. *PLoS Pathogens*, *21*(4), e1013053. https://doi.org/10.1371/journal.ppat.1013053

Mesén-Ramírez, P., Bergmann, B., Tran, T. T., Garten, M., Stäcker, J., Naranjo-Prado, I., Höhn, K., Zimmerberg, J., & Spielmann, T. (2019). EXP1 is critical for nutrient uptake across the parasitophorous vacuole membrane of malaria parasites. *PLOS Biology*, *17*(9), e3000473. https://doi.org/10.1371/journal.pbio.3000473

Mesén-Ramírez, P., Reinsch, F., Blancke Soares, A., Bergmann, B., Ullrich, A.-K., Tenzer, S., & Spielmann, T. (2016). Stable Translocation Intermediates Jam Global Protein Export in Plasmodium falciparum Parasites and Link the PTEX Component EXP2 with Translocation Activity. *PLoS Pathogens*, *12*(5), e1005618. https://doi.org/10.1371/journal.ppat.1005618

Meyer, C., Zizioli, D., Lausmann, S., Eskelinen, E. L., Hamann, J., Saftig, P., von Figura, K., & Schu, P. (2000). mu1A-adaptin-deficient mice: Lethality, loss of AP-1 binding and rerouting of mannose 6-phosphate receptors. *The EMBO Journal*, *19*(10), 2193–2203. https://doi.org/10.1093/emboj/19.10.2193

Milani, K. J., Schneider, T. G., & Taraschi, T. F. (2015). Defining the morphology and mechanism of the hemoglobin transport pathway in Plasmodium falciparum-infected erythrocytes. *Eukaryotic Cell*, *14*(4), 415–426. https://doi.org/10.1128/EC.00267-14

Mills, I. G., Praefcke, G. J. K., Vallis, Y., Peter, B. J., Olesen, L. E., Gallop, J. L., Butler, P. J. G., Evans, P. R., & McMahon, H. T. (2003). EpsinR. *The Journal of Cell Biology*, *160*(2), 213–222. https://doi.org/10.1083/jcb.200208023

Mitok, K. A., Keller, M. P., & Attie, A. D. (2022). Sorting through the extensive and confusing roles of sortilin in metabolic disease. *Journal of Lipid Research*, *63*(8), 100243. https://doi.org/10.1016/j.jlr.2022.100243

Morgan, J. R., Prasad, K., Hao, W., Augustine, G. J., & Lafer, E. M. (2000). A conserved clathrin assembly motif essential for synaptic vesicle endocytosis. *The Journal of Neuroscience: The Official Journal of the Society for Neuroscience*, *20*(23), 8667–8676. https://doi.org/10.1523/JNEUROSCI.20-23-08667.2000

Motley, A., Bright, N. A., Seaman, M. N. J., & Robinson, M. S. (2003). Clathrin-mediated endocytosis in AP-2-depleted cells. *The Journal of Cell Biology*, *162*(5), 909–918. https://doi.org/10.1083/jcb.200305145

Müdsam, C., Wollschläger, P., Sauer, N., & Schneider, S. (2018). Sorting of *Arabidopsis* NRAMP3 and NRAMP4 depends on adaptor protein complex AP4 and a dileucine-based motif. *Traffic*, *19*(7), 503–521. https://doi.org/10.1111/tra.12567

Mullis, K., Faloona, F., Scharf, S., Saiki, R., Horn, G., & Erlich, H. (1986). Specific enzymatic amplification of DNA in vitro: The polymerase chain reaction. *Cold Spring Harbor Symposia on Quantitative Biology*, *51 Pt 1*, 263–273. https://doi.org/10.1101/sqb.1986.051.01.032

Mundwiler-Pachlatko, E., & Beck, H.-P. (2013). Maurer's clefts, the enigma of Plasmodium falciparum. *Proceedings of the National Academy of Sciences of the United States of America*, *110*(50), 19987–19994. https://doi.org/10.1073/pnas.1309247110

Nakatsu, F., & Ohno, H. (2003). Adaptor protein complexes as the key regulators of protein sorting in the post-Golgi network. *Cell Structure and Function*, *28*(5), 419–429. https://doi.org/10.1247/csf.28.419

Narum, D. L., & Thomas, A. W. (1994). Differential localization of full-length and processed forms of PF83/AMA-1 an apical membrane antigen of Plasmodium falciparum merozoites. *Molecular and Biochemical Parasitology*, *67*(1), 59–68. https://doi.org/10.1016/0166-6851(94)90096-5

Naudi-Fabra, S., Elena-Real, C. A., Vedel, I. M., Tengo, M., Motzny, K., Jiang, P.-L., Schmieder, P., Liu, F., & Milles, S. (2024). An extended interaction site determines binding between AP180 and AP2 in clathrin mediated endocytosis. *Nature Communications*, *15*(1), 5884. https://doi.org/10.1038/s41467-024-50212-4

Nevin, W. D., & Dacks, J. B. (2009). Repeated secondary loss of adaptin complex genes in the Apicomplexa. *Parasitology International*, *58*(1), 86–94. https://doi.org/10.1016/j.parint.2008.12.002

Ngô, H. M., Yang, M., Paprotka, K., Pypaert, M., Hoppe, H., & Joiner, K. A. (2003). AP-1 in Toxoplasma gondii Mediates Biogenesis of the Rhoptry Secretory Organelle from a Post-Golgi Compartment. *Journal of Biological Chemistry*, *278*(7), 5343–5352. https://doi.org/10.1074/jbc.M208291200

Nie, Z., Boehm, M., Boja, E. S., Vass, W. C., Bonifacino, J. S., Fales, H. M., & Randazzo, P. A. (2003). Specific Regulation of the Adaptor Protein Complex AP-3 by the Arf GAP AGAP1. *Developmental Cell*, *5*(3), 513–521. https://doi.org/10.1016/S1534-5807(03)00234-X

Nielsen, M. S., Madsen, P., Christensen, E. I., Nykjaer, A., Gliemann, J., Kasper, D., Pohlmann, R., & Petersen, C. M. (2001). The sortilin cytoplasmic tail conveys Golgi-endosome transport and binds the VHS domain of the GGA2 sorting protein. *The EMBO Journal*, *20*(9), 2180–2190. https://doi.org/10.1093/emboj/20.9.2180

Nordmann, M., Cabrera, M., Perz, A., Bröcker, C., Ostrowicz, C., Engelbrecht-Vandré, S., & Ungermann, C. (2010). The Mon1-Ccz1 Complex Is the GEF of the Late Endosomal Rab7 Homolog Ypt7. *Current Biology*, *20*(18), 1654–1659. https://doi.org/10.1016/j.cub.2010.08.002

Nosten, F., Richard-Lenoble, D., & Danis, M. (2022). A brief history of malaria. *Presse Medicale (Paris, France: 1983)*, *51*(3), 104130. https://doi.org/10.1016/j.lpm.2022.104130

Ohno, H., Stewart, J., Fournier, M. C., Bosshart, H., Rhee, I., Miyatake, S., Saito, T., Gallusser, A., Kirchhausen, T., & Bonifacino, J. S. (1995). Interaction of tyrosine-based sorting signals with clathrin-associated proteins. *Science (New York, N.Y.)*, *269*(5232), 1872–1875. https://doi.org/10.1126/science.7569928

Ooi, C. E., Dell'Angelica, E. C., & Bonifacino, J. S. (1998). ADP-Ribosylation factor 1 (ARF1) regulates recruitment of the AP-3 adaptor complex to membranes. *The Journal of Cell Biology*, *142*(2), 391–402. https://doi.org/10.1083/jcb.142.2.391

Ooi, C. E., Moreira, J. E., Dell'Angelica, E. C., Poy, G., Wassarman, D. A., & Bonifacino, J. S. (1997). Altered expression of a novel adaptin leads to defective pigment granule biogenesis in the Drosophila eye color mutant garnet. *The EMBO Journal*, *16*(15), 4508–4518. https://doi.org/10.1093/emboj/16.15.4508

Outlaw, D. C., & Ricklefs, R. E. (2011). Rerooting the evolutionary tree of malaria parasites. *Proceedings of the National Academy of Sciences of the United States of America*, *108*(32), 13183–13187. https://doi.org/10.1073/pnas.1109153108

Owen, D. J., Vallis, Y., Noble, M. E., Hunter, J. B., Dafforn, T. R., Evans, P. R., & McMahon, H. T. (1999). A structural explanation for the binding of multiple ligands by the alpha-adaptin appendage domain. *Cell*, *97*(6), 805–815. https://doi.org/10.1016/s0092-8674(00)80791-6

Owen, D. J., Vallis, Y., Pearse, B. M., McMahon, H. T., & Evans, P. R. (2000). The structure and function of the beta 2-adaptin appendage domain. *The EMBO Journal*, *19*(16), 4216–4227. https://doi.org/10.1093/emboj/19.16.4216

Paczkowski, J. E., Richardson, B. C., & Fromme, J. C. (2015). Cargo adaptors: Structures illuminate mechanisms regulating vesicle biogenesis. *Trends in Cell Biology*, *25*(7), 408–416. https://doi.org/10.1016/j.tcb.2015.02.005

Painter, H. J., Morrisey, J. M., Mather, M. W., & Vaidya, A. B. (2007). Specific role of mitochondrial electron transport in blood-stage Plasmodium falciparum. *Nature*, *446*(7131), 88–91. https://doi.org/10.1038/nature05572

Park, S. Y., & Guo, X. (2014). Adaptor protein complexes and intracellular transport. *Bioscience Reports*, *34*(4), e00123. https://doi.org/10.1042/BSR20140069

Parkar, N. S., Akpa, B. S., Nitsche, L. C., Wedgewood, L. E., Place, A. T., Sverdlov, M. S., Chaga, O., & Minshall, R. D. (2009). Vesicle formation and endocytosis: Function, machinery, mechanisms, and modeling. *Antioxidants & Redox Signaling*, *11*(6), 1301–1312. https://doi.org/10.1089/ars.2008.2397

Peden, A. A., Oorschot, V., Hesser, B. A., Austin, C. D., Scheller, R. H., & Klumperman, J. (2004). Localization of the AP-3 adaptor complex defines a novel endosomal exit site for lysosomal membrane proteins. *The Journal of Cell Biology*, *164*(7), 1065–1076. https://doi.org/10.1083/jcb.200311064

Peden, A. A., Park, G. Y., & Scheller, R. H. (2001). The Di-leucine Motif of Vesicle-associated Membrane Protein 4 Is Required for Its Localization and AP-1 Binding. *Journal of Biological Chemistry*, *276*(52), 49183–49187. https://doi.org/10.1074/jbc.M106646200

Peden, A. A., Rudge, R. E., Lui, W. W. Y., & Robinson, M. S. (2002). Assembly and function of AP-3 complexes in cells expressing mutant subunits. *The Journal of Cell Biology*, *156*(2), 327–336. https://doi.org/10.1083/jcb.200107140

Piel, F. B., Patil, A. P., Howes, R. E., Nyangiri, O. A., Gething, P. W., Williams, T. N., Weatherall, D. J., & Hay, S. I. (2010). Global distribution of the sickle cell gene and geographical confirmation of the malaria hypothesis. *Nature Communications*, *1*, 104. https://doi.org/10.1038/ncomms1104

Pieperhoff, M. S., Schmitt, M., Ferguson, D. J. P., & Meissner, M. (2013). The Role of Clathrin in Post-Golgi Trafficking in Toxoplasma gondii. *PLoS ONE*, *8*(10), e77620. https://doi.org/10.1371/journal.pone.0077620

Plemel, R. L., Lobingier, B. T., Brett, C. L., Angers, C. G., Nickerson, D. P., Paulsel, A., Sprague, D., & Merz, A. J. (2011). Subunit organization and Rab interactions of Vps-C protein complexes that control endolysosomal membrane traffic. *Molecular Biology of the Cell*, *22*(8), 1353–1363. https://doi.org/10.1091/mbc.E10-03-0260

Preuss, D., Mulholland, J., Franzusoff, A., Segev, N., & Botstein, D. (1992). Characterization of the Saccharomyces Golgi complex through the cell cycle by immunoelectron microscopy. *Molecular Biology of the Cell*, *3*(7), 789–803. https://doi.org/10.1091/mbc.3.7.789

Prichard, K. L., O'Brien, N. S., Murcia, S. R., Baker, J. R., & McCluskey, A. (2021). Role of Clathrin and Dynamin in Clathrin Mediated Endocytosis/Synaptic Vesicle Recycling and Implications in Neurological Diseases. *Frontiers in Cellular Neuroscience*, *15*, 754110. https://doi.org/10.3389/fncel.2021.754110

Prudêncio, M., Rodriguez, A., & Mota, M. M. (2006). The silent path to thousands of merozoites: The Plasmodium liver stage. *Nature Reviews. Microbiology*, *4*(11), 849–856. https://doi.org/10.1038/nrmicro1529

Ralph, S. A., van Dooren, G. G., Waller, R. F., Crawford, M. J., Fraunholz, M. J., Foth, B. J., Tonkin, C. J., Roos, D. S., & McFadden, G. I. (2004). Tropical infectious diseases: Metabolic maps and functions of the Plasmodium falciparum apicoplast. *Nature Reviews. Microbiology*, *2*(3), 203–216. https://doi.org/10.1038/nrmicro843

Rapoport, I., Chen, Y. C., Cupers, P., Shoelson, S. E., & Kirchhausen, T. (1998). Dileucine-based sorting signals bind to the beta chain of AP-1 at a site distinct and regulated differently from the tyrosine-based motif-binding site. *The EMBO Journal*, *17*(8), 2148–2155. https://doi.org/10.1093/emboj/17.8.2148

Rehling, P., Darsow, T., Katzmann, D. J., & Emr, S. D. (1999). Formation of AP-3 transport intermediates requires Vps41 function. *Nature Cell Biology*, *1*(6), 346–353. https://doi.org/10.1038/14037

Ren, X., Farías, G. G., Canagarajah, B. J., Bonifacino, J. S., & Hurley, J. H. (2013). Structural basis for recruitment and activation of the AP-1 clathrin adaptor complex by Arf1. *Cell*, *152*(4), 755–767. https://doi.org/10.1016/j.cell.2012.12.042

Riglar, D. T., Rogers, K. L., Hanssen, E., Turnbull, L., Bullen, H. E., Charnaud, S. C., Przyborski, J., Gilson, P. R., Whitchurch, C. B., Crabb, B. S., Baum, J., & Cowman, A. F. (2013). Spatial association with PTEX complexes defines regions for effector export into Plasmodium falciparum-infected erythrocytes. *Nature Communications*, *4*, 1415. https://doi.org/10.1038/ncomms2449

Rivadeneira, E. M., Wasserman, M., & Espinal, C. T. (1983). Separation and concentration of schizonts of Plasmodium falciparum by Percoll gradients. *The Journal of Protozoology*, *30*(2), 367–370. https://doi.org/10.1111/j.1550-7408.1983.tb02932.x

Roach, T. G., Lång, H. K. M., Xiong, W., Ryhänen, S. J., & Capelluto, D. G. S. (2021). Protein Trafficking or Cell Signaling: A Dilemma for the Adaptor Protein TOM1. *Frontiers in Cell and Developmental Biology*, *9*, 643769. https://doi.org/10.3389/fcell.2021.643769

Robinson, M. S. (2004). Adaptable adaptors for coated vesicles. *Trends in Cell Biology*, *14*(4), 167–174. https://doi.org/10.1016/j.tcb.2004.02.002

Robinson, M. S. (2015). Forty Years of Clathrin-coated Vesicles. *Traffic (Copenhagen, Denmark)*, *16*(12), 1210–1238. https://doi.org/10.1111/tra.12335

Robinson, M. S., Antrobus, R., Sanger, A., Davies, A. K., & Gershlick, D. C. (2024). The role of the AP-1 adaptor complex in outgoing and incoming membrane traffic. *Journal of Cell Biology*, *223*(7), e202310071. https://doi.org/10.1083/jcb.202310071

Robinson, M. S., Sahlender, D. A., & Foster, S. D. (2010). Rapid Inactivation of Proteins by Rapamycin-Induced Rerouting to Mitochondria. *Developmental Cell*, *18*(2), 324–331. https://doi.org/10.1016/j.devcel.2009.12.015

Ross, B. H., Lin, Y., Corales, E. A., Burgos, P. V., & Mardones, G. A. (2014). Structural and functional characterization of cargo-binding sites on the μ4-subunit of adaptor protein complex 4. *PloS One*, *9*(2), e88147. https://doi.org/10.1371/journal.pone.0088147

Rossati, A., Bargiacchi, O., Kroumova, V., Zaramella, M., Caputo, A., & Garavelli, P. L. (2016). Climate, environment and transmission of malaria. *Le Infezioni in Medicina*, *24*(2), 93–104.

Rowe, J. A., Moulds, J. M., Newbold, C. I., & Miller, L. H. (1997). P. falciparum rosetting mediated by a parasite-variant erythrocyte membrane protein and complement-receptor 1. *Nature*, *388*(6639), 292–295. https://doi.org/10.1038/40888

Rudlaff, R. M., Kraemer, S., Marshman, J., & Dvorin, J. D. (2020). Three-dimensional ultrastructure of Plasmodium falciparum throughout cytokinesis. *PLoS Pathogens*, *16*(6), e1008587. https://doi.org/10.1371/journal.ppat.1008587

Ruwende, C., & Hill, A. (1998). Glucose-6-phosphate dehydrogenase deficiency and malaria. *Journal of Molecular Medicine (Berlin, Germany)*, *76*(8), 581–588. https://doi.org/10.1007/s001090050253

Sabitzki, R. (2022). *Identification and functional analysis of proteins involved in host cell cytosol uptake of the human malaria parasite Plasmodium falciparum*. University Hamburg.

Sabitzki, R., Roßmann, A.-L., Schmitt, M., Flemming, S., Guillén-Samander, A., Behrens, H. M., Jonscher, E., Höhn, K., Fröhlke, U., & Spielmann, T. (2024). Role of Rabenosyn-5 and Rab5b in host cell cytosol uptake reveals conservation of endosomal transport in malaria parasites. *PLOS Biology*, *22*(5), e3002639. https://doi.org/10.1371/journal.pbio.3002639

Sakura, T., Sindikubwabo, F., Oesterlin, L. K., Bousquet, H., Slomianny, C., Hakimi, M.-A., Langsley, G., & Tomavo, S. (2016). A Critical Role for Toxoplasma gondii Vacuolar Protein Sorting VPS9 in Secretory Organelle Biogenesis and Host Infection. *Scientific Reports*, *6*(1), 38842. https://doi.org/10.1038/srep38842

Salanti, A., Staalsoe, T., Lavstsen, T., Jensen, A. T. R., Sowa, M. P. K., Arnot, D. E., Hviid, L., & Theander, T. G. (2003). Selective upregulation of a single distinctly structured var gene in chondroitin sulphate A-adhering Plasmodium falciparum involved in pregnancy-associated malaria. *Molecular Microbiology*, *49*(1), 179–191. https://doi.org/10.1046/j.1365-2958.2003.03570.x

Saliba, K. J., Allen, R. J. W., Zissis, S., Bray, P. G., Ward, S. A., & Kirk, K. (2003). Acidification of the malaria parasite's digestive vacuole by a H+-ATPase and a H+-pyrophosphatase. *The Journal of Biological Chemistry*, *278*(8), 5605–5612. https://doi.org/10.1074/jbc.M208648200

Sangaré, L. O., Alayi, T. D., Westermann, B., Hovasse, A., Sindikubwabo, F., Callebaut, I., Werkmeister, E., Lafont, F., Slomianny, C., Hakimi, M.-A., Van Dorsselaer, A., Schaeffer-Reiss, C., & Tomavo, S. (2016). Unconventional endosome-like compartment and retromer complex in Toxoplasma gondii govern parasite integrity and host infection. *Nature Communications*, *7*(1), 11191. https://doi.org/10.1038/ncomms11191

Sanger, A., Hirst, J., Davies, A. K., & Robinson, M. S. (2019). Adaptor protein complexes and disease at a glance. *Journal of Cell Science*, *132*(20), jcs222992. https://doi.org/10.1242/jcs.222992

Sauer, M., Delgadillo, M. O., Zouhar, J., Reynolds, G. D., Pennington, J. G., Jiang, L., Liljegren, S. J., Stierhof, Y.-D., De Jaeger, G., Otegui, M. S., Bednarek, S. Y., & Rojo, E. (2013). MTV1 and MTV4 Encode Plant-Specific ENTH and ARF GAP Proteins That Mediate Clathrin-Dependent Trafficking of Vacuolar Cargo from the Trans-Golgi Network. *The Plant Cell*, *25*(6), 2217–2235. https://doi.org/10.1105/tpc.113.111724

Sayers, C. P., Mollard, V., Buchanan, H. D., McFadden, G. I., & Goodman, C. D. (2018). A genetic screen in rodent malaria parasites identifies five new apicoplast putative membrane transporters, one of which is essential in human malaria parasites. *Cellular Microbiology*, *20*(1). https://doi.org/10.1111/cmi.12789

Scheiner, M., Burda, P.-C., & Ingmundson, A. (2024). Moving on: How malaria parasites exit the liver. *Molecular Microbiology*, *121*(3), 328–340. https://doi.org/10.1111/mmi.15141

Schmidt, S., Wichers-Misterek, J. S., Behrens, H. M., Birnbaum, J., Henshall, I. G., Dröge, J., Jonscher, E., Flemming, S., Castro-Peña, C., Mesén-Ramírez, P., & Spielmann, T. (2023). The Kelch13 compartment contains highly divergent vesicle trafficking proteins in malaria parasites. *PLoS Pathogens*, *19*(12), e1011814. https://doi.org/10.1371/journal.ppat.1011814

Schoppe, J., Mari, M., Yavavli, E., Auffarth, K., Cabrera, M., Walter, S., Fröhlich, F., & Ungermann, C. (2020). AP-3 vesicle uncoating occurs after HOPS-dependent vacuole tethering. *The EMBO Journal*, *39*(20), e105117. https://doi.org/10.15252/embj.2020105117

Schoppe, J., Schubert, E., Apelbaum, A., Yavavli, E., Birkholz, O., Stephanowitz, H., Han, Y., Perz, A., Hofnagel, O., Liu, F., Piehler, J., Raunser, S., & Ungermann, C. (2021). Flexible open conformation of the AP-3 complex explains its role in cargo recruitment at the Golgi. *Journal of Biological Chemistry*, *297*(5), 101334. https://doi.org/10.1016/j.jbc.2021.101334

Seaman, M. N. J. (2007). Identification of a novel conserved sorting motif required for retromer-mediated endosome-to-TGN retrieval. *Journal of Cell Science*, *120*(Pt 14), 2378–2389. https://doi.org/10.1242/jcs.009654

Sharp, P. M., Plenderleith, L. J., Culleton, R. L., & Hahn, B. H. (2024). Origin of the human malaria parasite Plasmodium vivax. *Trends in Parasitology*, *40*(7), 562–572. https://doi.org/10.1016/j.pt.2024.05.001

Shih, W., Gallusser, A., & Kirchhausen, T. (1995). A clathrin-binding site in the hinge of the beta 2 chain of mammalian AP-2 complexes. *The Journal of Biological Chemistry*, *270*(52), 31083–31090. https://doi.org/10.1074/jbc.270.52.31083

Shimizu, Y., Takagi, J., Ito, E., Ito, Y., Ebine, K., Komatsu, Y., Goto, Y., Sato, M., Toyooka, K., Ueda, T., Kurokawa, K., Uemura, T., & Nakano, A. (2021). Cargo sorting zones in the trans-Golgi network visualized by super-resolution confocal live imaging microscopy in plants. *Nature Communications*, *12*(1), 1901. https://doi.org/10.1038/s41467-021-22267-0

Shimizu, Y., & Uemura, T. (2022). The sorting of cargo proteins in the plant trans-Golgi network. *Frontiers in Plant Science*, *13*, 957995. https://doi.org/10.3389/fpls.2022.957995

Silamut, K., Phu, N. H., Whitty, C., Turner, G. D., Louwrier, K., Mai, N. T., Simpson, J. A., Hien, T. T., & White, N. J. (1999). A quantitative analysis of the microvascular sequestration of malaria parasites in the human brain. *The American Journal of Pathology*, *155*(2), 395–410. https://doi.org/10.1016/S0002-9440(10)65136-X

Sim, B. K., Chitnis, C. E., Wasniowska, K., Hadley, T. J., & Miller, L. H. (1994). Receptor and ligand domains for invasion of erythrocytes by Plasmodium falciparum. *Science (New York, N.Y.)*, *264*(5167), 1941–1944. https://doi.org/10.1126/science.8009226

Simmen, T., Höning, S., Icking, A., Tikkanen, R., & Hunziker, W. (2002). AP-4 binds basolateral signals and participates in basolateral sorting in epithelial MDCK cells. *Nature Cell Biology*, *4*(2), 154–159. https://doi.org/10.1038/ncb745

Simpson, F., Bright, N. A., West, M. A., Newman, L. S., Darnell, R. B., & Robinson, M. S. (1996). A novel adaptor-related protein complex. *The Journal of Cell Biology*, *133*(4), 749–760. https://doi.org/10.1083/jcb.133.4.749

Simpson, F., Peden, A. A., Christopoulou, L., & Robinson, M. S. (1997). Characterization of the Adaptor-related Protein Complex, AP-3. *The Journal of Cell Biology*, *137*(4), 835–845. https://doi.org/10.1083/jcb.137.4.835

Singh, B., Kim Sung, L., Matusop, A., Radhakrishnan, A., Shamsul, S. S. G., Cox-Singh, J., Thomas, A., & Conway, D. J. (2004). A large focus of naturally acquired Plasmodium knowlesi infections in human beings. *Lancet (London, England)*, *363*(9414), 1017–1024. https://doi.org/10.1016/S0140-6736(04)15836-4

Singh, S., Alam, M. M., Pal-Bhowmick, I., Brzostowski, J. A., & Chitnis, C. E. (2010). Distinct external signals trigger sequential release of apical organelles during erythrocyte invasion by malaria parasites. *PLoS Pathogens*, *6*(2), e1000746. https://doi.org/10.1371/journal.ppat.1000746

Sinka, M. E., Bangs, M. J., Manguin, S., Rubio-Palis, Y., Chareonviriyaphap, T., Coetzee, M., Mbogo, C. M., Hemingway, J., Patil, A. P., Temperley, W. H., Gething, P. W., Kabaria, C. W., Burkot, T. R., Harbach, R. E., & Hay, S. I. (2012). A global map of dominant malaria vectors. *Parasites & Vectors*, *5*, 69. https://doi.org/10.1186/1756-3305-5-69

Sirkis, D. W., Edwards, R. H., & Asensio, C. S. (2013). Widespread dysregulation of peptide hormone release in mice lacking adaptor protein AP-3. *PLoS Genetics*, *9*(9), e1003812. https://doi.org/10.1371/journal.pgen.1003812

Sloves, P.-J., Delhaye, S., Mouveaux, T., Werkmeister, E., Slomianny, C., Hovasse, A., Dilezitoko Alayi, T., Callebaut, I., Gaji, R. Y., Schaeffer-Reiss, C., Van Dorsselear, A., Carruthers, V. B., & Tomavo, S. (2012). Toxoplasma Sortilin-like Receptor Regulates Protein Transport and Is Essential for Apical Secretory Organelle Biogenesis and Host Infection. *Cell Host & Microbe*, *11*(5), 515–527. https://doi.org/10.1016/j.chom.2012.03.006

Smith, D., Kannan, G., Coppens, I., Wang, F., Nguyen, H. M., Cerutti, A., Olafsson, E. B., Rimple, P. A., Schultz, T. L., Mercado Soto, N. M., Di Cristina, M., Besteiro, S., & Carruthers, V. B. (2021). Toxoplasma TgATG9 is critical for autophagy and long-term persistence in tissue cysts. *eLife*, *10*, e59384. https://doi.org/10.7554/eLife.59384

Smith, J. D., Craig, A. G., Kriek, N., Hudson-Taylor, D., Kyes, S., Fagan, T., Pinches, R., Baruch, D. I., Newbold, C. I., & Miller, L. H. (2000). Identification of a Plasmodium falciparum intercellular adhesion molecule-1 binding domain: A parasite adhesion trait implicated in cerebral malaria. *Proceedings of the National Academy of Sciences of the United States of America*, *97*(4), 1766–1771. https://doi.org/10.1073/pnas.040545897

Snounou, G., Sharp, P. M., & Culleton, R. (2024). The two parasite species formerly known as Plasmodium ovale. *Trends in Parasitology*, *40*(1), 21–27. https://doi.org/10.1016/j.pt.2023.11.004

Song, J., Lee, M. H., Lee, G.-J., Yoo, C. M., & Hwang, I. (2006). Arabidopsis EPSIN1 plays an important role in vacuolar trafficking of soluble cargo proteins in plant cells via interactions with clathrin, AP-1, VTI11, and VSR1. *The Plant Cell*, *18*(9), 2258–2274. https://doi.org/10.1105/tpc.105.039123

Spielmann, T., Fergusen, D. J. P., & Beck, H.-P. (2003). Etramps, a new Plasmodium falciparum gene family coding for developmentally regulated and highly charged membrane proteins located at the parasite-host cell interface. *Molecular Biology of the Cell*, *14*(4), 1529–1544. https://doi.org/10.1091/mbc.e02-04-0240

Spielmann, T., Gras, S., Sabitzki, R., & Meissner, M. (2020). Endocytosis in Plasmodium and Toxoplasma Parasites. *Trends in Parasitology*, *36*(6), 520–532. https://doi.org/10.1016/j.pt.2020.03.010

Stamnes, M. A., & Rothman, J. E. (1993). The binding of AP-1 clathrin adaptor particles to Golgi membranes requires ADP-ribosylation factor, a small GTP-binding protein. *Cell*, *73*(5), 999–1005. https://doi.org/10.1016/0092-8674(93)90277-w

Stepp, J. D., Huang, K., & Lemmon, S. K. (1997). The yeast adaptor protein complex, AP-3, is essential for the efficient delivery of alkaline phosphatase by the alternate pathway to the vacuole. *The Journal of Cell Biology*, *139*(7), 1761–1774. https://doi.org/10.1083/jcb.139.7.1761

Stockhammer, A., Adarska, P., Natalia, V., Heuhsen, A., Klemt, A., Bregu, G., Harel, S., Rodilla-Ramirez, C., Spalt, C., Özsoy, E., Leupold, P., Grindel, A., Fox, E., Mejedo, J. O., Zehtabian, A., Ewers, H., Puchkov, D., Haucke, V., & Bottanelli, F. (2024a). ARF1 compartments direct cargo flow via maturation into recycling endosomes. *Nature Cell Biology*, *26*(11), 1845–1859. https://doi.org/10.1038/s41556-024-01518-4

Stockhammer, A., Spalt, C., Klemt, A., Benz, L. S., Harel, S., Natalia, V., Wiench, L., Freund, C., Kuropka, B., & Bottanelli, F. (2024b). When less is more – a fast TurboID knock-in approach for high-sensitivity endogenous interactome mapping. *Journal of Cell Science*, *137*(16), jcs261952. https://doi.org/10.1242/jcs.261952

Striepen, B., He, C. Y., Matrajt, M., Soldati, D., & Roos, D. S. (1998). Expression, selection, and organellar targeting of the green fluorescent protein in Toxoplasma gondii. *Molecular and Biochemical Parasitology*, *92*(2), 325–338. https://doi.org/10.1016/s0166-6851(98)00011-5

Striepen, B., Soldati, D., Garcia-Reguet, N., Dubremetz, J. F., & Roos, D. S. (2001). Targeting of soluble proteins to the rhoptries and micronemes in Toxoplasma gondii. *Molecular and Biochemical Parasitology*, *113*(1), 45–53. https://doi.org/10.1016/s0166-6851(00)00379-0

Struck, N. S., de Souza Dias, S., Langer, C., Marti, M., Pearce, J. A., Cowman, A. F., & Gilberger, T. W. (2005). Re-defining the Golgi complex in Plasmodium falciparum using the novel Golgi marker PfGRASP. *Journal of Cell Science*, *118*(Pt 23), 5603–5613. https://doi.org/10.1242/jcs.02673

Struck, N. S., Herrmann, S., Schmuck-Barkmann, I., de Souza Dias, S., Haase, S., Cabrera, A. L., Treeck, M., Bruns, C., Langer, C., Cowman, A. F., Marti, M., Spielmann, T., & Gilberger, T. W. (2008). Spatial dissection of the cis- and trans-Golgi compartments in the malaria parasite Plasmodium falciparum. *Molecular Microbiology*, *67*(6), 1320–1330. https://doi.org/10.1111/j.1365-2958.2008.06125.x

Sturm, A., Amino, R., van de Sand, C., Regen, T., Retzlaff, S., Rennenberg, A., Krueger, A., Pollok, J.-M., Menard, R., & Heussler, V. T. (2006). Manipulation of host hepatocytes by the malaria parasite for delivery into liver sinusoids. *Science (New York, N.Y.)*, *313*(5791), 1287–1290. https://doi.org/10.1126/science.1129720

Sutherland, C. J., Tanomsing, N., Nolder, D., Oguike, M., Jennison, C., Pukrittayakamee, S., Dolecek, C., Hien, T. T., do Rosário, V. E., Arez, A. P., Pinto, J., Michon, P., Escalante, A. A., Nosten, F., Burke, M., Lee, R., Blaze, M., Otto, T. D., Barnwell, J. W., … Polley, S. D. (2010). Two nonrecombining sympatric forms of the human malaria parasite Plasmodium ovale occur globally. *The Journal of Infectious Diseases*, *201*(10), 1544–1550. https://doi.org/10.1086/652240

Ta, T. H., Hisam, S., Lanza, M., Jiram, A. I., Ismail, N., & Rubio, J. M. (2014). First case of a naturally acquired human infection with Plasmodium cynomolgi. *Malaria Journal*, *13*, 68. https://doi.org/10.1186/1475-2875-13-68

Tan, J. Z. A., & Gleeson, P. A. (2019). Cargo Sorting at the trans-Golgi Network for Shunting into Specific Transport Routes: Role of Arf Small G Proteins and Adaptor Complexes. *Cells*, *8*(6), 531. https://doi.org/10.3390/cells8060531

Tawk, L., Chicanne, G., Dubremetz, J.-F., Richard, V., Payrastre, B., Vial, H. J., Roy, C., & Wengelnik, K. (2010). Phosphatidylinositol 3-Phosphate, an Essential Lipid in Plasmodium, Localizes to the Food Vacuole Membrane and the Apicoplast. *Eukaryotic Cell*, *9*(10), 1519–1530. https://doi.org/10.1128/EC.00124-10

Taylor, H. M., McRobert, L., Grainger, M., Sicard, A., Dluzewski, A. R., Hopp, C. S., Holder, A. A., & Baker, D. A. (2010). The Malaria Parasite Cyclic GMP-Dependent Protein

Kinase Plays a Central Role in Blood-Stage Schizogony. *Eukaryotic Cell*, *9*(1), 37–45. https://doi.org/10.1128/EC.00186-09

Teh, O.-K., Shimono, Y., Shirakawa, M., Fukao, Y., Tamura, K., Shimada, T., & Hara-Nishimura, I. (2013). The AP-1 μ adaptin is required for KNOLLE localization at the cell plate to mediate cytokinesis in Arabidopsis. *Plant & Cell Physiology*, *54*(6), 838–847. https://doi.org/10.1093/pcp/pct048

Ter Haar, E., Harrison, S. C., & Kirchhausen, T. (2000). Peptide-in-groove interactions link target proteins to the β-propeller of clathrin. *Proceedings of the National Academy of Sciences*, *97*(3), 1096–1100. https://doi.org/10.1073/pnas.97.3.1096

Timmann, C., & Meyer, C. G. (2010). King Tutankhamun's family and demise. *JAMA*, *303*(24), 2473; author reply 2473-2475. https://doi.org/10.1001/jama.2010.822

Toh, W. H., Tan, J. Z. A., Zulkefli, K. L., Houghton, F. J., & Gleeson, P. A. (2017). Amyloid precursor protein traffics from the Golgi directly to early endosomes in an Arl5b- and AP4-dependent pathway. *Traffic (Copenhagen, Denmark)*, *18*(3), 159–175. https://doi.org/10.1111/tra.12465

Tomavo, S. (2014). Evolutionary repurposing of endosomal systems for apical organelle biogenesis in Toxoplasma gondii. *International Journal for Parasitology*, *44*(2), 133–138. https://doi.org/10.1016/j.ijpara.2013.10.003

Tonkin, C. J., Pearce, J. A., McFadden, G. I., & Cowman, A. F. (2006a). Protein targeting to destinations of the secretory pathway in the malaria parasite Plasmodium falciparum. *Current Opinion in Microbiology*, *9*(4), 381–387. https://doi.org/10.1016/j.mib.2006.06.015

Tonkin, C. J., Struck, N. S., Mullin, K. A., Stimmler, L. M., & McFadden, G. I. (2006b). Evidence for Golgi-independent transport from the early secretory pathway to the plastid in malaria parasites. *Molecular Microbiology*, *61*(3), 614–630. https://doi.org/10.1111/j.1365-2958.2006.05244.x

Tonkin, C. J., van Dooren, G. G., Spurck, T. P., Struck, N. S., Good, R. T., Handman, E., Cowman, A. F., & McFadden, G. I. (2004). Localization of organellar proteins in Plasmodium falciparum using a novel set of transfection vectors and a new immunofluorescence fixation method. *Molecular and Biochemical Parasitology*, *137*(1), 13–21. https://doi.org/10.1016/j.molbiopara.2004.05.009

Torii, M., Adams, J. H., Miller, L. H., & Aikawa, M. (1989). Release of merozoite dense granules during erythrocyte invasion by Plasmodium knowlesi. *Infection and Immunity*, *57*(10), 3230–3233. https://doi.org/10.1128/iai.57.10.3230-3233.1989

Trager, W., & Jensen, J. B. (1976). Human malaria parasites in continuous culture. *Science (New York, N.Y.)*, *193*(4254), 673–675. https://doi.org/10.1126/science.781840

Treeck, M., Struck, N. S., Haase, S., Langer, C., Herrmann, S., Healer, J., Cowman, A. F., & Gilberger, T. W. (2006). A Conserved Region in the EBL Proteins Is Implicated in Microneme Targeting of the Malaria Parasite Plasmodium falciparum. *Journal of*

Biological Chemistry, *281*(42), 31995–32003. https://doi.org/10.1016/S0021-9258(19)84113-3

Tutor, M. V., Shami, G. J., Siddiqui, G., Creek, D. J., Tilley, L., & Ralph, S. A. (2023). *The Plasmodium falciparum artemisinin resistance-associated protein Kelch 13 is required for formation of normal cytostomes*. https://doi.org/10.7554/eLife.90290.1

Ungermann, C., & Moeller, A. (2025). Structuring of the endolysosomal system by HOPS and CORVET tethering complexes. *Current Opinion in Cell Biology*, *94*, 102504. https://doi.org/10.1016/j.ceb.2025.102504

Ungewickell, E., & Branton, D. (1981). Assembly units of clathrin coats. *Nature*, *289*(5796), 420–422. https://doi.org/10.1038/289420a0

Vaidya, A. B., Akella, R., & Suplick, K. (1989). Sequences similar to genes for two mitochondrial proteins and portions of ribosomal RNA in tandemly arrayed 6-kilobase-pair DNA of a malarial parasite. *Molecular and Biochemical Parasitology*, *35*(2), 97–107. https://doi.org/10.1016/0166-6851(89)90112-6

Vaidya, A. B., Lashgari, M. S., Pologe, L. G., & Morrisey, J. (1993). Structural features of Plasmodium cytochrome b that may underlie susceptibility to 8-aminoquinolines and hydroxynaphthoquinones. *Molecular and Biochemical Parasitology*, *58*(1), 33–42. https://doi.org/10.1016/0166-6851(93)90088-f

Vaidya, A. B., & Mather, M. W. (2009). Mitochondrial evolution and functions in malaria parasites. *Annual Review of Microbiology*, *63*, 249–267. https://doi.org/10.1146/annurev.micro.091208.073424

Valdivia, R. H., Baggott, D., Chuang, J. S., & Schekman, R. W. (2002). The yeast clathrin adaptor protein complex 1 is required for the efficient retention of a subset of late Golgi membrane proteins. *Developmental Cell*, *2*(3), 283–294. https://doi.org/10.1016/s1534-5807(02)00127-2

Vallintine, T., & van Ooij, C. (2023). Timing of dense granule biogenesis in asexual malaria parasites. *Microbiology (Reading, England)*, *169*(8), 001389. https://doi.org/10.1099/mic.0.001389

Van Der Beek, J., Jonker, C., Van Der Welle, R., Liv, N., & Klumperman, J. (2019). CORVET, CHEVI and HOPS – multisubunit tethers of the endo-lysosomal system in health and disease. *Journal of Cell Science*, *132*(10), jcs189134. https://doi.org/10.1242/jcs.189134

van Dooren, G. G., Stimmler, L. M., & McFadden, G. I. (2006). Metabolic maps and functions of the Plasmodium mitochondrion. *FEMS Microbiology Reviews*, *30*(4), 596–630. https://doi.org/10.1111/j.1574-6976.2006.00027.x

Van Wye, J., Ghori, N., Webster, P., Mitschler, R. R., Elmendorf, H. G., & Haldar, K. (1996). Identification and localization of rab6, separation of rab6 from ERD2 and implications for an "unstacked" Golgi, in Plasmodium falciparum. *Molecular and Biochemical Parasitology*, *83*(1), 107–120. https://doi.org/10.1016/s0166-6851(96)02759-4

Varadi, M., Bertoni, D., Magana, P., Paramval, U., Pidruchna, I., Radhakrishnan, M., Tsenkov, M., Nair, S., Mirdita, M., Yeo, J., Kovalevskiy, O., Tunyasuvunakool, K., Laydon, A., Žídek, A., Tomlinson, H., Hariharan, D., Abrahamson, J., Green, T., Jumper, J., … Velankar, S. (2024). AlphaFold Protein Structure Database in 2024: Providing structure coverage for over 214 million protein sequences. *Nucleic Acids Research*, *52*(D1), D368–D375. https://doi.org/10.1093/nar/gkad1011

Venugopal, K., Werkmeister, E., Barois, N., Saliou, J.-M., Poncet, A., Huot, L., Sindikubwabo, F., Hakimi, M. A., Langsley, G., Lafont, F., & Marion, S. (2017). Dual role of the Toxoplasma gondii clathrin adaptor AP1 in the sorting of rhoptry and microneme proteins and in parasite division. *PLOS Pathogens*, *13*(4), e1006331. https://doi.org/10.1371/journal.ppat.1006331

Vercesi, A. E., Moreno, S. N., & Docampo, R. (1994). Ca2+/H+ exchange in acidic vacuoles of Trypanosoma brucei. *The Biochemical Journal, 304 (Pt 1)*(Pt 1), 227–233. https://doi.org/10.1042/bj3040227

Verhoef, J. M. J., Boshoven, C., Evers, F., Akkerman, L. J., Gijsbrechts, B. C. A., van de Vegte-Bolmer, M., van Gemert, G.-J., Vaidya, A. B., & Kooij, T. W. A. (2024). Detailing organelle division and segregation in Plasmodium falciparum. *The Journal of Cell Biology*, *223*(12), e202406064. https://doi.org/10.1083/jcb.202406064

Voinson, M., Nunn, C. L., & Goldberg, A. (2022). Primate malarias as a model for cross-species parasite transmission. *eLife*, *11*, e69628. https://doi.org/10.7554/eLife.69628

Voß, Y., Klaus, S., Guizetti, J., & Ganter, M. (2023). Plasmodium schizogony, a chronology of the parasite's cell cycle in the blood stage. *PLoS Pathogens*, *19*(3), e1011157. https://doi.org/10.1371/journal.ppat.1011157

Votýpka, J., Modrý, D., Oborník, M., Šlapeta, J., & Lukeš, J. (2017). Apicomplexa. In J. M. Archibald, A. G. B. Simpson, & C. H. Slamovits (Eds.), *Handbook of the Protists* (pp. 567–624). Springer International Publishing. https://doi.org/10.1007/978-3-319-28149-0_20

Wallace, N. S., Gadbery, J. E., Cohen, C. I., Kendall, A. K., & Jackson, L. P. (2024). Tepsin binds LC3B to promote ATG9A trafficking and delivery. *Molecular Biology of the Cell*, *35*(4), ar56. https://doi.org/10.1091/mbc.E23-09-0359-T

Waller, R. F., Keeling, P. J., Donald, R. G., Striepen, B., Handman, E., Lang-Unnasch, N., Cowman, A. F., Besra, G. S., Roos, D. S., & McFadden, G. I. (1998). Nuclear-encoded proteins target to the plastid in Toxoplasma gondii and Plasmodium falciparum. *Proceedings of the National Academy of Sciences of the United States of America*, *95*(21), 12352–12357. https://doi.org/10.1073/pnas.95.21.12352

Walliker, D., Quakyi, I. A., Wellems, T. E., McCutchan, T. F., Szarfman, A., London, W. T., Corcoran, L. M., Burkot, T. R., & Carter, R. (1987). Genetic Analysis of the Human Malaria Parasite *Plasmodium falciparum*. *Science*, *236*(4809), 1661–1666. https://doi.org/10.1126/science.3299700

Wan, W., Dong, H., Lai, D.-H., Yang, J., He, K., Tang, X., Liu, Q., Hide, G., Zhu, X.-Q., Sibley, L. D., Lun, Z.-R., & Long, S. (2023). The Toxoplasma micropore mediates endocytosis for selective nutrient salvage from host cell compartments. *Nature Communications*, *14*(1), 977. https://doi.org/10.1038/s41467-023-36571-4

Wang, T., Liu, N. S., Seet, L.-F., & Hong, W. (2010). The emerging role of VHS domain-containing Tom1, Tom1L1 and Tom1L2 in membrane trafficking. *Traffic (Copenhagen, Denmark)*, *11*(9), 1119–1128. https://doi.org/10.1111/j.1600-0854.2010.01098.x

Wang, Y. J., Wang, J., Sun, H. Q., Martinez, M., Sun, Y. X., Macia, E., Kirchhausen, T., Albanesi, J. P., Roth, M. G., & Yin, H. L. (2003). Phosphatidylinositol 4 phosphate regulates targeting of clathrin adaptor AP-1 complexes to the Golgi. *Cell*, *114*(3), 299–310. https://doi.org/10.1016/s0092-8674(03)00603-2

Wasiak, S., Legendre-Guillemin, V., Puertollano, R., Blondeau, F., Girard, M., De Heuvel, E., Boismenu, D., Bell, A. W., Bonifacino, J. S., & McPherson, P. S. (2002). Enthoprotin. *The Journal of Cell Biology*, *158*(5), 855–862. https://doi.org/10.1083/jcb.200205078

Weatherall, D. J. (2008). Genetic variation and susceptibility to infection: The red cell and malaria. *British Journal of Haematology*, *141*(3), 276–286. https://doi.org/10.1111/j.1365-2141.2008.07085.x

White, N. J. (2004). Antimalarial drug resistance. *The Journal of Clinical Investigation*, *113*(8), 1084–1092. https://doi.org/10.1172/JCI21682

White, N. J. (2008). Plasmodium knowlesi: The fifth human malaria parasite. *Clinical Infectious Diseases: An Official Publication of the Infectious Diseases Society of America*, *46*(2), 172–173. https://doi.org/10.1086/524889

WHO. (2024). *World malaria report 2024: Addressing inequity in the global malaria response*.

Wichers, J. S., Mesén-Ramírez, P., Fuchs, G., Yu-Strzelczyk, J., Stäcker, J., von Thien, H., Alder, A., Henshall, I., Liffner, B., Nagel, G., Löw, C., Wilson, D., Spielmann, T., Gao, S., Gilberger, T.-W., Bachmann, A., & Strauss, J. (2022). PMRT1, a Plasmodium-Specific Parasite Plasma Membrane Transporter, Is Essential for Asexual and Sexual Blood Stage Development. *mBio*, *13*(2), e0062322. https://doi.org/10.1128/mbio.00623-22

Wickham, M. E., Culvenor, J. G., & Cowman, A. F. (2003). Selective inhibition of a two-step egress of malaria parasites from the host erythrocyte. *The Journal of Biological Chemistry*, *278*(39), 37658–37663. https://doi.org/10.1074/jbc.M305252200

Willnow, T. E., Petersen, C. M., & Nykjaer, A. (2008). VPS10P-domain receptors—Regulators of neuronal viability and function. *Nature Reviews. Neuroscience*, *9*(12), 899–909. https://doi.org/10.1038/nrn2516

Wilson, R. J., Denny, P. W., Preiser, P. R., Rangachari, K., Roberts, K., Roy, A., Whyte, A., Strath, M., Moore, D. J., Moore, P. W., & Williamson, D. H. (1996). Complete gene map of the plastid-like DNA of the malaria parasite Plasmodium falciparum. *Journal of Molecular Biology*, *261*(2), 155–172. https://doi.org/10.1006/jmbi.1996.0449

Wilson, R. J., & Williamson, D. H. (1997). Extrachromosomal DNA in the Apicomplexa. *Microbiology and Molecular Biology Reviews: MMBR*, *61*(1), 1–16. https://doi.org/10.1128/mmbr.61.1.1-16.1997

Witkowski, B., Amaratunga, C., Khim, N., Sreng, S., Chim, P., Kim, S., Lim, P., Mao, S., Sopha, C., Sam, B., Anderson, J. M., Duong, S., Chuor, C. M., Taylor, W. R. J., Suon, S., Mercereau-Puijalon, O., Fairhurst, R. M., & Menard, D. (2013). Novel phenotypic assays for the detection of artemisinin-resistant Plasmodium falciparum malaria in Cambodia: In-vitro and ex-vivo drug-response studies. *The Lancet. Infectious Diseases*, *13*(12), 1043–1049. https://doi.org/10.1016/S1473-3099(13)70252-4

Wong-Dilworth, L., Rodilla-Ramirez, C., Fox, E., Restel, S. D., Stockhammer, A., Adarska, P., & Bottanelli, F. (2023). STED imaging of endogenously tagged ARF GTPases reveals their distinct nanoscale localizations. *Journal of Cell Biology*, *222*(7), e202205107. https://doi.org/10.1083/jcb.202205107

Wu, B., Rambow, J., Bock, S., Holm-Bertelsen, J., Wiechert, M., Soares, A. B., Spielmann, T., & Beitz, E. (2015). Identity of a Plasmodium lactate/H+ symporter structurally unrelated to human transporters. *Nature Communications*, *6*(1), 6284. https://doi.org/10.1038/ncomms7284

Wunderlich, J. (2022). Updated List of Transport Proteins in Plasmodium falciparum. *Frontiers in Cellular and Infection Microbiology*, *12*, 926541. https://doi.org/10.3389/fcimb.2022.926541

Wunderlich, J., Kotov, V., Votborg-Novél, L., Ntalla, C., Geffken, M., Peine, S., Portugal, S., & Strauss, J. (2024). Iron transport pathways in the human malaria parasite Plasmodium falciparum revealed by RNA-sequencing. *Frontiers in Cellular and Infection Microbiology*, *14*, 1480076. https://doi.org/10.3389/fcimb.2024.1480076

Yamakami, M., Yoshimori, T., & Yokosawa, H. (2003). Tom1, a VHS domain-containing protein, interacts with tollip, ubiquitin, and clathrin. *The Journal of Biological Chemistry*, *278*(52), 52865–52872. https://doi.org/10.1074/jbc.M306740200

Yamaoka, S., Shimono, Y., Shirakawa, M., Fukao, Y., Kawase, T., Hatsugai, N., Tamura, K., Shimada, T., & Hara-Nishimura, I. (2013). Identification and dynamics of Arabidopsis adaptor protein-2 complex and its involvement in floral organ development. *The Plant Cell*, *25*(8), 2958–2969. https://doi.org/10.1105/tpc.113.114082

Yap, C. (2003). Adaptor protein complex-4 (AP-4) is expressed in the central nervous system neurons and interacts with glutamate receptor δ2. *Molecular and Cellular Neuroscience*, *24*(2), 283–295. https://doi.org/10.1016/S1044-7431(03)00164-7

Yap, N. J., Hossain, H., Nada-Raja, T., Ngui, R., Muslim, A., Hoh, B.-P., Khaw, L. T., Kadir, K. A., Simon Divis, P. C., Vythilingam, I., Singh, B., & Lim, Y. A.-L. (2021). Natural Human Infections with Plasmodium cynomolgi, P. inui, and 4 other Simian Malaria Parasites, Malaysia. *Emerging Infectious Diseases*, *27*(8), 2187–2191. https://doi.org/10.3201/eid2708.204502

Yeh, E., & DeRisi, J. L. (2011). Chemical rescue of malaria parasites lacking an apicoplast defines organelle function in blood-stage Plasmodium falciparum. *PLoS Biology*, *9*(8), e1001138. https://doi.org/10.1371/journal.pbio.1001138

Yeoh, S., O'Donnell, R. A., Koussis, K., Dluzewski, A. R., Ansell, K. H., Osborne, S. A., Hackett, F., Withers-Martinez, C., Mitchell, G. H., Bannister, L. H., Bryans, J. S., Kettleborough, C. A., & Blackman, M. J. (2007). Subcellular discharge of a serine protease mediates release of invasive malaria parasites from host erythrocytes. *Cell*, *131*(6), 1072–1083. https://doi.org/10.1016/j.cell.2007.10.049

Yeoman, J. A., Hanssen, E., Maier, A. G., Klonis, N., Maco, B., Baum, J., Turnbull, L., Whitchurch, C. B., Dixon, M. W. A., & Tilley, L. (2011). Tracking Glideosome-associated protein 50 reveals the development and organization of the inner membrane complex of Plasmodium falciparum. *Eukaryotic Cell*, *10*(4), 556–564. https://doi.org/10.1128/EC.00244-10

Yeung, B. G., Phan, H. L., & Payne, G. S. (1999). Adaptor complex-independent clathrin function in yeast. *Molecular Biology of the Cell*, *10*(11), 3643–3659. https://doi.org/10.1091/mbc.10.11.3643

Yoshinari, A., Shimizu, Y., Hosokawa, T., Nakano, A., Uemura, T., & Takano, J. (2024). Rapid Vacuolar Sorting of the Borate Transporter BOR1 Requires the Adaptor Protein Complex AP-4 in Arabidopsis. *Plant & Cell Physiology*, *65*(11), 1801–1811. https://doi.org/10.1093/pcp/pcae096

Zeno, W. F., Hochfelder, J. B., Thatte, A. S., Wang, L., Gadok, A. K., Hayden, C. C., Lafer, E. M., & Stachowiak, J. C. (2021). Clathrin senses membrane curvature. *Biophysical Journal*, *120*(5), 818–828. https://doi.org/10.1016/j.bpj.2020.12.035

Zhang, S., Hama, Y., & Mizushima, N. (2021). The evolution of autophagy proteins—Diversification in eukaryotes and potential ancestors in prokaryotes. *Journal of Cell Science*, *134*(13), jcs233742. https://doi.org/10.1242/jcs.233742

Zimmermann, L., Stephens, A., Nam, S.-Z., Rau, D., Kübler, J., Lozajic, M., Gabler, F., Söding, J., Lupas, A. N., & Alva, V. (2018). A Completely Reimplemented MPI Bioinformatics Toolkit with a New HHpred Server at its Core. *Journal of Molecular Biology*, *430*(15), 2237–2243. https://doi.org/10.1016/j.jmb.2017.12.007

Zlatic, S. A., Grossniklaus, E. J., Ryder, P. V., Salazar, G., Mattheyses, A. L., Peden, A. A., & Faundez, V. (2013). Chemical-genetic disruption of clathrin function spares adaptor complex 3-dependent endosome vesicle biogenesis. *Molecular Biology of the Cell*, *24*(15), 2378–2388. https://doi.org/10.1091/mbc.E12-12-0860

Zwiewka, M., Feraru, E., Möller, B., Hwang, I., Feraru, M. I., Kleine-Vehn, J., Weijers, D., & Friml, J. (2011). The AP-3 adaptor complex is required for vacuolar function in Arabidopsis. *Cell Research*, *21*(12), 1711–1722. https://doi.org/10.1038/cr.2011.99

Appendix

Appendix 1 – Oligonucleotides

Appendix 1.1 – Oligonucleotides for cloning

Name	**sequence 5'→3'**
AP-1M NotI fw	ctcggcggccgctaaGTTAATGGTTTAACATATTGTTGGGTAG CTC
AP-1M AvrII rv	aggacctaggGGACATTCTGACCTGATAGTCGCCATTTTGC G
AP-3M NotI fw	ctcggcggccgctaaGGACCCTCTCCTTTATATAATAACAATG
AP-3M AvrII rv	aggacctaggTAGCCTAAATTCTATGTTATTATATATGGT
AP-4M NotI fw	ctcggcggccgctaaTTATTAGGAAATCCATTTATCAAAATAG C
AP-4M AvrII rv	aggacctaggGTTCAAACGGTAAACATATGAAGAAGATTG
Clathrin HC NotI fw	ctatttaggtgacactatagaatactcgcggccgctaaTTAACTGCATGCTAT TTGAAATTAAAAG
Clathrin HC AvrII rv	aatcactgcctcacccttactcaccatcctaggAAAATGGGTATTGTTGTT GAACATGTC
STEVOR$_{1-30}$ XhoI fw	gttttttttaatttcttacatataactcgagATGAAGATGTATAACCTTAAA ATG
mScarlet-SDEL XmaI rv	gaaaaacgaacattaagctgccatatccctcgacccgggTTATAATTCATCA CTCTTGTAAAGC
mScarlet XhoI fw	gttttttttaatttcttacatataactcgagATGGTGAGTAAGGGTGAGGC AGTGATTAAG
mScarlet AvrII KpnI rv	GAAATTCATCCATGGTACCTAATGTTGCAACTGGTGCA TAATCTGGATTATCATATGGATAACTTGTCCTAGGCTT GTAAAGCTCATCCATACCACC

Rab6 KpnI fw	cattaggtaccATGGATGAATTTCAAAACTCGGGACTAAATAAATACAAACTTGTTTTCTTAGGAGAACAAGCTGTTGGTAAAACATCTATAATTACAAGATTC
Rab6 XmaI rv	gaaaaacgaacattaagctgccatatccctcgacccgggTTAACATAAACATTTACTTAACATATTTTTGTC
Rab7 KpnI fw	cagttgcaacattaggtaccATGTCAAATAAAAAAAGAACCATATTAAAAG
Rab7 XmaI rv	gccatatccctcgacccgggTTAACAACAACGACTTTTGTACATTTTTTG
SP XhoI fw	gttttttttaatttcttacatataactcgagATGAAGAATAAACTTTCTAC
SP XmaI rv	cattaagctgccatatccctcgacccgggTTACTTGTAAAGCTCATCCATAC
GRASP XhoI fw	gttttttttaatttcttacatataactcgagATGGGAGCAGGACAAACtAAGGAAATTATG
GRASP AvrII rv	cataatctggattatcatatggataacttgtcctaggTATGTTCTTTCTTACATCATGAACATAATTAAATG
CLC XhoI fw	gttttttttaatttcttacatataactcgagATGAGCGAATTGAAAGAGTTCGATG
CLC AvrII rv	cataatctggattatcatatggataacttgtcctaggTGAACTTTCCTTTTGTATTAGTTTAAG
Tepsin XhoI fw	gttttttttaatttcttacatataactcgagATGATGAATAGGTTAATTTTGAACAAGGCCAC
Tepsin rv	GGACCTCCAAGGTTTCTATAAGAGTTTCTTTTTCTTC
Tepsin fw	GAAGAAAAAGAAACTCTTATAGAAACCTTGGAGGTCC
Tepsin AvrII rv	cataatctggattatcatatggataacttgtcctaggTAGTTTCATATGATCCGATAATAGTTCGAAG
Sortilin XhoI fw	gttttttttaatttcttacatataactcgagATGAAAAAAAAGCTTGAAAAGCAAAAGAAGTTG
Sortilin rv	CTTTATTAAACGAAATAACAGTTCTAACAGCATC
Sortilin fw	GATGCTGTTAGAACTGTTATTTCGTTTAATAAAG
Sortilin AvrII rv	cataatctggattatcatatggataacttgtcctaggTAATAATTCAATATTATCAGCATAATTTTTTG

Plasmepsin II XhoI fw	gttttttttaatttcttacatataactcgagATGGATATTACAGTAAGAGAACATG
Plasmepsin II AvrII rv	cataatctggattatcatatggataacttgtcctaggTAAATTCTTTTTAGCAAGAGCAATACCAAC
CDF XhoI fw	gttttttttaatttcttacatataactcgagATGCCCACCGAAATGAACTCTTCGTTGCTAG
CDF AvrII rv	cataatctggattatcatatggataacttgtcctaggAGTATCCCCTTTCAATGTGGAACATTTAAG
VIT XhoI fw	gttttttttaatttcttacatataactcgagATGGTTAGTAAAAAAACGATAGAAGCTAG
VIT AvrII rv	cataatctggattatcatatggataacttgtcctaggTTCGGAAATGTTATTTTTAAGTACAACTC
FNT XhoI fw	gttttttttaatttcttacatataactcgagATGCCCCCCAACAACAGCAAGTACGTGCTGG
FNT AvrII rv	ctggattatcatatggataacttgtcctaggGTTGCGCAGTTCAATGCTCAGGGATTTCATTTG
RON12 KpnI fw	GGGggtaccATGAAAAGAGTATATACGTGTTTG
RON12 AvrII rv	GGGGGcctaggTTCTTGTGTTAAATCGGAAACGTTC
EXP2 recod KpnI fw	CTGGctcgagATGAAGGTGTCCTACATTTTCTCTTTC
EXP2 recod AvrII rv	TCCTcctaggCTCCTTGTTCTCGTCCTTCTTCTCG

Appendix 1.2 – Oligonucleotides to assess correct integration

Name	**sequence 5'→3'**
P1 - AP1 int 5’ fw	CAGAGGTGTTTTATAATTGTGTTATTGATC
P2 - AP1 int 3’ rv	GCTACATTTGAATTTTCCATCAATTAATATGTTTC
P1 - AP3 int 5’ fw	CTTCTGCATTATTATGATAAAATTCTG
P2 - AP3 int 3' rv	GGTAACACGTGGCTACTATATATTGTACG
P1 - AP4 int 5’ fw	CAGTGAAAAAATTTGCCAACCTACC
P2 - AP4 int 3’ rv	GTGTAATTATATAATTCTTTGTTTAC
P3 - GFP 272 as	CCTTCGGGCATGGCACTC
P4 - pARLsense 55	ggaattgtgagcggataacaatttcacacagg

P5 - Clathrin HC int 5’ fw	CAAATAATCCAGAAGCATATAAAGAAGTTATAG
P6 - Clathrin HC int 3’ rv	CATCTATTATAAGGAAAAAATTATTTGTC
P7 - mScarlet 38 rv	CCCTCCATGTGCACCTTAAAACGC
P8 - pARLsense 55	ggaattgtgagcggataacaatttcacacagg

Appendix 2 – Plasmids

1) Plasmids for integration using SLI (Birnbaum et al., 2017)	
pSLI-AP-1 sandwich	this study
pSLI-AP-3 sandwich	this study
pSLI-AP-4 sandwich	this study
2) Plasmid for integration using SLI2 (Cronshagen et al., 2024)	
pSLI2-CHC	this study
3) Plasmids for colocalisation and KS	
pARL_*crt*-STEVOR$_{1\text{-}30}$-mScarlet-SDEL_*nmd3*-NLS-FRB-T2A-yDHODH	this study
pARL_*crt*-mScarlet-Rab6_*nmd3*-NLS-FRB-T2A-yDHODH	this study
pARL_*crt*-mScarlet-Rab7_*nmd3*-NLS-FRB-T2A-yDHODH	this study
pARL_*crt*-SP-mScarlet_*nmd3*-NLS-FRB-T2A-yDHODH	this study
pARL_*crt*-GRASP-mScarlet_*nmd3*-NLS-FRB-T2A-yDHODH	this study
pARL_*crt*-CLC-mScarlet_*nmd3*-NLS-FRB-T2A-yDHODH	this study
pARL_*crt*-Tepsin-mScarlet_*nmd3*-NLS-FRB-T2A-yDHODH	this study
pARL_*crt*-Sortilin-mScarlet_*nmd3*-NLS-FRB-T2A-yDHODH	this study
pARL_*crt*-PlmII-mScarlet_*nmd3*-NLS-FRB-T2A-yDHODH	this study
pARL_*crt*-CDF-mScarlet_*nmd3*-NLS-FRB-T2A-yDHODH	this study
pARL_*crt*-VIT-mScarlet_*nmd3*-NLS-FRB-T2A-yDHODH	this study
pARL_*crt*-FNT-mScarlet_*nmd3*-NLS-FRB-T2A-yDHODH	this study
pARL_*ama1*-RON12-mCherry_*nmd3*-NLS-FRB-T2A-yDHODH	this study
pARL_*ama1*-EXP2-mCherry_*nmd3*-NLS-FRB-T2A-yDHODH	this study

Appendix 3 – Efficiency of knock sideways

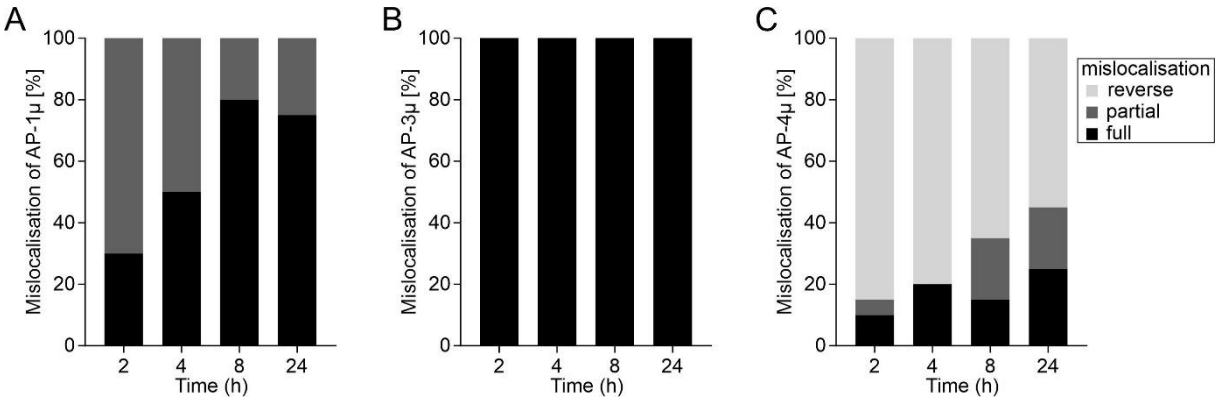

Appendix 4 – Growth curve

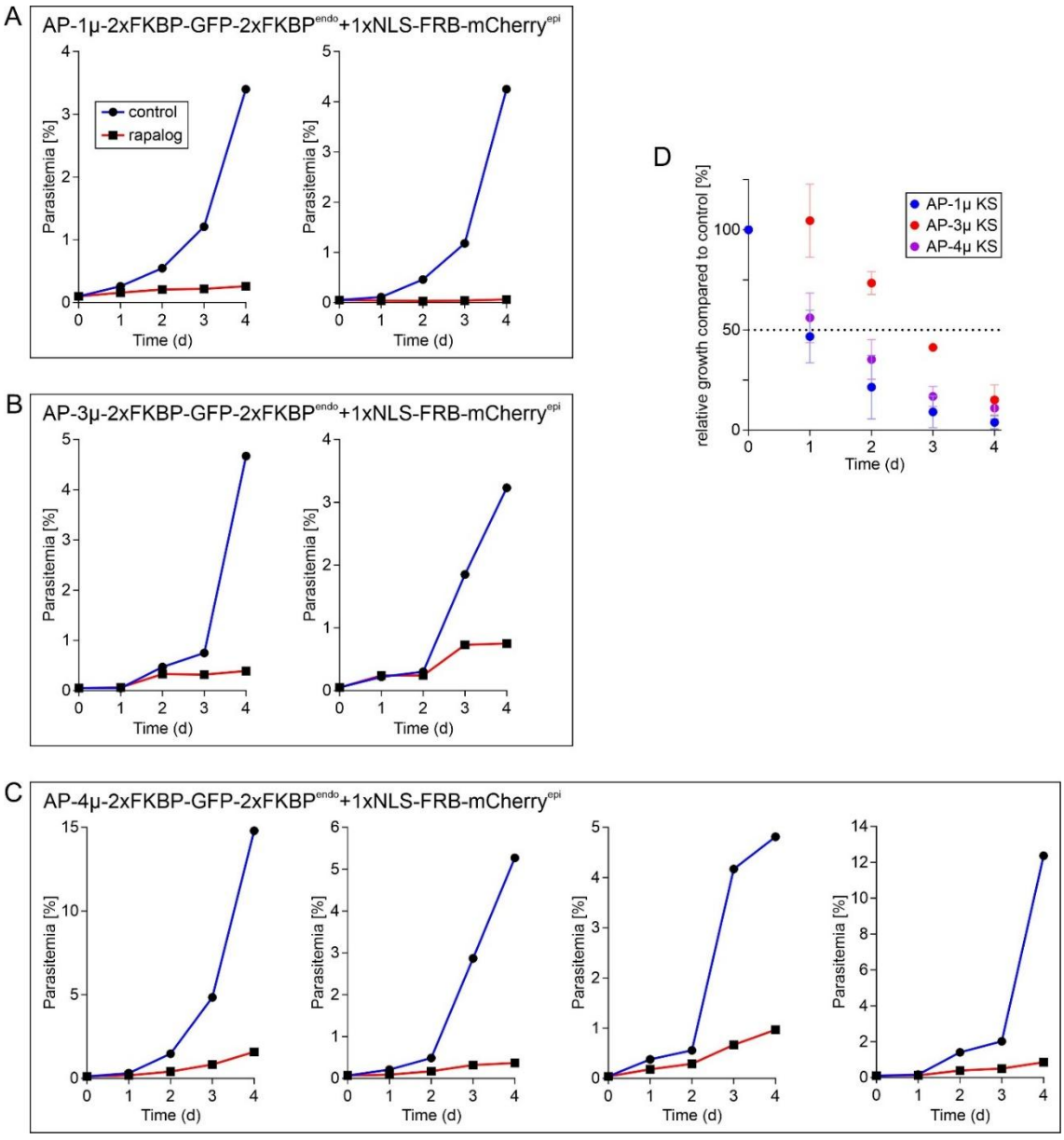

Appendix 5 – Stage assays

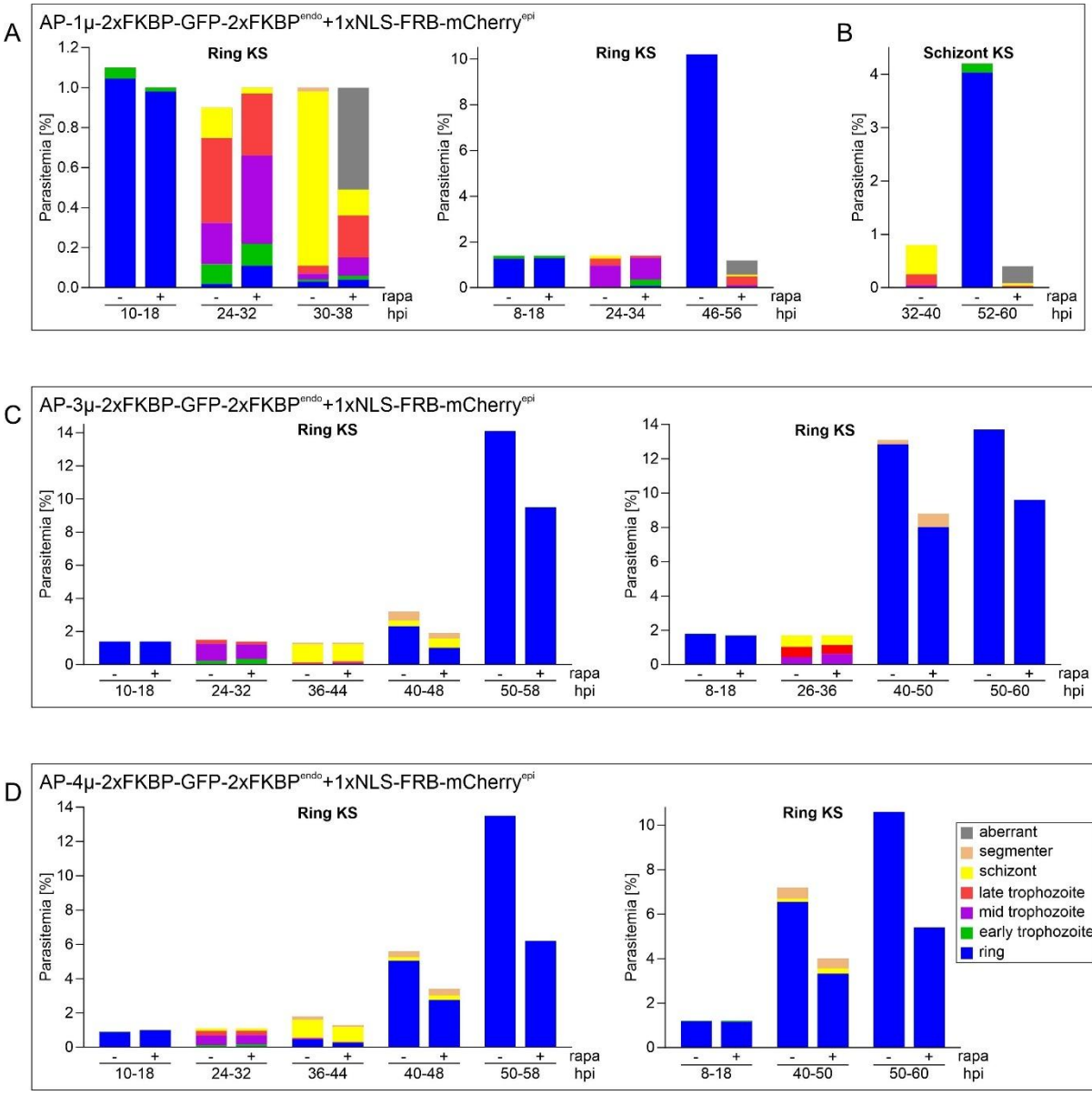

Appendix 6 – DiQ-BioID of AP-1

Majority protein IDs	gene_product	Ratio H/L normalized AP1_mT_Nt_Fw	Ratio H/L normalized AP1_mT_Nt_Rv	Ratio H/L normalized AP1_mT_Ct_Fw	Ratio H/L normalized AP1_mT_Ct_Rv	T-test Difference
PF3D7_1118100	AP-1 complex subunit sigma, putative	4,8039	4,4115	3,91303	4,13593	4,31609
PF3D7_1247400	peptidyl-prolyl cis-trans isomerase FKBP35	2,62129	2,60674	4,55912	4,13128	3,47961
PF3D7_1455500	AP-1 complex subunit gamma, putative	4,39869	4,46868	4,15437	3,8969	4,22966
PF3D7_1459600	AP-4 complex accessory subunit Tepsin, putative	4,04885	4,20919	2,95086	3,06504	3,56849
PF3D7_1435500	clathrin light chain, putative	3,75649	4,07958	3,2454	3,41923	3,62517
PF3D7_1219100	clathrin heavy chain, putative	3,69443	3,62211	3,17513	3,15869	3,41259
PF3D7_0419500	conserved Plasmodium membrane protein, unknown function	3,45628	3,58528	2,78224	3,02268	3,21162
PF3D7_1210100	syntaxin, Qa-SNARE family	2,89039	3,14714	3,4665	2,44199	2,9865
PF3D7_1432800	HP12 protein homolog, putative	3,44082	3,35767	2,53386	3,10942	3,11044
PF3D7_1411300	DnaJ protein, putative	3,22554	3,37273	1,98947	1,92413	2,62797
PF3D7_1247500	serine/threonine protein kinase, putative	3,42828	3,13924	2,99848	2,73543	3,07536
PF3D7_0915400	ATP-dependent 6-phosphofructokinase	3,27971	3,25388	1,15737	1,17277	2,21593
PF3D7_1227300	conserved Plasmodium protein, unknown function	2,50096	NaN	2,00252	3,40802	2,63717
PF3D7_0804900	GTPase-activating protein, putative	3,23541	3,25842	2,47988	2,60858	2,89557
PF3D7_1311400	AP-1 complex subunit mu-1	3,06366	2,71862	2,76617	2,54515	2,7734
PF3D7_1421000	DIX domain-containing protein, putative	3,07663	3,1702	1,85925	2,08688	2,54824
PF3D7_0526200	ADP-ribosylation factor GTPase-activating protein 2	3,02551	3,07899	1,65421	2,08314	2,46046
PF3D7_1307700	TOM1-like protein, putative	2,81506	3,03268	2,18495	2,45648	2,62229
PF3D7_0503500	protein kinase, putative	2,58866	2,65544	2,32887	2,14458	2,42939
PF3D7_1405100	GTPase-activating protein, putative	2,81711	2,89787	2,15682	2,2099	2,52043
PF3D7_0406700	KLRAQ domain-containing protein, putative	3,02428	2,23155	2,05884	2,16385	2,36963
PF3D7_0202600;PF3D7_0202600	nucleic acid-binding protein, putative	2,8394	2,90444	1,97394	2,18442	2,47555
PF3D7_1451800	sortilin	1,96096	2,06413	2,16941	1,86549	2,015
PF3D7_0530100	SNARE protein, putative	3,0804	2,27802	1,70208	1,73025	2,19769
PF3D7_1365700	SNARE associated Golgi protein, putative	NaN	1,04832	2,24059	1,56465	1,61785
PF3D7_0724000	Rab GTPase activator and protein kinase, putative	2,78821	2,22405	2,26649	1,51986	2,19965
PF3D7_0528100	AP-1/2 complex subunit beta, putative	2,50118	1,91061	2,02276	1,6736	2,02704
PF3D7_1408700	conserved protein, unknown function	2,43063	2,49753	1,83406	1,85017	2,1531
PF3D7_0929700	conserved Plasmodium protein, unknown function	2,74653	1,94364	1,94744	1,59366	2,05782
PF3D7_1205400	kelch domain-containing protein, putative	2,27149	1,80601	2,17728	1,36323	1,9045
PF3D7_1432000	syntaxin, Qa-SNARE family	2,23189	2,41396	1,93512	1,58251	2,04087
PF3D7_0704400	phosphoinositide-binding protein, putative	2,23177	2,26798	1,61127	1,88865	1,99992
PF3D7_1469100	Golgi SNAP receptor complex member 1, putative	NaN	2,2258	1,26813	1,54448	1,67947
PF3D7_0314100	vesicle transport v-SNARE protein, putative	1,92615	2,30052	1,55739	1,87107	1,91378
PF3D7_1332000	syntaxin, Qa-SNARE family	1,84157	2,48997	1,38333	1,5894	1,82607
PF3D7_0411800	conserved Plasmodium protein, unknown function	2,14261	2,23006	1,19182	1,19393	1,68961
PF3D7_1313800	conserved Plasmodium membrane protein, unknown function	1,18916	1,4089	1,09532	1,74792	1,36033
PF3D7_0916000	major facilitator superfamily domain-containing protein, putative	2,01221	2,29025	0,326882	0,654694	1,32101
PF3D7_0815800	vacuolar protein sorting-associated protein 9, putative	1,86616	1,82741	1,37217	1,46737	1,63328
PF3D7_1017600	conserved Plasmodium protein, unknown function	NaN	2,14254	-0,09445	0,554888	0,86766
PF3D7_0305200	GRIP domain-containing protein, putative	1,99048	1,95394	1,32164	1,50951	1,69389
PF3D7_1017300;PF3D7_1017300	golgi re-assembly stacking protein 1	1,70146	1,55678	1,4881	1,29039	1,50918
PF3D7_0914900	BSD-domain protein, putative	1,68684	1,61387	1,34238	1,42612	1,5173
PF3D7_0320100	protein transport protein SEC22	1,06736	2,10234	0,990519	1,72399	1,47105
PF3D7_1019600	conserved Plasmodium protein, unknown function	1,47669	1,42225	1,29531	1,23814	1,3581
PF3D7_0216400	vacuolar protein sorting-associated protein 45	1,37334	1,54662	1,29113	1,19027	1,35034
PF3D7_0711000	AAA family ATPase, CDC48 subfamily	NaN	1,66979	0,410775	0,136839	0,739135
PF3D7_1111300	protein transport protein BOS1, putative	1,42256	1,44878	1,15192	1,29156	1,3287
PF3D7_0919900	regulator of chromosome condensation-PP1-interacting protein	1,15192	1,413	1,06025	1,32536	1,23763
PF3D7_0820500	protein transport protein YIF1, putative	1,48471	1,29435	1,26921	1,08562	1,28347
PF3D7_1227200	potassium channel K1	2,02109	0,693061	0,856946	NaN	1,19037
PF3D7_1034000	Sec1 family protein, putative	0,813771	0,566635	1,20163	1,05412	0,909039
PF3D7_0609300	conserved Plasmodium protein, unknown function	1,24866	1,07403	1,26802	0,752948	1,08591
PF3D7_0904100	AP-4 complex subunit epsilon, putative	1,19925	1,23328	0,709379	0,816037	0,989486
PF3D7_1104300	conserved Plasmodium protein, unknown function	0,406972	1,30639	0,917699	1,04171	0,918193
PF3D7_1145100	coatomer subunit gamma, putative	1,19906	1,18863	0,609377	0,718711	0,928944
PF3D7_0721000	conserved Plasmodium membrane protein, unknown function	1,23235	1,06891	0,963622	NaN	1,08829
PF3D7_0505200	actin-like protein, putative	0,220949	-0,35242	1,04376	0,853684	0,441493
PF3D7_0209100	patatin-like phospholipase 1	1,26412	1,06951	0,828225	-0,33845	0,70585
PF3D7_0412000	LITAF-like zinc finger protein, putative	1,03668	0,995793	1,09943	0,763048	0,973738
PF3D7_1308000	conserved Plasmodium membrane protein, unknown function	0,914488	1,23759	0,868687	0,963729	0,996123
PF3D7_0408100	conserved Plasmodium protein, unknown function	1,28582	0,968661	0,538339	0,68952	0,870585
PF3D7_0625800	conserved Plasmodium protein, unknown function	0,768248	0,67013	0,77349	0,997175	0,802261
PF3D7_0716300	conserved protein, unknown function	0,842134	1,20779	0,864731	0,790809	0,926366
PF3D7_1414100	zinc finger protein, putative	0,004609	0,352308	1,22725	0,401044	0,496303
PF3D7_1132400	conserved Plasmodium membrane protein, unknown function	1,23008	0,797087	0,606821	0,856763	0,872688
PF3D7_1450000	serine/threonine protein kinase, putative	0,8279	-0,21636	0,810731	NaN	0,47409
PF3D7_0913600	conserved Plasmodium protein, unknown function	0,803475	0,32771	1,05012	0,571086	0,688098
PF3D7_0215400	conserved Plasmodium protein, unknown function	0,290542	1,72495	0,781905	0,782099	0,894874
PF3D7_0829000	conserved Plasmodium membrane protein, unknown function	0,939076	0,90717	0,815248	0,779497	0,860248
PF3D7_0505100	trafficking protein particle complex subunit 8, putative	0,927821	1,04397	0,786429	0,798918	0,889284
PF3D7_0935200	vacuolar protein sorting-associated protein 33, putative	0,745452	1,18076	0,885184	0,580267	0,847916
PF3D7_0705500	inositol-phosphate phosphatase, putative	0,958286	0,893866	0,71352	0,862287	0,85699
PF3D7_0512600	ras-related protein Rab-1B	0,742437	0,390529	0,93644	0,638771	0,677044
PF3D7_0501900	trafficking protein particle complex subunit 13, putative	1,097	0,705782	0,68428	0,547067	0,758532
PF3D7_0511300	MORN repeat protein, putative	NaN	0,538325	0,92691	0,611491	0,692242
PF3D7_0627100	ankyrin-repeat protein, putative	1,27882	0,51513	0,076149	0,14299	0,503272
PF3D7_1303500	sodium/hydrogen exchanger	0,299948	1,47017	-0,00357	0,895529	0,66552
PF3D7_1236300	conserved protein, unknown function	0,756767	0,991628	0,68724	0,70557	0,785301
PF3D7_1361000	protein arginine N-methyltransferase 5, putative	-1,38304	1,85439	-0,03021	1,55368	0,498706
PF3D7_1326500	conserved Plasmodium protein, unknown function	1,91411	-0,22243	-0,53253	-0,00331	0,288957
PF3D7_0107000	centrin-1	NaN	0,801632	0,264476	-0,14379	0,307441
PF3D7_1127600	CRAL/TRIO domain-containing protein, putative	0,559541	1,0407	0,546759	0,325449	0,618112
PF3D7_1147500	protein farnesyltransferase subunit beta	0,918844	-0,86354	NaN	0,731589	0,262297
PF3D7_1351200	conserved Plasmodium protein, unknown function	-0,2035	1,76489	-1,23797	0,951122	0,318635
PF3D7_0206500	conserved Plasmodium protein, unknown function	-0,45734	-0,17351	0,711142	NaN	0,026765
PF3D7_1434800	mitochondrial acidic protein MAM33, putative	NaN	0,756989	0,01407	-0,18777	0,19443
PF3D7_0703000	conserved Plasmodium protein, unknown function	0,37951	0,551585	0,50284	0,896872	0,582702
PF3D7_1219000	formin 2	0,707083	0,750955	0,410558	0,425521	0,573529
PF3D7_1401200	Plasmodium exported protein, unknown function	-0,4347	0,56126	0,338567	1,0534	0,379633
PF3D7_0102500	erythrocyte binding antigen-181	0,457752	0,997693	0,335026	0,157094	0,486891
PF3D7_1015400	RMI1 domain-containing protein, putative	0,351289	-0,30416	-0,13641	1,46462	0,343834
PF3D7_0804000	cactin homolog, putative	NaN	0,706041	-0,29431	0,029087	0,146938
PF3D7_1427600	CorA-like Mg2+ transporter protein, putative	0,985646	0,417251	0,172231	0,373196	0,487081
PF3D7_1239700	ATP-dependent zinc metalloprotease FTSH 1	0,782492	0,598719	0,76528	0,394809	0,635325
PF3D7_1455200	methyltransferase AAMT	0,157173	0,389149	0,632175	0,678672	0,464292
PF3D7_1364000	conserved protein, unknown function	0,643394	0,721159	0,799419	0,302297	0,616567
PF3D7_1363100	conserved Plasmodium protein, unknown function	1,50716	-0,14313	0,703632	-0,28416	0,445875
PF3D7_0407800	protein CINCH	0,524365	0,741324	0,164786	0,136474	0,391737
PF3D7_1104100	syntaxin, Qa-SNARE family	0,595313	0,454407	0,798673	0,46937	0,579441
PF3D7_0912400	alkaline phosphatase, putative	NaN	0,632092	-0,28634	0,589833	0,311862
PF3D7_0806800	V-type proton ATPase subunit a, putative	0,518535	0,724755	0,458382	-0,04404	0,414407
PF3D7_1465100	conserved oligomeric Golgi complex subunit 6, putative	0,55562	0,587966	0,921893	0,265674	0,582788
PF3D7_0926700	glutamine-dependent NAD(+) synthetase, putative	1,09694	0,116692	0,362778	0,47305	0,512365
PF3D7_0301600	Plasmodium exported protein (hyp1), unknown function	0,566474	0,46895	1,20596	-0,02475	0,55416
PF3D7_1318800	translocation protein SEC63, putative	0,584289	NaN	1,19805	-0,08963	0,564235
PF3D7_1026800	40S ribosomal protein S2	0,53436	0,320702	0,687419	0,490821	0,508325
PF3D7_1017000	DNA polymerase delta catalytic subunit	-0,03425	0,46909	0,854395	0,314194	0,400858
PF3D7_0305500	protein dopey homolog, putative	0,655993	0,485398	0,309525	0,423971	0,468722
PF3D7_1239900	vacuolar protein sorting-associated protein 16, putative	0,312433	0,481888	0,612211	0,541408	0,486985
PF3D7_1034500	armadillo repeat protein, putative	0,24123	0,731925	0,504264	0,628541	0,52649
PF3D7_0416800	small GTP-binding protein sar1	0,684639	0,440792	0,650856	0,339236	0,528881
PF3D7_1336800	nuclear movement protein, putative	0,697507	0,369781	0,703366	0,413615	0,546067

PF3D7_1320600	ras-related protein Rab-11A	0,473215	0,649933	0,241718	0,679435	0,511075
PF3D7_1205900	conserved protein, unknown function	0,654619	0,420511	0,370611	0,742265	0,547001
PF3D7_0613500	AP-3 complex subunit beta, putative	0,270828	0,840913	0,142348	0,557688	0,452944
PF3D7_1118200	heat shock protein 90, putative	0,322505	0,318506	-0,84814	1,95797	0,43771
PF3D7_1316100	inositol polyphosphate kinase, putative	0,554933	NaN	0,244278	0,304861	0,368024
PF3D7_1211300	DNA helicase MCM8, putative	0,194087	0,907576	0,573956	0,148433	0,456013
PF3D7_0813200	CS domain protein, putative	-0,05065	-1,0383	0,465295	0,641626	0,004492
PF3D7_1365900;PF3D7_1211800	ubiquitin-60S ribosomal protein L40	0,483468	0,613101	0,001586	-0,23156	0,21665
PF3D7_1014900	protein KIC8	0,649569	0,445009	0,346531	0,202688	0,410949
PF3D7_0918000	glideosome-associated protein 50	0,606063	0,471729	1,15225	-0,09153	0,534628
PF3D7_1462900	AAA ATPase, putative	0,350271	-0,14639	0,549817	NaN	0,251231
PF3D7_0826500	ubiquitin conjugation factor E4 B, putative	-0,51932	NaN	0,726483	0,366578	0,191247
PF3D7_0910800	cytosolic Fe-S cluster assembly factor NBP35, putative	0,293841	-1,03773	0,343806	0,733795	0,083428
PF3D7_0829200	prohibitin 1, putative	0,809497	0,255288	0,448267	0,219774	0,433207
PF3D7_1412100	mini-chromosome maintenance complex-binding protein	0,726831	0,331609	-0,2409	0,10729	0,231209
PF3D7_0104300	ubiquitin carboxyl-terminal hydrolase 1, putative	0,03196	0,638973	0,528171	NaN	0,399701
PF3D7_0615600	zinc finger protein, putative	-0,01245	1,05568	0,086512	0,152917	0,320666
PF3D7_0820900	conserved Plasmodium protein, unknown function	0,233152	-0,04138	0,146003	0,893839	0,307903
PF3D7_0702500	Plasmodium exported protein, unknown function	0,097341	0,936	-0,51476	0,530031	0,262153
PF3D7_0611900	lsm12, putative	-0,02626	-0,00547	0,516822	NaN	0,161695
PF3D7_0916700	RNA-binding protein musashi, putative	0,7122	0,312491	0,0842	0,129103	0,309499
PF3D7_1466100	protein phosphatase containing kelch-like domains	NaN	0,328399	0,852798	0,179172	0,453456
PF3D7_0717600	inner membrane complex protein, putative	0,364685	0,654445	0,289598	0,17119	0,369979
PF3D7_0509800	phosphatidylinositol 4-kinase beta	0,481919	0,530364	0,396159	0,611359	0,50495
PF3D7_0806000	AAA family ATPase, putative	-0,03236	0,910936	NaN	0,508465	0,462347
PF3D7_1429800	coatomer subunit beta, putative	0,569297	0,442791	0,407516	0,563241	0,495711
PF3D7_1238100	calcyclin binding protein, putative	0,208517	0,127605	0,503145	0,510991	0,337564
PF3D7_1135900	3-oxo-5-alpha-steroid 4-dehydrogenase, putative	0,509949	0,487763	0,576861	0,166972	0,435386
PF3D7_1119000	acyl-CoA-binding protein, putative	-0,34207	0,072999	0,500598	NaN	0,077177
PF3D7_1309700	vacuolar protein sorting-associated protein 18, putative	0,543595	0,434266	0,722816	0,243369	0,486012
PF3D7_0419800	60S ribosomal protein L7ae/L30e, putative	0,691266	0,285073	-0,34944	0,658196	0,321274
PF3D7_1462100	conserved Plasmodium protein, unknown function	0,292546	0,181248	0,514198	0,48459	0,368145
PF3D7_1346400	VPS13 domain-containing protein, putative	0,531269	0,444773	0,494774	0,404783	0,4689
PF3D7_1442900	Sec7 domain-containing protein ARFGEF, putative	0,294194	0,088761	0,522759	0,465162	0,342719
PF3D7_1022600	kelch protein K10	0,484602	NaN	-0,25758	-0,32792	-0,03363
PF3D7_1329400	AMP deaminase	0,600936	0,365314	0,193204	0,171417	0,332718
PF3D7_0501200	parasite-infected erythrocyte surface protein	-0,51899	1,48128	-0,19423	-0,05922	0,177211
PF3D7_1312600	2-oxoisovalerate dehydrogenase subunit alpha, mitochondrial, putative	NaN	0,172311	0,510354	0,456762	0,379809
PF3D7_1002700	conserved Plasmodium protein, unknown function	0,464982	0,489139	0,076833	0,45595	0,371726
PF3D7_0502000	vacuolar protein sorting-associated protein 11, putative	0,439783	0,51019	0,065986	0,500483	0,37911
PF3D7_1116700	dipeptidyl aminopeptidase 1	0,729705	-0,06461	NaN	0,479734	0,381611
PF3D7_0513800	ras-related protein Rab-1A	0,312781	0,635383	0,088142	-0,01364	0,255666
PF3D7_1451000	conserved Plasmodium protein, unknown function	0,077653	0,499218	0,251446	0,688171	0,379122
PF3D7_0313000	conserved Plasmodium protein, unknown function	0,41738	0,528677	0,446891	0,264686	0,414408
PF3D7_0606700	coatomer alpha subunit, putative	0,406972	0,535123	0,449007	0,395207	0,446577
PF3D7_0922500	phosphoglycerate kinase	0,51924	0,273901	0,495081	0,432007	0,430057
PF3D7_1473100	GTPase-activating protein, putative	0,185993	0,746277	0,327917	0,150849	0,352759
PF3D7_1144900	ras-related protein Rab-6	NaN	0,141812	0,551295	0,37501	0,356039
PF3D7_1230700	protein transport protein SEC13	0,523662	0,403675	0,187641	0,114644	0,307405
PF3D7_1230000	TBC domain-containing protein, putative	0,359184	0,20141	0,659194	0,254444	0,368558
PF3D7_0314700	RING finger protein RNF1	0,372283	0,554803	0,411318	0,459953	0,449589
PF3D7_1246800	signal recognition particle receptor subunit beta, putative	0,531668	0,389848	0,416948	0,243182	0,395411
PF3D7_0523400	DnaJ protein, putative	0,447315	0,465062	0,323543	0,359027	0,398737
PF3D7_0808100	AP-3 complex subunit delta, putative	-0,00606	0,313405	0,384381	0,521722	0,303363
PF3D7_0717100	CRAL/TRIO domain-containing protein, putative	-0,10199	1,00636	-0,32511	0,186098	0,191342
PF3D7_1020900	ADP-ribosylation factor 1	0,573665	0,18043	0,527571	0,374561	0,414057
PF3D7_0919800	TLD domain-containing protein	0,323312	0,577509	0,360533	0,326787	0,397035
PF3D7_1212400	tetratricopeptide repeat protein, putative	-0,83049	0,130776	0,786262	0,114441	0,050249
PF3D7_1465900	40S ribosomal protein S3	0,389567	0,294668	0,459012	0,441595	0,39621
PF3D7_0802300	periodic tryptophan protein 2, putative	0,019915	0,875434	-0,22582	0,054332	0,180966
PF3D7_0612200	leucine-rich repeat protein	0,514602	0,375459	0,16221	0,105473	0,289436
PF3D7_1034900	methionine--tRNA ligase	0,245861	0,104992	0,390227	0,49981	0,310222
PF3D7_0504000	cation transporting P-ATPase	0,573762	0,304986	0,238909	0,328399	0,361514
PF3D7_1308700	conserved Plasmodium protein, unknown function	-0,07926	0,061571	-0,0627	0,948363	0,216992
PF3D7_0106800	ras-related protein Rab-5C	0,246712	0,000577	0,259062	0,620335	0,281672
PF3D7_0310700	trafficking protein particle complex subunit 4, putative	0,436588	NaN	0,301002	-0,10996	0,209209
PF3D7_0301700	Plasmodium exported protein, unknown function	0,206893	0,139999	0,187134	0,685802	0,304957
PF3D7_0828500	translation initiation factor eIF-2B subunit alpha, putative	0,200253	0,671278	0,214498	0,548269	0,408574
PF3D7_1433100	HID1 domain-containing protein, putative	-0,01092	0,781678	0,677441	0,188414	0,409153
PF3D7_0302100	serine/threonine protein kinase	0,319734	0,533952	0,276556	0,384998	0,37881
PF3D7_1332900	isoleucine--tRNA ligase, putative	0,285816	0,365295	0,454597	0,406522	0,378058
PF3D7_1461300	40S ribosomal protein S28e, putative	0,644871	0,20568	0,289834	0,267896	0,35207
PF3D7_0815200	importin subunit beta, putative	0,560519	0,185638	0,636358	0,210496	0,398253
PF3D7_0212900	arginyl-tRNA--protein transferase	0,416407	0,42463	0,319502	0,072073	0,308153
PF3D7_0727000	vacuolar protein sorting-associated protein 53, putative	0,249991	0,524541	0,14991	0,693178	0,404405
PF3D7_0801500	nucleolar protein 10, putative	1,04879	-0,21164	0,038998	-0,53047	0,086421
PF3D7_0917700	GPN-loop GTPase, putative	0,122209	0,262884	0,420402	NaN	0,268498
PF3D7_1110500	vacuolar protein sorting-associated protein 35, putative	-0,16036	0,976191	-0,22048	0,323552	0,229725
PF3D7_1408000	plasmepsin II	0,347325	0,199852	0,466862	0,36736	0,34535
PF3D7_0935800	cytoadherence linked asexual protein 9	0,441165	0,361175	0,302758	0,058458	0,290889
PF3D7_1471200	inorganic anion exchanger, inorganic anion antiporter	0,251325	-0,23634	0,661567	0,170637	0,211797
PF3D7_0812100	proteasome activator complex subunit 4, putative	0,515006	0,285108	0,170694	0,435827	0,351659
PF3D7_1115300;PF3D7_1115700	cysteine proteinase falcipain 2b	0,363339	0,323678	0,343578	0,48748	0,379519
PF3D7_1117900	conserved Plasmodium protein, unknown function	0,204016	0,590463	0,016068	0,352805	0,290838
PF3D7_1440700	AP-3 complex subunit mu, putative	-0,09599	-0,02574	0,590434	0,239072	0,176945
PF3D7_1311300	ATP synthase subunit gamma, mitochondrial	NaN	-0,80232	0,327572	0,492931	0,006062
PF3D7_0521700	ATP-dependent RNA helicase DDX1, putative	0,218223	0,069149	0,408494	0,404248	0,275029
PF3D7_1312100	GYF domain-containing protein, putative	0,455965	0,336828	0,133169	0,409796	0,33394
PF3D7_1344900	conserved Plasmodium protein, unknown function	-0,24451	0,507501	0,072037	0,729866	0,266223
PF3D7_1426700	phosphoenolpyruvate carboxylase	0,388575	0,39876	0,263034	-0,00676	0,260901
PF3D7_1211400	heat shock protein DNAJ homologue Pfj4	0,205893	0,209161	0,278936	0,51837	0,30309
PF3D7_0933500	gamma-tubulin complex component, putative	0,070115	0,710402	-0,00038	0,102729	0,220718
PF3D7_0918300	eukaryotic translation initiation factor 3 subunit F, putative	0,252416	0,238119	0,502942	0,290639	0,321029
PF3D7_1338100	26S proteasome regulatory subunit RPN3, putative	0,242572	0,299418	0,405012	0,388337	0,333835
PF3D7_1458500	spindle assembly abnormal protein 4, putative	0,341416	0,433019	-0,0904	0,308126	0,248039
PF3D7_0612100	eukaryotic translation initiation factor 3 subunit L, putative	0,082021	0,158929	0,549817	0,241902	0,258167
PF3D7_0629200	DnaJ protein, putative	0,458277	0,314499	0,177471	0,092386	0,260658
PF3D7_1314100	conserved Plasmodium protein, unknown function	NaN	0,086936	0,486663	0,296545	0,290048
PF3D7_1031500	ATP-dependent DNA helicase DDX3X	-0,87729	-0,12446	0,198243	0,582469	-0,05526
PF3D7_1003500	40S ribosomal protein S20e, putative	0,450802	0,315558	0,31313	0,186525	0,316504
PF3D7_0914500	conserved Plasmodium protein, unknown function	0,212009	-0,35671	0,275961	0,498749	0,157503
PF3D7_0621800	nascent polypeptide-associated complex subunit alpha, putative	0,925999	-0,16363	-0,24049	0,204216	0,181525
PF3D7_0316800	40S ribosomal protein S15A, putative	0,124328	0,156933	0,346191	0,407153	0,258651
PF3D7_0920800	inosine-5-monophosphate dehydrogenase	1,318	-0,56599	-1,08036	1,1003	0,192988
PF3D7_0719700	40S ribosomal protein S10, putative	0,344488	-0,00877	0,74829	0,003409	0,271853
PF3D7_0413500	phosphoglucomutase-2	0,437121	0,310737	0,349478	0,080561	0,294474
PF3D7_1331800	60S ribosomal protein L23, putative	0,378623	0,090189	0,634779	0,112599	0,304047
PF3D7_1108700	heat shock protein J2	0,364909	0,372617	0,210389	0,01265	0,240141
PF3D7_1124100	BEACH domain-containing protein, putative	0,274649	0,4617	0,260387	0,195566	0,298075
PF3D7_1231100	ras-related protein Rab-2	0,447421	0,287061	0,420725	0,19962	0,338707
PF3D7_0303000	N-ethylmaleimide-sensitive fusion protein	0,239276	0,034825	0,412619	0,322686	0,252352
PF3D7_1142100	conserved Plasmodium protein, unknown function	0,306146	0,427692	0,11929	0,379489	0,308154
PF3D7_1105700	tRNA-splicing ligase RtcB, putative	0,429964	0,102341	0,405448	0,328417	0,316543
PF3D7_0404600	conserved Plasmodium membrane protein, unknown function	-0,10903	0,02078	0,810731	-0,07943	0,160762
PF3D7_0529800	conserved Plasmodium protein, unknown function	0,380286	0,341427	-0,06475	0,196211	0,213293
PF3D7_1245500	conserved Plasmodium protein, unknown function	0,281431	0,149009	0,403049	0,32366	0,289287
PF3D7_0617000	mitochondrial import receptor subunit TOM40, putative	0,56589	0,154811	0,411426	0,265171	0,349325
PF3D7_1361100	protein transport protein Sec24A	0,36042	0,360008	0,358284	0,171303	0,312504
PF3D7_0626800	pyruvate kinase	0,421048	0,298549	0,304628	0,319046	0,335818
PF3D7_1014700	prohibitin 2, putative	0,562474	0,154072	0,338909	0,19679	0,313061
PF3D7_1311900	V-type proton ATPase catalytic subunit A	0,240009	0,243472	0,338681	0,38069	0,300713
PF3D7_1106700	DNA replication ATP-dependent helicase/nuclease DNA2, putative	0,337311	0,376227	0,128689	0,260204	0,275608

Appendix 7 – DiQ-BioID of AP-3

Majority protein IDs	gene_product	Ratio H/L normalized cterm_F	Ratio H/L normalized cterm_R	Ratio H/L normalized nterm_F	Ratio H/L normalized nterm_R	AVERAGE
PF3D7_1247400	peptidyl-prolyl cis-trans isomerase FKBP35	5,50925	5,03056	2,76335	2,8132	4,02909
PF3D7_0613500	AP-3 complex subunit beta, putative	4,07998	4,23189	3,8802	3,59228	3,946088
PF3D7_0808100	AP-3 complex subunit delta, putative	3,43376	3,15213	4,17369	3,9652	3,681195
PF3D7_1440700	AP-3 complex subunit mu, putative	3,55213	3,62558	1,97049	3,0424	3,04765
PF3D7_0915400	ATP-dependent 6-phosphofructokinase	1,57415	1,63774	3,19947	3,27844	2,42245
PF3D7_0920800	inosine-5-monophosphate dehydrogenase	1,48872	1,74884	1,14613	1,37363	1,43933
PF3D7_0626400	CRAL/TRIO domain-containing protein, putative	3,9607	-1,28983	-0,22813	3,18285	1,406397
PF3D7_1352800	vacuolar fusion protein MON1, putative	1,40376	1,47377	1,36827	1,37012	1,40398
PF3D7_1220300	cell cycle associated protein, putative	0,708055	1,50693	NaN	1,86355	1,359512
PF3D7_0619800	conserved Plasmodium membrane protein, unknown function	1,26327	1,38832	1,08773	1,34205	1,270343
PF3D7_1453700	HSP90 co-chaperone p23	1,34409	1,44179	NaN	0,95023	1,24537
PF3D7_0916400	conserved Plasmodium protein, unknown function	1,21282	1,19942	NaN	1,28856	1,2336
PF3D7_1147300	conserved Plasmodium protein, unknown function	1,15004	1,09792	1,04942	1,04704	1,086105
PF3D7_0502000	vacuolar protein sorting-associated protein 11, putative	0,898015	1,05962	1,10487	0,968435	1,007735
PF3D7_0813200	CS domain protein, putative	0,991608	1,08204	0,887447	NaN	0,987032
PF3D7_0305200	GRIP domain-containing protein, putative	0,55562	0,802915	1,04775	1,48746	0,973436
PF3D7_0419500	conserved Plasmodium membrane protein, unknown function	0,560715	1,05544	0,904349	1,34103	0,965384
PF3D7_1211300	DNA helicase MCM8, putative	0,82326	0,995103	1,04698	NaN	0,955114
PF3D7_0721200	conserved Plasmodium protein, unknown function	1,53953	1,3095	0,448901	0,498199	0,949033
PF3D7_1026800	40S ribosomal protein S2	1,18675	1,18311	0,702037	0,596165	0,917016
PF3D7_0218600	patatin-like phospholipase, putative	0,508632	0,484812	1,72735	NaN	0,906931
PF3D7_1410300	WD repeat-containing protein, putative	1,2112	0,976958	0,562474	0,811472	0,890526
PF3D7_0621800	nascent polypeptide-associated complex subunit alpha, putative	0,135404	0,456999	1,68495	1,22445	0,875451
PF3D7_1017000	DNA polymerase delta catalytic subunit	1,10903	0,954445	0,768502	0,51835	0,837582
PF3D7_1332900	isoleucine--tRNA ligase, putative	1,07245	1,00046	0,674099	0,563135	0,827536
PF3D7_0525100	acyl-CoA synthetase	1,07772	0,796385	0,83463	0,465201	0,793484
PF3D7_0314700	RING finger protein RNF1	0,866868	0,785626	0,876645	0,642752	0,792973
PF3D7_1454200	conserved Plasmodium protein, unknown function	1,05019	0,586298	0,881508	0,520293	0,759572
PF3D7_1034900	methionine--tRNA ligase	1,17018	1,03389	0,427713	0,40133	0,758278
PF3D7_1336800	nuclear movement protein, putative	0,86481	0,447466	NaN	0,948586	0,753621
PF3D7_1127600	CRAL/TRIO domain-containing protein, putative	0,84149	0,96948	0,7612	0,411905	0,746019
PF3D7_0219600	replication factor C subunit 1	0,989284	1,06371	0,541812	0,324491	0,729824
PF3D7_0812100	proteasome activator complex subunit 4, putative	0,75873	0,755308	0,666757	0,693388	0,718546
PF3D7_1134700	DNA-directed RNA polymerase I subunit RPA2, putative	0,665302	0,94167	0,517427	NaN	0,708133
PF3D7_1408700	conserved protein, unknown function	0,624616	0,665203	0,662388	0,879728	0,707984
PF3D7_1355100	DNA replication licensing factor MCM6	0,858458	0,733987	0,578601	0,621999	0,698261
PF3D7_1426700	phosphoenolpyruvate carboxylase	0,475396	0,488836	1,18161	0,543509	0,672338
PF3D7_0416900	conserved Plasmodium protein, unknown function	0,595695	0,944554	0,517931	0,599396	0,664394
PF3D7_1104000	phenylalanine--tRNA ligase beta subunit	1,00985	0,449139	0,531469	NaN	0,663486
PF3D7_1355300	histone-lysine N-methyltransferase, putative	0,872789	0,498016	0,607011	NaN	0,659272
PF3D7_0624000	hexokinase	0,774671	0,680544	0,522759	0,656081	0,658514
PF3D7_0627100	ankyrin-repeat protein, putative	0,176067	-0,09248	1,74928	0,770757	0,650906
PF3D7_1466800	NOC3 domain-containing protein, putative	0,233765	-0,00461	1,93051	0,416539	0,644051
PF3D7_0926700	glutamine-dependent NAD(+) synthetase, putative	0,752149	0,613013	0,544584	NaN	0,636582
PF3D7_1466100	protein phosphatase containing kelch-like domains	1,35552	1,0508	-0,29304	0,401616	0,628724
PF3D7_1106700	DNA replication ATP-dependent helicase/nuclease DNA2, putative	0,42825	0,490436	0,96229	NaN	0,626992
PF3D7_0808400	coatomer subunit epsilon, putative	0,158854	0,474813	NaN	1,21809	0,617252
PF3D7_1118300	insulinase, putative	0,574053	0,486166	0,701239	0,658083	0,604885
PF3D7_1107200	conserved protein, unknown function	0,766298	0,550761	0,556895	0,526639	0,600148
PF3D7_1459200	WD repeat-containing protein, putative	1,1171	0,7393	-0,07739	NaN	0,593003
PF3D7_0704400	phosphoinositide-binding protein, putative	0,569199	0,384452	0,61551	0,767094	0,584064
PF3D7_1008800	nucleolar protein 5, putative	0,74786	-0,08719	1,06571	NaN	0,57546
PF3D7_0405400	pre-mRNA-processing-splicing factor 8, putative	0,549916	0,609618	0,653977	0,463768	0,56932
PF3D7_1205900	conserved protein, unknown function	0,231187	0,94931	NaN	0,520169	0,566889
PF3D7_0904100	AP-4 complex subunit epsilon, putative	-0,1432	0,181607	NaN	1,64778	0,562063
PF3D7_1313800	conserved Plasmodium membrane protein, unknown function	0,851679	0,442262	NaN	0,392024	0,561988
PF3D7_1404000	DNA-directed RNA polymerase II subunit RPB4, putative	0,679154	0,218028	1,28842	0,014368	0,549993
PF3D7_1226300	haloacid dehalogenase-like hydrolase, putative	0,235114	0,36669	0,681944	0,909716	0,548366
PF3D7_0414000	structural maintenance of chromosomes protein 3	0,660929	0,397733	0,575603	NaN	0,544755
PF3D7_1416100	protein SEY1, putative	0,365021	0,321063	0,934932	NaN	0,540339
PF3D7_0527500	Hsc70-interacting protein	0,043205	0,114301	1,41749	0,583398	0,539598
PF3D7_1358200	conserved Plasmodium protein, unknown function	-0,16086	0,011181	0,989066	1,31326	0,538161
PF3D7_1318800	translocation protein SEC63, putative	0,693052	0,86247	0,380286	0,195021	0,532707
PF3D7_0803200	filament assembling protein, putative	-0,02873	0,420607	NaN	1,20294	0,531604
PF3D7_0802300	periodic tryptophan protein 2, putative	-0,68478	0,859405	NaN	1,4135	0,529374
PF3D7_1012400	hypoxanthine-guanine phosphoribosyltransferase	0,584193	0,443419	0,329296	0,758062	0,528743
PF3D7_1410600	eukaryotic translation initiation factor 2 subunit gamma, putative	0,615416	0,681793	0,37629	0,412904	0,521601
PF3D7_1116800	heat shock protein 101	0,272023	NaN	1,09646	0,187264	0,518582
PF3D7_0505100	trafficking protein particle complex subunit 8, putative	0,427606	0,516883	0,752749	0,352363	0,5124
PF3D7_0413600	26S protease regulatory subunit 6B, putative	0,535555	0,389205	0,594644	0,521411	0,510204
PF3D7_0903400	ATP-dependent RNA helicase DDX60, putative	0,583038	0,654785	0,579663	0,208378	0,506466
PF3D7_1309700	vacuolar protein sorting-associated protein 18, putative	0,416407	-0,01521	0,798341	0,804753	0,501072
PF3D7_1340600	RNA lariat debranching enzyme, putative	0,663937	0,441909	NaN	0,388034	0,49796
PF3D7_1015900	enolase	0,577924	0,525226	0,419323	0,466516	0,497247
PF3D7_0630300	DNA polymerase epsilon catalytic subunit A, putative	0,618427	0,486469	0,371726	NaN	0,492207
PF3D7_1443600	gamma-tubulin complex component, putative	0,621337	0,444184	0,407407	0,465002	0,484483
PF3D7_0308200	T-complex protein 1 subunit eta	0,203013	0,518639	0,455229	0,759527	0,484102
PF3D7_1461300	40S ribosomal protein S28e, putative	0,524064	0,138775	NaN	0,785651	0,48283
PF3D7_1126000	threonine--tRNA ligase	0,302641	0,580871	0,572987	0,472429	0,482232
PF3D7_0309600	60S acidic ribosomal protein P2	0,276318	0,24542	1,14359	0,253481	0,479702
PF3D7_0826700	receptor for activated c kinase	0,664392	0,567041	0,285698	0,398817	0,478987
PF3D7_0503800	60S ribosomal protein L31	-0,53671	1,38813	0,401303	0,641446	0,473542
PF3D7_1242800	rab specific GDP dissociation inhibitor	0,285106	0,3928	0,735349	NaN	0,471085
PF3D7_1417800	DNA replication licensing factor MCM2	0,556012	0,688846	0,404031	0,221539	0,467607
PF3D7_1329000	DNA-directed RNA polymerase III subunit RPC1, putative	0,415434	-0,06461	1,50635	0,003452	0,465157
PF3D7_1364200	nucleoporin NUP205, putative	0,539928	0,5771	0,492417	0,236673	0,46153
PF3D7_0504000	cation transporting P-ATPase	0,351402	0,434422	0,389236	0,663534	0,459649
PF3D7_1463200	replication factor C subunit 3, putative	0,393306	0,455851	0,161565	0,822529	0,458313
PF3D7_0914900	BSD-domain protein, putative	0,393965	0,302262	0,705226	0,423294	0,456187
PF3D7_0922600	glutamine synthetase, putative	0,644779	0,383831	0,593402	0,192233	0,453561
PF3D7_1132200	T-complex protein 1 subunit alpha	0,415759	0,319208	0,610794	0,428993	0,443689
PF3D7_0708400	heat shock protein 90	0,529371	0,516842	0,497025	0,23121	0,443612
PF3D7_1428300	proliferation-associated protein 2g4, putative	0,385818	0,107959	0,896543	0,383605	0,443481
PF3D7_1238800	acyl-CoA synthetase	0,205893	0,494576	0,559051	0,510478	0,4425
PF3D7_1412400	conserved Plasmodium protein, unknown function	0,7876	0,42492	-0,04986	0,605925	0,442146
PF3D7_1108400	casein kinase 2, alpha subunit	0,479851	0,28773	0,844064	0,144919	0,439141
PF3D7_1443000	serine/threonine protein kinase	0,01407	-0,01293	0,845992	0,905115	0,438063
PF3D7_1303800	conserved Plasmodium protein, unknown function	0,232292	0,332353	1,20914	-0,03125	0,435633
PF3D7_0627500	protein DJ-1	0,242328	1,01704	-0,198	0,643022	0,426098
PF3D7_1238100	calcyclin binding protein, putative	0,393636	0,442301	0,480162	0,38794	0,42601
PF3D7_0202600;PF3D7_0202600	nucleic acid-binding protein, putative	0,386038	0,545319	0,29537	0,475395	0,425531
PF3D7_0509400	RNA polymerase I	0,523763	0,528761	0,244644	0,395815	0,423246
PF3D7_0422200	erythrocyte membrane-associated antigen	0,656817	0,33712	0,539531	0,138807	0,418069
PF3D7_1311900	V-type proton ATPase catalytic subunit A	0,49293	0,509307	0,490878	0,168123	0,41531
PF3D7_1420200	myosin-specific chaperone UNC, putative	0,50782	0,218296	0,515511	NaN	0,413876
PF3D7_1134000	heat shock protein 70	0,359634	0,485842	0,235114	0,55222	0,408203
PF3D7_0513300	purine nucleoside phosphorylase	0,553754	NaN	0,28155	0,38743	0,407578
PF3D7_0609000	nucleoporin NUP637, putative	0,495183	0,44782	0,338339	0,344758	0,406525
PF3D7_0517400	FACT complex subunit SPT16, putative	0,228973	0,389924	0,531569	0,472789	0,405814
PF3D7_0215700	DNA-directed RNA polymerase II subunit RPB2, putative	0,437867	0,426625	0,39846	0,344465	0,401854
PF3D7_0411800	conserved Plasmodium protein, unknown function	0,183455	0,394411	0,641361	0,386167	0,401349
PF3D7_1123400	eukaryotic peptide chain release factor GTP-binding subunit, putative	0,430821	0,602569	0,243913	0,316798	0,398525
PF3D7_1106000	RuvB-like helicase 2	0,125387	0,142099	0,751549	0,572501	0,397884

PF3D7_1015600	heat shock protein 60	0,597889	0,358842	0,256165	0,372132	0,396257
PF3D7_0511800	inositol-3-phosphate synthase	0,359521	0,582901	0,296428	0,330629	0,39237
PF3D7_0708800	heat shock protein 110	0,645056	0,350118	0,423524	0,134049	0,388187
PF3D7_0722400	Obg-like ATPase 1, putative	0,481816	0,348354	0,378068	0,330647	0,384721
PF3D7_0921000	ubiquitin-conjugating enzyme E2, putative	0,545672	0,253103	0,505484	0,233871	0,384533
PF3D7_1017300;PF3D7_1017300	golgi re-assembly stacking protein 1	0,099497	0,269217	0,598175	0,564478	0,382842
PF3D7_0517700	eukaryotic translation initiation factor 3 subunit B, putative	0,328607	0,31919	0,456911	0,423952	0,382165
PF3D7_0801800	mannose-6-phosphate isomerase, putative	0,430821	0,356421	0,299127	0,426296	0,378166
PF3D7_1219600	phospholipid-transporting ATPase 2	0,417056	0,370116	0,469886	0,231125	0,372046
PF3D7_0309500	asparagine synthetase [glutamine-hydrolyzing], putative	0,135666	0,083753	0,501617	0,766357	0,371848
PF3D7_0724700	bromodomain protein 6, putative	0,590722	0,266941	0,225522	0,403256	0,37161
PF3D7_1349200	glutamate--tRNA ligase, putative	0,37362	0,260653	0,486148	0,341025	0,365362
PF3D7_1353600	ER lumen protein retaining receptor	0,116365	0,418928	0,557386	NaN	0,364226
PF3D7_1434500	dynein-related AAA-type ATPase, putative	0,435522	0,183277	0,697329	0,139474	0,363901
PF3D7_0310500	ATP-dependent RNA helicase DHX57, putative	0,398131	0,314984	0,486457	0,243916	0,360872
PF3D7_0320300	T-complex protein 1 subunit epsilon	0,461529	0,376901	0,080931	0,521018	0,360095
PF3D7_1223500	conserved Plasmodium protein, unknown function	0,478195	0,454961	0,314755	0,182131	0,357511
PF3D7_1115300;PF3D7_1115700	cysteine proteinase falcipain 2b	0,53963	0,31493	0,509949	0,064043	0,357138
PF3D7_0932800	importin alpha re-exporter, putative	0,11703	0,333098	0,617863	NaN	0,355997
PF3D7_0517000	60S ribosomal protein L12, putative	0,545968	0,325539	0,565792	-0,01977	0,354381
PF3D7_1445100	histidine--tRNA ligase, putative	0,179256	0,721944	0,155102	NaN	0,352101
PF3D7_1347500	DNA/RNA-binding protein Alba 4	0,139731	0,225042	0,690641	0,348703	0,351029
PF3D7_0728000	eukaryotic translation initiation factor 2 subunit alpha	0,36042	0,222111	0,45249	0,364534	0,349889
PF3D7_1124600	ethanolamine kinase	0,378845	0,098552	NaN	0,57025	0,349216
PF3D7_0802000	glutamate dehydrogenase, putative	0,352194	0,293041	0,329526	0,406885	0,345412
PF3D7_1211200	conserved Plasmodium protein, unknown function	0,538141	0,555884	0,07738	0,206179	0,344396
PF3D7_1349500	conserved Plasmodium protein, unknown function	0,257373	0,449454	0,543298	0,115894	0,341505
PF3D7_0629200	DnaJ protein, putative	0,265677	0,407631	0,36233	0,32896	0,34115
PF3D7_0317000	proteasome subunit alpha type-3, putative	-0,23336	0,294862	0,944784	0,35716	0,340861
PF3D7_1008700	tubulin beta chain	0,13014	0,492018	0,376513	0,363846	0,340629
PF3D7_1433500	DNA topoisomerase 2	0,486457	0,436217	0,223175	0,215613	0,340366
PF3D7_0309000	dual specificity protein phosphatase	0,385928	0,159219	0,317999	0,462316	0,331366
PF3D7_1345800	conserved Plasmodium protein, unknown function	0,679063	0,058683	0,443182	0,140078	0,330252
PF3D7_0401800	Plasmodium exported protein (PHISTb), unknown function	0,094642	0,362918	0,380619	0,47696	0,328785
PF3D7_1130400	26S protease regulatory subunit 6A, putative	0,123401	0,302902	0,69537	0,179123	0,325199
PF3D7_1432100	voltage-dependent anion-selective channel protein, putative	NaN	0,45504	0,093695	0,42254	0,323758
PF3D7_1306400	26S protease regulatory subunit 10B, putative	0,394843	0,197021	0,407081	0,291433	0,322595
PF3D7_1130200	60S ribosomal protein P0	0,340961	0,293094	0,476537	0,176577	0,321792
PF3D7_1213800	proline--tRNA ligase	0,232047	0,221909	0,342669	0,482331	0,319739
PF3D7_1248900	26S protease regulatory subunit 8, putative	0,277866	0,297626	0,423417	0,276765	0,318919
PF3D7_0922500	phosphoglycerate kinase	0,254836	0,368179	0,338909	0,312814	0,318685
PF3D7_1115400	cysteine proteinase falcipain 3	0,04712	0,433584	0,348346	0,445657	0,318677
PF3D7_0625800	conserved Plasmodium protein, unknown function	0,267116	0,609905	0,063227	NaN	0,313416
PF3D7_0629100	nicotinate phosphoribosyltransferase, putative	0,431676	0,2994	0,182184	0,340222	0,313371
PF3D7_0214100	protein transport protein SEC31	0,172616	0,011835	0,595504	0,46949	0,312361
PF3D7_0909900	helicase SKI2W, putative	0,443394	0,136585	0,349252	NaN	0,309744
PF3D7_0922800	conserved Plasmodium protein, unknown function	0,296545	0,417695	0,080658	0,435905	0,307701
PF3D7_1227800	elongator complex protein 3, putative	0,141564	0,38879	0,386149	0,313925	0,307607
PF3D7_0829000	conserved Plasmodium membrane protein, unknown function	0,305445	0,318398	0,34153	0,264946	0,30758
PF3D7_1233900	sentrin-specific protease 1	NaN	-0,36536	1,32941	-0,04628	0,305924
PF3D7_1124900	60S ribosomal protein L35, putative	-0,29947	0,672888	-0,84272	1,68158	0,303069
PF3D7_1437900	HSP40, subfamily A	0,33308	0,440087	0,077106	0,358269	0,302136
PF3D7_1116100	serine esterase, putative	0,015069	0,243387	NaN	0,645548	0,301335
PF3D7_0212300	eukaryotic peptide chain release factor subunit 1, putative	0,18954	0,253292	0,59388	0,16372	0,300108
PF3D7_1134800	coatomer subunit delta	0,030265	0,18061	0,337654	0,647422	0,298988
PF3D7_0611600	basal complex transmembrane protein 1	0,186627	0,180626	0,687329	0,137806	0,298097
PF3D7_1218200	symplekin domain-containing protein, putative	0,312433	0,211314	0,369048	NaN	0,297598
PF3D7_1437200	ribonucleoside-diphosphate reductase large subunit, putative	0,297133	0,156386	0,50853	0,223323	0,296343
PF3D7_0932300	M18 aspartyl aminopeptidase	0,302407	0,056431	0,732486	0,089175	0,295125
PF3D7_1356100	conserved Plasmodium protein, unknown function	0,18916	0,287395	NaN	0,404172	0,293576
PF3D7_0716800	eukaryotic translation initiation factor 3 subunit I, putative	0,202136	0,293748	0,379843	NaN	0,291909
PF3D7_0206700	adenylosuccinate lyase	0,201508	0,142783	0,527571	NaN	0,290621
PF3D7_1346400	VPS13 domain-containing protein, putative	0,308594	0,302529	0,239642	0,306787	0,289388
PF3D7_0406100	V-type proton ATPase subunit B	0,295018	0,118649	0,345964	0,384245	0,285969
PF3D7_1304500	small heat shock protein, putative	0,38084	0,327385	0,172487	0,259806	0,28513
PF3D7_0821600	polyribonucleotide 5-hydroxyl-kinase Clp1, putative	0,565012	-0,287	NaN	0,572844	0,283619
PF3D7_1013900	translation initiation factor eIF-2B subunit delta, putative	0,216858	0,386223	0,248292	0,281877	0,283313
PF3D7_1308300	40S ribosomal protein S27	0,255078	0,177376	0,367707	0,315325	0,278872
PF3D7_0509800	phosphatidylinositol 4-kinase beta	0,165558	0,338196	0,219958	0,385394	0,277277
PF3D7_1311500	26S protease regulatory subunit 7, putative	0,348459	0,175273	0,276199	0,308019	0,276988
PF3D7_1203700	nucleosome assembly protein	0,224411	0,205197	0,347892	0,326914	0,276104
PF3D7_0322700	conserved Plasmodium protein, unknown function	-0,17596	0,490882	NaN	0,494638	0,269854
PF3D7_1020900	ADP-ribosylation factor 1	0,154065	0,185687	0,368936	0,365593	0,26857
PF3D7_1130100	60S ribosomal protein L38	0,053111	-0,14796	-0,36114	1,52899	0,268251
PF3D7_1426800	conserved Plasmodium protein, unknown function	0,145743	0,352308	0,051442	0,518784	0,267069
PF3D7_0727400	proteasome subunit alpha type-5, putative	0,378623	0,155422	0,324695	0,208494	0,266809
PF3D7_1412500	actin II	0,435522	0,155743	0,281431	0,193387	0,266521
PF3D7_0613600	conserved Plasmodium protein, unknown function	0,276318	0,623398	-0,1088	NaN	0,263639
PF3D7_0525000	zinc finger protein, putative	0,221939	-0,05339	0,746571	0,135174	0,262574
PF3D7_1302800	40S ribosomal protein S7, putative	0,287945	0,179939	0,126312	0,453103	0,261825
PF3D7_1439000	copper transporter	0,389016	-0,04474	0,433921	NaN	0,259398
PF3D7_0217600	conserved Plasmodium protein, unknown function	0,115166	0,195137	1,1165	-0,39517	0,257908
PF3D7_1361100	protein transport protein Sec24A	0,352646	0,250663	0,152638	0,27528	0,257807
PF3D7_0507800	conserved protein, unknown function	0,125916	0,143166	0,326767	0,433078	0,257232
PF3D7_0418300	conserved Plasmodium protein, unknown function	0,194717	0,022229	0,32008	0,491125	0,257038
PF3D7_0628300	choline/ethanolaminephosphotransferase, putative	0,095317	0,271374	0,261471	0,389017	0,254295
PF3D7_1247500	serine/threonine protein kinase, putative	0,007195	0,655558	NaN	0,087365	0,25004
PF3D7_1441400	FACT complex subunit SSRP1, putative	0,041243	0,241799	0,583134	0,13065	0,249207
PF3D7_1135900	3-oxo-5-alpha-steroid 4-dehydrogenase, putative	0,213503	0,288435	0,258579	0,236011	0,249132
PF3D7_1470900	proteasome subunit beta type-2, putative	-0,00248	0,004523	0,736821	NaN	0,246287
PF3D7_0707200	conserved Plasmodium protein, unknown function	0,02772	0,153029	0,525969	0,274128	0,245212
PF3D7_1367600	ribosome biogenesis protein MRT4, putative	0,019204	0,260912	0,065434	0,635136	0,245172
PF3D7_0212400	conserved Plasmodium membrane protein, unknown function	0,154583	0,103457	0,719052	0,001675	0,244692
PF3D7_1421000	DIX domain-containing protein, putative	0,10608	-0,09261	0,813935	0,147969	0,243843
PF3D7_1443400	WD repeat-containing protein	0,52667	0,346445	0,278461	-0,17875	0,243208
PF3D7_0903700;PF3D7_0422300	alpha tubulin 1	0,201634	0,156402	0,294547	0,3191	0,242921
PF3D7_0903200	ras-related protein RAB7	0,256286	0,230872	0,295958	0,181035	0,241038
PF3D7_1368900	conserved protein, unknown function	0,098285	-0,06198	0,685716	NaN	0,240672
PF3D7_1231100	ras-related protein Rab-2	0,216982	0,166049	0,441271	0,137172	0,240369
PF3D7_1468700	eukaryotic initiation factor 4A	0,143655	0,155084	0,322159	0,334935	0,238958
PF3D7_1108700	heat shock protein J2	0,088277	0,423816	0,16954	0,271931	0,238391
PF3D7_0303500	spindle pole body protein, putative	0,398898	0,441772	0,017494	0,090849	0,237253
PF3D7_0626800	pyruvate kinase	0,188021	0,202871	0,267955	0,288734	0,236895
PF3D7_0519400	40S ribosomal protein S24	0,269751	0,128724	0,221939	0,325268	0,236421
PF3D7_1407800	plasmepsin IV	0,182565	0,128314	0,471552	0,160831	0,235816
PF3D7_1213900	W2 domain-containing protein, putative	0,378512	0,110371	0,1153	0,337995	0,235545
PF3D7_0719900	conserved Plasmodium membrane protein, unknown function	0,275484	0,25515	0,203514	0,202505	0,234163
PF3D7_1102400	phosphopantothenate--cysteine ligase, putative	0,260146	0,148081	0,418568	0,107555	0,233588
PF3D7_0933200	calcyclin-binding protein, putative	0,234256	0,028705	0,397803	0,265345	0,231527
PF3D7_0918900	gamma-glutamylcysteine synthetase	0,36614	0,235892	0,293724	0,026058	0,230454
PF3D7_0929000	transcription initiation factor TFIID subunit 7, putative	0,199123	0,26866	0,023326	0,426839	0,229487
PF3D7_1459600	AP-4 complex accessory subunit Tepsin, putative	0,189287	0,21677	0,155879	0,354907	0,229211
PF3D7_1328300	conserved protein, unknown function	0,179893	0,134382	NaN	0,372561	0,228945
PF3D7_0628600	DNA methyltransferase 1-associated protein 1, putative	0,518032	NaN	-0,07707	0,238834	0,226598
PF3D7_0211800	asparagine--tRNA ligase	0,168385	0,393975	NaN	0,115816	0,226059
PF3D7_1442900	Sec7 domain-containing protein ARFGEF, putative	0,365133	0,223374	0,235972	0,07391	0,224597
PF3D7_0322900	40S ribosomal protein S3A, putative	-0,03922	0,145972	0,460795	0,327493	0,22376
PF3D7_1409400	conserved protein, unknown function	0,230941	0,264755	0,294782	0,100778	0,222814
PF3D7_0821000	conserved Plasmodium protein, unknown function	0,407516	0,705547	-0,25193	0,028631	0,22244
PF3D7_1137300	CLPTM1 domain-containing protein, putative	0,380397	0,126124	0,172616	0,204649	0,220947
PF3D7_1211400	heat shock protein DNAJ homologue Pfj4	0,298776	0,40154	0,107286	0,071436	0,21976
PF3D7_0501900	trafficking protein particle complex subunit 13, putative	-0,20616	-0,59913	NaN	1,46045	0,218387

Appendix 8 – DiQ-BioID of AP-4

Majority protein IDs	gene_product	Ratio H/L normalized cterm_F	Ratio H/L normalized cterm_R	Ratio H/L normalized nterm_F	Ratio H/L normalized nterm_R	AVERAGE
PF3D7_1247400	peptidyl-prolyl cis-trans isomerase FKBP35	5,61777	5,4885	4,05242	3,78635	4,73626
PF3D7_0904100	AP-4 complex subunit epsilon, putative	4,31041	4,17895	4,93701	4,85058	4,569238
PF3D7_0408100	conserved Plasmodium protein, unknown function	4,8388	4,27475	3,80395	4,82235	4,434963
PF3D7_1219100	clathrin heavy chain, putative	2,79473	2,73159	3,32582	3,18141	3,008388
PF3D7_1119500	AP-4 complex subunit mu, putative	1,64496	2,63828	3,76871	3,95937	3,00283
PF3D7_1459600	AP-4 complex accessory subunit Tepsin, putative	2,48646	2,47057	3,51816	3,35977	2,95874
PF3D7_1205400	kelch domain-containing protein, putative	2,54863	2,32981	3,15515	2,29011	2,580925
PF3D7_0730200	AP-4 complex subunit beta, putative	1,74257	3,13416	2,78706	2,62193	2,57143
PF3D7_0904900	copper-transporting ATPase	2,08929	2,11766	2,79645	2,83393	2,459333
PF3D7_0715900	cation diffusion facilitator family protein, putative	2,39665	1,90401	3,04296	2,44473	2,447088
PF3D7_1435500	clathrin light chain, putative	1,68661	1,93088	2,53067	2,49924	2,16185
PF3D7_1236000	vesicle transport v-SNARE protein VTI1, putative	2,03759	2,2346	1,8979	2,182	2,088023
PF3D7_0815500	conserved Plasmodium protein, unknown function	NaN	2,09105	1,6931	2,11397	1,96604
PF3D7_1432800	HP12 protein homolog, putative	1,86754	1,75575	1,9923	2,05026	1,916463
PF3D7_0929300	conserved Plasmodium protein, unknown function	3,02768	NaN	1,79705	0,675927	1,833552
PF3D7_0419500	conserved Plasmodium membrane protein, unknown function	1,72744	1,71478	1,62396	2,17293	1,809778
PF3D7_1365700	SNARE associated Golgi protein, putative	1,59703	1,61096	NaN	1,95445	1,720813
PF3D7_0915400	ATP-dependent 6-phosphofructokinase	0,689568	0,482674	2,80016	2,68205	1,663613
PF3D7_0412000	LITAF-like zinc finger protein, putative	1,65274	1,5569	NaN	1,74077	1,650137
PF3D7_0305200	GRIP domain-containing protein, putative	1,16215	1,49289	1,87259	1,86939	1,599255
PF3D7_0920800	inosine-5-monophosphate dehydrogenase	1,26364	1,41396	1,771	1,74739	1,548998
PF3D7_1132400	conserved Plasmodium membrane protein, unknown function	1,45307	1,14407	1,64007	1,85095	1,52204
PF3D7_0721200	conserved Plasmodium protein, unknown function	1,70995	1,3128	1,64044	1,14784	1,452758
PF3D7_0804900	GTPase-activating protein, putative	1,33199	1,21722	1,62415	1,58044	1,43845
PF3D7_0503500	protein kinase, putative	1,12002	1,38071	1,41808	1,73015	1,41224
PF3D7_1453700	HSP90 co-chaperone p23	1,73414	1,70129	1,18688	0,93093	1,38831
PF3D7_1147300	conserved Plasmodium protein, unknown function	0,941933	0,962913	1,51602	1,90552	1,331597
PF3D7_0806800	V-type proton ATPase subunit a, putative	1,37901	1,43538	1,07224	1,33676	1,305848
PF3D7_1026800	40S ribosomal protein S2	1,16034	0,889289	1,39961	1,56563	1,253717
PF3D7_1332000	syntaxin, Qa-SNARE family	1,00267	1,10917	1,41808	1,47674	1,251665
PF3D7_1008900	adenylate kinase	1,19182	1,0391	1,15743	1,49574	1,221023
PF3D7_1247500	serine/threonine protein kinase, putative	1,09112	1,23097	1,23186	1,32272	1,219168
PF3D7_0609300	conserved Plasmodium protein, unknown function	1,28605	0,765572	1,12757	1,68534	1,216133
PF3D7_0813200	CS domain protein, putative	1,26291	1,10644	1,19169	1,22901	1,197513
PF3D7_1427600	CorA-like Mg2+ transporter protein, putative	1,07087	1,04287	1,48109	1,12664	1,180368
PF3D7_0523400	DnaJ protein, putative	1,13842	1,42504	0,866235	1,24458	1,168569
PF3D7_1332900	isoleucine--tRNA ligase, putative	1,1375	1,11026	1,24647	1,14379	1,159505
PF3D7_1336900	tryptophan--tRNA ligase	0,734135	0,624777	2,21114	1,0463	1,154088
PF3D7_1455500	AP-1 complex subunit gamma, putative	1,13179	0,902039	1,20006	1,32637	1,140065
PF3D7_1104300	conserved Plasmodium protein, unknown function	1,07957	1,09425	1,19402	1,18361	1,137863
PF3D7_0525100	acyl-CoA synthetase	1,19698	1,35997	0,908813	1,06172	1,131871
PF3D7_1112500	RNA transcription, translation and transport factor protein, putative	1,22151	1,08519	1,18884	1,028	1,130885
PF3D7_1421000	DIX domain-containing protein, putative	0,733875	0,606847	1,65673	1,50022	1,124418
PF3D7_1336800	nuclear movement protein, putative	1,1753	0,831769	1,3151	1,11095	1,10828
PF3D7_1017000	DNA polymerase delta catalytic subunit	1,20683	0,770289	1,26808	1,13866	1,095965
PF3D7_1127600	CRAL/TRIO domain-containing protein, putative	0,88495	0,964798	1,12367	1,37692	1,087585
PF3D7_1466100	protein phosphatase containing kelch-like domains	0,991318	1,03274	1,42771	0,8851	1,084217
PF3D7_1211300	DNA helicase MCM8, putative	0,746915	1,20506	1,12697	1,23715	1,079024
PF3D7_0216400	vacuolar protein sorting-associated protein 45	0,6291	1,69367	1,25042	0,739709	1,078225
PF3D7_1104100	syntaxin, Qa-SNARE family	0,797096	1,05526	1,27316	1,14995	1,068867
PF3D7_1408700	conserved protein, unknown function	1,00899	0,839106	1,23156	1,17811	1,064442
PF3D7_1034900	methionine--tRNA ligase	1,04264	1,20397	0,999423	1,00494	1,062743
PF3D7_1223700	vacuolar iron transporter	-0,58929	1,44674	1,43552	1,94375	1,05918
PF3D7_1210100	syntaxin, Qa-SNARE family	1,14971	1,0122	0,736735	1,31973	1,054594
PF3D7_1017300;PF3D7_1017300	golgi re-assembly stacking protein 1	0,966209	0,886913	1,15698	1,1755	1,046401
PF3D7_0926700	glutamine-dependent NAD(+) synthetase, putative	0,921208	0,66534	1,32372	1,26119	1,042865
PF3D7_1464700	ATP synthase (C/AC39) subunit, putative	0,908121	1,66315	1,72923	-0,19131	1,027298
PF3D7_1452600	conserved Plasmodium protein, unknown function	0,863939	NaN	1,24677	0,952462	1,021057
PF3D7_0314700	RING finger protein RNF1	1,17581	1,03428	0,941782	0,782943	0,983704
PF3D7_1461900	valine--tRNA ligase, putative	0,844948	0,820667	1,1279	1,1224	0,978979
PF3D7_0617100	AP-2 complex subunit alpha, putative	NaN	1,27327	1,52937	0,114113	0,972251
PF3D7_1454200	conserved Plasmodium protein, unknown function	1,143	0,805131	1,06833	0,858907	0,968842
PF3D7_1019600	conserved Plasmodium protein, unknown function	0,848398	1,16114	1,20495	0,625066	0,959889
PF3D7_1411300	DnaJ protein, putative	0,688136	0,495675	1,41922	1,23331	0,959085
PF3D7_0612100	eukaryotic translation initiation factor 3 subunit L, putative	1,20927	0,953439	0,560617	1,06398	0,946827
PF3D7_0615900	protein phosphatase, putative	0,951662	NaN	0,732747	1,14194	0,942116
PF3D7_0215400	conserved Plasmodium protein, unknown function	1,11083	1,17361	0,505688	0,901985	0,923028
PF3D7_0411800	conserved Plasmodium protein, unknown function	0,924252	0,67275	1,0005	1,05748	0,913746
PF3D7_1355100	DNA replication licensing factor MCM6	0,916324	0,968181	0,872789	0,890145	0,91186
PF3D7_0704400	phosphoinositide-binding protein, putative	0,864176	0,877075	0,893595	0,892285	0,881783
PF3D7_0914900	BSD-domain protein, putative	0,775935	0,754626	1,0767	0,822019	0,85732
PF3D7_1111700	conserved Plasmodium protein, unknown function	1,0059	0,877871	0,761626	0,752413	0,849453
PF3D7_1410300	WD repeat-containing protein, putative	1,00971	0,601628	1,04404	0,684944	0,835081
PF3D7_0803400	DNA repair and recombination protein RAD54, putative	0,624709	0,801732	0,632734	1,2746	0,833444
PF3D7_1465100	conserved oligomeric Golgi complex subunit 6, putative	0,998773	0,976503	0,837217	0,505451	0,829486
PF3D7_1318800	translocation protein SEC63, putative	0,924024	0,758379	0,831958	0,790285	0,826162
PF3D7_1239700	ATP-dependent zinc metalloprotease FTSH 1	0,203514	2,012	0,256165	NaN	0,823893
PF3D7_0624000	hexokinase	0,740539	0,642865	0,989139	0,904953	0,819374
PF3D7_0416900	conserved Plasmodium protein, unknown function	1,10715	0,929363	0,696706	0,531114	0,816083
PF3D7_1331700	glutamine--tRNA ligase, putative	0,699285	0,912836	0,90327	0,734011	0,812351
PF3D7_0202600;PF3D7_0202600	nucleic acid-binding protein, putative	0,671927	0,72423	0,993276	0,850533	0,809992
PF3D7_0812100	proteasome activator complex subunit 4, putative	0,849999	0,591375	0,862828	0,931315	0,808879
PF3D7_1034000	Sec1 family protein, putative	0,545573	1,0068	1,09167	0,574498	0,804635
PF3D7_1462100	conserved Plasmodium protein, unknown function	0,735955	0,821304	0,770956	0,881056	0,802318
PF3D7_0505100	trafficking protein particle complex subunit 8, putative	0,768333	0,711464	0,903193	0,81165	0,79866
PF3D7_0308000	DNA polymerase delta small subunit, putative	0,582652	0,802588	0,662114	1,12548	0,793209
PF3D7_0511300	MORN repeat protein, putative	1,04865	0,572201	0,613154	0,917543	0,787887
PF3D7_1311400	AP-1 complex subunit mu-1	0,654985	1,03733	0,791689	0,656581	0,785146
PF3D7_0219600	replication factor C subunit 1	0,893751	0,981508	0,664847	0,594225	0,783583
PF3D7_0626000	conserved Plasmodium protein, unknown function	0,783499	0,512658	NaN	1,03481	0,776989
PF3D7_0820500	protein transport protein YIF1, putative	0,826925	0,78339	0,921208	0,553723	0,771312
PF3D7_1410600	eukaryotic translation initiation factor 2 subunit gamma, putative	0,913339	0,723039	0,71308	0,663374	0,753208
PF3D7_1368800	DNA repair endonuclease XPF, putative	0,048934	0,469749	1,72351	NaN	0,747398
PF3D7_0526200	ADP-ribosylation factor GTPase-activating protein 2	0,402504	0,649797	0,919988	0,982192	0,73862
PF3D7_0922600	glutamine synthetase, putative	0,718263	0,783613	0,715718	0,726377	0,735993
PF3D7_0809900	JmjC domain-containing protein 1, putative	0,774924	0,949171	0,590051	0,618008	0,733039
PF3D7_1205900	conserved protein, unknown function	0,599413	0,946166	0,413052	0,966996	0,731407
PF3D7_0530100	SNARE protein, putative	0,805292	0,599965	0,698663	0,805585	0,727376
PF3D7_0209100	patatin-like phospholipase 1	0,689925	0,693528	0,661658	0,814311	0,714856
PF3D7_1218600	arginine--tRNA ligase	0,970117	0,207261	1,00741	0,672727	0,714379
PF3D7_0931000	elongation factor Tu, putative	0,788017	0,95534	0,394185	NaN	0,712514
PF3D7_1104000	phenylalanine--tRNA ligase beta subunit	0,764856	0,789661	0,718789	0,569865	0,710793
PF3D7_0514200	conserved Plasmodium protein, unknown function	0,795019	0,969113	0,363451	0,714089	0,710418
PF3D7_0829000	conserved Plasmodium membrane protein, unknown function	0,685985	0,513996	0,811389	0,809625	0,705249
PF3D7_0501900	trafficking protein particle complex subunit 13, putative	0,533264	0,596951	0,562768	1,10976	0,700686
PF3D7_1368200	ABC transporter E family member 1, putative	0,604071	0,751878	0,787182	0,651768	0,698725
PF3D7_1238100	calcyclin binding protein, putative	0,748719	0,635652	0,780898	0,618096	0,695841
PF3D7_0305300	transporter, putative	0,637471	0,591766	0,460166	1,08985	0,694813
PF3D7_0903400	ATP-dependent RNA helicase DDX60, putative	0,523161	0,694485	0,791522	0,746035	0,688801
PF3D7_0826700	receptor for activated c kinase	0,516015	0,670681	0,635337	0,8044	0,656608
PF3D7_1016200	Rab3 GTPase-activating protein non-catalytic subunit, putative	0,134221	0,12562	1,05255	1,24475	0,639285
PF3D7_1238800	acyl-CoA synthetase	0,578794	0,531323	0,643856	0,767266	0,63031

PF3D7_1451800	sortilin	0,546561	0,680359	0,682304	0,609464	0,629672
PF3D7_0622800	leucine--tRNA ligase, putative	0,479231	0,539645	0,442652	1,05014	0,627917
PF3D7_0308600	pre-mRNA-processing factor 19, putative	NaN	0,381705	1,06267	0,438972	0,627782
PF3D7_0625800	conserved Plasmodium protein, unknown function	0,425996	0,764714	0,834549	0,474412	0,624918
PF3D7_1134700	DNA-directed RNA polymerase I subunit RPA2, putative	0,659011	0,49354	0,606442	0,730225	0,622305
PF3D7_0414000	structural maintenance of chromosomes protein 3	0,564427	1,16152	0,391108	0,369278	0,621583
PF3D7_1350100	lysine--tRNA ligase	0,61155	0,448824	0,796266	0,618694	0,618834
PF3D7_0524400	ribosome-interacting GTPase 1, putative	1,081	0,630461	0,263876	0,483702	0,61476
PF3D7_1349200	glutamate--tRNA ligase, putative	0,521955	0,5771	0,642933	0,716457	0,614611
PF3D7_0511800	inositol-3-phosphate synthase	0,543199	0,578133	0,679874	0,654649	0,613964
PF3D7_1432000	syntaxin, Qa-SNARE family	0,682304	0,523359	0,679874	0,555418	0,610239
PF3D7_1218500	dynamin-like protein, putative	0,776104	0,161605	0,90666	0,594596	0,609741
PF3D7_1335700	conserved oligomeric Golgi complex subunit 3, putative	0,516015	0,592615	0,593497	0,708114	0,60256
PF3D7_0922400	para-aminobenzoic acid synthetase	0,449958	0,276677	1,05262	0,615375	0,598658
PF3D7_0831700	heat shock protein 70	0,547055	0,810764	0,472904	0,556521	0,596811
PF3D7_1340600	RNA lariat debranching enzyme, putative	0,492212	0,581454	0,727354	0,580742	0,595441
PF3D7_1028400	ribosome biogenesis protein RPF2, putative	NaN	1,94608	-0,28969	0,127415	0,594603
PF3D7_1013100	U3 small nucleolar RNA-associated protein 13, putative	1,11537	0,784707	0,381948	0,084747	0,591693
PF3D7_0703000	conserved Plasmodium protein, unknown function	0,595408	0,530823	0,640991	0,577724	0,586237
PF3D7_1420400	glycine--tRNA ligase	1,02432	0,488289	0,256165	0,574541	0,585829
PF3D7_1451400	transcriptional regulatory protein sir2b	0,547055	0,349824	0,727964	0,706771	0,582904
PF3D7_1128500	Fe-S cluster assembly factor HCF101, putative	NaN	0,85964	0,394295	0,490679	0,581538
PF3D7_1364200	nucleoporin NUP205, putative	0,406428	0,495105	0,691355	0,722777	0,578916
PF3D7_1433500	DNA topoisomerase 2	0,440952	0,6173	0,482022	0,769035	0,577327
PF3D7_0616800	malate:quinone oxidoreductase	0,584	0,570807	0,435629	0,703079	0,573379
PF3D7_1242800	rab specific GDP dissociation inhibitor	0,493237	0,703384	0,732139	0,359287	0,572012
PF3D7_1417800	DNA replication licensing factor MCM2	0,582074	0,472669	0,642378	0,590354	0,571869
PF3D7_0303000	N-ethylmaleimide-sensitive fusion protein	0,623399	0,568644	0,59703	0,496997	0,571518
PF3D7_1344800	aspartate carbamoyltransferase	0,010064	0,737567	0,604736	0,927002	0,569842
PF3D7_0934100	TFIIH basal transcription factor complex helicase XPD subunit	0,247806	0,573832	0,62882	0,816698	0,566789
PF3D7_1230000	TBC domain-containing protein, putative	0,522156	0,683947	0,39846	0,654717	0,56482
PF3D7_0933500	gamma-tubulin complex component, putative	0,387252	0,79001	0,603692	0,477201	0,564539
PF3D7_0705300	origin recognition complex subunit 2	0,118758	0,31276	0,282499	1,5438	0,564454
PF3D7_0617000	mitochondrial import receptor subunit TOM40, putative	0,582363	0,190915	0,05797	1,36877	0,550005
PF3D7_1107400	DNA repair protein RAD51	0,635522	0,190618	1,0504	0,311435	0,546994
PF3D7_0630300	DNA polymerase epsilon catalytic subunit A, putative	0,59579	0,57962	0,585347	0,423352	0,546027
PF3D7_0722400	Obg-like ATPase 1, putative	0,50457	0,415268	0,671203	0,569501	0,540136
PF3D7_0801800	mannose-6-phosphate isomerase, putative	0,512176	0,313119	0,661294	0,672979	0,539892
PF3D7_1345800	conserved Plasmodium protein, unknown function	0,460481	0,336737	0,617204	0,743497	0,53948
PF3D7_0717700	serine--tRNA ligase, putative	0,334568	0,558134	0,762902	0,497812	0,538354
PF3D7_1307700	TOM1-like protein, putative	0,491391	0,43298	0,682304	0,543846	0,53763
PF3D7_0615800	conserved oligomeric Golgi complex subunit 4, putative	-0,47229	0,713923	1,36983	NaN	0,537155
PF3D7_1002700	conserved Plasmodium protein, unknown function	0,598365	0,446797	0,419215	0,665821	0,53255
PF3D7_0813000	protein KIC7	1,71334	-0,03605	0,014355	0,434344	0,531498
PF3D7_1029600	adenosine deaminase	0,121944	0,497812	0,722553	0,780835	0,530786
PF3D7_0509400	RNA polymerase I	0,462052	0,500442	0,652785	0,506742	0,530505
PF3D7_0619500	acyl-CoA synthetase	1,04383	-0,19055	0,697685	0,56339	0,528588
PF3D7_0608900	conserved Plasmodium protein, unknown function	0,260146	0,252724	0,284988	1,31136	0,527305
PF3D7_0405100	protein transport protein Sec24B, putative	0,331247	0,178861	1,23818	0,356624	0,526228
PF3D7_1308000	conserved Plasmodium membrane protein, unknown function	NaN	0,644375	0,664483	0,269147	0,526002
PF3D7_0320100	protein transport protein SEC22	0,212009	0,59586	0,618896	0,67229	0,524764
PF3D7_1445100	histidine--tRNA ligase, putative	0,454176	0,618495	0,326882	0,685965	0,52138
PF3D7_1126000	threonine--tRNA ligase	0,475915	0,563518	0,547746	0,494902	0,52052
PF3D7_1412400	conserved Plasmodium protein, unknown function	0,394404	0,589615	0,490467	0,606167	0,520163
PF3D7_1313800	conserved Plasmodium membrane protein, unknown function	0,009491	0,813094	0,621055	0,6348	0,51961
PF3D7_1108400	casein kinase 2, alpha subunit	0,550211	0,362473	0,656908	0,500667	0,517565
PF3D7_1118300	insulinase, putative	0,566377	0,363884	0,556601	0,568067	0,513732
PF3D7_1453800	glucose-6-phosphate dehydrogenase-6-phosphogluconolactonase	0,327687	0,406675	0,477263	0,837893	0,51238
PF3D7_0314100;PF3D7_0314100	vesicle transport v-SNARE protein, putative	0,699196	0,355535	0,266277	0,722801	0,510952
PF3D7_1471400	diacylglycerol kinase, putative	1,06523	0,591592	1,02645	-0,64828	0,508748
PF3D7_1034500	armadillo repeat protein, putative	0,452806	0,59778	0,49211	0,489646	0,508086
PF3D7_1355300	histone-lysine N-methyltransferase, putative	0,476641	0,858384	0,378845	0,318254	0,508031
PF3D7_1443400	WD repeat-containing protein	0,536252	0,748408	0,231555	0,505267	0,505371
PF3D7_0922500	phosphoglycerate kinase	0,440846	0,293306	0,663208	0,611182	0,502136
PF3D7_0708400	heat shock protein 90	0,581207	0,399007	0,512176	0,494983	0,496843
PF3D7_1349500	conserved Plasmodium protein, unknown function	0,697863	0,388658	0,435629	0,464246	0,496599
PF3D7_0821000	conserved Plasmodium protein, unknown function	0,479955	0,404286	0,624896	0,47309	0,495557
PF3D7_0405400	pre-mRNA-processing-splicing factor 8, putative	0,506805	0,430178	0,511974	0,525995	0,493738
PF3D7_1360800	falcilysin	0,47633	0,582836	0,419862	0,490902	0,492483
PF3D7_0824800	conserved Plasmodium membrane protein, unknown function	0,564037	1,3599	-0,22305	0,26479	0,491418
PF3D7_1441600	acid cluster protein 33 homologue, putative	0,410233	0,484631	0,657091	0,41227	0,491056
PF3D7_0413600	26S protease regulatory subunit 6B, putative	0,658828	0,616193	0,35095	0,326661	0,488158
PF3D7_0630500	ribosome biogenesis protein YTM1, putative	0,481092	0,449178	0,52687	NaN	0,485713
PF3D7_1012400	hypoxanthine-guanine phosphoribosyltransferase	0,295488	0,137584	0,776609	0,725136	0,483704
PF3D7_0626800	pyruvate kinase	0,470198	0,308662	0,60046	0,520645	0,474991
PF3D7_0528100	AP-1/2 complex subunit beta, putative	0,359634	0,68022	NaN	0,381254	0,473703
PF3D7_1356100	conserved Plasmodium protein, unknown function	0,409472	0,427072	0,406863	0,646428	0,472459
PF3D7_0728000	eukaryotic translation initiation factor 2 subunit alpha	0,545968	0,561303	0,422341	0,359398	0,472253
PF3D7_1405800	ribosome biogenesis protein BOP1, putative	0,176578	0,217776	NaN	1,01967	0,471341
PF3D7_1451000	conserved Plasmodium protein, unknown function	0,460166	0,454071	0,523963	0,446345	0,471136
PF3D7_1311900	V-type proton ATPase catalytic subunit A	0,532467	0,500585	0,382169	0,461343	0,469141
PF3D7_1223500	conserved Plasmodium protein, unknown function	0,415434	0,581087	0,333767	0,541828	0,468029
PF3D7_1408400	FANCJ-like helicase, putative	0,377957	0,299525	0,579663	0,603271	0,465104
PF3D7_1223400	phospholipid-transporting ATPase, putative	0,529071	0,345858	0,354678	0,62765	0,464314
PF3D7_1132200	T-complex protein 1 subunit alpha	0,54893	0,38116	0,482952	0,442889	0,463983
PF3D7_1117300	conserved protein, unknown function	0,122739	0,535123	NaN	0,730799	0,462887
PF3D7_1346400	VPS13 domain-containing protein, putative	0,491186	0,43014	0,47228	0,455297	0,462226
PF3D7_1442900	Sec7 domain-containing protein ARFGEF, putative	0,671837	0,444262	0,35208	0,378288	0,461617
PF3D7_0803700	tubulin gamma chain	0,776946	0,229518	0,183201	0,654013	0,46092
PF3D7_1250800	DNA repair protein rhp16, putative	0,118891	NaN	0,281431	0,981309	0,460544
PF3D7_0413700	lysine decarboxylase-like protein, putative	0,158596	0,508075	0,645978	0,516058	0,457177
PF3D7_0909900	helicase SKI2W, putative	0,673556	0,178388	0,578214	0,39369	0,455962
PF3D7_1440700	AP-3 complex subunit mu, putative	0,399773	0,264894	0,217479	0,936387	0,454633
PF3D7_1344100	TLD domain-containing protein, putative	0,435949	0,310504	0,584674	0,485479	0,454152
PF3D7_0218600	patatin-like phospholipase, putative	0,696083	0,376695	0,346985	0,391399	0,452791
PF3D7_0320300	T-complex protein 1 subunit epsilon	0,472592	0,29465	0,49057	0,551099	0,452228
PF3D7_0609000	nucleoporin NUP637, putative	0,396598	0,298903	0,528371	0,549156	0,443257
PF3D7_0910800	cytosolic Fe-S cluster assembly factor NBP35, putative	0,69439	0,448646	NaN	0,177506	0,440181
PF3D7_1007900	eukaryotic translation initiation factor 3 subunit D, putative	0,367707	0,369669	0,550408	0,457712	0,436374
PF3D7_1123400	eukaryotic peptide chain release factor GTP-binding subunit, putative	0,411752	0,336373	0,551393	0,445028	0,436137
PF3D7_0308200	T-complex protein 1 subunit eta	0,776862	0,397239	0,193961	0,369315	0,434344
PF3D7_0907200	GTPase-activating protein, putative	0,309991	0,238715	0,514804	0,665203	0,432178
PF3D7_0310300	phosphoglycerate mutase, putative	0,374066	0,749815	0,25411	0,349235	0,431807
PF3D7_0106100	V-type proton ATPase subunit C, putative	0,328147	0,224402	0,715981	0,453459	0,430497
PF3D7_0415200	conserved Plasmodium protein, unknown function	0,310456	0,127841	0,423524	0,859195	0,430254
PF3D7_1107000	U6 snRNA-associated Sm-like protein LSm4, putative	0,094642	0,515192	0,702569	0,40053	0,428233
PF3D7_1412100	mini-chromosome maintenance complex-binding protein	0,284869	0,302902	0,654436	0,46552	0,426932
PF3D7_0503800	60S ribosomal protein L31	0,148218	0,356365	0,858299	0,343806	0,426672
PF3D7_0309000	dual specificity protein phosphatase	0,189919	0,337904	0,564622	0,610191	0,425659
PF3D7_0720700	phosphoinositide-binding protein PX1	0,277271	0,473871	0,291368	0,655717	0,424557
PF3D7_1454700	6-phosphogluconate dehydrogenase, decarboxylating	0,502229	0,295801	0,481402	0,416712	0,424036
PF3D7_0613500	AP-3 complex subunit beta, putative	0,473631	0,562453	0,276318	0,376489	0,422223
PF3D7_1428300	proliferation-associated protein 2g4, putative	0,474358	0,199438	0,536351	0,465341	0,418872
PF3D7_1203900	ubiquitin-conjugating enzyme E2	NaN	-0,26772	0,723777	0,793507	0,416523
PF3D7_1116700	dipeptidyl aminopeptidase 1	0,149259	0,631466	0,664119	0,218917	0,41594
PF3D7_1433100	HID1 domain-containing protein, putative	0,311619	0,309073	0,55395	0,488249	0,415723
PF3D7_0802000	glutamate dehydrogenase, putative	0,357608	0,250972	0,536451	0,517482	0,415628
PF3D7_0919800	TLD domain-containing protein	0,291721	0,265345	0,67708	0,426994	0,415285
PF3D7_0527200	ubiquitin carboxyl-terminal hydrolase 14	0,582074	0,386864	0,321928	0,367769	0,414659
PF3D7_1443600	gamma-tubulin complex component, putative	0,280244	0,437311	0,476226	0,463768	0,414387
PF3D7_1219600	phospholipid-transporting ATPase 2	0,38648	0,401597	0,37362	0,49287	0,413642
PF3D7_0621800	nascent polypeptide-associated complex subunit alpha, putative	0,333424	0,125038	0,795102	0,399178	0,413186
PF3D7_0932800	importin alpha re-exporter, putative	0,116365	0,406522	0,480265	0,644984	0,412034

Appendix 9 – Proxiome of AP-1µ

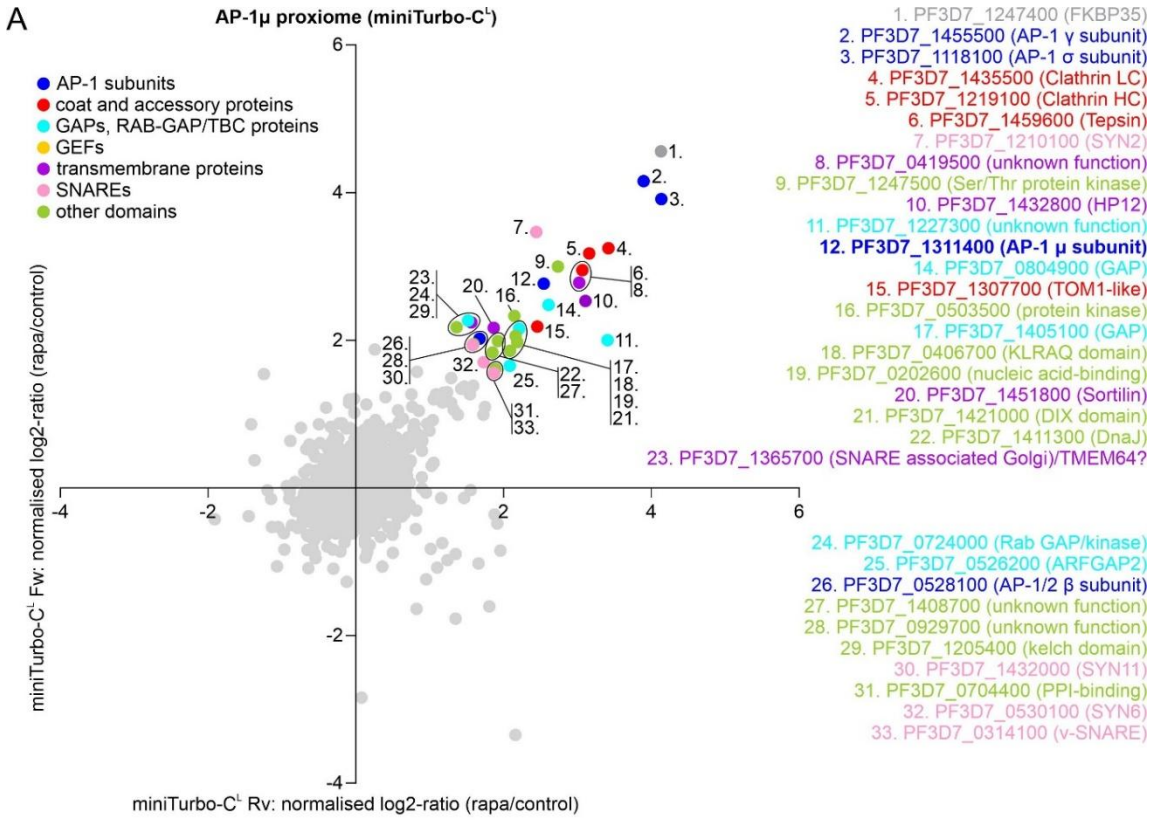

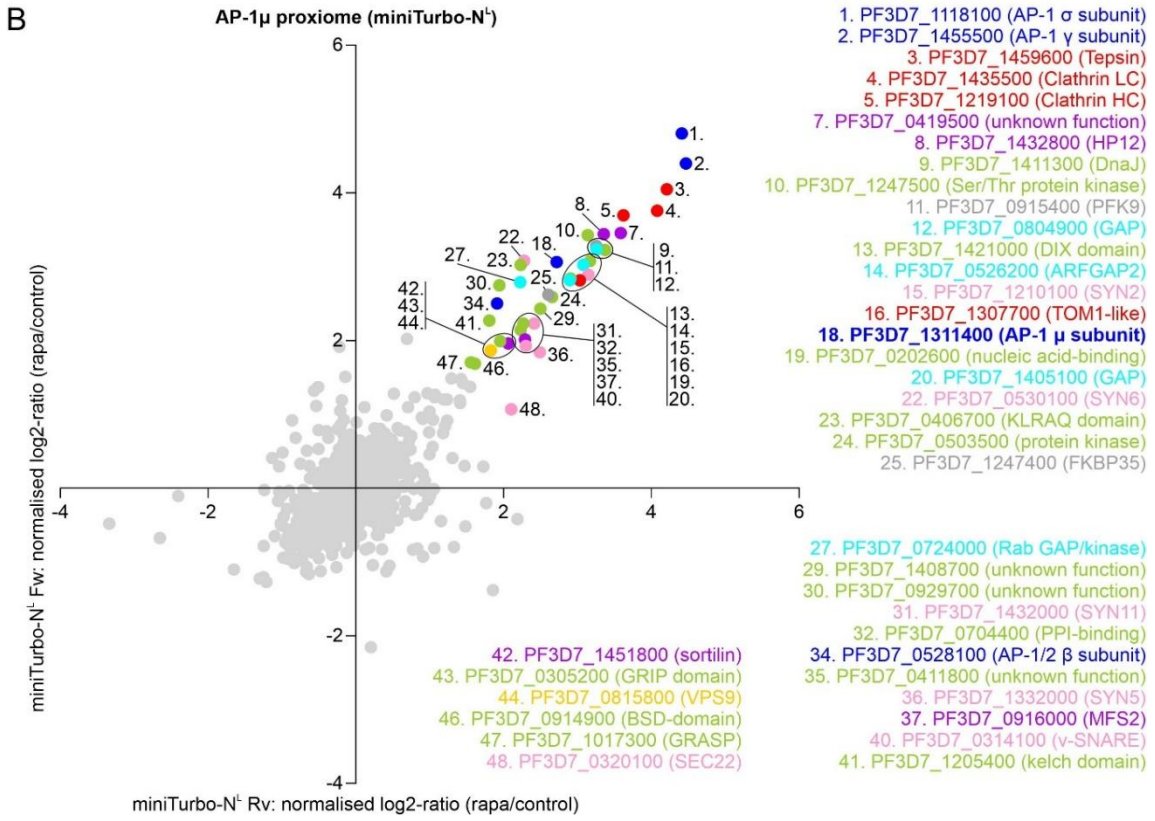

Appendix 10 – Proxiome of AP-3µ

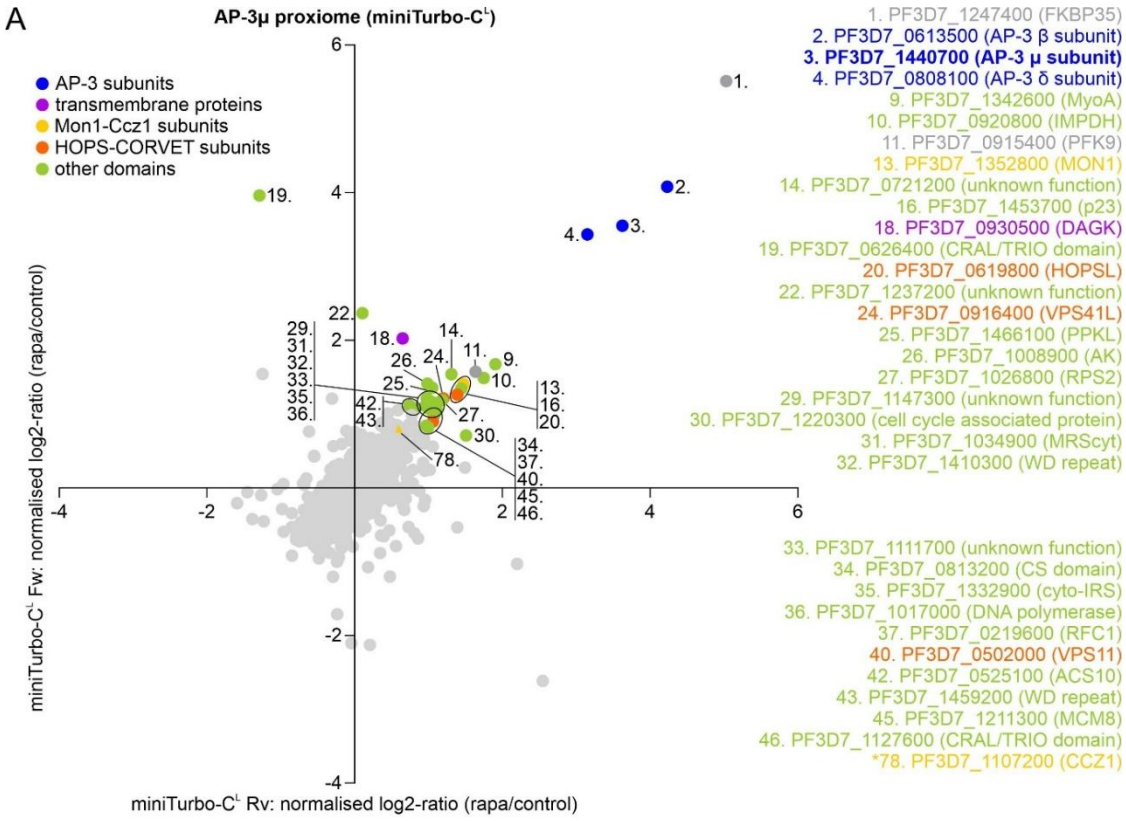

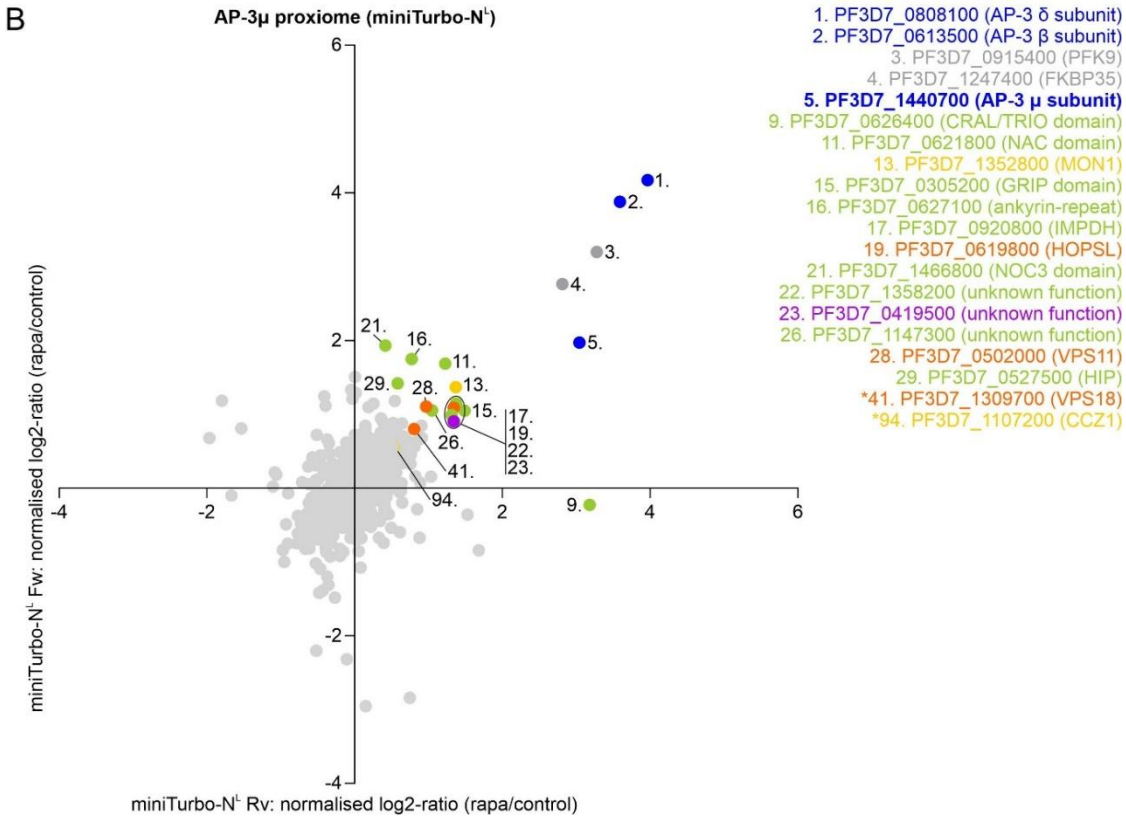

Appendix 11 – Proxiome of AP-4µ

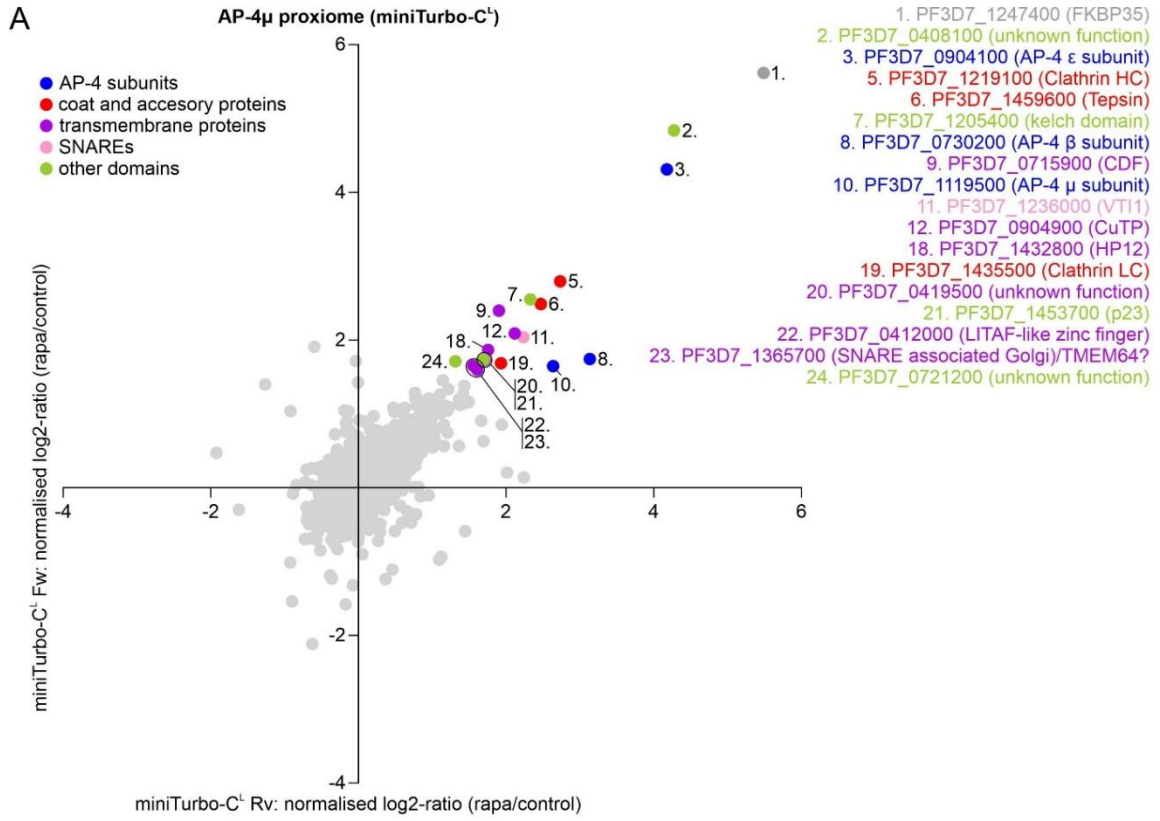

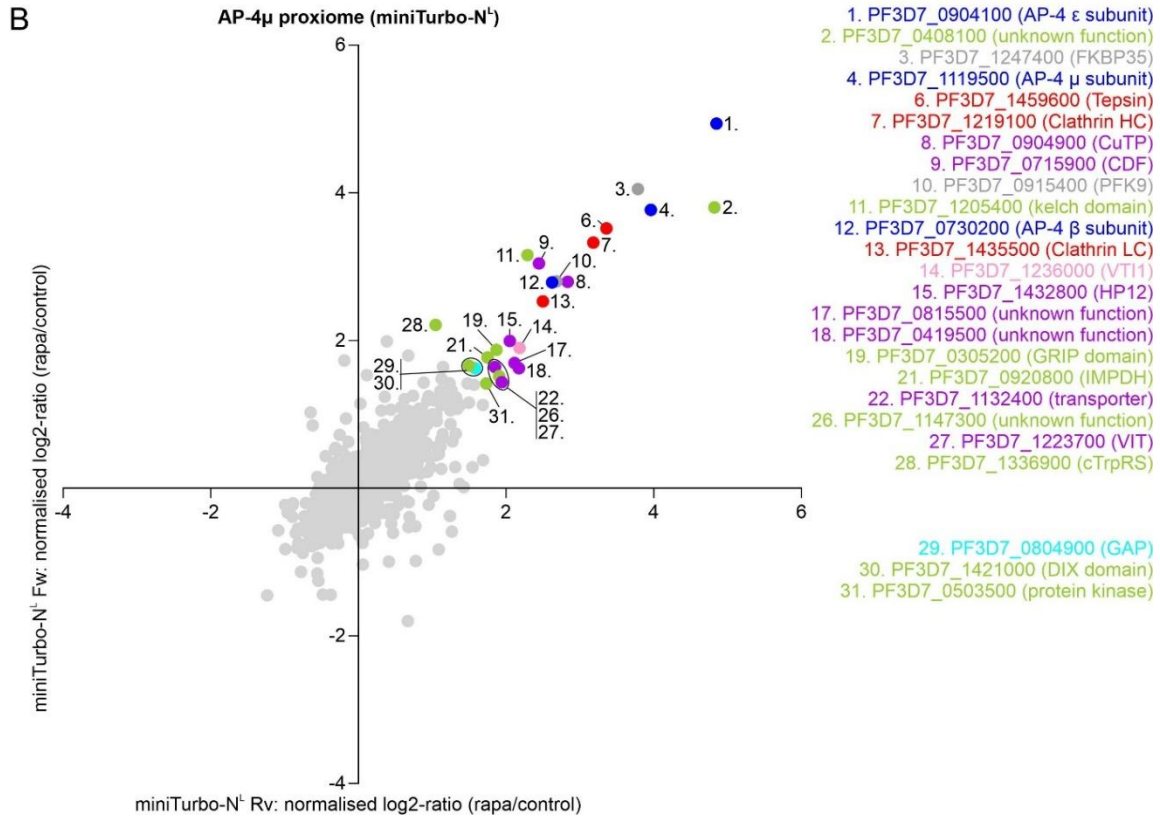

Appendix 12 – Bioinformatic analysis of the unstructured C-terminus of tepsin

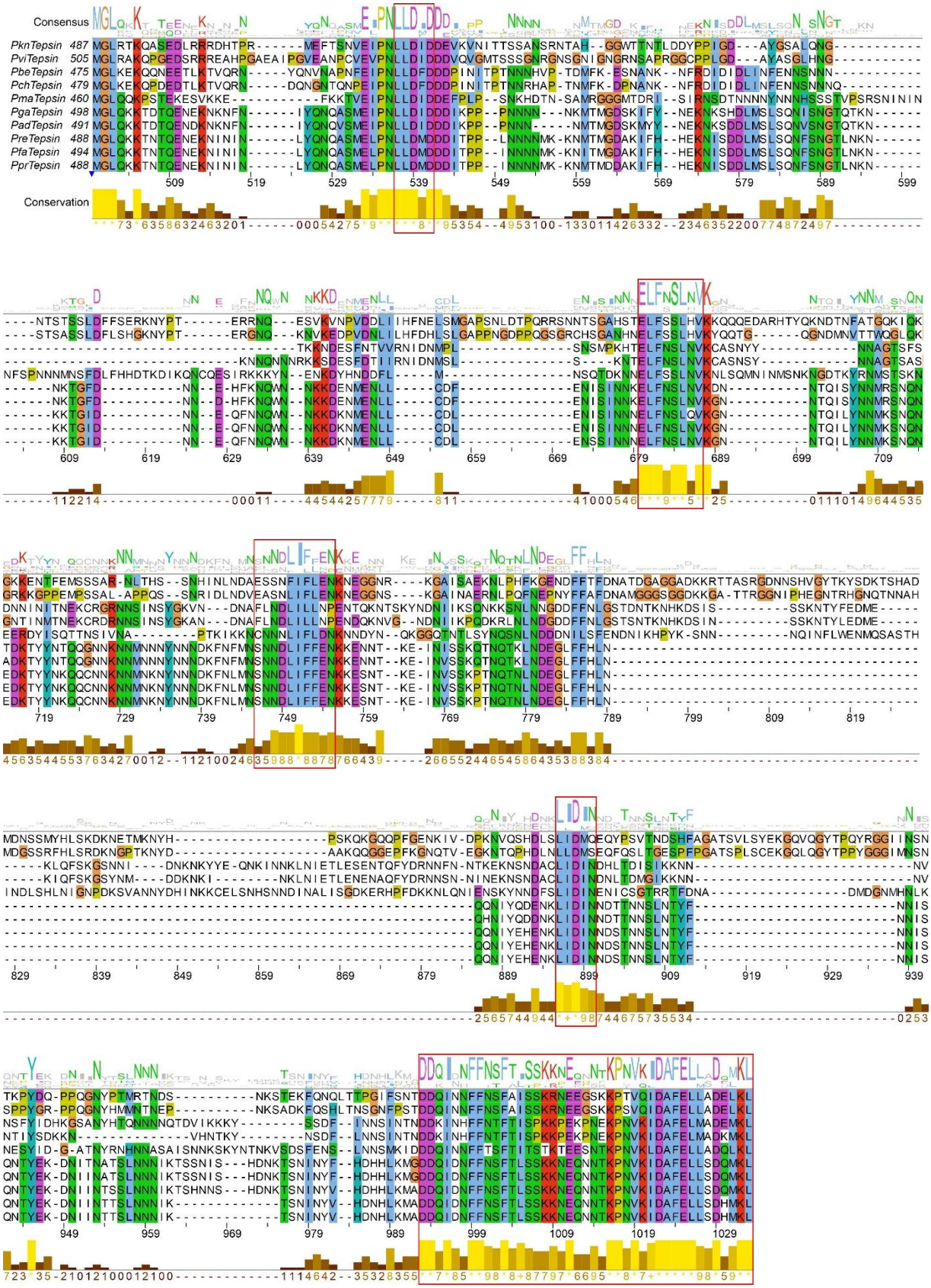

Publications

Mesén-Ramírez, J. P., Fuchs, G., Burmester, J., Farias, G. B., Alape-Flores, A. M., Singla, S., Alder, A., Cubillán-Marín, J., Castro-Peña, C., Lemcke, S., Sondermann, H., Prado, M., Spielmann, T., Wilson, D., & Gilberger, T.-W. (2025). HOPS/CORVET tethering complexes are critical for endocytosis and protein trafficking to invasion related organelles in malaria parasites. PLoS Pathogens, 21(4), e1013053. https://doi.org/10.1371/journal.ppat.1013053

Cubillán-Marín J., Fröhlke U., Ramón-Zamorano G., Mainye S., Mesén-Ramírez J.P.; Farias G.B., Höhn K., Gilberger T.-W., Bártfai R., & Spielmann S. (in revision) Vesicle adaptors in malaria parasites show conservation and flexibility of protein sorting machinery

Acknowledgements

First of all, I would like to express my deepest gratitude to Dr. Tobias Spielmann for giving me the opportunity to do this doctoral thesis. I greatly appreciate his time, dedication and the stimulating discussions we had at each meeting. Your willingness and understanding throughout my PhD were invaluable. I am especially grateful for having allowed you to work with a certain degree of freedom in the development of my doctoral thesis.

I would also like to thank Prof. Tim W. Gilberger for his collaboration, support, and valuable advice, as well as for his role as co-supervisor and thesis reviewer.

I would also like to thank my co-supervisors at the institute's graduate school, Dr. Esther Schnettler and Dr. César Muñoz-Fontela for their advice, guidance and support during the PhD.

My sincere thanks to Dr. Richard Bartfai and Dr. Gala Ramón-Zamorano for their contribution in the project.

I thank Dr. Kathrina Höhn for her dedication and expertise in EM analysis, as well as for her kind conversations and encouragement throughout the process.

I thank the lab technicians, especially Ulrike, for her dedication and important contributions to the adaptor protein studies, and Bärbel (now retired) for her warm welcome and support when I joined the lab.

I would like to acknowledge the financial support provided by the DAAD for my PhD scholarship. I also thank the RTG 2771 programme and the Vereinigung der Freunde des Tropeninstituts Hamburg e.V for their support.

Many thanks to the members of the AG Spielmann team. Thank you for your kindness, good humour, and for creating such a warm, inclusive, and motivating work environment. You truly made the lab feel like a second home, and I will always look back on our time together with great fondness. It was truly a pleasure to be part of this team. Thank you, all guys!

I would also like to thank Dr. Carolina Castro and Dr. Sheila Mainye for their unwavering support, solidarity and cherished friendship. Caro, thank you once again!

Finally, I would like to thank my family – Valeria, Oriana and little Bruno – from the bottom of my heart for accompanying me on this incredible adventure. Your love and support have meant everything to me.